Generic Monte Carlo Event Generator for NLO Processes

Dissertation

zur
Erlangung der naturwissenschaftlichen Doktorwürde
(Dr. sc. nat.)
vorgelegt der
Mathematisch-naturwissenschaftlichen Fakultät
der
Universität Zürich
von

Tobias Motz

aus
Deutschland

Promotionskomitee

Prof. Dr. Daniel Wyler (Vorsitz)
Prof. Dr. Ansgar Denner (Leiter der Dissertation)
Prof. Dr. Thomas Gehrmann
Prof. Dr. Ulrich Straumann

Zürich, 2011

meinen Eltern
meinem Bruder

Zusammenfassung

Für viele Prozesse am LHC (Large Hadron Collider) ist die Berechnung von Korrekturen nächstführender Ordnung zwingend erforderlich. Da diese Prozesse typischerweise viele Teilchen im Endzustand beinhalten, ist für die Berechnung relevanter Observablen die Integration über einen hoch-dimensionalen Phasenraum notwendig. Der angemessenste Algorithmus für eine derartige viel-dimensionale Integration ist eine Monte Carlo Integration. Er ermöglicht die Berechnung eines Resultats in relativ kurzer Zeit mit verhältnimässig geringem Rechenaufwand. Die zentrale Aufgabe der vorliegenden Doktorarbeit war es, einen Monte Carlo Event Generator für LHC Prozesse in nächstführender Ordnung zu implementieren. Zur Verbesserung der Effizienz des Monte Carlo Integrationsalgorithmus wurden verschiedene Optimierungsmethoden eingebaut. Um die Ergebnisse der Monte Carlo Integration mit experimentellen Resultaten zu vergleichen, wurde ferner ein Clustering- und Rekombinations-Algorithmus sowie ein auf elementare Weise generischer Cut-Algorithmus implementiert. Um die in nächstführender Ordnung auftretenden weichen und kollinearen Singularitäten zu regularisieren, wurde eine numerische Methode — konkret der Catani–Seymour Subtraktionsformalismus — eingebaut. Abschliessend wurde das Programm auf Vektor-Boson Streuprozesse angewendet.

Abstract

For many processes at the LHC the calculation of next-to-leading-order (NLO) corrections is mandatory. Since these processes typically involve many particles in the final state, the calculation of the relevant observables requires to integrate over a multidimensional phase space. The most suitable approach for such a multidimensional integration is a Monte Carlo algorithm. This algorithm leads to a result in a reasonable amount of time while ensuring low computational cost. Therefore the goal for the doctoral thesis was the construction of an efficient generic Monte Carlo integrator for LHC processes at NLO. Different optimization schemes that improve the efficiency of the Monte Carlo integration have been implemented. In order to compare the results with experimental data a clustering and recombination algorithm has been implemented and a basic generic cut scheme is provided. Since the Monte Carlo integrator will be used for processes at NLO a treatment of the soft and collinear singularities has to be included. Therefore the Catani–Seymour dipole subtraction formalism has been implemented, also including the phase-space restriction parameter. Finally the program was applied to weak-boson fusion processes.

Contents

List of Figures

List of Tables

1

Introduction

The Monte Carlo method is a statistical sampling method whose beginnings go back to the 1940's. Scientists around Stanislaw Ulam and John von Neumann including Enrico Fermi, Nicholas Metropolis and Robert Richtmyer were searching for methods in order to explore the behavior of neutron chain reactions in fission processes [2], [3]. They were intrigued of sampling these reactions with the help of the newly developed electronic computing devices. John von Neumann states in a letter to Robert Richtmyer in March 1947 that "the statistical approach is very well suited to a digital treatment" [1]. Therein he described in detail how this method could be a solution to the neutron diffusion problem and their interaction with surrounding material in fission devices. This was the first conception of a Monte Carlo computation on an electronic computing device.

For the process under consideration von Neumann started with basic simplifications such as spherically symmetric geometry and isotropically generated neutrons with known velocity. Furthermore he assumed an appropriate statistical probability for the number of neutrons generated in each fission process and that the crosssections for absorption and scattering were functions of the neutron velocity only. John von Neumann's idea was to track the trajectory of a given neutron through the various interactions along its way. At each decision- and interaction-point random numbers were used to determine the subsequent part of the history of the neutron. The random numbers accounted for path length, direction, type of collision as well as velocity after scattering. For every newly generated neutron a trajectory was constructed in the same algorithmic way. One of the main quantities of interest for von Neumann was of course the multiplication rate, i.e. how many neutrons would be present after a time interval Δt assuming n-initial neutrons. In his formulation random numbers were needed at each point of choice of the trajectory of the neutron.

In order to perform Monte Carlo computations of fission processes techniques for picking uniformly distributed random numbers on the unit interval were necessary. The

[1] Letter from John von Neumann to Robert Richtmyer on March 17, 1947.

trajectory of a neutron is generated by a series of different interactions. Each of these is correlated with a known - and usually nonuniform - probability distribution of possible outcomes of the physical event. There is for example the travel distance of the neutron before it interacts with a nucleus again. Due to the exponential decay of neutron path lengths, the probability of an interaction in shorter distances is higher than in longer distances. Therefore, random numbers according to nonuniform distributions were needed and corresponding techniques were developed. In their correspondence Ulam and von Neumann discussed two techniques for generating nonuniform distributions of random numbers out of uniform distributions. In order to generate exponentially decreasing random numbers, Ulam suggested to use the inverse of the desired function $f = g^{-1}$. In the case where an analytical calculation of the inverse is very difficult or even impossible, von Neumann proposed the so called acceptance-rejection technique. The techniques had to be adapted to the probability distributions of the different decision points.

In this framework of von Neumann, the extraction of meaningful information was straightforward. The average energy of the neutrons at a particular time step is calculated by taking the average energy of all neutrons generated up to that point in time. The uncertainty of this value is proportional to the square root of the ratio of variance and number of neutrons generated.

This outline of von Neumann for exploring the behavior of neutrons in neutron fission processes was the first application of a Monte Carlo calculation which was run on an electronic computation device named ENIAC. The potential applications of the Monte Carlo methods were much broader than anticipated until then. In the following years, possible applications were discussed and spread quickly, supplemented by the growing power of computers. More involved problems could be studied, such as the equations of state based on the two-dimensional motion of hard spheres. The growth in complexity of the considered issues lead to optimization of the various ingredients of a Monte Carlo algorithm. The random number generators and techniques for reducing the uncertainty on the result were significantly improved. One of the first random number generators in use - the so called "middle-square digits"-algorithm - was proposed by von Neumann himself. In this algorithm a n-digit integer is squared yielding a $2n$-digit product wherefrom the middle n-digits were extracted. Repeating this process forms a chain of integers used as random numbers. Since then the quality of random number generators has immensely improved, also inspired by mathematical methods (see chapter 2.6). Error reducing techniques for the Monte Carlo result such as variance reducing methods were developed and individualized for the actual problem. The requirements for an efficient Monte Carlo integration in particle physics are outlined in Chapter 2.3.

In the beginning of the 1970s spin glasses came into the focus of Monte Carlo simulations [4]. The Edwards-Anderson Model in 1975 allowed with its abstraction

and generalizations a numerical approach to spin glasses. The basic idea was to find energetically optimal configurations using the Metropolis-Algorithm [5] and a set of possible moves inside the considered spin glass. The Monte Carlo setup for spin glasses found its application also in a physically inspired solutions to optimization problems like the traveling salesman problem. In this case the quantity to be minimized was not the energy, but the path length. Even more sophisticated problems like a time dependent traveling salesman problem with additional constraints were successfully accounted for by Monte Carlo algorithms.

So far the study of physical systems was the main focus. But random sampling is also a powerful way to calculate complicated high-dimensional integrals. The classical numerical integration has been done by quadrature formulas, which can be categorized in two groups. The Newton-Cotes type formulae evaluate the integral on equidistant values, whereas the Gaussian quadrature rules evaluate the integrand at specially chosen values using orthogonal polynomials. For both types of classical numerical integration an absolute bound on specific derivatives of the integrand has to be known in order to get an exact error estimate. These numerical integration methods are very powerful for one-dimensional integrals, provided that the integrand is smooth enough (i.e. knowing absolute bounds on specific derivations of the integrand). The phase space integrals occurring in particle physics are d-dimensional integrals. Cassical numerical integration achieves with N evaluations of the integral an error scaling of about $N^{-\frac{s}{d}}$, where s is an integer number depending on the integration method chosen (e.g. $s = 4$ for the Simpson rule). Therefore, the efficiency of the quadrature rules reduces with increasing number of dimensions. As we will see in Chapter 2.1, the Monte Carlo integration error scales with $1/\sqrt{N}$ independent of the number of dimensions. Furthermore, integrands in particle physics are not necessarily as smooth as required in classical numerical methods. These arguments render the Monte Carlo integration the method of choice for phase-space integration in particle physics.

In this work we present a generic Next-to-Leading Order Monte Carlo code that is optimized for phase space integration of squared matrix elements in particle physics. The mathematical basics of the Monte Carlo method, the construction of the phase space and its implementation are shown in Chapter 4. At Next-to-Leading Order soft and/or collinear singularities occur in the phase-space integration, which have to be numerically regulated. In chapter 3 the Catani–Seymour Dipole Subtraction Formalism [6] is shortly reviewed and the details of its implementation are explained.

2

Monte Carlo Integration

In this chapter we introduce the main mathematical concepts for Monte Carlo Integration. We will show that the error scales like $1/\sqrt{N}$ independent of the number integration dimensions. This makes the Monte Carlo integration the method of choice for the high-dimensional phase-space integrals occuring in particle physics. As a next step, optimization techniques such as stratified sampling, importance sampling and adaptive optimization for efficiency improvement are explained. They are followed by a subsection on random-number generators. A discussion of the multi-channel Monte Carlo approach closes this chapter. The reviewed mathematical background will follow [7] and the lecture [8].

2.1 Monte Carlo Integration

For the phase-space integration in particle physics, one has to evaluate the integral $I(f)$ of a function f on a manifold M using a measure μ

$$I(f) = \int_M f \mathrm{d}\mu. \tag{2.1}$$

In general an analytic evaluation of this integral is not possible and one has to rely on numerical integration methods for estimating $I(f)$. According to the multi-particle final states considered in particle physics, one has to deal with high-dimensional integrals. Since, in that case, standard quadrature formulae are not practical, Monte Carlo integration is the preferred method. The Monte Carlo estimate for the integral Eq. (2.1) is given by

$$E(f) = \frac{1}{N} \sum_{i=1}^{N} f(x_i), \tag{2.2}$$

where the x_i are randomly distributed. The law of large numbers ensures the convergence of Eq. (2.2) to $I(f)$

$$\lim_{N\to\infty} \frac{1}{N} \sum_{i=1}^{N} f(x_i) = I(f). \tag{2.3}$$

A measure for the dispersion around the expectation value is the variance given by

$$\mathrm{Var}(f) = \int \left(f(x) - I(f)\right)^2 \mathrm{d}x. \tag{2.4}$$

The standard deviation is given by the square root of the variance. However, this formula is unpractical since the exact value of the integral $I(f)$ is unknown. Instead of the exact value of $I(f)$, the expectation value $E_N(f) = \frac{1}{N}\sum_{i=1}^{N} f(x_i)$ after N evaluations is used for the calculation of the variance of the Monte Carlo estimate

$$\mathrm{Var}(f) = \frac{1}{N-1} \sum_{i=1}^{N} \left(f(x_i) - E_N\left(f\right)\right)^2 = \frac{1}{N} \sum_{i=1}^{N} \left(f(x_i)\right)^2 - E_N\left(f\right)^2 \ , \tag{2.5}$$

where the standard deviation is given by

$$\sigma(f) = \sqrt{\left(\frac{1}{N} \sum_{i=1}^{N} \left(f(x_i)\right)^2 - E_N\left(f\right)^2\right)}. \tag{2.6}$$

With the help of the central limit theorem the probability that the Monte Carlo estimate lies in the Interval $\left[I(f) - a\frac{\sigma(f)}{\sqrt{N}}, I(f) + b\frac{\sigma(f)}{\sqrt{N}}\right]$ is given by

$$\lim_{N\to\infty} P\left(-a\frac{\sigma(f)}{\sqrt{N}} \leq \frac{1}{N}\sum_{i=1}^{N} f(x_i) - I(f) \leq b\frac{\sigma(f)}{\sqrt{N}}\right) = \frac{1}{\sqrt{2\pi}} \int_{-a}^{b} e^{-\frac{t^2}{2}} \mathrm{d}t \tag{2.7}$$

This shows that the error of the Monte Carlo integration scales independent of the number of dimensions like $\frac{1}{\sqrt{N}}$. The Tschebyschew inequality illustrates that the constant controlling the absolute value of the error depends on the variance of the integrated function. This is used by variance reducing techniques to optimize the integration by reducing the error. Nevertheless, only a probabilistic error bound on the Monte Carlo integration can be given, whereas for standard quadrature integration methods the error bound is deterministic. It should be pointed out that the integrated function f has to be square-integrable, i.e. $\sqrt{\int |f(x)|^2 \mathrm{d}x} < \infty$, in order to ensure reliable error estimates. This condition is fulfilled by the squared matrix elements that have to be integrated over the phase space.

2.2 Mathematical Background

A main part of the thesis is providing an optimized Monte Carlo integration algorithm. Thus, it is necessary to explain the mathematical basis for this type of integration algorithm. In this section we present the basic definitions and theorems in order to put the Monte Carlo integration in a mathematical framework and to understand the principles of the optimization methods. First we define the characteristic function.

Definition 2.2.1 (Characteristic Function)
The characteristic function $\mathbf{1}_A$ *of a subset* A *of* $\mathcal{A}$ *is defined as*

$$\begin{aligned} \mathbf{1}_A &: \mathcal{A} \mapsto 0,1 \\ \mathbf{1}_A(x) &= \begin{cases} 1 & \text{if } x \in A, \\ 0 & \text{if } x \notin A. \end{cases} \end{aligned} \tag{2.8}$$

In order to clearly define the probability space and to define random variables acting on it, we need the following definitions.

Definition 2.2.2 (σ- Algebra)
Let A *be an arbitrary set and* $\mathcal{P}(A)$ *be the power set (i.e. the set of all subsets of* A*). Then a subset* $\mathcal{A} \in \mathcal{P}(A)$ *is called* σ*-Algebra, if it satisfies the following properties:*

- $\mathcal{A}$ *is non-empty*
- $M \in \mathcal{A} \Rightarrow M^C \in \mathcal{A}$
- $M_1, M_2, M_3, \cdots \in \mathcal{A} \Rightarrow \bigcup_{i=1}^{\infty} M_i \in \mathcal{A}$

Definition 2.2.3 (Measurable Space)
A measurable space is a pair $(\Omega, \mathcal{A})$ *consisting of a non-empty set* Ω *and a* σ*-Algebra* $\mathcal{A}$ *of subsets in* Ω*.*

Definition 2.2.4 (Probability Measure)
A probability measure P *is a mapping* $\mathcal{A} \mapsto [0,1]$ *that fullfills the following conditions*

- $P(A) \geq 0 \quad \forall A \in \mathcal{A}$
- $P(\Omega) = 1$
- P *is* σ*-additive, i.e. for disjoint* $A_1, A_2, ... \in \mathcal{A}$ *it holds* $P\left(\bigcup_{i=1}^{\infty} A_i\right) = \sum_{i=1}^{\infty} P(A_i)$*.*

Definition 2.2.5 (Probability Space)
$(\Omega, \mathcal{A}, P)$ *is called probability space and subsets* $A \in \Omega$ *are called events.*

Definition 2.2.6 (Measurable Function)
Let $(\Omega, \mathcal{A})$ *and* $(\Omega^{'}, \mathcal{A}^{'})$ *be measurable spaces. A mapping* $f : \Omega \mapsto \Omega^{'}$ *is called measurable if*

$$f^{-1}(A^{'}) \in \mathcal{A} \quad \forall A^{'} \in \mathcal{A}^{'}, \tag{2.9}$$

where $f^{-1}(A^{'}) := \{\omega \in \Omega | f(\omega) \in \mathcal{A}^{'}\}$. *A random variable is a measurable function defined on* Ω *of a probability space* $(\Omega, \mathcal{A}, P)$.

In a discrete space, every mapping $X : \Omega \mapsto \Re$ is a random variable. Two random variables X and Y are called uncorrelated if the covariance

$$\mathrm{Cov}(X, Y) = E\left((X - EX)(Y - EY)\right) = 0. \tag{2.10}$$

The probability measure defined by

$$P_X(A^{'}) = P(X \in A^{'}) \tag{2.11}$$

is called distribution of X. If X is real-valued the distribution function of X can uniquely be written as

$$F_X(x) = P(X \leq x) = P_X(]-\infty, x[). \tag{2.12}$$

The probability density on $\Re$ is a nonnegative function f that fulfills

$$\int_{-\infty}^{\infty} f(x)\mathrm{d}x = 1. \tag{2.13}$$

The density f can be used to describe a probability distribution function F via

$$F(x) = \int_{-\infty}^{x} f(t)\mathrm{d}t. \tag{2.14}$$

Analogously to F being an arbitrary, continous distribution function defined on $\Re$, which is continuously differentiable on the complement of a finite or empty set C, a probability density f can be defined through

$$f(x) = \frac{\mathrm{d}}{\mathrm{d}x}F(x) \quad (x \in \Re \setminus C). \tag{2.15}$$

Let g be a continuous function on $\Re$. The expectation value of the real-valued random variable X, whose distribution has the probability density f, is given by

$$E_f\left[g(x)\right] = \int g(x)f(x)\mathrm{d}x = \int g(x)\mathrm{d}F(x). \tag{2.16}$$

These definitions of density and distribution functions can be generalized to $\Re^n$ as follows. Let now be $\vec{x} \in \Re^n$ with $\vec{x} = (x_1, \ldots, x_n)$ and for $\vec{y} \in \Re^n$ with $\vec{y} = (y_1, \ldots, y_n)$

denote $x_1 \leq y_1 \wedge \cdots \wedge x_n \leq y_n$ with $\vec{x} \leq \vec{y}$. A probability density in $\mathcal{R}^n$ is a non-negative function f, that fulfills

$$\int_{-\infty}^{\infty} f(x_1, \ldots, x_n) \mathrm{d}x_1 \ldots \mathrm{d}x_n = 1. \tag{2.17}$$

The probability distribution function F in n dimensions with $\vec{b} = (b_1, \ldots, b_n) \in \mathcal{R}^n$ reads

$$F\left(\vec{b}\right) = P(\{\vec{x} \in \mathcal{R}^n | \vec{x} \leq \vec{b}\}) = \int_{-\infty}^{b_1} \ldots \int_{-\infty}^{b_n} f(x_1, \ldots, x_n) \mathrm{d}x_1 \ldots \mathrm{d}x_n \tag{2.18}$$

and can be used to define a probability density function f via

$$f\left(\vec{x}\right) = \frac{\partial^n}{\partial x_1 \ldots \partial x_n} F\left(\vec{x}\right). \tag{2.19}$$

2.2.1 Distribution of mapped random variables

For the optimization techniques used in the Monte Carlo integration, it is useful to study the distribution of a mapped random variable. Let $\phi : \mathcal{R}^n \mapsto \mathcal{R}^n$ be a continuously differentiable mapping and $Y = \phi(X)$. For simplification, we restrict to the case that ϕ is bijective and continuously differentiable in both directions on an open set $G \subset \mathcal{R}^n$ with $P(X \in G) = 1$. Denote the components of the vector $\phi(x)$ by $\phi_i(x)(i = 1, \ldots, n)$ and the jacobian of ϕ by

$$\triangle(x) = \det\left(\left(\frac{\partial \phi_i}{\partial x_k}\right)_{i,k=1,\ldots,n}\right). \tag{2.20}$$

If $\vec{y} = \phi(\vec{x})$, it clearly holds $(\triangle(x))^{-1} = \left(\triangle\left(\phi^{-1}(y)\right)\right)^{-1}$ and $G^{'} = \phi(G)$ is also an open set. The transformation theorem for integrals yields for a continuous function f on G

$$\int_G f(x) \mathrm{d}x = \int_{G'} f\left(\phi^{-1}(y)\right) \left|\left(\triangle\left(\phi^{-1}(y)\right)\right)\right|^{-1} \mathrm{d}y. \tag{2.21}$$

For $A^{'} \subset G^{'}$ we can now calculate

$$P\left(\phi(X) \in A^{'}\right) = \int \mathbf{1}_{\phi^{-1}A'}(x) f(x) \mathrm{d}x \tag{2.22}$$

and with Eq. (2.21) we get

$$P\left(\phi(X) \in A^{'}\right) = \int_{A'} f\left(\phi^{-1}(y)\right) \left|\left(\triangle\left(\phi^{-1}(y)\right)\right)\right|^{-1} \mathrm{d}y. \tag{2.23}$$

If $A^{'}$ a measurable set and $A^{'} \in \Re \setminus G^{'}$, it holds $P\left(\phi(X) \in A^{'}\right) = 0$. The density of $\phi(X)$ is therefore given by

$$g(y) = \begin{cases} f\left(\phi^{-1}(y)\right) \left|\left(\triangle\left(\phi^{-1}(y)\right)\right)\right|^{-1} & \text{if } y \in G^{'} \\ 0 & \text{if } y \in \Re \setminus G^{'} \end{cases}. \tag{2.24}$$

The distribution of mapped variables plays an important role in the multi-channel approach and optimization methods therin.

2.2.2 Conditional Probability

For the proof of the variance reduction of stratified sampling — one of the optimization techniques shown in the next subsection — a theorem on the total variance is needed and derived in the following by means of conditional probability.

Definition 2.2.7 *If X and Y are discrete random variables the conditional probability density function of X given $Y = y$ is defined as*

$$p_{X|Y}(x|y) = P(X = x|Y = y) = \frac{p_{X,Y}(x, y)}{p_Y(y)}. \tag{2.25}$$

In this case, the conditional expectation value of X given $Y = y$ is defined by

$$E[X|Y = y] = \sum_x xP(X = x|Y = y) = \sum_x xp_{X|Y}(x|y). \tag{2.26}$$

Similarly, for continuous random variables X and Y the conditional expectation value is

$$E[X|Y = y] = \int_{-\infty}^{\infty} xp_{X|Y}(x|y). \tag{2.27}$$

Definition 2.2.8 *If X and Y are random variables defined on the same probability space, then the conditional variance of X given that $Y = y$ is the quantity*

$$\mathrm{Var}(X|Y = y) = E[(X - E[X|Y = y])^2|Y = y] \tag{2.28}$$

and similarly the conditional variance of X given Y is

$$\mathrm{Var}(X|Y) = E[(X - E[X|Y])^2|Y]. \tag{2.29}$$

As the following theorem shows, the expected conditional variance of a random variable is less than its variance.

Theorem 2.2.1 Law of total variance

$$\mathrm{Var}(X) = E[\mathrm{Var}(X|Y)] + \mathrm{Var}(E[X|Y]) \tag{2.30}$$

Proof With the basic calculation rules for the variance one observes

$$\mathrm{Var}(X|Y) = E[X^2|Y] + (E[X|Y])^2 \tag{2.31}$$

and

$$E[\mathrm{Var}(X|Y)] = E[E[X^2|Y]] + E[(E[X|Y])^2] = E[X^2] - E[(E[X|Y])^2]. \tag{2.32}$$

Especially because $E[X^2] = E[E[X^2|Y]]$ the variance of the conditional expectation of X given Y can be written as

$$\mathrm{Var}(E[X|Y]) = E[(E[X|Y])^2] - (E[X])^2. \tag{2.33}$$

Adding the last two equation proves the theorem.

∎

2.2.3 The law of large numbers

For the proof of the key theorem for Monte Carlo integration the Tschebyschew inequality is a necessary tool and shown first.

Theorem 2.2.2 *Let (Ω, P) be a discrete probability space and X a real-valued random variable with finite variance. For every $\epsilon > 0$ the inequality*

$$P\left(|X - E[X]| \geq \epsilon\right) \leq \frac{\mathrm{Var}(X)}{\epsilon^2} \tag{2.34}$$

holds.

Proof Let $Z = X - E[X]$, $Y(\omega) = 0$ for ω with $|Z(\omega)| < \epsilon$ and $Y(\omega) = \epsilon^2$ for ω with $|Z(\omega)| \geq \epsilon$. Therefore $Y \leq |Z|^2$ and it follows

$$\mathrm{Var}(X) = E(|Z|^2) \geq E(Y) = \epsilon^2 P(Y = \epsilon^2) = \epsilon^2 P(|X - EX| \geq \epsilon). \tag{2.35}$$

∎

Theorem 2.2.3 *Let $X_1, \ldots, X_n$ be uncorrelated random variables with equal expectation value and finite variance $Var(X_i) \leq M < \infty$. Then for all $\epsilon > 0$ it holds*

$$P\left(\left|\frac{1}{n}\left(X_1 + \cdots + X_n\right) - EX_1\right| > \epsilon\right) \leq \frac{M}{\epsilon^2 n}. \tag{2.36}$$

Proof Let $X = \frac{1}{n}\left(X_1 + \cdots + X_n\right)$. It follows, that $EX = EX_1$ and

$$\mathrm{Var}(X) = \frac{1}{n^2}\mathrm{Var}\left(X_1 + \cdots + X_n\right) = \frac{1}{n^2}\left(\mathrm{Var}\left(X_1\right) + \cdots + \mathrm{Var}\left(X_n\right)\right) \leq \frac{M}{n}. \tag{2.37}$$

The Tschebyschew inequality proves the claim. ∎

This means that the probability that the sum $\frac{1}{n}\sum_{i=1}^{n} X_i$ differs from the expectation value by more than ϵ goes to zero if $n \to \infty$.

2.3 Optimization Methods

2.3.1 Stratified Sampling

The main idea of stratified sampling is to divide the integration domain $M = [0,1]^d$ into several disjoint subdomains $M_1, \ldots, M_n$ such that

$$\bigcup_{i=1}^{n} M_i = M, \tag{2.38}$$

which leads, due to the linearity of the integral, to the following sum

$$\int_M f(x)\mathrm{d}x = \sum_{i=1}^{n} \int_{M_i} f(x)\mathrm{d}x. \tag{2.39}$$

In each subdomain we perform a Monte Carlo integration with total N_j points, which gives in total $N_{rn} = n \cdot N_j$ points, and obtain for the estimate

$$E[f] = \frac{1}{n}\sum_{i=1}^{n} E[f] \restriction_{M_i}, \tag{2.40}$$

where $E[f] \restriction_{M_i}$ means that the expectation value of f is only calculated on the subdomain M_i. For the variance of the stratified estimator, we calculate the following expression

$$\begin{aligned} \mathrm{Var}_{\mathrm{strat}}[E[f]] &= \mathrm{Var}\left[\frac{1}{n}\sum_{i=1}^{n} E[f] \restriction_{M_i}\right] = \\ &= \frac{1}{nN_{rn}}\sum_{i=1}^{n} \mathrm{Var}\left[f \restriction_{M_i}\right] \end{aligned} \tag{2.41}$$

In order to compare the estimates, we now have to compute the variance of the corresponding unstratified estimator. To obtain this result one can use the fact that an unstratified sample is equivalent to first choosing a random subdomain M_j according to the discrete probability density $Vol(M_i)$ (corresponding to the random variable Y) and then randomly choosing x_i in M_j (corresponding to the random variable X). From the point of view of conditional probability this means that X is chosen conditionally on Y. So, we can use (2.30) and get

$$\mathrm{Var}_{\mathrm{unstrat}}[f] = \frac{1}{n}\sum_{i=1}^{n} \frac{\mathrm{Var}\left[f \restriction_{M_i}\right]}{N_{rn}} + \frac{1}{n}\sum_{i=1}^{n} \frac{N_i}{n}(E\left[f \restriction_{M_i}\right] - I(f)^2)$$

Comparison with Eq. (2.41) shows that stratified sampling can significantly reduce the variance. Since the last sum in Eq.(2.42) is always non-negative, stratified sampling can never increase the variance. A further advantage of stratified sampling is that nothing has to be known about the shape of the integrand in order to improve the integration. This varies from the following optimization technique.

2.3.2 Importance Sampling

The idea of importance sampling refers to the principle of choosing a probability density p that is similar to the integrand f. It is well known that the best choice is $p(x) = cf(x)$, where the proportionality constant is determined to be $c = \frac{1}{I(f)}$. This would lead to an estimator with zero variance, since we integrate a constant. Of course, this is not a practical choice, because we have to know the value of the desired integral in order to compute the constant c. Although this is not possible, a probability density p whose shape is similar to f can reduce the variance. This is typically done by determining an analytically integrable function g that is similar to the integrand and let $p \propto g$. Importance sampling is particularly useful in performing the phase space integration of squared matrix elements , because it is powerful for integrands that have large values on small parts of the integration domain M. Mathematically importance sampling corresponds to a change of integration variables and is based on the identity

$$P(X \in M) = \int_M f(x)\mathrm{d}x = \int_M g(x)\frac{f(x)}{g(x)}\mathrm{d}x = \int_M w(x)g(x)\mathrm{d}x \tag{2.42}$$

for all g, such that $g(x) > 0$ for almost all x with $f(x) > 0$. This identity can be used to find a generalized expression for the expectation value

$$\begin{aligned} E_f[h(X)] &= \int_M f(x)h(x)\mathrm{d}x = \int_M h(x)g(x)\frac{f(x)}{g(x)}\mathrm{d}x \\ &= \int_M w(x)h(x)g(x)\mathrm{d}x = E_g[w(X)h(X)]. \end{aligned} \tag{2.43}$$

Assume we have a sample of random variables $X_1, \ldots, X_n$ created according to a probability density g and given that the expectation value $E_g[w(X)h(X)]$ exists, then

$$\frac{1}{n}\sum_{i=1}^{n} w(X_i)h(X_i) \to E_g[w(X)h(X)], \quad n \to \infty \tag{2.44}$$

and by (2.43)

$$\frac{1}{n}\sum_{i=1}^{n} w(X_i)h(X_i) \to E_f[h(X)], \quad n \to \infty. \tag{2.45}$$

The estimate for the integral is thus given by

$$\mu' = \frac{1}{n}\sum_{i=1}^{n} w(X_i)h(X_i). \tag{2.46}$$

The above equation (2.43) holds for every g as long as the domain of f/g is contained in the domain of g. One typically tries to find the best choice for g in order to reduce the variance. The following theorem proves, for which choice of g the variance is minimal.

Theorem 2.3.1 (Optimal Proposal) *The proposal distribution g' that minimizes the variance of $\mu'$is given by*

$$g'(x) = \frac{|h(x)|f(x)}{\int_M |h(t)|f(t)\mathrm{d}t}. \tag{2.47}$$

Proof From the basic calculation rules for the variance we have

$$\begin{aligned} n \cdot \mathrm{Var}\left(\mu'\right) &= \mathrm{Var}\left(w(X)h(X)\right) = \mathrm{Var}_g\left(\frac{h(X)f(X)}{g(X)}\right) \\ &= E_g\left(\left(\frac{h(X)f(X)}{g(X)}\right)^2\right) - \left(E_g\left(\frac{h(X)f(X)}{g(X)}\right)\right)^2 \\ &= E_g\left(\left(\frac{h(X)f(X)}{g(X)}\right)^2\right) - \left(E_g[\mu']\right)^2. \end{aligned} \tag{2.48}$$

We only have to minimize the first part of the equation, namely $E_g\left(\left(\frac{h(X)f(X)}{g(X)}\right)^2\right)$. Plugging in g', we obtain

$$\begin{aligned} E_{g'}\left(\left(\frac{h(X)f(X)}{g'(X)}\right)^2\right) &= \int_M \frac{h(x)^2 f(x)^2}{g'(x)}\mathrm{d}x \\ &= \left(\int_M \frac{h(x)^2 f(x)^2}{|h(x)|\, f(x)}\mathrm{d}x\right) \cdot \left(\int_M |h(t)|\, f(t)\mathrm{d}t\right) \\ &= \left(\int_M |h(x)|\, f(x)\mathrm{d}x\right)^2 \end{aligned} \tag{2.49}$$

On the other hand, we can use the Jensen inequality to get a lower bound for $E_g\left(\left(\frac{h(X)f(X)}{g(X)}\right)^2\right)$

$$\begin{aligned} E_g\left(\left(\frac{h(X)f(X)}{g(X)}\right)^2\right) &\geq \left(E_g\left(\frac{h(X)f(X)}{g(X)}\right)\right)^2 \\ &= \left(\int_M |h(x)|\, f(x)\mathrm{d}x\right)^2, \end{aligned} \tag{2.50}$$

which concludes the proof. ∎

However this theorem is a rather formal optimality result and from a first point of view unpractical, since we need to know the exact value of the desired integral. Later we will show a way to find a probability distribution g suited for the phase space integration in particle physics whose shape is similar to the shape of the function to be integrated.

2.4 VEGAS

VEGAS [9], [10] is an iterative algorithm that adjusts the probability density in each step such that it minimizes the variance of the integration. The idea is to start from uniformly distributed random points $\vec{x} \in [0,1]^n$, i.e. $g(\vec{x}) = const$ and modify $g(\vec{x})$ so that the variance is reduced. Following [9] and [10], this is explained in the one-dimensional case integrating the function $f(x)$. Dividing the integration axis x into N intervals Δx_i with $\sum_{i=1}^{N} \Delta x_i = 1$, one defines the probability density as the step function

$$g(x) = \frac{1}{N \Delta x_i} \quad \text{if} \quad x_i - \Delta x_i \leq x < x_i. \tag{2.51}$$

After the first M evaluations of the integrand $f(x)$ the N intervals are subdivided into m_i subintervals, where

$$m_i = C \cdot \frac{\bar{f}_i \Delta x_i}{\sum_{j=1}^{N} \bar{f}_j \Delta x_j} \tag{2.52}$$

with

$$\bar{f}_i = \sum_{x \in x_i - \Delta x_i}^{x_i} |f(x)| \tag{2.53}$$

and C being a large constant. The choice (2.52) is mainly guided by the optimal proposal for $g(x)$, because in that way m_i is a weight for the contribution of $|f|$ in the interval Δx_i - if $|f|$ has large contributions, m_i is also large and the other way round. Since one wants to restore the original number of intervals N, the subintervals have to be regrouped and merged to larger intervals such that their number in each group is constant and the increment density $\frac{m_i}{N}$ is preserved. Accordingly, the increment size Δx_i is varied, while the total number N is kept constant, so that Δx_i is small where $|f(x)|$ has a large contribution. In the next step, the new grid is used and refined by the above steps. The optimal grid is reached if the increment density is constant, i.e. the number of subintervals per interval is equal to all others ($m_i = m_j, \forall i,j \in \{1,...,N\}$). The generalization to n dimensions is straightforward. Supposing a factorizable probability density $g(x_1,\ldots,x_n) = g_{x_1}(x_1) \cdot \cdots \cdot g_{x_n}(x_n)$ the optimal proposal is given by

$$g_{x_i}(x_i) = \frac{\left[\int \mathrm{d}\hat{x}_i \frac{f(\vec{x})}{\prod_{j\neq i}^{n} g_{x_j}(x_j)}\right]^{\frac{1}{n}}}{\int \mathrm{d}x_i \left[\int d\hat{x}_i \frac{f(\vec{x})}{\prod_{j\neq i}^{n} g_{x_j}(x_j)}\right]^{\frac{1}{n}}}, \tag{2.54}$$

where $\hat{x}_i = (x_1,\ldots,x_{i-1},x_{i+1},\ldots,x_n)$. By defining

$$\bar{f}_i^n = \sum_{x \in x_i - \Delta x_i}^{x_i} \sum_{\hat{x}_i} \left(\frac{f(\vec{x})}{\prod_{j\neq i}^{n} g_{x_j}(x_j)} \right)^n, \tag{2.55}$$

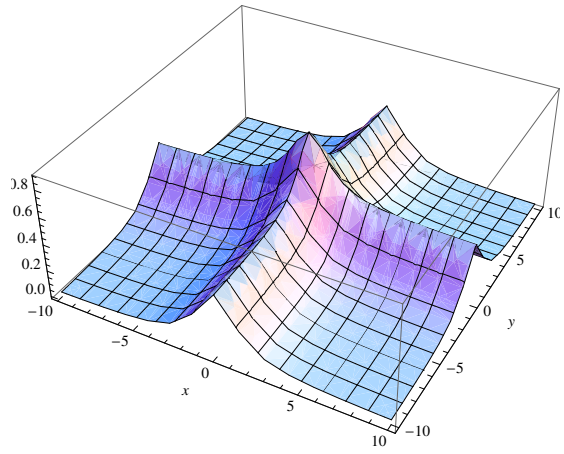

Figure 2.1: Plot of $f_1(x, y)$

the one-dimensional algorithm can now be applied for all axis x_i. VEGAS is an adaptive integration algorithm, i.e. the information gained about the integrand in the first evaluations is used to define a variance reducing new probability density. Visually spoken, this is done by refining the grid perpendicular to the axis, so that the volume of the hypercubes where the integrand has large contributions is small. Over many iterations this algorithm concentrates the density of points to suit the integrand.

2.5 Non factorizable distributions

As shown in the section above, VEGAS can be used [11] for optimization in the case of factorizable distribution g and measures μ. Factorizable means that singularities occur along the coordinate axis. The factorization property clearly depends on the coordinate system chosen. As an example take the two well-known functions

$$f_1(x, y) = \frac{1}{(x)^2 + 1.5^2} + \frac{1}{(y)^2 + 1.5^2} \tag{2.56}$$

and

$$f_2(x, y) = \frac{1}{(\sqrt{x^2 + y^2})^2 + 4}. \tag{2.57}$$

Both functions shown in figure 2.1 and 2.2 are factorizable f_1 in cartesian coordinates and f_2 in polar coordinates. Therefore VEGAS will integrate both functions efficiently in suitable coordinate system. Nevertheless, from a first point of view, there is no coordinate system in which VEGAS can integrate the sum of f_1 and f_2. In [11], a generalization of the VEGAS algorithm to the sum of factorizable distributions, where each term can be factorizable in a different coordinate system is proposed. It uses

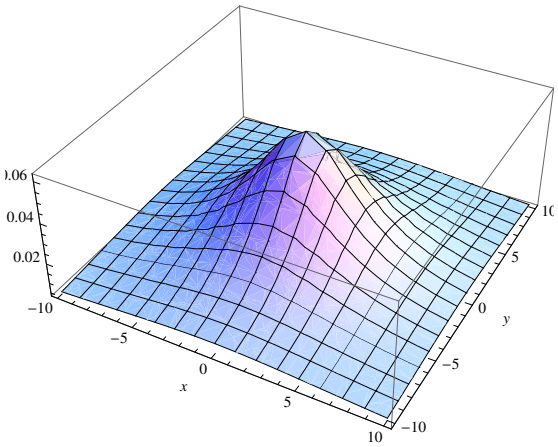

Figure 2.2: Plot of $f_2(x, y)$

importance sampling in combination with an adaptive optimization technique. After a transformation of variables, the desired integral $I(f)$ has the form

$$I(f) = \int_0^1 d^n x (f \circ \phi)(x) \left| \frac{\partial \phi}{\partial x} \right|, \tag{2.58}$$

with $\phi : [0,1]^n \mapsto M$. For the numerical integration it remains to sample $(f \circ \phi)(x) \left| \frac{\partial \phi}{\partial x} \right|$ on the n-dimensional unit hypercube U. In our case, f can be seen as a sum of terms, which have each singularities that factorize in different coordinate systems. One now tries to exploit the fact that there is more than one mapping from U to M to take account for the individual singularity structure. The task is still to choose the most suitable mappings for our integration purposes. Since it is almost impossible to get the optimal proposal, one tries to find ϕ such that the integrand of (2.58) has factorizable singularities. For all different peaking structures, one gets associated mappings $\phi_i : U \mapsto M$ with their corresponding probability densities $g_i : M \mapsto [0, \infty)$. For the integration of f, a probability density g on M is required and defined through

$$g = \sum_{i=1}^{N} \alpha_i (g_i \circ \phi_i^{-1}) \left| \frac{\partial \phi_i^{-1}}{\partial x} \right|. \tag{2.59}$$

Given the following normalization of g_i and α_i

$$\int_0^1 g_i(x) d^n x = 1, \quad \sum_{i=1}^{N} \alpha_i = 1, \quad 0 \leq \alpha_i \leq 1, \tag{2.60}$$

the probability density $g : M \mapsto [0, \infty)$ fulfills

$$\int_M g(p) \mathrm{d}\mu(p) = 1. \tag{2.61}$$

Inserting (2.59) in the integration $I(f)$, we find

$$\begin{aligned} I(f) &= \int_M \mathrm{d}\mu(p) g(p) \frac{f(p)}{g(p)} \\ &= \sum_{i=1}^{N} \alpha_i \int_M \mathrm{d}\mu(p) (g_i \circ \phi_i^{-1})(p) \left| \frac{\partial \phi_i^{-1}}{\partial x} \right| \frac{f(p)}{g(p)} \\ &= \sum_{i=1}^{N} \alpha_i \int_0^1 d^n x g_i(x) \frac{f(\phi_i(x))}{g(\phi_i(x))}. \end{aligned} \tag{2.62}$$

This shows that the estimate for the integration does not depend on the chosen parametrization of M. This allows to optimize the integration by choosing N mappings ϕ_i and their corresponding densities g_i that account for the different singularity structures appearing in f, which is shown in [12]. So far, the only precondition to the so called *a-priori weights* $\alpha_i \in [0,1]$ is the normalization condition

$$\sum_{i=1}^{N} \alpha_i = 1. \tag{2.63}$$

Once this is fulfilled, Eq. (2.62) shows that the estimate of the integral $I(f)$ will not depend on the values of the *a-priori weights*, but the error will. So another possible scope of optimization is the adjustment of the *a-priori weights* α_i. The goal of this optimization scheme is to modify the α_i in order to minimize the variance (2.5) of the Monte Carlo result. This is equal to minimizing

$$W(f, \alpha) = \int_M \mathrm{d}\mu(p) g(p) \left(\frac{f(p)}{g(p)} \right)^2 \tag{2.64}$$

with respect to $\alpha = \{\alpha_1, \cdots, \alpha_i\}$ with the auxiliary condition $\sum_{i=1}^{N} \alpha_i = 1$. W depends via g on the set α_i. The integration error is proportional to $\left[\left(W(\alpha) - I(f)^2 \right) \right]$. In order to reduce the error, one tries to modify the α_i to minimize the quantity $W(\alpha)$. As shown above, changing the α_i during the integration routine does not affect the result, since the value of $I(f)$ does not depend on the set α_i. This means that the optimization will lead to an unbiased result. Thus the task of this optimization scheme is to find $\overline{\alpha}$ such that $W(\overline{\alpha})$ is minimized. The extremum of $W(\overline{\alpha})$ is obtained at values of $\overline{\alpha}$ for which

$$W_i(f, \overline{\alpha}) = W(\overline{\alpha}), \quad \forall i \tag{2.65}$$

with

$$W_i(f, \overline{\alpha}) = -\frac{\partial}{\partial \alpha_i} W(\overline{\alpha}) = \int_0^1 d^n x g_i(x) \left(\frac{(f \circ \phi_i)(x)}{(g \circ \phi_i)(x)} \right)^2 \tag{2.66}$$

and

$$W\left(f,\overline{\alpha}\right)=\sum_{i=1}^{N}\alpha_i W_i\left(f,\overline{\alpha}\right). \tag{2.67}$$

This is due to the fact that $W\left(\alpha\right)$ is homogeneous of degree $n_{deg}=-1$, which implies

$$n_{deg}\cdot W\left(\alpha\right)=\sum_{i=1}^{n}\frac{\partial W}{\partial\alpha_i}\cdot\alpha_i \quad\Leftrightarrow\quad n_{deg}\cdot W\left(\alpha\right)=\alpha\cdot\nabla W\left(\alpha\right) \tag{2.68}$$

via Eulers theorem. To prove that this is indeed a minimum, let $\alpha_i=\overline{\alpha_i}+\beta_i$ with small β_i. Since α_i and $\overline{\alpha_i}$ describe a simplex, it holds $\sum_{i=1}^{n}\beta_i=0$ and

$$W\left(\alpha\right)=W\left(\overline{\alpha}\right)+\frac{1}{2}\int \mathrm{d}^n x\frac{(f\circ\phi_i)(x_i)^2}{(g\circ\phi_i)(x)^3}\left(\sum_{i=1}^{N}\beta_i(g\circ\phi_i)(x)\right)^2+\mathcal{O}\left(\beta_i^3\right). \tag{2.69}$$

From the Taylor expansion around $\overline{\alpha}$ and $g\geq 0$ it is clear that $W\left(\alpha\right)$ has a minimum at $\overline{\alpha}$, although not necessarily a unique one. Now one has to set up a procedure in order to find a set of α_i during a Monte Carlo run that minimizes $W\left(\alpha\right)$. Starting with an arbitrary set α the Monte Carlo creates a number of phase-space points in each channel. At each point, $W_i\left(\alpha\right)$ is estimated using

$$W_i\left(\alpha\right)=\left\langle\frac{g_i\left(\vec{x}\right)}{g\left(\vec{x}\right)}w\left(\vec{x}\right)^2\right\rangle \tag{2.70}$$

and this information helps to improve α_i. If $W_i\left(\alpha\right)$ is small (large), the optimization should lead to a new α_i^{new} that is smaller (larger), because the contributions to the final result from this bin are smaller (larger). We use according to [12]

$$\alpha_i^{new}\propto\alpha_i\sqrt{W_i\left(\alpha\right)}. \tag{2.71}$$

as a concrete optimization prescription. In that way, the α_i are proportional to the probability that a given channel i is evaluated. After a given number of points (should be chosen such that each channel was chosen reasonably often) the α_i are refined according to relation Eq (2.71) building a new grid. The refinement of the α_i should be done until they converge to a reasonable grid. In general the refinement should take about 10% of the total number of events needed for the full integration.

2.6 Random Number Generator

A main component of Monte Carlo methods are independent and identically distributed (i.i.d.) random numbers chosen from the uniform distribution of the interval $[0,1]$. Using physical phenomena to get random numbers is of course not feasible. The random numbers are generated by a definite, deterministic computational process. If they mimic

a sequence of i.i.d. random numbers, they are called pseudo-random numbers. In the Monte Carlo code [13], the pseudo random numbers should work as a good replacement for true random numbers, i.e. the program should produce the same results independently of whether pseudo random numbers or true random numbers were used. Hence computational indistinguishability of the output is one of the main requirements for a random number generator. Other requirements for a good random number generator are listed in the following:

- random numbers are almost uniformly distributed
- random numbers are uncorrelated
- period between identical number is sufficiently long
- unless a seed is given, the numbers should be unpredictable

Before 1990s good random number generators were hard to find, as Park and Miller stated in 1989 [14]. But in 1998, Matsumoto and Nishimura [15] invented an algorithm whose period ($s^{19937}-1$) exeeded the number of electron spin changes since the creation of the universe (10^{6000} vs. 10^{120}). L'Ecuyer [16] defined a basic structure (S, μ, f, U, g) of pseudo random number generators, where

- S is a finite set of states
- the initial distribution μ is a probability distribution on S
- f is a transition function $f : S \mapsto S$
- U is a finite output set
- g is an output function defined as $g : S \mapsto U$.

The random number are generated according to the following algorithm:

- generate the initial state (the so called seed s_0) according to the initial distribution
- compute $u_0 = g(s_0)$
- for $i = 1, \ldots, n$ do: $s_i = f(s_{i-1})$ and $u_i = g(s_i)$

In most cases, the machine clock timer is used to generate the initial seed. One of the key characters of the random number generator is the period - defined as the smallest integer l, such that $s_{l+n} = s_n \forall n \in \mathbb{N}$. The two main families of these types of random number generators are Linear Congruential Generators (LCG) and Multiple Recursive

Generators (MRG), where the main difference of these two is the transfer function. In case of a LCG, the transfer function is such that

$$x_n = (a x_{n+1} + c) \ \ mod \ \ m \tag{2.72}$$

and in case of a MCG the transfer function reads

$$x_n = (a_1 x_{n-1} + \cdots + a_k x_{n-k} + c) \ \ mod \ \ m \ , \tag{2.73}$$

where $a \in \mathbb{N}$ is the multiplier, $c \in \mathbb{N}$ the increment, $m \in \mathbb{N}$ the modulus and $k \in \mathbb{N}$ a fixed integer. In order to maximize the period, there are number theoretical theorems, which put constraints on these parameters. We use the random number generator RANLUX implemented by [17]. It is a very fast random number generator that provides decorrelated numbers at a high level of randomness with a proven period of about 10^{171}.

2.7 Multi-Channel Monte Carlo

The methods introduced above can be combined to a *multichannel* Monte Carlo integration using *a-priori-weights* α. According to [18] and [19], the phase space integral reads

$$I_n = \int \mathrm{d}\Phi_n \ \rho\left(p_i\left(\Phi\right)\right) \ \ f\left(p_i\left(\Phi\right)\right), \tag{2.74}$$

where

$$f\left(p_i\left(\Phi\right)\right) = \frac{1}{F} \left|\mathcal{M}\left(p_1, p_2, p_i\left(\Phi\right)\right)\right|^2, \tag{2.75}$$

ρ denotes the phase space density and F is the flux factor given by

$$F = 2\lambda\left(s, m_1^2, m_2^2\right)^{\frac{1}{2}}. \tag{2.76}$$

In order to apply the Monte Carlo integration the phase space $\mathrm{d}\Phi$ has to be built out of uncorrelated random numbers r_i in the unit hypercube $[0,1]$. We denote this mapping with $h(\mathbf{r}) = \mathbf{\Phi}$ and obtain

$$I_n = \int \mathrm{d}\Phi_n \ \rho\left(p_i\left(\Phi\right)\right) \ \ f\left(p_i\left(\Phi\right)\right) = \int_0^1 d\mathbf{r} \rho\left(p_i\left(h(\mathbf{r})\right)\right) f\left(p_i\left(h(\mathbf{r})\right)\right) \left|\frac{\partial h(\mathbf{r})}{\partial \mathbf{r}}\right|_{\mathbf{r}=h^{-1}(\Phi)} \tag{2.77}$$

With

$$\frac{1}{g\left(p_i\left(h(\mathbf{r})\right)\right)} = \rho\left(p_i\left(h(\mathbf{r})\right)\right) \left|\frac{\partial h(\mathbf{r})}{\partial \mathbf{r}}\right|_{\mathbf{r}=h^{-1}(\Phi)}, \tag{2.78}$$

we can rewrite I_n as

$$I_n = \int_0^1 d\mathbf{r} \frac{f\left(p_i\left(h(\mathbf{r})\right)\right)}{g\left(p_i\left(h(\mathbf{r})\right)\right)}. \tag{2.79}$$

So far, we used a transformation of variables, which allows for importance sampling as an optimization technique according to Section 2.3.2. Mappings $h(\mathbf{r})$ have to be constructed such that their jacobian determinants mimic the peaking structure of the integrand. They are deducted in Section 4.2 guided by the optimal proposal (2.3.1). The peaking structure of the integrand follows the topologies appearing in the Feynman diagrams of squared matrix elements . Those can have a very complex propagator - and therefore also peaking - structure. For complicated processes, one mapping is usually not enough for an efficient Monte Carlo integration. A way out was shown in Section 2.5, where a *multi-channel-approach* based on [20], [21] with adaptive weight optimization according to [12] and [11] was introduced. We now have N mappings $h_i : U \mapsto \Phi$ with their corresponding densities $g_i : \Phi \mapsto [0, \infty)$ and N *a-priori-weights* α_i that fulfill

$$\sum_{i=1}^{N} \alpha_i = 1, \quad 0 \leq \alpha_i \leq 1. \tag{2.80}$$

The phase space mapping is chosen by taking a random number z uniformly distributed in $[0, 1]$ and defining cumulative weights by $\beta_0 = 0$, $\beta_N = 1$ and $\beta_i = \sum_{l=1}^{i} \alpha_l$. The channel h_l is chosen if $\beta_{i-1} \leq z \leq \beta_i$. Using

$$\int_0^1 dz\, \Theta\left(\beta_{i-1} \leq z \leq \beta_i\right) = \beta_i - \beta_{i-1} = \alpha_i \tag{2.81}$$

we can rewrite Eq. (2.79) with the help of Theorem **??** and Eq. (2.62) as follows

$$I_n = \int_0^1 dz \sum_{k=1}^{N} \Theta(z - \beta_{k-1})\Theta(\beta_k - z) \int_0^1 d\mathbf{r} \frac{f\left(p_i\left(h_k(\mathbf{r})\right)\right)}{g_{tot}\left(p_i\left(h_k(\mathbf{r})\right)\right)}, \tag{2.82}$$

with a total density given by

$$g_{tot}\left(p_i\left(h_k(\mathbf{r})\right)\right) = \sum_{l=1}^{N} \alpha_l g_l\left(p_i\left(h_k(\mathbf{r})\right)\right). \tag{2.83}$$

The *a-priori-weights* α_i can be optimized according to the adaptive optimization scheme explained in Section 2.5. The advantages of a multi-channel Monte Carlo integration are obvious. The integrands are squared matrix elements that exhibit a peaking structure due to the propagators in the corresponding topologies of the Feynman diagrams. Each of the peaking structures can be accounted for in a specific channel by introducing a set of mappings that smoothens the singularity structure of a given topology. The construction of the mappings is led by Theorem (2.3.1) and worked out in Section 4.2. The smoothening of densities constructed in that way is shown in Section 2.3.2 and reduces the Monte Carlo error significantly. Whereas basic information of the shape of the integrand has to be known in order to construct appropriate mappings, the

adaptive optimization of the *a-priori-weights* α can be done without any knowledge of the integrand. A combination of both error reducing techniques is given in a multi-channel Monte Carlo approach.

3

Dipole Subtraction Formalism

This Chapter briefly reviews the dipole subtraction formalism. After explaining the basic structure of the subtraction concept, the subtraction terms and the integrated subtraction terms are listed both in the α-dependent and α-independent way. Also the phase space factorization for each of the different emitter–spectator cases is given. At the end of this Chapter, the evaluation of the x_+ and +-distributions is discussed. The Chapters 3.3 and 3.4 collect and present the dipole subtraction and integrated dipole subtraction terms that are implemented and present in the literature at NLO. The review of the dipole subtraction formalism will follow [6] and [22].

3.1 Dipole Subtraction Formalism

The dipole subtraction formalism is well suited for numerical calculation of NLO cross-sections. Starting with the LO cross-section with m final-state partons

$$\sigma^{\mathrm{LO}} = \int_m \mathrm{d}\sigma^{\mathrm{B}}, \tag{3.1}$$

the NLO crossection σ is given by

$$\sigma = \sigma^{\mathrm{LO}} + \sigma^{\mathrm{NLO}} = \int \mathrm{d}\sigma^{\mathrm{B}} + \int \mathrm{d}\sigma^{\mathrm{NLO}}. \tag{3.2}$$

Here, the phase-space integration in Eq. (3.1) yields a finite LO cross-section. The NLO cross-section consists of the real radiation part $\mathrm{d}\sigma^{\mathrm{R}}$ belonging to the $m+1$ particle phase space and the virtual part $\mathrm{d}\sigma^{\mathrm{V}}$ which belongs to the m parton phase space:

$$\sigma^{\mathrm{NLO}} = \int_{m+1} \mathrm{d}\sigma^{\mathrm{R}} + \int_m \mathrm{d}\sigma^{\mathrm{V}}. \tag{3.3}$$

Both the integrals on the right hand side of Eq. (3.3) are separately divergent in four dimensions, whereas their sum is finite. Since both of the integrands $\mathrm{d}\sigma^{\mathrm{V}}$ and $\mathrm{d}\sigma^{\mathrm{R}}$

are integrated over different phase spaces $\mathrm{d}\Phi_m$ and $\mathrm{d}\Phi_{m+1}$ respectively, they have to be regularized before any numerical calculation can be performed. In dimensional regularization the divergencies are contained in ϵ-poles and occur in the limit $\epsilon \to 0$, which is equivalent to dimension $d \to 4$. The dipole subtraction formalism steps in after the renormalization procedure for ultraviolet divergencies has been carried out. In this case, only soft and/or collinear singularities that occur at NLO in $\frac{1}{\epsilon^2}$ poles (soft and collinear) or in $\frac{1}{\epsilon}$ poles (soft or collinear) are left over. The main idea of the subtraction formalism according to [6] is given by the following equation

$$\sigma^{\mathrm{NLO}} = \int_{m+1} \left(\mathrm{d}\sigma^{\mathrm{R}} - \mathrm{d}\sigma^{\mathrm{A}}\right) + \left[\int_{m+1} \mathrm{d}\sigma^{\mathrm{A}} + \int_m \mathrm{d}\sigma^V\right] \quad . \tag{3.4}$$

The term $\mathrm{d}\sigma^{\mathrm{A}}$ is constructed in such a way that it approximates pointwise the singular structure of the real radiation part $\mathrm{d}\sigma^{\mathrm{R}}$. Hence $\mathrm{d}\sigma^{\mathrm{A}}$ is a local counterterm for the soft- and/or collinear singularities in $\mathrm{d}\sigma^{\mathrm{R}}$, which allows to safely build the limit $\epsilon \to 0$ on the integrand level in the phase space integral

$$\sigma^{\mathrm{NLO}}_{m+1} = \int_{m+1} \left[\lim_{\epsilon\to 0} \mathrm{d}\sigma^{\mathrm{R}} - \lim_{\epsilon\to 0} \mathrm{d}\sigma^{\mathrm{A}}\right] \quad . \tag{3.5}$$

The $m+1$ parton phase space integral can now be computed numerically in four dimensions. The only singularities left are contained in the square bracket of Eq. (3.4). Assuming one is able to integrate $\mathrm{d}\sigma^{\mathrm{A}}$ analytically over the one parton subspace leading to the ϵ poles, the sum of these poles with the ones in $\mathrm{d}\sigma^V$ cancels the leftover divergencies. After building the limes $\epsilon \to 0$ the sum of $\mathrm{d}\sigma^V + \int_1 \mathrm{d}\sigma^{\mathrm{A}}$ can be integrated numerically over the m-parton phase space

$$\sigma^{\mathrm{NLO}} = \int_{m+1} \left[\lim_{\epsilon\to 0} \mathrm{d}\sigma^{\mathrm{R}} - \lim_{\epsilon\to 0} \mathrm{d}\sigma^{\mathrm{A}}\right] + \int_m \lim_{\epsilon\to 0} \left[\mathrm{d}\sigma^V + \int_1 \mathrm{d}\sigma^{\mathrm{A}}\right] \quad . \tag{3.6}$$

The fact that the singularities in the second integral of Eq. (3.6) cancel is not a property of all hadronic crossections. It is due to the fact that [6] only consider so called jet observables. These jet observables F_{J} are a function of the momenta $(p_i)_{i=1,\ldots,m}$ and have to fulfill the following properties:

- $F_{\mathrm{J}}^{(m+1)}(p_1, .., p_j = \lambda q, .., p_{m+1}) \to F_{\mathrm{J}}^{(m)}(p_1, ..., p_{m+1}) \quad \text{if} \quad \lambda \to 0$
- $F_{\mathrm{J}}^{(m+1)}(p_1, .., p_i, .., p_j, .., p_{m+1}) \to F_{\mathrm{J}}^{(m)}(p_1, .., p, .., p_{m+1}) \quad \text{if} \quad p_i \to zp \ , p_j \to (1-z)p$
- $F_{\mathrm{J}}^{(m)}(p_1, ..., p_m) \to 0 \quad \text{if} \quad p_i \cdot p_j \to 0$

These formal definitions imply that the jet observable F_{J} has the same value for a given m-parton configuration and all $m+1$-parton configurations which are kinematically degenerate with the m-parton configuration. A $m+1$-parton configuration is kinematically degenerate if it is obtained from a m-parton configuration by adding a soft or collinear parton, such that the final-state carries the same total momentum. For a generic Monte-Carlo generator it is necessary to have also a generic subtraction prescription, in the sense that it must be able to construct $\mathrm{d}\sigma^{\mathrm{A}}$ independent of the jet observable considered. This sums up the three main conditions $\mathrm{d}\sigma^{\mathrm{A}}$ must fulfill:

1. $\mathrm{d}\sigma^{\mathrm{A}}$ matches pointwise exactly the singularity structure of $\mathrm{d}\sigma^{\mathrm{R}}$,
2. $\mathrm{d}\sigma^{\mathrm{A}}$ is analytically integrable over the one parton subspace, that leads to soft and/or collinear divergencies,
3. $\mathrm{d}\sigma^{\mathrm{A}}$ is constructable independent of the jet observable considered.

For only QCD partons Reference [6] derived the so called dipole formula that fits the above conditions. This formula allows to write schematically

$$\mathrm{d}\sigma^{\mathrm{A}} = \sum_{\text{dipole}} \mathrm{d}\sigma^{\mathrm{B}} \otimes \mathrm{d}V_{\text{dipole}}, \tag{3.7}$$

where $\otimes$ denotes a proper phase space convolution in combination with sums over spins and colours and $\mathrm{d}\sigma^{\mathrm{B}}$ is the corresponding spin and colour projection of the squared Born matrix element. In $\sum_{\text{dipole}}$ it is summed up over all contributing emitter-spectator pairs, where the emitter can be any QCD-parton that emits the unresolved parton with respect to the LO process and the spectator can be any other QCD parton in the considered process. The so called dipole factors $\mathrm{d}V_{\text{dipole}}$ meet all the three above conditions. They are constructed in a process independent manner, such that they match pointwise exactly the singularities of $\mathrm{d}\sigma^{\mathrm{R}}$ and are integrable over the singularity-causing subspace. The number and form of dipole terms occuring depend on the different kinematic configurations of the $m+1$-parton phase space in relation to the m-parton phase space. Each of the $m+1$-parton configurations are obtained out of the m-parton configurations by the decay of one of the partons in the m-parton phase space into two partons. In this way, each of the kinematically degenerate configurations corresponds to one dipole factor in $\mathrm{d}\sigma^{\mathrm{A}}$ that approximates exactly this singularity. The existence of a mapping from the $m+1$-parton phase space to an m-parton phase space times a one-parton phase space,

$$\mathrm{d}\Phi_{m+1} \mapsto \mathrm{d}\Phi_m \times \mathrm{d}\Phi_1 \tag{3.8}$$

allows to derive the following identity by integrating Eq. (3.7)

$$\int_{m+1} \mathrm{d}\sigma^{\mathrm{A}} = \sum_{\text{dipole}} \int_m \mathrm{d}\sigma^{\mathrm{B}} \otimes \int_1 \mathrm{d}V_{\text{dipole}} = \int_m \left[\mathrm{d}\sigma^{\mathrm{B}} \otimes \mathbf{I}\right], \tag{3.9}$$

where $\mathbf{I} = \sum_{\mathbf{dipoles}} \int_{\mathbf{1}} \mathrm{d}\mathbf{V}_{\mathrm{dipole}}$. After the analytical one-parton subspace integration is performed, Eq. (3.9) relates the $m+1$-parton phase space to the m-parton phase space. Since the integral $\int_1 \mathrm{d}V_{\mathrm{dipole}}$ is performed over the singularity-causing one-parton subspace using dimensional-regularization, $\mathbf{I}$ contains all the ϵ-poles that cancel the poles from the virtual part $\mathrm{d}\sigma^{\mathrm{V}}$. In the case of no initial-state hadrons, this leads to the concluding schematical formula

$$\sigma^{\mathrm{NLO}} = \int_{m+1} \left[\left(\mathrm{d}\sigma^{\mathrm{R}}\right)_{\epsilon=0} - \left(\mathrm{d}\sigma^{\mathrm{A}}\right)_{\epsilon=0}\right] + \int_m \left[\mathrm{d}\sigma^{\mathrm{V}} + \mathrm{d}\sigma^{\mathrm{B}} \otimes \mathbf{I}\right]_{\epsilon=0}. \tag{3.10}$$

Hence, the two integrations over the $m+1$-parton phase space and the m-parton phase space can now be separately numerically performed. In addition to the real radiation and virtual matrix element appropriate colour and helicity projections of the Born matrix element are needed to implement the procedure for a given process.
In the case of initial-state hadrons the formalism has to be extended. Initial-state partons ruin the cancellation of collinear singularities. The left-over singularities have to be factorized and absorbed into the non-perturbative parton distribution functions for the incoming partons. The main difference to the case with no initial-state hadrons are additional singular regions where one of the final-state partons becomes collinear to the initial-state parton. Additional dipole terms $\mathrm{d}V'_{\mathrm{dipole}}$ subtract divergencies arising in these kinematical areas. Since the hadronic cross Section is the result of the convolution of the partonic cross-section with the non-perturbative parton distribution functions, the phase-space integration has to be performed while keeping the momentum of the initial-state parton fixed. This leads to an additional constraint to the auxiliary cross-section arising through the dipole terms $\mathrm{d}V'_{\mathrm{dipole}}$. They have to be fully analytically integrable over the one parton subspace from which the soft and collinear divergencies arise, even if the parton momentum is kept fixed. The auxiliary cross Section now reads

$$\mathrm{d}\sigma^{\mathrm{A}} = \sum_{\mathrm{dipole}} \mathrm{d}\sigma^{\mathrm{B}} \otimes \left(\mathrm{d}V_{\mathrm{dipole}} + \mathrm{d}V'_{\mathrm{dipole}}\right). \tag{3.11}$$

Using the phase space factorization and performing the analytical one-parton subspace integration the additional dipole terms $\mathrm{d}V'_{\mathrm{dipole}}$

$$\sum_{\mathrm{dipole}} \int_m \mathrm{d}\sigma^{\mathrm{B}} \otimes \int_1 \left(\mathrm{d}V_{\mathrm{dipole}} + \mathrm{d}V'_{\mathrm{dipole}}\right) = \int_m \left[\mathrm{d}\sigma^{\mathrm{B}} \otimes \mathbf{I}(\epsilon)\right] + \left[\mathrm{d}\sigma^{\mathrm{B}} \otimes (\mathbf{K}+\mathbf{P})\right], \tag{3.12}$$

lead to the so called **K**- and **P**-Operators. Both depend on the momentum fraction x carried by the colliding parton. The final subtraction formula is similar to Eq. (3.10)

$$\sigma^{\mathrm{NLO}} = \int_{m+1} \left[\left(\mathrm{d}\sigma^{\mathrm{R}}\right)_{\epsilon=0} - \left(\mathrm{d}\sigma^{\mathrm{A}}\right)_{\epsilon=0}\right] + \int_m \left[\mathrm{d}\sigma^{\mathrm{V}} + \mathrm{d}\sigma^{\mathrm{B}} \otimes \mathbf{I}\right]_{\epsilon=0}$$

$$+ \quad \int_0^1 dx \int_m \left[\mathrm{d}\sigma^{\mathrm{B}} \otimes (\mathbf{K} + \mathbf{P}) \right]_{\epsilon=0} . \tag{3.13}$$

All in all the dipole subtraction formalism is very well suited for a generic implementation. For a full calculation of cross-section at NLO, which intrinsically implies that one has already the real radiation contribution $\mathrm{d}\sigma^{\mathrm{R}}$ and the one-loop contribution $\mathrm{d}\sigma^{\mathrm{V}}$ at hand, one additionally needs the following ingredients in order to apply the dipole subtraction formalism:

1. the colour-projected squared Born matrix elements, summed over polarizations in d-dimensions and

2. in case of a gluon–gluon splitting, one additionally needs the projection of the Born matrix element according to the helicities of the gluon.

3.2 Factorization in singular regions

For the construction of the auxiliary cross-section $\mathrm{d}\sigma^{\mathrm{A}}$ that fulfills all the requirements stated above, it is necessary to study the behavior of a tree-level matrix element in the possible singular regions. By doing this, [6] represent the matrix element in the different singular areas by a sum of dipole terms leading to the dipole factorization formula. The starting point is a tree-level matrix element $\mathcal{M}_{m+1}$ with $m+1$ final-state QCD partons representing the real matrix element. Since the singularities arise form the denominators of propagators $1/(p_i+p_j)^2$, one finds that the squared matrix element $|\mathcal{M}_{m+1}|^2$ behaves in the *soft* region as $1/\lambda^2$ (if the soft region is parametrized as $p_j = \lambda q$, $\lambda \to 0$ with q as an arbitrary four-momentum) and in the *collinear* region as $1/p_i p_j$. The important observation is that the singular behavior of $|\mathcal{M}_{m+1}|^2$ is *universal*, i.e. independent of the detailed structure of the matrix element. The universality means that the $|\mathcal{M}_{m+1}|^2$ can be understood as constructed by the insertion of parton j onto all the possible external legs of the squared m-parton matrix element $|\mathcal{M}_m|^2$. The singular factor therefore only depends on the momenta and quantum numbers of the QCD partons in $|\mathcal{M}_m|^2$. This factorization property can schematically be written as

$$|\mathcal{M}_{m+1,a\ldots}|^2 \to |\mathcal{M}_{m,a\ldots}|^2 \otimes \boldsymbol{V}_{ij,k} \ , \tag{3.14}$$

where $\boldsymbol{V}_{ij,k}$ is the singular factor depending only on the partons i — the so called emitter —, j and k — the so called spectator.

3.2.1 Soft Limit

In this Section, we review the behavior of the squared matrix element $|\mathcal{M}_{m+1}|^2$ in the soft limit. The corresponding parametrization for a soft gluon j with momentum p_j given an arbitrary four vector q^μ and a scale factor λ is: $p_j = \lambda q, \quad \lambda \to 0$. The eikonal current for the emission of the soft gluon is given by

$$\boldsymbol{J}^\mu(q) = \sum_i \boldsymbol{T}_i \frac{p_i^\mu}{p_i \cdot q} + \boldsymbol{T}_a \frac{p_a^\mu}{p_a \cdot q} + \boldsymbol{T}_b \frac{p_b^\mu}{p_b \cdot q} \quad , \tag{3.15}$$

where the sum $\sum_i$ indicates a sum over final-state QCD partons and a and b label possible initial-state partons. In the given soft limit the squared matrix element behaves as

$$|\mathcal{M}_{m+1;a,b}|^2 \to -\frac{1}{\lambda^2}\, 4\pi\mu^{2\epsilon}\alpha_s \ \left[\mathcal{M}^*_{m;a,b}\, [\boldsymbol{J}^\mu(q)]^\dagger\, \boldsymbol{J}_\mu(q) \mathcal{M}_{m;a,b}\right] \tag{3.16}$$

The matrix element $|\mathcal{M}_{m;a,b}|^2$ and its corresponding vector in colour and helicity space $|..., i-1, i+1, ...; a, b\rangle_{m,a,b}$ is created out of $|\mathcal{M}_{m+1;a,b}|^2$ and accordingly out of the vector $|..., i-1, i, i+1, ...; a, b\rangle_{m+1,a,b}$ by removing parton i. It is important to note that the factorization is not exact in the sense of left over colour and helicity correlations. Evaluating $[\boldsymbol{J}^\mu(q)]^\dagger\, \boldsymbol{J}_\mu(q)$ while supposing massless particles leads to

$$\begin{aligned} [\boldsymbol{J}^\mu(q)]^\dagger\, \boldsymbol{J}_\mu(q) \quad &= \quad \sum_{k,i} \boldsymbol{T}_k \cdot \boldsymbol{T}_i \, \frac{p_k p_i}{(p_k q)(p_i q)} + 2 \left(\sum_i \boldsymbol{T}_a \cdot \boldsymbol{T}_i \, \frac{p_a p_i}{(p_a q)(p_i q)} \right. \\ &+ \quad \left. \sum_i \boldsymbol{T}_b \cdot \boldsymbol{T}_i \, \frac{p_b p_i}{(p_b q)(p_i q)} + \boldsymbol{T}_a \cdot \boldsymbol{T}_b \, \frac{p_a p_b}{(p_a q)(p_b q)} \right) \quad . \end{aligned} \tag{3.17}$$

Partional fractioning of the term

$$\frac{p_k p_i}{(p_k q)(p_i q)} = \frac{p_k p_i}{p_k \cdot q \ (p_i + p_k) \cdot q} + \frac{p_k p_i}{p_i \cdot q \ (p_i + p_k) \cdot q} \tag{3.18}$$

allows to disentangle the collinear singularities that occur when the momentum q is collinear to p_i, p_k, p_a or p_b. Using the identity

$$\frac{p_k p_i}{(p_k q)(p_i q)} = \frac{1}{p_i q}\left[\frac{p_k p_i}{(p_i + p_k) q}\right] + \frac{1}{p_k q}\left[\frac{p_k p_i}{(p_k + p_i) q}\right], \tag{3.19}$$

Eq. (3.16) can be rewritten as

$$|\mathcal{M}_{m+1;a,b}|^2 \to -\frac{1}{\lambda^2}\, 8\pi\mu^{2\epsilon}\alpha_s \cdot \sum_i \frac{1}{p_i q} \sum_{k \neq i} \left[\mathcal{M}^*_{m;a,b} \frac{\boldsymbol{T}_k \cdot \boldsymbol{T}_i \, p_k p_i}{(p_i + p_k) q} \mathcal{M}_{m;a,b}\right]$$

where terms involving initial-state partons a and b are left out. The dipole terms $\boldsymbol{V}_{ij,k}$ to be constructed will mimic exactly this behaviour

$$\boldsymbol{V}_{ij,k} \propto \frac{p_k p_i}{(p_i + p_k) p_j} \tag{3.20}$$

in the soft limit.

3.2.2 Collinear Limit

In the collinear region one has to distinguish between two possible cases. Two final-state particles can become parallel to each other or a final-state to an initial-state particle. The behavior of the matrix element is similar, but the parametrization of the two parallel momenta with respect to the collinear direction and the corresponding phase-space factorization is different. Given a lightlike vector p^μ specifying the collinear direction and an auxiliary lightlike vector n^μ determining the transverse component ${k_\perp}^\mu$ the collinearity of two final-state momenta p_i and p_j can be parametrized according to [6] as

$$\begin{aligned} p_i^\mu &= zp^\mu + k_\perp^\mu - \frac{k_\perp^2}{z}\frac{n^\mu}{2pn} \ , \\ p_j^\mu &= (1-z)p^\mu - k_\perp^\mu - \frac{k_\perp^2}{1-z}\frac{n^\mu}{2pn} \ . \end{aligned} \tag{3.21}$$

In the collinear limit of $k_\perp \to 0$ the matrix element behaves as

$$|\mathcal{M}_{m+1;a,b}|^2 \to -\frac{1}{\lambda^2}\frac{1}{p_i p_j}\, 4\pi\mu^{2\epsilon}\alpha_s \, \left[\mathcal{M}^*_{m;a,b}\, \hat{P}_{(ij),i}(z;\epsilon)\, \mathcal{M}_{m;a,b}\right] \tag{3.22}$$

In order to obtain the m-parton matrix element, parton j is emitted and the momentum of parton i is replaced by the momentum of parton $\tilde{ij}$. $\hat{P}_{(ij),i}(z,k_\perp;\epsilon)$ are the d-dimensional Altarelli-Parisi splitting functions that depend on the momentum fraction z, $k_\perp$, the dimension d and the helicity of the splitting particle, which comes only into play if a gluon is splitting into a parton pair. The case of a final-state momentum p_i becoming collinear to an initial-state momentum p_{ai}, yielding the splitting $a \to ai+i$, can be parametrized as

$$\begin{aligned} p_i^\mu &= (1-x)p_a^\mu + k_\perp^\mu - \frac{k_\perp^2}{1-x}\frac{n^\mu}{2p_a n} \ , \\ 2p_i p_a &= -\frac{k_\perp^2}{1-x} \ , \qquad k_\perp \to 0 \ . \end{aligned} \tag{3.23}$$

The collinear limit in this case is roughly the same as in Eq. (3.22) except for an additional factor of $1/x$ on the right hand side of the equation and the initial-state parton p_{ai} carrying the momentum xp_a.

3.3 Dipole Subtraction Terms

The differential auxiliary cross Section $\mathrm{d}\sigma^{\mathrm{A}}$ which is subtracted from the differential real cross Section as in Eq. (3.13) is in the most general case, i.e. two initial-state hadrons given by

$$\mathrm{d}\sigma^{\mathrm{A}}_{ab} = \mathcal{N}_{in}\frac{1}{n_s(a)n_s(b)\Phi(p_a p_b)}\sum_{\{m+1\}}\mathrm{d}\phi_{m+1}(p_1,...,p_{m+1};p_a+p_b+Q)\frac{1}{S_{\{m+1\}}}$$

DipoleTerm	Emitter	Spectator
$\mathcal{D}_{ij,k}$	FS	FS
$\mathcal{D}^{a}_{ij}$	FS	IS
$\mathcal{D}^{ai}_{k}$	IS	FS
$\mathcal{D}^{ai,b}$	IS	IS

Table 3.1: Four cases of Dipole Subtraction Terms

$$
\begin{aligned}
\cdot \quad & \Bigg\{ \sum_{\substack{\text{pairs}\\ i,j}} \sum_{k\neq i,j} \mathcal{D}_{ij,k}(\{p\})\; F_{\mathrm{J}}^{(m)}(\{\widetilde{p}\}) \\
+ \quad & \sum_{\substack{\text{pairs}\\ i,j}} \Big[\mathcal{D}^{a}_{ij}(\{p\})\; F_{\mathrm{J}}^{(m)}(\{\widetilde{p}\}) + (a \leftrightarrow b) \Big] \\
+ \quad & \sum_{i} \sum_{k\neq i} \Big[\mathcal{D}^{ai}_{k}(\{p\})\; F_{\mathrm{J}}^{(m)}(\{\widetilde{p}\}) + (a \leftrightarrow b) \Big] \\
+ \quad & \sum_{i} \Big[\mathcal{D}^{ai,b}(\{p\})\; F_{\mathrm{J}}^{(m)}(\{\widetilde{p}\}) + (a \leftrightarrow b) \Big] \Bigg\} \;, \qquad (3.24)
\end{aligned}
$$

where $\{p\}$ denotes the set of momenta $\{p_1, ..., p_{m+1}; p_a, p_b\}$ of the the $m+1$-parton phase space and $\{\widetilde{p}\}$ stands for the mapped momenta in the specific emitter-spectator case. In this formula, $\frac{1}{n_s(a)n_s(b)}$ accounts for the average of initial-state polarizations, $\Phi(p_a p_b)$ denotes the flux factor and $\mathcal{N}_{in}$ includes all non QCD factors. The sum $\sum_{\substack{\text{pairs}\\ i,j}}$ stands for the combination of all possible emitter pairs ($\widetilde{ij} \to i+j$), whereas the indices k and i in the sums $\sum_k$ and $\sum_i$ denote summation over final-state particles. The F_{J} are jet functions with the properties defined in Chapter 3 requiring additionally that both intial-state partons p_a and p_b fulfill the factorizability condition of collinear initial-state singularities. The dipole terms $\mathcal{D}_{ij,k}$, $\mathcal{D}^{a}_{ij}$, $\mathcal{D}^{ai}_{k}$ and $\mathcal{D}^{ai,b}$ correspond each to one of the four possible emitter-spectator cases that can occur.

The dipole subtraction terms in all four cases are schematically the product of the singular propagator and a colour- and helicity-correlated Born matrix element multiplied with a splitting function $\mathbf{V}$

$$
\begin{aligned}
&\mathcal{D}_{ij,k}(p_1, \ldots, p_{m+1}) = \\
&\quad -\frac{1}{(p_i + p_j)^2 - m_{ij}^2} \;\otimes {}_m\langle \ldots, \widetilde{ij}, \ldots, \tilde{k}, \ldots | \mathbf{V} | \ldots, \widetilde{ij}, \ldots, \tilde{k}, \ldots \rangle_m \;, \qquad (3.25)
\end{aligned}
$$

where in the presence of massless particles only the propagator simplifies to $1/2p_ip_j$. The m-parton Born matrix element on the right hand side of the equation denoted with ${}_m\langle | \cdots | \rangle_m$ is obtained from the real correction $m+1$-parton matrix element by replacing the partons i and j by the emitter-parton $\widetilde{ij}$ and the spectator k by a mapped

spectator $\tilde{k}$. The mapping from the partons $\{i, j, k\}$ to the partons $\{\tilde{ij}, \tilde{k}\}$ must fulfill the following requirements:

- spectator parton $\tilde{k}$ has the same quantum numbers as parton k
- emitter parton $\tilde{ij}$ has quantum numbers according to the collinear splitting $\tilde{ij} \to i + j$
- momentum conservation: $p_i + p_j + p_k = \widetilde{p}_{ij} + \widetilde{p}_k$

3.3.1 Notation

In this Section we explain in detail the notation for the dipole subtraction formalism. In general we follow the notation of [6]. The letters a and b label initial-state particles and i,j and k label final-state particles. Massless quarks are labelled with small letters q and massive quarks with capital letters Q. In the two cases of a final-state singularity (final-state emitter) the $\{i, j, k\}$ and $\{i, j, a\}$ respectively label each the corresponding particles, i.e. $\tilde{ij}$ labels the emitter parton, emitting i and j, and $k(a)$ denote the spectator partons as figures 3.1 and 3.2 show.

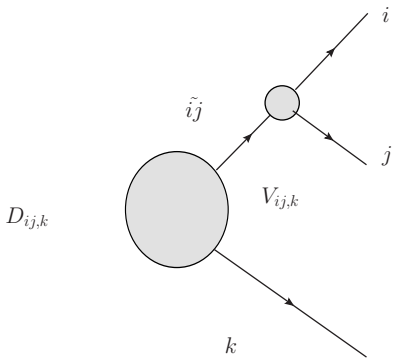

Figure 3.1: Notation: $D_{ij,k}$

In the case of an initial-state singularity (initial-state emitter) and the spectator in either the final state or the initial state the notation according to [6] differs a bit. For example in D_k^{ai} a is the original emitting particle, which emits parton i that goes into the final state and parton $\tilde{ai}$ that contributes to the hard scattering process, as figures 3.3 and 3.4 show.

For the integrated subtraction terms we stick to the notation of origin of the corresponding term. This leads to two notations, e.g. $\mathcal{V}^{q,qg}$ and I_{gg}^{a}. Their notation is straightforward, i.e. $\mathcal{V}^{q,qg}$ denotes the integrated splitting term, which corresponds to the initial-state splitting of a quark q into the parton q, which contributes to the hard scattering process, and a final-state gluon g. I_{gg}^{q} stands for the integrated subtraction

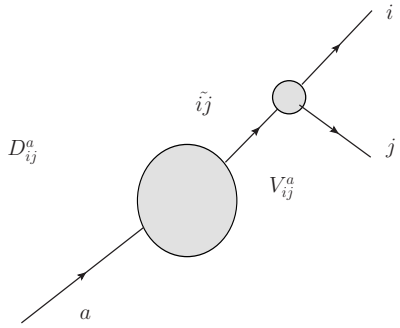

Figure 3.2: Notation: D^a_{ij}

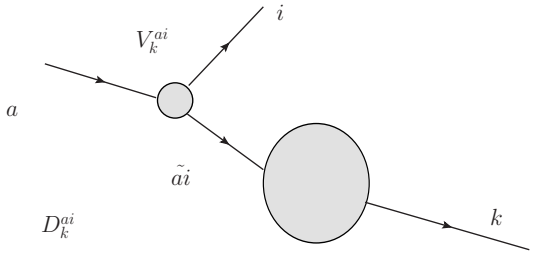

Figure 3.3: Notation: D^{ai}_k

term corresponding to a final-state gluon-gluon splitting with an initial-state spectator a. In the following we also denote with C_A and C_F the Casimir operators of the adjoint and fundamental representation respectively. N_f is the number of quark flavours and T_R denotes the norm of the trace of the colour matrices, i.e. $\mathrm{Tr}[t^a t^b] = T_\mathrm{R}\delta^{ab}$.

3.3.2 Phase Space Restriction

In [23], an additional parameter $\alpha \in (0, 1]$ was introduced to optimize numerical integration. The auxiliary cross Section becomes dependent on the new parameter. Since it is sufficient for the numerical subtraction to evaluate the dipole subtraction terms only around singular regions, the α parameter is intended to restrict the phase space region of dipole subtraction term evaluations. The new auxiliary cross Section $\mathrm{d}\sigma^\mathrm{A}_{ab}$ now reads as

$$\begin{aligned}\mathrm{d}\sigma^\mathrm{A}_{ab} \;=\; & \mathcal{N}_{in}\frac{1}{n_s(a)n_s(b)\Phi(p_a p_b)}\sum_{\{m+1\}}\mathrm{d}\phi_{m+1}(p_1,...,p_{m+1};p_a+p_b+Q)\frac{1}{S_{\{m+1\}}} \\ & \cdot\;\left\{\sum_{\substack{\text{pairs}\\ i,j}}\sum_{k\neq i,j}\mathcal{D}_{ij,k}(\{p\})\;F^{(m)}_\mathrm{J}(\{\widetilde{p}\})\Theta(\alpha-y_{ij,k})\right.\end{aligned}$$

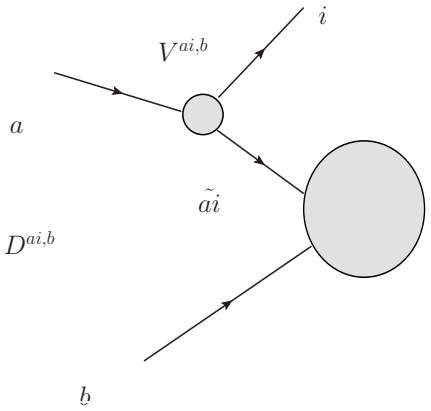

Figure 3.4: Notation: $D^{ai,b}$

$$
\begin{aligned}
&+ \sum_{\substack{\text{pairs}\\ i,j}} \Big[\mathcal{D}^{a}_{ij}(\{p\})\; F^{(m)}_{\mathrm{J}}(\{\widetilde{p}\}) + (a \leftrightarrow b)\Big]\,\Theta(\alpha - 1 + x_{ij,a}) \\
&+ \sum_{i} \sum_{k\neq i} \Big[\mathcal{D}^{ai}_{k}(\{p\})\; F^{(m)}_{\mathrm{J}}(\{\widetilde{p}\}) + (a \leftrightarrow b)\Big]\,\Theta(\alpha - u_i) \\
&+ \sum_{i} \Big[\mathcal{D}^{ai,b}(\{p\})\; F^{(m)}_{\mathrm{J}}(\{\widetilde{p}\}) + (a \leftrightarrow b)\Big]\,\Theta(\alpha - \tilde{v}_i)\Bigg\}\;. \qquad (3.26)
\end{aligned}
$$

By setting $\alpha = 1$, one gets the α-independent $\mathrm{d}\sigma^{\mathrm{A}}$ of Eq. (3.24) and all subtraction terms are evaluated. One big advantage of $\alpha \neq 0$ is saving CPU time, because evaluating a large number of partly complicated dipole subtraction terms is rather time consuming. Taking α-dependent integrated subtraction terms into account, the sum in Eq. (3.13) is still independent of α. Therefore, consistency checks of the calculation can be performed by varying α.

The following Sections based on [6], provide an overview over the different mappings and splitting functions in each of the four cases.

3.3.3 Spectator: final-state - Emitter: final-state

The contribution $\mathcal{D}_{ij,k}$ accounts for final-state singularities with a final-state spectator. The general structure is

$$
\begin{aligned}
\mathcal{D}_{ij,k}(p_1,\dots,p_{m+1}) &= -\frac{1}{(p_i+p_j)^2 - m^2_{ij}} \\
&\times {}_m\langle \dots, \widetilde{ij}, \dots, \tilde{k}, \dots | \frac{\boldsymbol{T}_k \cdot \boldsymbol{T}_{ij}}{\boldsymbol{T}^2_{ij}} \mathbf{V}_{ij,k} | \dots, \widetilde{ij}, \dots, \tilde{k}, \dots \rangle_m . \qquad (3.27)
\end{aligned}
$$

where $\mathbf{V}_{ij,k}$ can contain implicit helicity correlations with the reduced matrix element. In the massless case, the singular propagator simplifies to $1/2p_ip_j$. All possible splittings

Nr.	Case	DipoleTerm	IntDipole
1	$q \to g + q$	$\boldsymbol{V}_{q_i g_j, k}$	$\mathcal{V}_{gq}$
2	$g \to g + g$	$\boldsymbol{V}_{g_i g_j, k}$	$\mathcal{V}_{gg}$
3	$g \to q + \bar{q}$	$\boldsymbol{V}_{q_i \bar{q}_j, k}$	$\mathcal{V}_{q\bar{q}}$

Table 3.2: FS Emitter - FS Spectator

with their corresponding dipole term names are listed in the table 3.2.

3.3.3.1 Massless

The dimensionless kinematical variables needed in this case are $y_{ij,k}$ and $\tilde{z}_i, \tilde{z}_j$, which are defined by

$$y_{ij,k} = \frac{p_i p_j}{p_i p_j + p_j p_k + p_k p_i} \tag{3.28}$$

and

$$\tilde{z}_i = \frac{p_i p_k}{p_j p_k + p_i p_k}, \quad \tilde{z}_j = 1 - \tilde{z}_i \ . \tag{3.29}$$

The mapping in the final-state emitter and a final-state spectator case is given by

$$\begin{aligned} \widetilde{p}_k^{\mu} &= \frac{1}{1 - y_{ij,k}} \, p_k^{\mu} \ , \\ \widetilde{p}_{ij}^{\mu} &= p_i^{\mu} + p_j^{\mu} - \frac{y_{ij,k}}{1 - y_{ij,k}} \, p_k^{\mu} \ . \end{aligned} \tag{3.30}$$

This mapping ensures momentum conservation and keeps both the emitter ($\widetilde{p}_{ij}$) and the spectator ($\widetilde{p}_k$) on-shell ($\widetilde{p}_{ij}^2 = \widetilde{p}_k^2 = 0$). For a quark splitting into a quark-gluon pair ($q \to q + g$), the splitting function $\mathbf{V}_{q_i g_j, k}$ is given in [6] as

$$\boldsymbol{V}_{q_i g_j, k}(\tilde{z}_i; y_{ij,k}) = 8\pi\mu^{2\epsilon}\alpha_s \, C_F \left[\frac{2}{1 - \tilde{z}_i(1 - y_{ij,k})} - (1 + \tilde{z}_i) - \epsilon(1 - \tilde{z}_i) \right] . \tag{3.31}$$

In case of a gluon splitting into a quark-anti-quark pair ($g \to q + \bar{q}$) or into a gluon-gluon pair ($g \to g + g$), the splitting functions $V^{\mu\nu}_{q_i \bar{q}_j, k}$ and $V^{\mu\nu}_{g_i g_j, k}$ respectively acquire a spin correlation to the emitting gluon ($\tilde{ij}$) via the spin indices μ and ν, yielding

$$\boldsymbol{V}^{\mu\nu}_{q_i \bar{q}_j, k} = 8\pi\mu^{2\epsilon}\alpha_s \, T_R \left[-g^{\mu\nu} - \frac{2}{p_i p_j} \left(\tilde{z}_i p_i^{\mu} - \tilde{z}_j p_j^{\mu} \right) \left(\tilde{z}_i p_i^{\nu} - \tilde{z}_j p_j^{\nu} \right) \right] , \tag{3.32}$$

$$\begin{aligned} \boldsymbol{V}^{\mu\nu}_{g_i g_j, k} &= 16\pi\mu^{2\epsilon}\alpha_s \, C_A \left[-g^{\mu\nu} \left(\frac{1}{1 - \tilde{z}_i(1 - y_{ij,k})} + \frac{1}{1 - \tilde{z}_j(1 - y_{ij,k})} - 2 \right) \right. \\ &+ \left. (1 - \epsilon) \frac{1}{p_i p_j} \left(\tilde{z}_i p_i^{\mu} - \tilde{z}_j p_j^{\mu} \right) \left(\tilde{z}_i p_i^{\nu} - \tilde{z}_j p_j^{\nu} \right) \right] . \end{aligned} \tag{3.33}$$

3.3.3.2 Massive

The massive case is treated in [22]. The mappings have to obey the mass-shell conditions

$$\widetilde{p}_{ij}^2 = m_{ij}^2, \quad \widetilde{p}_k^2 = m_k^2. \tag{3.34}$$

By introducing

$$Q^\mu = \widetilde{p}_{ij}^\mu + \widetilde{p}_k^\mu, \tag{3.35}$$

one can define rescaled parton masses

$$\mu_n = \frac{m_n}{\sqrt{Q^2}}. \tag{3.36}$$

The mapping in the massive final-state emitter and final-state spectator case is defined by

$$\begin{aligned}
\widetilde{p}_k^\mu &= \frac{\sqrt{\lambda(Q^2, m_{ij}^2, m_k^2)}}{\sqrt{\lambda(Q^2, (p_i+p_j)^2, m_k^2)}} \left(p_k^\mu - \frac{Qp_k}{Q^2} Q^\mu \right) + \frac{Q^2 + m_k^2 - m_{ij}^2}{2Q^2} Q^\mu \,, \\
\widetilde{p}_{ij}^\mu &= Q^\mu - \widetilde{p}_k^\mu \,.
\end{aligned} \tag{3.37}$$

The relative velocity of the two momenta p and q

$$v_{p,q} = \frac{\sqrt{\lambda((p+q)^2, p^2, q^2)}}{(p+q)^2 - p^2 - q^2} \tag{3.38}$$

leading to

$$\begin{aligned}
v_{ij,k} &= \frac{\sqrt{[2\mu_k^2 + (1-\mu_i^2-\mu_j^2-\mu_k^2)(1-y_{ij,k})]^2 - 4\mu_k^2}}{(1-\mu_i^2-\mu_j^2-\mu_k^2)(1-y_{ij,k})}, \\
v_{ij,i} &= \frac{\sqrt{(1-\mu_i^2-\mu_j^2-\mu_k^2)^2 y_{ij,k}^2 - 4\mu_i^2\mu_j^2}}{(1-\mu_i^2-\mu_j^2-\mu_k^2) y_{ij,k} + 2\mu_i^2}
\end{aligned} \tag{3.39}$$

and the additional kinematical variables defined in the following are needed to compute the splitting functions in this Chapter

$$\begin{aligned}
y_- &= \frac{2\mu_i\mu_j}{1-\mu_i^2-\mu_j^2-\mu_k^2} \,, \qquad y_+ = 1 - \frac{2\mu_k(1-\mu_k)}{1-\mu_i^2-\mu_j^2-\mu_k^2} \,, \\
z_\pm(y_{ij,k}) &= \frac{2\mu_i^2 + (1-\mu_i^2-\mu_j^2-\mu_k^2) y_{ij,k}}{2[\mu_i^2+\mu_j^2+(1-\mu_i^2-\mu_j^2-\mu_k^2) y_{ij,k}]} (1 \pm v_{ij,i} v_{ij,k}) \,,
\end{aligned} \tag{3.40}$$

$$\tilde{z}_i^{(m)} = \tilde{z}_i - \frac{1}{2}(1 - v_{ij,k}) \,, \quad \tilde{z}_j^{(m)} = \tilde{z}_j - \frac{1}{2}(1 - v_{ij,k}) \,. \tag{3.41}$$

The splitting function $\mathcal{V}_{gQ,k}$ of a quark with mass m_Q splitting into a massless gluon g_i and a massive quark with m_Q reads

$$\mathbf{V}_{gQ,k} = 8\pi\mu^{2\varepsilon}\alpha_{\mathrm{s}}C_{\mathrm{F}}\left\{\frac{2}{1-\tilde{z}_j(1-y_{ij,k})} - \frac{\tilde{v}_{ij,k}}{v_{ij,k}}\left[1+\tilde{z}_j+\frac{m_Q^2}{p_ip_j}+\varepsilon(1-\tilde{z}_j)\right]\right\}. \quad (3.42)$$

The massive splitting functions for a gluon emitting a quark-antiquark pair $\mathbf{V}_{Q\bar{Q},k}$ or a gluon pair $\mathbf{V}_{gg,k}$ both acquire the helicity indices of the emitting gluon

$$\begin{aligned}\mathbf{V}^{\mu,\nu}_{Q\bar{Q},k} &= 8\pi\mu^{2\varepsilon}\alpha_{\mathrm{s}}T_{\mathrm{R}}\frac{1}{v_{ij,k}}\left\{-g^{\mu\nu}\left[1-\frac{2\kappa}{1-\varepsilon}\left(z_+z_- - \frac{m_Q^2}{(p_i+p_j)^2}\right)\right]\right.\\ &\quad - \frac{4}{(p_i+p_j)^2}\left[\tilde{z}_i^{(m)}p_i^\mu - \tilde{z}_j^{(m)}p_j^\mu\right]\\ &\quad \left.\cdot\left[\tilde{z}_i^{(m)}p_i^\nu - \tilde{z}_j^{(m)}p_j^\nu\right]\right\}, \quad (3.43)\\ \mathbf{V}^{\mu,\nu}_{gg,k} &= 16\pi\mu^{2\varepsilon}\alpha_{\mathrm{s}}C_{\mathrm{A}}\left\{-g^{\mu\nu}\left[\frac{1}{1-\tilde{z}_i(1-y_{ij,k})}+\frac{1}{1-\tilde{z}_j(1-y_{ij,k})}\right.\right.\\ &\quad - \left.\frac{2-\kappa z_+z_-}{v_{ij,k}}\right] + \frac{1}{v_{ij,k}}\frac{1-\varepsilon}{p_ip_j}\left[\tilde{z}_i^{(m)}p_i^\mu - \tilde{z}_j^{(m)}p_j^\mu\right]\\ &\quad \times \left.\left[\tilde{z}_i^{(m)}p_i^\nu - \tilde{z}_j^{(m)}p_j^\nu\right]\right\}. \quad (3.44)\end{aligned}$$

The parameter κ can be chosen arbitrarily since it just redistributes regular terms between the auxiliary cross Section $\mathrm{d}\sigma^{\mathrm{A}}$ and the integrated subtraction terms $\int_1 \mathrm{d}\sigma^{\mathrm{A}}$. Simplifying choices are $\kappa = \frac{2}{3}$ or $\kappa = 0$.

3.3.4 Spectator: initial-state - Emitter: final-state

The subtraction term $\mathcal{D}_j^{ai}$ is closely related to Eq. (3.27) except for the additional factor of $\frac{1}{x_{ij,a}}$ due to the initial-state spectator

$$\begin{aligned}&\mathcal{D}_j^{ai}(p_1,\dots,p_{m+1};p_a,\dots) =\\ &\quad -\frac{1}{2p_ap_i}\,\frac{1}{x_{ij,a}}\;{}_{m,\widetilde{ai}}\langle\dots,\tilde{j},\dots;\widetilde{ai},\dots|\frac{\boldsymbol{T}_j\cdot\boldsymbol{T}_{ai}}{\boldsymbol{T}_{ai}^2}\mathbf{V}_j^{ai}|\dots,\tilde{j},\dots;\widetilde{ai},\dots\rangle_{m,\widetilde{ai}}. \quad (3.45)\end{aligned}$$

The denotation of the splittings and their corresponding dipole subtraction terms is shown in table 3.3.

3.3.4.1 Massless

In the mapping from the $m+1$- into the m-parton phase space, the momentum conservation is ensured by the momentum of an initial-state spectator. With the kinematical variable

$$x_{ij,a} = \frac{p_ip_a + p_jp_a - p_ip_j}{(p_i+p_j)p_a} \quad (3.46)$$

Nr.	Case	DipoleTerm	IntDipole
11	$q \to g + q$	$\boldsymbol{V}^a_{q_i g_j}$	I^a_{qg}
12	$g \to g + g$	$\boldsymbol{V}^a_{g_i g_j}$	I^a_{gg}
13	$g \to q + \bar{q}$	$\boldsymbol{V}^a_{q_i \bar{q}_j}$	$I^a_{q\bar{q}}$

Table 3.3: FS Emitter - IS Spectator

and the redefined $\tilde{z}_i$ and $\tilde{z}_j$

$$\tilde{z}_i = \frac{p_i p_a}{p_i p_a + p_j p_a} \,, \quad \tilde{z}_j = \frac{p_j p_a}{p_j p_a + p_i p_a} = 1 - \tilde{z}_i \,, \tag{3.47}$$

the mapping can be defined as

$$\widetilde{p}^{\mu}_a = x_{ij,a}\, p^{\mu}_a \,, \quad \widetilde{p}^{\mu}_{ij} = p^{\mu}_i + p^{\mu}_j - (1 - x_{ij,a})\, p^{\mu}_a \,, \tag{3.48}$$

where p_a is the momentum of the initial-state spectator. Three splittings are possible

1. $q \to q_i + g_j$
2. $g \to g_i + g_j$
3. $g \to q_i + \bar{q}_j$.

The corresponding splitting function in case 1 is

$$\begin{aligned} \boldsymbol{V}^a_{q_i g_j}(\tilde{z}_i; x_{ij,a}) &= 8\pi\mu^{2\epsilon}\alpha_s\, C_F \left[\frac{2}{1 - \tilde{z}_i + (1 - x_{ij,a})}\right. \\ &- \left. (1 + \tilde{z}_i) - \epsilon(1 - \tilde{z}_i)\right]. \end{aligned} \tag{3.49}$$

In case 2 and case 3 the dipole splitting functions read

$$\begin{aligned} \left(\boldsymbol{V}^a_{g_i g_j}\right)^{\mu,\nu}(\tilde{z}_i; x_{ij,a}) &= 16\pi\mu^{2\epsilon}\alpha_s\, C_A \left[-g^{\mu\nu}\left(\frac{1}{1 - \tilde{z}_i + (1 - x_{ij,a})}\right.\right. \\ &+ \left.\frac{1}{1 - \tilde{z}_j + (1 - x_{ij,a})} - 2\right) \\ &+ \left.(1 - \epsilon)\frac{1}{p_i p_j}\left(\tilde{z}_i p^{\mu}_i - \tilde{z}_j p^{\mu}_j\right)\left(\tilde{z}_i p^{\nu}_i - \tilde{z}_j p^{\nu}_j\right)\right] \,, \end{aligned} \tag{3.50}$$

and

$$\left(\boldsymbol{V}^a_{q_i \bar{q}_j}\right)^{\mu,\nu}(\tilde{z}_i) = 8\pi\mu^{2\epsilon}\alpha_s\, T_R \left[-g^{\mu\nu} - \frac{2}{p_i p_j}\left(\tilde{z}_i p^{\mu}_i - \tilde{z}_j p^{\mu}_j\right)\left(\tilde{z}_i p^{\nu}_i - \tilde{z}_j p^{\nu}_j\right)\right]. \tag{3.51}$$

3.3.4.2 Massive

The final-state momenta p_i and p_j can have arbitrary masses m_i and m_j, but the initial-state momentum p_a is supposed to be massless. The total transferred momentum Q is given by $Q^\mu = p_i^\mu + p_j^\mu - p_a^\mu$. Auxiliary kinematical variables needed in this Section are defined in the following

$$\begin{aligned} x_{ij,a} &= \frac{p_a p_i + p_a p_j - p_i p_j + \frac{1}{2}(m_{ij}^2 - m_i^2 - m_j^2)}{p_a p_i + p_a p_j}, \\ \tilde{z}_i &= \frac{p_a p_i}{p_a p_i + p_a p_j}, \qquad \tilde{z}_j = \frac{p_a p_j}{p_a p_i + p_a p_j}, \\ x_+ &= 1 + \mu_{ij}^2 - (\mu_i + \mu_j)^2, \\ z_\pm(x) &= \frac{1 - x + \mu_{ij}^2 + \mu_i^2 - \mu_j^2 \pm \sqrt{(1 - x + \mu_{ij}^2 - \mu_i^2 - \mu_j^2)^2 - 4\mu_i^2\mu_j^2}}{2(1 - x + \mu_{ij}^2)}. \end{aligned} \tag{3.52}$$

With the mapping

$$\widetilde{p}_a^\mu = x_{ij,a}\, p_a^\mu \,, \quad \widetilde{p}_{ij}^\mu = p_i^\mu + p_j^\mu - (1 - x_{ij,a})\, p_a^\mu \,, \tag{3.53}$$

the rescaled parton masses now read

$$\mu_n = \frac{m_n}{\sqrt{2\widetilde{p}_{ij} p_a}}. \tag{3.54}$$

The dipole splitting function $\mathbf{V}_{gQ}^a$ for the splitting $Q \to g_i + Q_j$ is given in [22] as

$$\mathbf{V}_{gQ}^a = 8\pi\mu^{2\varepsilon}\alpha_\mathrm{s} C_\mathrm{F} \left\{ \frac{2}{2 - x_{ij,a} - \tilde{z}_j} - 1 - \tilde{z}_j - \frac{m_Q^2}{p_i p_j} - \varepsilon(1 - \tilde{z}_j) \right\}. \tag{3.55}$$

Since we have no massive initial-state partons the splitting $g \to g + g$ is already covered by Eq. (3.51). The only splitting left is $g \to Q_i + \bar{Q}_j$ with the helicity dependent dipole term

$$\left(\mathbf{V}_{Q\bar{Q}}^a\right)^{\mu,\nu} = 8\pi\mu^{2\varepsilon}\alpha_\mathrm{s} T_\mathrm{R} \left\{ -g^{\mu\nu} - \frac{4}{(p_i + p_j)^2} \left[\tilde{z}_i p_i^\mu - \tilde{z}_j p_j^\mu\right] \left[\tilde{z}_i p_i^\nu - \tilde{z}_j p_j^\nu\right] \right\}. \tag{3.56}$$

3.3.5 Spectator: final-state - Emitter: initial-state

Since we consider only massless particles in the initial-state, the structure of the dipole subtraction terms simplifies to

$$\begin{aligned} &\mathcal{D}_j^{ai}(p_1, \dots, p_{m+1}; p_a, \dots) = \\ &\quad -\frac{1}{2p_a p_i} \frac{1}{x_{ij,a}} \, {}_{m,\widetilde{ai}}\langle \dots, \tilde{j}, \dots; \widetilde{ai}, \dots | \frac{\boldsymbol{T}_j \cdot \boldsymbol{T}_{ai}}{\boldsymbol{T}_{ai}^2} \mathbf{V}_j^{ai} | \dots, \tilde{j}, \dots; \widetilde{ai}, \dots \rangle_{m,\widetilde{ai}} \,. \end{aligned} \tag{3.57}$$

With a labeling the parton that emits the final state parton i and the parton that contributes to the hard scattering process , one gets the following splittings and denoted dipole terms:

Nr.	Case	DipoleTerm	IntDipole
21	$\bar{q}_a \to \bar{q} + g_i$	$\boldsymbol{V}_k^{q_a g_i}$	$\mathcal{V}^{q,qg}$
22	$\bar{q}_a \to g + \bar{q}_i$	$\boldsymbol{V}_k^{q_a q_i}$	$\mathcal{V}^{g,gq}$
24	$g_a \to q + \bar{q}_i$	$\boldsymbol{V}_k^{g_a q_i}$	$\mathcal{V}^{q,gq}$
25	$g_a \to g + g_i$	$\boldsymbol{V}_k^{q_a g_i}$	$\mathcal{V}^{g,gg}$

Table 3.4: IS Emitter - FS Spectator

3.3.5.1 Massless

The kinematical variables for the calculation of the mapping and dipole functions are

$$x_{ik,a} = \frac{p_k p_a + p_i p_a - p_i p_k}{(p_k + p_i) p_a}$$

and

$$u_i = \frac{p_i p_a}{p_i p_a + p_k p_a} \quad . \tag{3.58}$$

The mapping is defined by

$$\widetilde{p}_{ai}^{\mu} = x_{ik,a}\, p_a^{\mu} \ , \tag{3.59}$$

$$\widetilde{p}_k^{\mu} = p_k^{\mu} + p_i^{\mu} - (1 - x_{ik,a})\, p_a^{\mu} \ . \tag{3.60}$$

This mapping keeps the emitter momentum $\widetilde{p}_{ai}$ parallel to p_a. By labeling the parton that goes into the hard process with the index $_a$ and the parton contributing to the final-state by index i, the four different splittings are

1. $q_a \to q + g_i$ with the splitting function $\boldsymbol{V}_k^{q_a g_i}$,
2. $g_a \to q + \bar{q}_i$ with the splitting function $\boldsymbol{V}_k^{g_a q_i}$,
3. $q_a \to g + q_i$ with the splitting function $\boldsymbol{V}_k^{q_a q_i}$,
4. $q_a \to g + g_i$ with the splitting function $\boldsymbol{V}_k^{q_a g_i}$.

Their splitting functions are

$$\begin{aligned} \boldsymbol{V}_k^{q_a g_i}(x_{ik,a}; u_i) &= 8\pi\mu^{2\epsilon}\alpha_s\, C_F \left[\frac{2}{1 - x_{ik,a} + u_i} - (1 + x_{ik,a}) \right. \\ &- \left. \epsilon(1 - x_{ik,a}) \right] , \end{aligned} \tag{3.61}$$

$$\boldsymbol{V}_k^{g_a \bar{q}_i}(x_{ik,a}) = 8\pi\mu^{2\epsilon}\alpha_s\, T_R\, \left[1 - \epsilon - 2x_{ik,a}(1 - x_{ik,a})\right] \ , \tag{3.62}$$

$$\left(\boldsymbol{V}_k^{q_a q_i}(x_{ik,a}; u_i)\right)^{\mu,\nu} = 8\pi\mu^{2\epsilon}\alpha_s\, C_F \left[-g^{\mu\nu} x_{ik,a} \right.$$

$$+ \frac{1-x_{ik,a}}{x_{ik,a}} \frac{2u_i(1-u_i)}{p_i p_k} \left(\frac{p_i^\mu}{u_i} - \frac{p_k^\mu}{1-u_i}\right) \cdot \left(\frac{p_i^\nu}{u_i} - \frac{p_k^\nu}{1-u_i}\right)\Bigg], \tag{3.63}$$

and

$$\begin{aligned}\left(\boldsymbol{V}_k^{g_a g_i}(x_{ik,a};u_i)\right)^{\mu,\nu} &= 16\pi\mu^{2\epsilon}\alpha_s\, C_A \Bigg[-g^{\mu\nu}\left(\frac{1}{1-x_{ik,a}+u_i} - 1 \right. \\ &+ \left. x_{ik,a}(1-x_{ik,a})\right) \\ &+ (1-\epsilon)\,\frac{1-x_{ik,a}}{x_{ik,a}}\,\frac{u_i(1-u_i)}{p_i p_k} \\ &\cdot \left(\frac{p_i^\mu}{u_i} - \frac{p_k^\mu}{1-u_i}\right)\left(\frac{p_i^\nu}{u_i} - \frac{p_k^\nu}{1-u_i}\right)\Bigg]\end{aligned} \tag{3.64}$$

respectively.

3.3.5.2 Massive

The kinematics here is closely related to Section 3.3.4.2. With the variables

$$\begin{aligned} x_{ij,a} &= \frac{p_a p_i + p_a p_j - p_i p_j}{p_a p_i + p_a p_j}, \qquad \tilde{z}_i = \frac{p_a p_i}{p_a p_i + p_a p_j}, \qquad \tilde{z}_j = \frac{p_a p_j}{p_a p_i + p_a p_j}, \\ \mu_j &= \frac{m_j}{\sqrt{2\widetilde{p}_j p_a}}, \qquad Q = p_i + p_j - p_a = \widetilde{p}_j - \widetilde{p}_{ai}. \end{aligned} \tag{3.65}$$

the mapping

$$\widetilde{p}_{ai}^{\,\mu} = x_{ij,a} p_a^\mu, \qquad \widetilde{p}_j^{\,\mu} = p_i^\mu + p_j^\mu - (1-x_{ij,a}) p_a^\mu, \tag{3.66}$$

obey the mass-shell relations $p_a^2 = \widetilde{p}_{ai}^{\,2} = p_i^2 = 0$ and $p_j^2 = \widetilde{p}_j^{\,2} = m_j^2$. Since we are considering only massless particles in the initial-state, only the spectator can be massive. Thus splittings $q \to q+g$, $g \to q+\bar{q}$ and $g \to g+g$ occur and their dipole functions are

$$\begin{aligned} \mathbf{V}_j^{qg} &= 8\pi\mu^{2\varepsilon}\alpha_{\mathrm{s}} C_{\mathrm{F}} \left\{\frac{2}{2-x_{ij,a}-\tilde{z}_j} - 1 - x_{ij,a} - \varepsilon(1-x_{ij,a})\right\}, \\ \mathbf{V}_j^{g\bar{q}} &= 8\pi\mu^{2\varepsilon}\alpha_{\mathrm{s}} T_{\mathrm{R}} \left\{1 - \varepsilon - 2x_{ij,a}(1-x_{ij,a})\right\}, \\ \left(\mathbf{V}_j^{qq}\right)^{\mu,\mu} &= 8\pi\mu^{2\varepsilon}\alpha_{\mathrm{s}} C_{\mathrm{F}} \left\{-g^{\mu\nu} x_{ij,a} + \frac{1-x_{ij,a}}{x_{ij,a}} \frac{2\tilde{z}_i\tilde{z}_j}{p_i p_j}\left(\frac{p_i^\mu}{\tilde{z}_i} - \frac{p_j^\mu}{\tilde{z}_j}\right)\right. \\ &\cdot \left.\left(\frac{p_i^\nu}{\tilde{z}_i} - \frac{p_j^\nu}{\tilde{z}_j}\right)\right\}, \end{aligned} \tag{3.67}$$

and

$$\left(\mathbf{V}_j^{gg}\right)^{\mu,\nu} = 16\pi\mu^{2\varepsilon}\alpha_{\mathrm{s}} C_{\mathrm{A}} \left\{-g^{\mu\nu}\left[\frac{1}{2-x_{ij,a}-\tilde{z}_j} - 1 + x_{ij,a}(1-x_{ij,a})\right]\right.$$

$$+ (1-\varepsilon)\frac{1-x_{ij,a}}{x_{ij,a}}\frac{\tilde{z}_i\tilde{z}_j}{p_i p_j} \cdot \left(\frac{p_i^\mu}{\tilde{z}_i} - \frac{p_j^\mu}{\tilde{z}_j}\right)\left(\frac{p_i^\nu}{\tilde{z}_i} - \frac{p_j^\nu}{\tilde{z}_j}\right)\Bigg\} \tag{3.68}$$

respectively.

3.3.6 Spectator: initial-state - Emitter: initial-state

This case only appears in the massless case and results in a dipole term $\mathcal{D}^{ai,b}$ that involves both initial-state partons a and b and reads

$$\mathcal{D}^{ai,b}(p_1,...,p_{m+1};p_a,p_b) = -\frac{1}{2p_a\cdot p_i}\,\frac{1}{x_{i,ab}} \\ {}_{m,ab}\langle\widetilde{1},..,\widetilde{m+1};\widetilde{ai},b|\,\frac{\boldsymbol{T}_b\cdot\boldsymbol{T}_{ai}}{\boldsymbol{T}_{ai}^2}\,\boldsymbol{V}^{ai,b}\,|\widetilde{1},..,\widetilde{m+1};\widetilde{ai},b\rangle_{m,ab}\ , \tag{3.69}$$

where the momenta of the emitter p_a and all final-state momenta $p_1,\ldots,p_m$ are mapped and only the spectator momentum p_b keeps unchanged. Sticking to the notation of the final-state spectator and initial-state emitter case the contributions are listed in table 3.5.

Nr.	Case	DipoleTerm	IntDipole
31	$\bar{q}_a \to \bar{q} + g_i$	$\boldsymbol{V}^{q_a g_i,k}$	$\tilde{\mathcal{V}}^{q,qg}$
32	$\bar{q}_a \to g + \bar{q}_i$	$\boldsymbol{V}^{q_a q_i,k}$	$\tilde{\mathcal{V}}^{g,gq}$
34	$g_a \to q + \bar{q}_i$	$\boldsymbol{V}^{g_a q_i,k}$	$\tilde{\mathcal{V}}^{q,qq}$
35	$g_a \to g + g_i$	$\boldsymbol{V}^{q_a g_i,k}$	$\tilde{\mathcal{V}}^{g,gg}$

Table 3.5: IS Emitter - IS Spectator

3.3.6.1 Massless

In this case, both emitter $(\tilde{ai})$ and spectator (i) are in the initial-state. Since we consider only massless initial-state partons, no massive dipole terms occur. In order to write the auxiliary cross Section as compact as in Eq. (3.24), it is convenient to keep the spectator momentum p_b unchanged. Hence, the mapping changes the emitter momentum $\widetilde{p}_{ai}$ and all the outgoing momenta $p_1,\ldots,p_n$. By defining

$$x_{i,ab} = \frac{p_a p_b - p_i p_a - p_i p_b}{p_a p_b}\ , \tag{3.70}$$

the initial-state emitter momentum maps as

$$\widetilde{p}_{ai}^{\,\mu} = x_{i,ab}\,p_a^\mu\ . \tag{3.71}$$

All other final-state momenta are mapped via

$$\widetilde{p}_j^{\,\mu} = p_j^\mu - \frac{2p_j\cdot(K+\widetilde{K})}{(K+\widetilde{K})^2}\,(K+\widetilde{K})^\mu + \frac{2p_j\cdot K}{K^2}\,\widetilde{K}^\mu\,, \tag{3.72}$$

where K^μ and $\widetilde{K}^\mu$ are defined as

$$\begin{array}{rcl} K^\mu &=& p_a^\mu + p_b^\mu - p_i^\mu\ , \\ \widetilde{K}^\mu &=& \widetilde{p}_{ai}^{\,\mu} + p_b^\mu\ . \end{array} \tag{3.73}$$

The splittings are the same as in the case of an initial-state emitter and a final-state spectator:

1. $q_a \to q + g_i$ with the splitting function $\boldsymbol{V}^{q_a g_i,k}$,
2. $g_a \to q + \bar{q}_i$ with the splitting function $\boldsymbol{V}^{g_a q_i,k}$,
3. $q_a \to g + q_i$ with the splitting function $\boldsymbol{V}^{q_a q_i,k}$,
4. $q_a \to g + g_i$ with the splitting function $\boldsymbol{V}^{q_a g_i,k}$.

Their splitting functions are given by

$$\boldsymbol{V}^{q_a g_i,b}(x_{i,ab}) = 8\pi\mu^{2\epsilon}\alpha_s\,C_F\,\delta_{ss'}\left[\frac{2}{1-x_{i,ab}} - \,(1+x_{i,ab}) - \epsilon(1-x_{i,ab}))\right]\,, \tag{3.74}$$

$$\boldsymbol{V}^{g_a \bar{q}_i,b}(x_{i,ab}) = 8\pi\mu^{2\epsilon}\alpha_s\,T_R\,\left[1-\epsilon-2x_{i,ab}(1-x_{i,ab})\right]\,, \tag{3.75}$$

$$\begin{array}{rcl} \left(\boldsymbol{V}^{q_a q_i,b}(x_{i,ab})\right)^{\mu,\nu} &=& 8\pi\mu^{2\epsilon}\alpha_s\,C_F\,\left[-g^{\mu\nu}x_{i,ab}\right. \\ &+& \dfrac{1-x_{i,ab}}{x_{i,ab}}\dfrac{2p_a\cdot p_b}{p_i\cdot p_a\;p_i\cdot p_b}\left(p_i^\mu - \dfrac{p_i p_a}{p_b p_a}p_b^\mu\right) \\ &\cdot& \left.\left(p_i^\nu - \dfrac{p_i p_a}{p_b p_a}p_b^\nu\right)\right]\,, \end{array} \tag{3.76}$$

and

$$\begin{array}{rcl} \left(\boldsymbol{V}^{g_a g_i,b}(x_{i,ab})\right)^{\mu,\nu} &=& 16\pi\mu^{2\epsilon}\alpha_s\,C_A\,\left[-g^{\mu\nu}\left(\dfrac{x_{i,ab}}{1-x_{i,ab}} + x_{i,ab}(1-x_{i,ab})\right)\right. \\ &+& (1-\epsilon)\,\dfrac{1-x_{i,ab}}{x_{i,ab}}\,\dfrac{p_a\cdot p_b}{p_i\cdot p_a\;p_i\cdot p_b} \\ &\cdot& \left.\left(p_i^\mu - \dfrac{p_i p_a}{p_b p_a}p_b^\mu\right)\left(p_i^\nu - \dfrac{p_i p_a}{p_b p_a}p_b^\nu\right)\right]\,. \end{array} \tag{3.77}$$

3.4 Integrated Dipole Terms

In the Sections above, the dipole subtraction terms needed to calculate $\mathrm{d}\sigma^{\mathrm{A}}$ were given for both the massless and the massive case. For the complete numerical implementation of Eq. (3.13), the analytic integration over the one-parton subspace $\int_1 \mathrm{d}\sigma^{\mathrm{A}}$ leading to poles in ϵ has to be performed. In [6], the strategy of the integration is outlined and schematically summarized as

$$\begin{aligned}
&\int \mathrm{d}\phi(p_i,p_j,p_k;Q)\ \ \mathcal{V}(p_i,p_j,p_k)\otimes \mathrm{d}\sigma^{\mathrm{B}}(p_i,p_j,p_k)\\
&\overset{(1)}{=} \int \mathrm{d}\phi(\widetilde{p}_{ij},\widetilde{p}_k;Q)\ \left[\int [dp_i(\widetilde{p}_{ij},\widetilde{p}_k)]\ \ \mathcal{V}(p_i)\ \right]\otimes \mathrm{d}\sigma^{\mathrm{B}}(\widetilde{p}_{ij},\widetilde{p}_k)\\
&= \int \mathrm{d}\phi(\widetilde{p}_{ij},\widetilde{p}_k;Q)\ \mathbf{I}\otimes \mathrm{d}\sigma^{\mathrm{B}}(\widetilde{p}_{ij},\widetilde{p}_k). \qquad (3.78)
\end{aligned}$$

Phase-space factorization used in (1) is the main ingredient for carrying out the integration above and makes a generic implementation of the dipole subtraction formalism possible. Taking the phase space restriction parameter into account, Eq. (3.78) changes to

$$\begin{aligned}
&\int d\phi(p_i,p_j,p_k;Q)\ \Theta(\alpha-x)\ \ \mathcal{V}(p_i,p_j,p_k)\otimes d\sigma^{\mathrm{B}}(p_i,p_j,p_k)\\
&= \int d\phi(\widetilde{p}_{ij},\widetilde{p}_k;Q)\ \left[\int [dp_i(\widetilde{p}_{ij},\widetilde{p}_k)]\ \Theta(\alpha-x)\ \ \mathcal{V}(p_i)\ \right]\otimes d\sigma^{\mathrm{B}}(\widetilde{p}_{ij},\widetilde{p}_k)\\
&= \int d\phi(\widetilde{p}_{ij},\widetilde{p}_k;Q)\ \ \mathbf{I}(\alpha)\otimes d\sigma^{\mathrm{B}}(\widetilde{p}_{ij},\widetilde{p}_k). \qquad (3.79)
\end{aligned}$$

where x denotes a kinematical variable that is correlated to the singularity being subtracted by $\mathcal{V}$. In this way the integrated subtraction terms $\mathbf{I}(\alpha)$ acquire a dependence on α. In the following Sections, the integrated subtraction terms based on the factorized phase space are listed in the four possible emitter-spectator cases. Thus the Θ-function of the α dependence only affects the integration boundaries and causes no singularities, we first present the α-dependent integrated subtraction terms. Performing the limit $\alpha \to 1$ provides the corresponding α-independent terms.

3.4.1 Massless, α-dependent Integrated Subtraction Terms

3.4.1.1 Spectator: final-state - Emitter: final-state

If both the emitter and the spectator are final-state partons, the phase space factorization is following [6], exemplarily worked out in the appendix of this thesis. It yields

$$\mathrm{d}\phi(p_i,p_j,p_k;Q) = \mathrm{d}\phi(\widetilde{p}_{ij},\widetilde{p}_k;Q)\ \ [dp_i(\widetilde{p}_{ij},\widetilde{p}_k)] \qquad (3.80)$$

with

$$[dp_i(\widetilde{p}_{ij},\widetilde{p}_k)] = \frac{(2\widetilde{p}_{ij}\widetilde{p}_k)^{1-\epsilon}}{16\pi^2}\,\frac{\mathrm{d}\Omega^{(d-3)}}{(2\pi)^{1-2\epsilon}}\,d\tilde{z}_i\,dy_{ij,k}\,\Theta(\tilde{z}_i(1-\tilde{z}_i)) \cdot \Theta(y_{ij,k}(1-y_{ij,k}))\;(\tilde{z}_i(1-\tilde{z}_i))^{-\epsilon}\;(1-y_{ij,k})^{1-2\epsilon}\,y_{ij,k}^{-\epsilon}\,, \quad (3.81)$$

referring to the kinematics of Section 3.3.3.1. The integration of the dipole term for the calculation of the integrated subtraction term $\mathcal{V}_{ij,k}$ is defined as follows:

$$\int [dp_i(\widetilde{p}_{ij},\widetilde{p}_k)]\;\frac{1}{2p_i\cdot p_j}\;<\boldsymbol{V}_{ij,k}> \equiv\; \frac{\alpha_s}{2\pi}\frac{1}{\Gamma(1-\epsilon)}\left(\frac{4\pi\mu^2}{2\widetilde{p}_{ij}\widetilde{p}_k}\right)^{\epsilon}\mathcal{V}_{ij}(\epsilon)\,. \quad (3.82)$$

By introducing the phase space restriction parameter α and substituting

$$\int [dp_i(\widetilde{p}_{ij},\widetilde{p}_k)] \to \int [dp_i(\widetilde{p}_{ij},\widetilde{p}_k)]\,\Theta(\alpha - y_{ij,k}), \quad (3.83)$$

the integrated subtraction terms acquire the α-dependence $\mathcal{V}_{ij,k}(\epsilon) \to \mathcal{V}_{ij,k}(\epsilon,\alpha)$. The three splittings that have to be considered in the presence of massless particles only are

1. $q(\overline{q}) \to q(\overline{q}) + g$ with massless final-state spectator,
2. $g \to q + \overline{q}$ with massless final-state spectator,
3. $g \to g + g$ with massless final-state spectator.

Their according numbering in the program is given in table 3.2. The α-dependent integrated subtraction terms are calculated in [23] and yield the following results

1. $q \to q + g$:

$$\mathcal{V}_{qg}(\epsilon,\alpha) = C_F\left\{\left(\frac{1}{\epsilon^2} - \ln^2\alpha\right) + \frac{3}{2}\left(\frac{1}{\epsilon} - 1 + \alpha - \ln\alpha\right) + \quad 5 - \frac{\pi^2}{2} + \mathrm{O}(\epsilon)\right\}\,, \quad (3.84)$$

2. $g \to q + \overline{q}$:

$$\mathcal{V}_{q\bar{q}}(\epsilon,\alpha) = T_R\left\{-\frac{2}{3}\left(\frac{1}{\epsilon} - 1 + \alpha - \ln\alpha\right) - \frac{16}{9} + \mathrm{O}(\epsilon)\right\}\,, \quad (3.85)$$

3. $g \to g + g$:

$$\mathcal{V}_{gg}(\epsilon,\alpha) = 2C_A\left\{\left(\frac{1}{\epsilon^2} - \ln^2\alpha\right) + \frac{11}{6}\left(\frac{1}{\epsilon} - 1 + \alpha - \ln\alpha\right) + \quad \frac{50}{9} - \frac{\pi^2}{2} + \mathrm{O}(\epsilon)\right\}\,. \quad (3.86)$$

These formulas for the integrated subtraction terms can be combined to a complete sum-formula for the **I** operator in the final-state emitter and final-state spectator case:

$$\begin{aligned}\boldsymbol{I}(\{p_i\};\epsilon,\alpha) = &-\frac{\alpha_s}{2\pi}\frac{1}{\Gamma(1-\epsilon)} \\ &\times\sum_{i=1}^{4}\ \frac{1}{\boldsymbol{T}_i^2}\ \mathcal{V}_i(\epsilon,\alpha)\ \sum_{k\neq i}\boldsymbol{T}_i\cdot\boldsymbol{T}_k\ \left(\frac{4\pi\mu^2}{2p_i\cdot p_k}\right)^{\epsilon}\ .\end{aligned} \tag{3.87}$$

Keeping in mind that the index i in $\mathcal{V}_i(\epsilon,\alpha)$ labels the emitter parton, the factors are given by

$$\mathcal{V}_i(\epsilon,\alpha) = \boldsymbol{T}_i^2\left(\frac{1}{\epsilon^2}-\frac{\pi^2}{3}-\ln^2\alpha\right)+\gamma_i\ \left(\frac{1}{\epsilon}+\alpha-\ln\alpha\right)+K_i+\mathrm{O}(\epsilon)\,, \tag{3.88}$$

where the constants are defined as

$$\begin{aligned}\gamma_q &= \frac{3}{2}C_F\,, & K_q &= \left(\frac{7}{2}-\frac{\pi^2}{6}\right)C_F\,, \\ \gamma_g &= \frac{11}{6}C_A-\frac{2}{3}T_R N_f\,, & K_g &= \left(\frac{67}{18}-\frac{\pi^2}{6}\right)C_A-\frac{10}{9}T_R N_f\,.\end{aligned} \tag{3.89}$$

The index q in the constants labels both q and $\bar{q}$.

3.4.1.2 Spectator: initial-state - Emitter: final-state

In the case where a final-state splitting is spectated by an initial-state parton, the phase-space factorization based on the kinematics of Section 3.3.4.1 obtains an additional convolution due to the momentum fraction $x_{ij,a}$ of the incoming hadron, that the initial-state parton carries. The factorization of the three-parton phase space $\mathrm{d}\phi(p_i,p_j;Q+p_a)$ into the two-parton phase space $\mathrm{d}\phi(\widetilde{p}_{ij};Q+xp_a)$ and the one parton subspace $[dp_i(\widetilde{p}_{ij};p_a,x)]$ is given by

$$\mathrm{d}\phi(p_i,p_j;Q+p_a) = \int_0^1 dx\ \mathrm{d}\phi(\widetilde{p}_{ij};Q+xp_a)\ \left[dp_i(\widetilde{p}_{ij};p_a,x)\right]\ , \tag{3.90}$$

where

$$\begin{aligned}\left[dp_i(\widetilde{p}_{ij};p_a,x)\right] \;=\; &\frac{(2\widetilde{p}_{ij}p_a)^{1-\epsilon}}{16\pi^2}\ \frac{\mathrm{d}\Omega^{(d-3)}}{(2\pi)^{1-2\epsilon}}\ d\tilde{z}_i\ dx_{ij,a}\ \Theta(\tilde{z}_i(1-\tilde{z}_i)) \\ &\cdot\Theta(x(1-x))\ (\tilde{z}_i(1-\tilde{z}_i))^{-\epsilon}\ \delta(x-x_{ij,a})\ (1-x)^{-\epsilon}\ .\end{aligned} \tag{3.91}$$

The integrated subtraction terms $I_{ij}^a(x;\epsilon)$ are defined analogously to the ones of the final–final case in Eq. (3.82). The only difference is the leftover x-dependence

$$\frac{\alpha_s}{2\pi}\frac{1}{\Gamma(1-\epsilon)}\left(\frac{4\pi\mu^2}{2\widetilde{p}_{ij}p_a}\right)^{\epsilon} I_{ij}^a(x;\epsilon) \equiv \int\left[dp_i(\widetilde{p}_{ij};p_a,x)\right]\frac{1}{2p_ip_j} < \boldsymbol{V}_{ij}^a(\tilde{z}_i;x_{ij,a}) > \ . \tag{3.92}$$

In order to avoid evaluation of the subtraction terms in specific phase-space regions, the kinematical variable $x_{ij,a}$ has to be restricted by the α parameter. This is done by the replacement

$$\int [dp_i(\widetilde{p}_{ij}; p_a, x)] \to \int [dp_i(\widetilde{p}_{ij}; p_a, x)]\, \Theta(\alpha - 1 + x_{ij,a}) \tag{3.93}$$

in the integration of the dipole terms and leads to the α-dependence in $I^a_{ij}(x; \alpha, \epsilon)$ The splittings occuring here are the same as in the final–final case, whereas now the spectator is in the initial-state

1. $q(\overline{q}) \to q(\overline{q}) + g$ with massless initial-state spectator
2. $g \to q + \overline{q}$ with massless initial-state spectator
3. $g \to g + g$ with massless initial-state spectator.

Table 3.3 shows their corresponding numbering in our code.

Case 1: $q(\overline{q}) \to q(\overline{q}) + g$

The α-dependent integrated subtraction terms for this case is calculated in [24]:

$$\begin{aligned} I^a_{qg}(x; \epsilon, \alpha) &= C_F \Bigg\{ \delta(1-x) \left(\frac{7}{2} - \frac{\pi^2}{2} - \frac{3}{2} \ln(\alpha) - \ln^2(\alpha) + \frac{3}{2\epsilon} + \frac{1}{\epsilon^2} \right) \\ &+ \frac{2\, \ln(2-x)}{1-x}\, \Theta(x - 1 + \alpha) - 2 \left(\frac{\ln(1-x)}{1-x} \right)_{1-\alpha} \\ &- \frac{3}{2} \left(\frac{1}{1-x} \right)_{1-\alpha} \Bigg\} + \mathrm{O}(\epsilon)\,. \end{aligned} \tag{3.94}$$

Case 2: $g \to q + \overline{q}$

For this case, the decomposition of the integrated subtraction term $I^a_{q\bar{q}}$ is performed according to [22] with $\mu_Q \to 0$

$$\begin{aligned} I^a_{q\bar{q}}(x; \alpha, \epsilon) &= T_{\mathrm{R}} \left\{ [J^a_{q\bar{q}}(x, 0; \alpha)]_{x_+} + \delta(x_+ - x) \left[J^{a;\mathrm{S}}_{q\bar{q}}(0; \alpha, \epsilon) + J^{a;\mathrm{NS}}_{q\bar{q}}(0; \alpha) \right] \right\} \\ &+ \mathrm{O}(\epsilon)\,. \end{aligned} \tag{3.95}$$

The results for this case were derived in [25] from the result of gluon splitting into a massive quark - antiquark pair by setting the corresponding masses to zero, i.e. $\lim_{\mu_Q \to 0}$. This gives the following contributions

$$[J^a_{q\bar{q}}(x, 0; \alpha)]_+ = \frac{2}{3} \left(\frac{1}{1-x} \right)_{1-\alpha}, \tag{3.96}$$

$$J^{a;\mathrm{S}}_{q\bar{q}}(0;\alpha,\epsilon) = -\frac{2}{3\varepsilon} - \frac{10}{9}\,, \tag{3.97}$$

and

$$J^{a;\mathrm{NS}}_{q\bar{q}}(0;\alpha) = \frac{2}{3}\ln(\alpha)\,. \tag{3.98}$$

Case 3: $g \to g + g$

The general structure of the integrated subtraction term in the case of gluon–gluon splitting is given in [22]

$$I^a_{gg}(x;\alpha,\epsilon) = 2C_\mathrm{A}\left\{[J^a_{gg}(x;\alpha)]_+ + \delta(1-x)\,J^{a;\mathrm{S}}_{gg}(\alpha,\epsilon)\right\} + \mathrm{O}(\epsilon)\,. \tag{3.99}$$

According to [25], the function $[J^a_{gg}(x;\alpha)]$ and $J^{a;\mathrm{S}}_{gg}(\alpha,\epsilon)$ are given by

$$[J^a_{gg}(x,\alpha)]_+ = \left(\frac{2}{1-x}\ln\frac{1}{1-x} - \frac{11}{6}\frac{1}{1-x}\right)_{1-\alpha} + \frac{2}{1-x}\ln(2-x)\Theta(\alpha-1+x) \tag{3.100}$$

and

$$J^{a;\mathrm{S}}_{gg}(x,\alpha) = \frac{1}{\varepsilon^2} + \frac{11}{6\varepsilon} + \frac{67}{18} - \frac{\pi^2}{2} - \ln^2\alpha - \frac{11}{6}\ln\alpha. \tag{3.101}$$

3.4.1.3 Spectator: final-state - Emitter: initial-state

With respect to the kinematics of Section 3.3.5.1, the phase-space factorization is schematically the same as in Eq. (3.90) after interchanging $\widetilde{p}_{ij} \leftrightarrow \widetilde{p}_k$

$$\mathrm{d}\phi(p_i,p_k;Q+p_a) = \int_0^1 dx\;\mathrm{d}\phi(\widetilde{p}_k;Q+xp_a)\;\;[dp_i(\widetilde{p}_k;p_a,x)]\;\,, \tag{3.102}$$

where $[dp_i(\widetilde{p}_k;p_a,x)]$ is explicitly given by

$$\begin{aligned}[dp_i(\widetilde{p}_k;p_a,x)] \;\;=\;\; & \frac{(2\widetilde{p}_k p_a)^{1-\epsilon}}{16\pi^2}\;\frac{\mathrm{d}\Omega^{(d-3)}}{(2\pi)^{1-2\epsilon}}\;du_i\;dx_{ik,a}\;\Theta(u_i(1-u_i)) \\ & \cdot\,\Theta(x(1-x))\;\;(u_i(1-u_i))^{-\epsilon}\;\;\delta(x-x_{ik,a})\;\;(1-x)^{-\epsilon}\,.\end{aligned} \tag{3.103}$$

The one parton subspace integral that has to be performed is defined by

$$\frac{\alpha_s}{2\pi}\frac{1}{\Gamma(1-\epsilon)}\left(\frac{4\pi\mu^2}{2\widetilde{p}_k p_a}\right)^{\epsilon}\mathcal{V}^{a,ai}(x;\epsilon) \equiv \int [dp_i(\widetilde{p}_k;p_a,x)]\,\frac{1}{2p_a p_i}\;\;<\tilde{\boldsymbol{V}}^{ai}_k(x_{ik,a};u_i)>\,, \tag{3.104}$$

where $<\tilde{\boldsymbol{V}}^{ai}_k(x_{ik,a};u_i)>$ includes already the ratio of the number of polarizations of the emitted parton a and the emitter $\widetilde{ai}$. (Keep in mind: $\tilde{\boldsymbol{V}}^{ai}_k(x_{ik,a};u_i) = \frac{n_s(\widetilde{ai})}{n_s(a)}\boldsymbol{V}^{ai}_k(x_{ik,a};u_i)$). The α dependence is again introduced by the substitution

$$\int [dp_i(\widetilde{p}_k;p_a,x)] \to \int [dp_i(\widetilde{p}_k;p_a,x)]\,\Theta(\alpha-z_i). \tag{3.105}$$

In the case of an initial-state singularity, i.e. the final-state NLO parton being emitted from the initial-state, and a final-state spectator, the following four cases can occur. (The index a labels the parton going into the hard scattering process and i labels the final-state parton.)

1. $q \to q_a + g_i$ with massless final-state spectator
2. $q \to g_a + q_i$ with massless final-state spectator
3. $g \to q_a + \bar{q}_i$ with massless final-state spectator
4. $g \to g_a + g_i$ with massless final spectator.

The numbers of the corresponding subtraction terms are shown in table 3.4.

Case 1: $q \to q_a + g_i$

The α-dependent integrated subtraction term was calculated in [24] and reads

$$\begin{aligned}
\mathcal{V}^{q,qg}(x;\epsilon,\alpha) &= C_F\Bigg\{(1-x) - \frac{2}{1-x}\ln\Big(\frac{1+\alpha-x}{\alpha}\Big) \\
&+ \Big(\frac{1}{\epsilon} - \ln(\alpha) - \ln(1-x)\Big)(1+x) \\
&+ \delta(1-x)\Big(\frac{1}{\epsilon^2} + \frac{\pi^2}{6}\Big) + 4\Big[\frac{\ln(1-x)}{(1-x)}\Big]_+ - \frac{2}{\epsilon}\Big[\frac{1}{1-x}\Big]_+\Bigg\} \\
&+ \mathrm{O}(\epsilon)
\end{aligned} \tag{3.106}$$

Case 2: $q \to g_a + q_i$

In the case of a massive spectator, the integrated subtraction term is given by [26]:

$$\begin{aligned}
& I_Q^{qg}(x;\epsilon,\alpha) = C_F\Bigg\{\frac{\Big(1+(1-x)^2\Big)}{x} \\
\times\ & \left[\ln\Big(\frac{(1-x)^2}{1-x+x\left(\frac{\mu}{x}\right)^2}\Big) - \frac{1}{\epsilon} - \Theta(z_+-\alpha)\ln\left(\frac{z_+}{\alpha}\right)\right] \\
+\ & 2\left(\frac{\mu}{x}\right)^2\ln\left(\frac{x\left(\frac{\mu}{x}\right)^2}{1-x+x\left(\frac{\mu}{x}\right)^2}\right) \\
-\ & \Theta(z_+-\alpha)2\left(\frac{\mu}{x}\right)^2\ln\left(\frac{1-z_+}{1-\alpha}\right) + x\Bigg\} + \mathrm{O}(\epsilon)\,.
\end{aligned} \tag{3.107}$$

A straightforward implementation of this term causes numerical issues due to terms like $\mu_Q \ln(\mu_Q)$. The analytical calculation of the limit $\mu_Q \to 0$

$$\lim_{\mu_Q \to 0} I_Q^{qg}(x;\epsilon,\alpha) = V^{g,gq}(x;\epsilon,\alpha) \tag{3.108}$$

gives

$$\begin{aligned} V^{g,gq}(x;\epsilon,\alpha) &= C_F \Bigg\{ \frac{\Big(1+(1-x)^2\Big)}{x} \\ \times \quad & \left[\ln\Big(1-x\Big) - \frac{1}{\epsilon} + \ln(\alpha) \right] + x \Bigg\} + \mathrm{O}(\epsilon)\,. \end{aligned} \tag{3.109}$$

Case 3: $g \to q_a + \bar{q}_i$

The integral of a massless splitting of a gluon into a quark-antiquark pair is given in [26]:

$$\begin{aligned} V^{q,gq}(x;\epsilon,\alpha) &= T_R \Bigg\{ \Big(x^2+(1-x)^2\Big) \\ \times \quad & \left[\ln\Big(\frac{(1-x)^2}{1-x+x\left(\frac{\mu}{x}\right)^2}\Big) - \frac{1}{\epsilon} + \ln(\alpha) \right] + 2\,x(1-x) \Bigg\} + \mathrm{O}(\epsilon)\,. \end{aligned} \tag{3.110}$$

Case 4: $g \to g_a + \bar{g}_i$

In presence of a massive spectator, the integrated subtraction term reads

$$\begin{aligned} I_Q^{gg}(x;\epsilon,\alpha) \;=\; & C_A \Bigg\{ \delta(1-x) \Bigg[\frac{1}{\epsilon^2} + \frac{1}{\epsilon} \ln(1+\Big(\frac{\mu}{x}\Big)^2) + \frac{\pi^2}{6} \\ & +2\mathrm{Li}_2(-\Big(\frac{\mu}{x}\Big)^2) + 2\ln(\Big(\frac{\mu}{x}\Big)^2)\ln(1+\Big(\frac{\mu}{x}\Big)^2) - \frac{1}{2}\ln^2(1+\Big(\frac{\mu}{x}\Big)^2) \Bigg] \\ & -\frac{1}{\epsilon}\,\frac{2}{[1-x]_+} - 2\,\frac{\ln(1+\tilde{\mu}^2)}{[1-x]_+} + 4\left[\frac{\ln(1-x)}{(1-x)}\right]_+ \\ & +2\left(x(1-x)+\frac{1-x}{x}-1\right)\Bigg[-\frac{1}{\epsilon} + \ln\Big(\frac{(1-x)^2}{1-x+x\left(\frac{\mu}{x}\right)^2}\Big) \\ & -\Theta(z_+-\alpha)\,\ln\Big(\frac{z_+}{\alpha}\Big)\Bigg] - \Theta(z_+-\alpha)\Bigg[2\Big(\frac{\mu}{x}\Big)^2 \ln\Big(\frac{1-z_+}{1-\alpha}\Big) \\ & -\frac{2}{(1-x)}\ln\Big(\frac{\alpha(1-x+z_+)}{z_+(1-x+\alpha)}\Big)\Bigg] + 2\Big(\frac{\mu}{x}\Big)^2 \ln\Big(\frac{x\left(\frac{\mu}{x}\right)^2}{1-x+x\left(\frac{\mu}{x}\right)^2}\Big) \end{aligned}$$

$$-\frac{2}{(1-x)}\ln\Big(\frac{2-x+x\left(\frac{\mu}{x}\right)^2}{1+\left(\frac{\mu}{x}\right)^2}\Big)\Bigg\}\,, \tag{3.111}$$

because $\lim_{x\to 0} x^l \ln x = 0$ for $l > 0$. Performing the same limit as in case 2,

$$\lim_{\mu_Q\to 0} I_Q^{gg}(x;\epsilon,\alpha) = V^{g,gg}(x;\epsilon,\alpha), \tag{3.112}$$

yields

$$\begin{aligned} V^{g,gg}(x;\epsilon,\alpha) = {} & C_A\Bigg\{\delta(1-x)\left[\frac{1}{\epsilon^2}+\frac{\pi^2}{6}\right] \\ - {} & \frac{1}{\epsilon}\frac{2}{[1-x]_+} + 4\left[\frac{\ln(1-x)}{(1-x)}\right]_+ \\ + {} & 2\Big(x(1-x)+\frac{1-x}{x}-1\Big)\left[-\frac{1}{\epsilon}+\ln\Big(1-x\Big)+\ln(\alpha)\right] \\ - {} & \left[-\frac{2}{(1-x)}\ln\Big(\frac{\alpha(2-x)}{(1-x+\alpha)}\Big)\right] - \frac{2}{(1-x)}\ln\Big(2-x\Big)\Bigg\}. \end{aligned} \tag{3.113}$$

3.4.1.4 Spectator: initial-state - Emitter: initial-state

The last possible case that can occur is due to an initial-state emitter and an initial-state spectator. The phase space factorization is given by

$$\mathrm{d}\phi(p_i,\{k\};p_a+p_b) = \int_0^1 dx\ \mathrm{d}\phi(\{\tilde{k}\};xp_a+p_b)\ \left[dp_i(p_a,p_b,x)\right]\,, \tag{3.114}$$

where $\{\tilde{k}\}$ ($\{\tilde{k}\}$) are the rescaled (non rescaled) final-state momenta using the kinematics of Section (3.3.6.1). The explicit phase space measure of the one parton subspace reads

$$\begin{aligned} \left[dp_i(p_a,p_b,x)\right] = {} & \frac{(2p_ap_b)^{1-\epsilon}}{16\pi^2}\,\frac{\mathrm{d}\Omega^{(d-3)}}{(2\pi)^{1-2\epsilon}}\,d\tilde{v}_i\,dx_{i,ab}\,\Theta(\tilde{v}_i)\,\Theta\Big(1-\frac{\tilde{v}_i}{1-x}\Big) \\ & \times\ (1-x)^{-2\epsilon}\ \Theta(x(1-x))\ \delta(x-x_{i,ab}) \\ & \times\ \left[\frac{\tilde{v}_i}{1-x}\left(1-\frac{\tilde{v}_i}{1-x}\right)\right]^{-\epsilon}\,. \end{aligned} \tag{3.115}$$

The integration of the splitting function can be written as

$$\frac{\alpha_s}{2\pi}\frac{1}{\Gamma(1-\epsilon)}\left(\frac{4\pi\mu^2}{2p_ap_b}\right)^{\epsilon}\widetilde{\mathcal{V}}^{a,ai}(x;\epsilon) \equiv \int\left[dp_i(p_a,p_b,x)\right]\frac{1}{2p_ap_i}\ <\tilde{\boldsymbol{V}}^{ai,b}(x_{i,ab})>\,, \tag{3.116}$$

where $<\tilde{\boldsymbol{V}}^{ai,b}(x_{i,ab})>$ is again already multiplied with the proper ratio of polarizations of partons taking part in the splitting. The integrated splitting terms acquire the

α-dependence by multiplying the integration measure with $\Theta(\alpha - \tilde{v}_i)$. The possible splitting are except for the initial-state spectator the same as in the Section above, namely

1. $q \to q_a + g_i$ with massless initial-state spectator
2. $q \to g_a + q_i$ with massless initial-state spectator
3. $g \to q_a + \bar{q}_i$ with massless initial-state spectator
4. $g \to g_a + g_i$ with massless initial spectator.

The corresponding numbers of the subtraction terms in the code are given in table 3.5. The results for these cases can be found in [24] and [26] and are listed below.

Case 1: $q \to q_a + g_i$

The result for the integrated splitting function in this case is given by

$$\begin{aligned}\tilde{\mathcal{V}}^{q,qg}(x;\epsilon,\alpha) &= C_F\Bigg\{\left(\frac{1}{\epsilon^2}-\frac{\pi^2}{6}\right)\delta(1-x)+(1-x)-(1+x)\\ &\quad\times\Big(2\ln(1-x)-\frac{1}{\epsilon}\Big)+\Theta(1-x-\alpha)\frac{(1+x^2)}{(1-x)}\\ &\quad\times\ln\left(\frac{\alpha}{1-x}\right)-\frac{2}{\epsilon}\frac{1}{\big[1-x\big]_+}+4\left[\frac{\ln(1-x)}{1-x}\right]_+\Bigg\}+\mathrm{O}(\epsilon)\,. \end{aligned} \tag{3.117}$$

Case 2: $q \to g_a + q_i$

The splitting $q \to g_a + q_i$ yields the following result:

$$\begin{aligned}\tilde{\mathcal{V}}^{g,gq}(x;\epsilon,\alpha) &= T_R\Bigg\{\Big((1-x)^2+x^2\Big)\times\Bigg[2\ln(1-x)-\frac{1}{\epsilon}\\ &\quad+\Theta(1-x-\alpha)\ln\left(\frac{\alpha}{1-x}\right)\Bigg]+2x(1-x)\Bigg\}+\mathrm{O}(\epsilon). \end{aligned} \tag{3.118}$$

Case 3: $g \to q_a + \bar{q}_i$

The integration of a gluon splitting into a massless quark-antiquark pair was performed in [26] and reads

$$\tilde{\mathcal{V}}^{q,qq}(x;\epsilon,\alpha) = C_F\Bigg\{\frac{\Big(1+(1-x)^2\Big)}{x}$$

$$\times \quad \left[2\ln(1-x) - \frac{1}{\epsilon} + \Theta(1-x-\alpha)\ln\left(\frac{\alpha}{1-x}\right)\right] + x\Bigg\} + \mathrm{O}(\epsilon)\,. \qquad (3.119)$$

Case 4: $g \to g_a + g_i$

The integrated subtraction term for a gluon-gluon splitting is given by

$$\begin{aligned}\tilde{\mathcal{V}}^{g,gg}(x;\epsilon,\alpha) &= C_A\Bigg\{\left(\frac{1}{\epsilon^2} - \frac{\pi^2}{6}\right)\delta(1-x) + 2\Big(x\,(1-x) + \frac{1-x}{x} - 1\Big)\\ &\times \quad \Big(2\ln(1-x) - \frac{1}{\epsilon}\Big) + \Theta(1-x-\alpha)\frac{2(x\,(1-x)-1)^2}{x(1-x)}\\ &\times \quad \ln\left(\frac{\alpha}{1-x}\right) - \frac{2}{\epsilon}\frac{1}{\big[1-x\big]_+} + 4\left[\frac{\ln(1-x)}{1-x}\right]_+\Bigg\} + \mathrm{O}(\epsilon)\,. \qquad (3.120)\end{aligned}$$

3.4.2 Massive, α-dependent Integrated Subtraction Terms

3.4.2.1 Spectator: final-state - Emitter: final-state

Nr.	Case	DipoleTerm	Type	α IntDipole
101	$Q \to Q + g$	$D_{gQ,k}$	$M_{sp} = 0$	$I_{gQ,k}$
			$M_{sp} \neq 0$	$I_{gQ,\mathbf{k}}$
101	$q \to q + g$	$D_{gq,k}$	$M_{sp} = 0$	-
			$M_{sp} \neq 0$	$I_{gq,\mathbf{k}}$
102	$g \to g + g$	$D_{gg,k}$	$M_{sp} = 0$	-
			$M_{sp} \neq 0$	$I_{g,g\mathbf{k}}$
103	$g \to q + \bar{q}$	$D_{q\bar{q},k}$	$M_{sp} = 0$	-
			$M_{sp} \neq 0$	$I_{qq,\mathbf{k}}$

Table 3.6: FS Emitter - FS Spectator

In the case of a final-state emitter and a final-state spectator, the exact phase-space factorization is

$$\mathrm{d}\phi(p_i,p_j,p_k;Q) = \mathrm{d}\phi(\widetilde{p}_{ij},\widetilde{p}_k;Q)\,[\mathrm{d}p_i(\widetilde{p}_{ij},\widetilde{p}_k)]\,\Theta(1-\mu_i-\mu_j-\mu_k)\,. \qquad (3.121)$$

Using the kinematics of Section 3.3.3.2 leads according to [22], to the one-parton phase-space integral

$$\begin{aligned}\int[\mathrm{d}p_i(\widetilde{p}_{ij},\widetilde{p}_k)] &= \frac{1}{4}(2\pi)^{-3+2\varepsilon}(Q^2)^{1-\varepsilon}(1-\mu_i^2-\mu_j^2-\mu_k^2)^{2-2\varepsilon}\left[\lambda(1,\mu_{ij}^2,\mu_k^2)\right]^{\frac{-1+2\varepsilon}{2}}\int \mathrm{d}^{d-3}\Omega\\ &\times \int_{y_-}^{y_+}\mathrm{d}y_{ij,k}\,(1-y_{ij,k})^{1-2\varepsilon}\left[\mu_i^2+\mu_j^2+(1-\mu_i^2-\mu_j^2-\mu_k^2)y_{ij,k}\right]^{-\varepsilon}\end{aligned}$$

$$\times \int_{z_-(y_{ij,k})}^{z_+(y_{ij,k})} \mathrm{d}\tilde{z}_i \, [z_+(y_{ij,k}) - \tilde{z}_i]^{-\varepsilon} \, [\tilde{z}_i - z_-(y_{ij,k})]^{-\varepsilon} \, . \tag{3.122}$$

In order to get the integrated subtraction terms, the product of the splitting functions and the corresponding propagator has to be integrated over the one-parton subspace leading to the singularity. For the implementation we use the following definition of $I_{ij,k}(\epsilon, m, p)$

$$\int [\mathrm{d}p_i(\widetilde{p}_{ij}, \widetilde{p}_k)] \, \frac{1}{(p_i + p_j)^2 - m_{ij}^2} \, \langle \mathbf{V}_{ij,k} \rangle \equiv \frac{\alpha_\mathrm{s}}{2\pi} \frac{1}{\Gamma(1-\varepsilon)} \left(\frac{4\pi\mu^2}{Q^2} \right)^{\varepsilon} I_{ij,k}(\varepsilon) \, . \tag{3.123}$$

In the case of a final-state emitter and a final-state spectator, the kinematical variable for the phase space restriction has to be applied to is $y_{ij,k}$ which leads to the additional Θ-function $\Theta(y_{ij,k} < \alpha)$ in the integral above yielding the α-dependence

$$\int [\mathrm{d}p_i(\widetilde{p}_{ij}, \widetilde{p}_k)] \, \to \int [\mathrm{d}p_i(\widetilde{p}_{ij}, \widetilde{p}_k)] \Theta(y_{ij,k} < \alpha). \tag{3.124}$$

The integrated subtraction term $I_{ij,k}$ can be decomposed into an eikonal part I^{eik} and a collinear part I^{coll}:

$$I_{ij,k}(\mu_i, \mu_j, \mu_k; \epsilon) \propto \left[2I^{\mathrm{eik}}(\mu_i, \mu_j, \mu_k; \varepsilon) + I_{ij,k}^{\mathrm{coll}}(\mu_i, \mu_j, \mu_k; \epsilon) \right] \, , \tag{3.125}$$

where the eikonal integral is defined as follows:

$$\frac{\alpha_\mathrm{s}}{2\pi} \frac{1}{\Gamma(1-\varepsilon)} \left(\frac{4\pi\mu^2}{Q^2} \right)^{\varepsilon} I^{\mathrm{eik}}(\mu_i, \mu_j, \mu_k; \varepsilon) = \int [\mathrm{d}p_i(\widetilde{p}_{ij}, \widetilde{p}_k)] \, \frac{1}{2p_i p_j} \, \frac{8\pi\mu^{2\varepsilon}\alpha_\mathrm{s}}{1 - \tilde{z}_j(1 - y_{ij,k})}. \tag{3.126}$$

As pointed out in Reference [22] the eikonal integral can be split up in a symmetric and antisymmetric part. In our implementation of the following three eikonal integrals we only took the symmetric part of the eikonal integral into account, which is completely sufficient for the calculation of a physical cross section.

Final $Q \to Q + g$ splitting

For a final-state $Q \to Q + g$ splitting three cases can occur:

1. $Q \to Q + g$ splitting with massless spectator
2. $Q \to Q + g$ with massive spectator.
3. $q \to q + g$ with massive spectator.

Case 1

The integrated subtraction terms $I_{Qg,k}$ is decomposed as follows:

$$I_{gQ,k}(\mu_Q,\mu_k;\epsilon) = C_{\mathrm{F}}\left[2I^{\mathrm{eik}}(\mu_Q,\mu_k;\varepsilon) + I^{\mathrm{coll}}_{gQ,k}(\mu_Q,\mu_k;\epsilon)\right] \tag{3.127}$$

Using the definition of the eikonal integral in Eq. (3.126) and taking the additional Θ-function of Eq. (3.124) into account, one obtains in terms of the kinematics of Section 3.3.4.2 according to [24]

$$\begin{aligned} I^{\mathrm{eik}}(\mu_Q,0;\epsilon) &= \frac{\ln(\mu_Q^2)}{2\epsilon} - 2\mathrm{Li}_2(1-\mu_Q^2) - \ln(\mu_Q^2)\ln(1-\mu_Q^2) - \frac{1}{4}\ln^2(\mu_Q^2) \\ &- \ln(\alpha)\ln(\mu_Q^2) - \mathrm{Li}_2\Big(\frac{\mu_Q^2-1}{\mu_Q^2}\Big) + \mathrm{Li}_2\Big(\frac{\alpha(\mu_Q^2-1)}{\mu_Q^2}\Big) \\ &+ \mathrm{O}(\epsilon)\,. \end{aligned} \tag{3.128}$$

Integrating the remaining terms of the dipole subtraction term gives the collinear integral

$$\begin{aligned} I^{\mathrm{coll}}(\mu_Q,0;\epsilon) &= \frac{1}{\epsilon} + 3 + \ln(\mu_Q^2)(1+\frac{1}{2}) + \ln(\mu_Q^2)\frac{(-1)}{1-\mu_Q^2} - 2\ln(1-\mu_Q^2) \\ &+ \frac{1}{2}\Big[3\alpha - 2 - \frac{(3-\mu_Q^2)}{(1-\mu_Q^2)}\ln(\alpha+(1-\alpha)\mu_Q^2) - \frac{\alpha}{(\alpha+(1-\alpha)\mu_Q^2)}\Big] \\ &- 2\ln(\alpha) + 2\frac{\ln(\alpha+(1-\alpha)\mu_Q^2)}{(1-\mu_Q^2)} + \mathrm{O}(\epsilon)\,. \end{aligned} \tag{3.129}$$

Case 2

The decomposition of the integrated subtraction term in this case follows [27] by separating the α and ϵ dependence of $I_{ij,k}$

$$I_{ij,k}(\epsilon) \to I_{ij,k}(\epsilon,\alpha) = I_{ij,k}(\epsilon) + \Delta I_{ij,k}(\alpha)\,. \tag{3.130}$$

The complete decomposition thus reads

$$I_{ij,k}(\epsilon,\alpha) = \Big[2\Big(I^{\mathrm{eik}}(\varepsilon) + \Delta I^{\mathrm{eik}}(\alpha)\Big) + \Big(I^{\mathrm{coll}}_{ij,k}(\epsilon) + \Delta I^{\mathrm{coll}}_{ij,k}(\alpha)\Big)\Big]\,. \tag{3.131}$$

According to [6], the α independent part $I^{\mathrm{eik}}(\varepsilon)$ of the eikonal integral after expansion in ϵ is given by

$$\begin{aligned} &I^{\mathrm{eik}}(\mu_Q,\mu_k;\varepsilon) = \\ &\quad\frac{1}{\tilde{v}_{iQ,k}}\left[\frac{1}{2\epsilon}\ln\rho - \ln\rho\,\ln\Big(1-(\mu_Q+\mu_k)^2\Big) - \frac{1}{2}\ln^2\rho_Q - \frac{1}{2}\ln^2\rho_k\right. \end{aligned}$$

$$+\frac{\pi^2}{6} + 2\mathrm{Li}_2(-\rho) - 2\mathrm{Li}_2(1-\rho) - \frac{1}{2}\mathrm{Li}_2(1-\rho_Q^2)$$
$$-\frac{1}{2}\mathrm{Li}_2(1-\rho_k^2)\Bigg] + \mathrm{O}(\epsilon)\,. \tag{3.132}$$

and the collinear part reads

$$\begin{aligned} I^{\mathrm{coll}}_{gQ,k}(\mu_Q,\mu_k;\varepsilon) \;=\; & \frac{3}{2\varepsilon} - \frac{1}{2\varepsilon} + \ln(\mu_Q) - 2 - 2\ln\left[(1-\mu_k)^2-\mu_Q^2\right] + \ln(1-\mu_k) \\ & - \frac{2\mu_Q^2}{1-\mu_Q^2-\mu_k^2}\ln\left(\frac{\mu_Q}{1-\mu_k}\right) + 5 - \frac{\mu_k}{1-\mu_k} - \frac{2\mu_k(1-2\mu_k)}{1-\mu_Q^2-\mu_k^2} \\ & + \mathrm{O}(\epsilon)\,, \end{aligned} \tag{3.133}$$

The α-dependence of both parts was calculated in [27]. The eikonal integral reads

$$\begin{aligned} \Delta I^{\mathrm{eik}} = \frac{1}{v_{jk}} \quad & \Bigg(-\mathrm{Li}_2\left(\frac{a+x}{a+x_+}\right) + \mathrm{Li}_2\left(\frac{a}{a+x_+}\right) + \mathrm{Li}_2\left(\frac{x_+-x}{x_+-b}\right) - \mathrm{Li}_2\left(\frac{x_+}{x_+-b}\right) \\ & + \mathrm{Li}_2\left(\frac{c+x}{c+x_+}\right) - \mathrm{Li}_2\left(\frac{c}{c+x_+}\right) + \mathrm{Li}_2\left(\frac{x_--x}{x_-+a}\right) - \mathrm{Li}_2\left(\frac{x_-}{x_-+a}\right) \\ & - \mathrm{Li}_2\left(\frac{b-x}{b-x_-}\right) + \mathrm{Li}_2\left(\frac{b}{b-x_-}\right) - \mathrm{Li}_2\left(\frac{x_--x}{x_-+c}\right) + \mathrm{Li}_2\left(\frac{x_-}{x_-+c}\right) \\ & + \mathrm{Li}_2\left(\frac{b-x}{b+a}\right) - \mathrm{Li}_2\left(\frac{b}{b+a}\right) - \mathrm{Li}_2\left(\frac{c+x}{c-a}\right) + \mathrm{Li}_2\left(\frac{c}{c-a}\right) \\ & + \ln(c+x)\ln\left(\frac{(a-c)(x_+-x)}{(a+x)(c+x_+)}\right) - \ln(c)\ln\left(\frac{(a-c)x_+}{a(c+x_+)}\right) \\ & + \ln(b-x)\ln\left(\frac{(a+x)(x_--b)}{(a+b)(x_--x)}\right) - \ln(b)\ln\left(\frac{a(x_--b)}{(a+b)x_-}\right) \\ & - \ln\left((a+x)(b-x_+)\right)\ln(x_+-x) + \ln\left(a(b-x_+)\right)\ln(x_+) \\ & + \ln(d)\ln\left(\frac{(a+x)x_+x_-}{a(x_+-x)(x_--x)}\right) + \ln\left(\frac{x_--x}{x_-}\right)\ln\left(\frac{c+x_-}{a+x_-}\right) \\ & + \frac{1}{2}\ln\left(\frac{a+x}{a}\right)\ln\left(a(a+x)(a+x_+)^2\right)\Bigg)\,, \end{aligned} \tag{3.134}$$

with the abbreviations

$$x = y_+ - \alpha + \sqrt{(y_+-\alpha)\left(\frac{1}{y_+} - \alpha + \frac{4\mu_j^2\mu_k^2}{(\mu_j^2-(1-\mu_k)^2)(1-\mu_j^2-\mu_k^2)}\right)}, \tag{3.135}$$

$$a = \frac{2\mu_k}{1-\mu_j^2-\mu_k^2}\,, \tag{3.136}$$

$$b = \frac{2(1-\mu_k)}{1-\mu_j^2-\mu_k^2}\,, \tag{3.137}$$

$$c = \frac{2\mu_k(1-\mu_k)}{1-\mu_j^2-\mu_k^2}\,, \tag{3.138}$$

$$d = \frac{1}{2}(1-\mu_j^2-\mu_k^2)\,. \tag{3.139}$$

In Eq. (3.134), one has to be careful in some specific cases. For example, if $b = x_+$, the following terms have to be rewritten

$$\begin{aligned}
&\mathrm{Li}_2\left(\frac{x_+-x}{x_+-b}\right) - \mathrm{Li}_2\left(\frac{x_+}{x_+-b}\right) - \ln\left((a+x)(b-x_+)\right)\ln\left(x_+-x\right)\\
&+\ln\left(a(b-x_+)\right)\ln(x_+)\\
&= -\mathrm{Li}_2\left(\frac{x_+-b}{x_+-x}\right) + \mathrm{Li}_2\left(\frac{x_+-b}{x_+}\right) + \frac{1}{2}\ln^2(x_+) - \frac{1}{2}\ln^2(x_+-x)\\
&-\ln(a+x)\ln(x_+-x) + \ln(a)\ln(x_+),
\end{aligned} \tag{3.140}$$

where $\mathrm{Li}_2\left(\frac{x_+-b}{x_+-x}\right) = \mathrm{Li}_2\left(\frac{x_+-b}{x_+}\right) = 0$ and the remaining terms are well defined. Another issue can occur in the case $x_- + b = 0$. In this case we also have to rewrite some terms

$$\begin{aligned}
&-\mathrm{Li}_2\left(\frac{x_--x}{x_-+c}\right) + \mathrm{Li}_2\left(\frac{x_-}{x_-+c}\right) + \ln\left(\frac{x_--x}{x_-}\right)\ln\left(\frac{c+x_-}{a+x_-}\right)\\
&= \mathrm{Li}_2\left(\frac{x_-+c}{x_--x}\right) - \mathrm{Li}_2\left(\frac{x_-+c}{x_-}\right)\\
&+\frac{1}{2}\left(-2\ln(a+x_-)\ln\left(1-\frac{x}{x_-}\right) + \ln^2(x-x_-) - \ln^2(-x_-)\right),
\end{aligned} \tag{3.141}$$

where the dilogs are again zero in the given case.

The α-dependence of collinear part for the case under consideration is given by

$$\begin{aligned}
\Delta I_{gQ,k} = &\left(\frac{3}{2}(1+\alpha) + \frac{1}{1-\mu_k} - \frac{2(2-2\mu_j^2-\mu_k)}{1-\mu_j^2-\mu_k^2}\right.\\
&+\frac{(1-\alpha)\mu_j^2}{2(\mu_j^2+\alpha(1-\mu_j^2-\mu_k^2))}\\
&-2\ln\left(\frac{\alpha(1-\mu_j^2-\mu_k^2)}{(1-\mu_k)^2-\mu_j^2}\right) + \frac{1+\mu_j^2-\mu_k^2}{2(1-\mu_j^2-\mu_k^2)}\\
&\left.\cdot\ln\left(\frac{\mu_j^2+\alpha(1-\mu_j^2-\mu_k^2)}{(1-\mu_k)^2}\right)\right)\,.
\end{aligned} \tag{3.142}$$

Case 3

The case of a massless quark splitting into a massless quark and a gluon with a massive spectator is closely related to case 2 above. The eikonal integrals are given in case 2 by replacing $m_Q \to 0$. The α-dependent collinear part can be found in Eq. (3.142) setting $m_Q \to 0$.

Final $g \to g + g$ splitting

The only massive parton in this case can be the spectator. The decomposition of the integrated subtraction term reads

$$I_{gg,k}(\epsilon, \alpha) = \left[2\left(I^{\text{eik}}(\varepsilon) + \Delta I^{\text{eik}}(\alpha)\right) + \left(I^{\text{coll}}_{gg,k}(\epsilon) + \Delta I^{\text{coll}}_{gg,k}(\alpha)\right)\right] . \tag{3.143}$$

The eikonal integrals are given in Eq. (3.132) and Eq. (3.134) with $m_Q \to 0$. The α-independent collinear integral was calculated in [22]

$$\begin{aligned} I^{\text{coll}}_{gg,k}(\mu_k; \varepsilon) \; = & \frac{11}{6\varepsilon} + \frac{50}{9} - \frac{11}{3}\left[\frac{\mu_k}{1+\mu_k} + \ln(1-\mu_k)\right] + \frac{(2-3\kappa)\mu_k^2}{3(1-\mu_k^2)} \ln\left(\frac{2\mu_k}{1+\mu_k}\right) \\ & + \mathrm{O}(\epsilon) , \end{aligned} \tag{3.144}$$

and the α-dependence in [27]

$$\begin{aligned} \Delta I_{gg,k} \;\; = \;\; & -\frac{11}{6}\left(\frac{1-\mu_k-\alpha(1+\mu_k)}{1+\mu_k} + \ln\left(\frac{\alpha(1+\mu_k)}{1-\mu_k}\right)\right) \\ & -\left(\kappa - \frac{2}{3}\right)\frac{\mu_k^2}{1-\mu_k^2} \ln\left(\frac{(1-\alpha)(1+\mu_k)}{2\mu_k}\right) . \end{aligned} \tag{3.145}$$

$gl \to q + \bar{q}$

In the case of a gluon splitting into a massless quark-antiquark pair with a massive spectator, only the collinear part of the integral is needed, since no soft singularity is present. The integral is split up into an ϵ-dependent part and an α-dependent part, according to [27]

$$I_{ij,k}(\epsilon) \to I_{ij,k}(\epsilon, \alpha) = I_{ij,k}(\epsilon) + \Delta I_{ij,k}(\alpha) . \tag{3.146}$$

The complete integrated subtraction is given by [22]

$$I_{q\bar{q},k}(0, \mu_k; \varepsilon) = T_{\text{R}}\, I^{\text{coll}}_{q\bar{q},k}(0, \mu_k; \varepsilon) . \tag{3.147}$$

By performing the limit $\mu_Q \to 0$ in

$$\begin{aligned} I^{\text{coll}}_{Q\bar{Q},k}(\mu_Q, \mu_k; \varepsilon) \;\; = \;\; & -\frac{2}{3}\left[\frac{1}{\varepsilon}\left(1 - \mu_Q^{-2\varepsilon}\right) - 2\ln(1-\mu_k)\right. \\ & - \;\; \left. 2\ln\left(\frac{1+\rho_1}{2}\right) + \frac{2}{3}\rho_1(3+\rho_1^2) - \frac{2\rho_1^3\mu_k}{1+\mu_k}\right] \\ & + \;\; \left(\kappa - \frac{2}{3}\right)\frac{2\mu_k^2}{1-\mu_k^2}\left[\rho_2^3 \ln\left(\frac{\rho_2-\rho_1}{\rho_2+\rho_1}\right)\right. \\ & - \;\; \left. \ln\left(\frac{1-\rho_1}{1+\rho_1}\right) - \frac{8\rho_1\mu_Q^2}{1-\mu_k^2}\right] + \mathrm{O}(\epsilon) , \end{aligned} \tag{3.148}$$

Nr.	Case	DipoleTerm	αIntDipole
111	$Q \to g + Q$	D^k_{gQ}	I^a_{gQ}

Table 3.7: FS Emitter - IS Spectator

one gets

$$I^{\text{coll}}_{q\bar{q},k}(0,\mu_k;\varepsilon) = -\frac{2}{3}\left[\frac{1}{\varepsilon} - 2\ln(1-\mu_k) + \frac{8}{3} - \frac{2\mu_k}{1+\mu_k}\right] + \left(\kappa - \frac{2}{3}\right)\frac{2\mu_k^2}{1-\mu_k^2}\left[\ln\left(\frac{2\mu_k}{\mu_k+1}\right)\right] + \mathrm{O}(\epsilon)\,. \tag{3.149}$$

The corresponding α-dependence was calculated in [27] and reads

$$\Delta I_{q\bar{q},k}(\alpha) = \frac{2}{3}\left(\frac{1-\mu_k-\alpha(1+\mu_k)}{1+\mu_k} + \ln\left(\frac{\alpha(1+\mu_k)}{1-\mu_k}\right)\right) \tag{3.150}$$

$$+ \left(\kappa - \frac{2}{3}\right)\frac{2\mu_k^2}{1-\mu_k^2}\ln\left(\frac{(1-\alpha)(1+\mu_k)}{2\mu_k}\right)\,. \tag{3.151}$$

3.4.2.2 Spectator: initial-state - Emitter: final-state

In the case of a final-state emitter and an initial-state spectator, the phase-space factorization gains an additional convolution due to the rescaled incoming momentum $\tilde{p}_a = xp_a$. Therefore, the factorization of the three-particle phase space $\mathrm{d}\phi(\widetilde{p}_i,\widetilde{p}_j;Q+\widetilde{p}_a)$ into the two-particle phase space $\mathrm{d}\phi(\widetilde{p}_{ij};Q+\widetilde{p}_a)$ and the one-parton subspace $[\mathrm{d}p_i(\widetilde{p}_{ij};p_a,x)]$ with the kinematics of Section (3.3.5.2) reads [22]

$$\mathrm{d}\phi(p_i,p_j;Q+p_a) = \int_0^1 \mathrm{d}x\;\mathrm{d}\phi\Big(\widetilde{p}_{ij};Q+xp_a\Big)\;[\mathrm{d}p_i(\widetilde{p}_{ij};p_a,x)]\;\Theta(x_+-x)\,, \tag{3.152}$$

with

$$x_+ = 1+\mu_{ij}^2-(\mu_i+\mu_j)^2. \tag{3.153}$$

The integration of the unresolved parton after the factorization is given by

$$\int[\mathrm{d}p_i(\widetilde{p}_{ij};p_a,x)] = \frac{1}{4}(2\pi)^{-3+2\varepsilon}(2\widetilde{p}_{ij}p_a)^{1-\varepsilon}\int_0^{x_+}\mathrm{d}x_{ij,a}\,\delta(x-x_{ij,a})\,(1-x+\mu_{ij}^2)^{-\varepsilon} \times \int \mathrm{d}^{d-3}\Omega\int_{z_-(x)}^{z_+(x)}\mathrm{d}\tilde{z}_i\;[z_+(x)-\tilde{z}_i]^{-\varepsilon}\,[\tilde{z}_i-z_-(x)]^{-\varepsilon} \tag{3.154}$$

where the integration boundaries are

$$z_\pm(x) = \frac{1-x+\mu_{ij}^2+\mu_i^2-\mu_j^2 \pm \sqrt{(1-x+\mu_{ij}^2-\mu_i^2-\mu_j^2)^2-4\mu_i^2\mu_j^2}}{2(1-x+\mu_{ij}^2)}. \tag{3.155}$$

The phase space restriction in the final-state emitter case with an initial-state spectator is applied to the kinematical variable

$$x_{ij,a} = \frac{p_a p_i + p_a p_j - p_i p_j + \frac{1}{2}(m_{ij}^2 - m_i^2 - m_j^2)}{p_a p_i + p_a p_j}. \tag{3.156}$$

Hence, the α-dependence of the integrated subtraction terms is due to the replacement

$$\int [\mathrm{d}p_i(\widetilde{p}_{ij}; p_a, x)] \to \int [\mathrm{d}p_i(\widetilde{p}_{ij}; p_a, x)] \Theta(x_{ij,a} - 1 + \alpha), \tag{3.157}$$

which affects the integration boundaries of the integration over the unresolved parton.

$Q \to Q + g$

Since we only consider massless particles in the initial-state, only the splitting of a massive quark into a gluon and a massive quark with a massless initial-state spectator occurs. In [24], the integration over the one parton subspace is performed. The result is decomposed into parts proportional to the delta-function, plus-distribution and a rational part according to

$$\begin{aligned} I^a_{gQ}(x_{gQ,a}; \epsilon, \alpha) &= C_F \Big\{ \delta(1 - x_{gQ,a})\, J^{a\,\delta}_{gQ}(\mu_Q, \epsilon, \alpha) + J^{a\,+}_{gQ}(x_{gQ,a}, \mu_Q, \alpha) \\ &+ J^{a\,\mathrm{R}}_{gQ}(x_{gQ,a}, \mu_Q, \alpha) \Big\} + \mathrm{O}(\epsilon). \end{aligned} \tag{3.158}$$

Defining μ_Q as

$$\mu_Q^2 = \frac{m^2}{2\tilde{p}_{ij} p_a} \tag{3.159}$$

the functions $J^{a\,\delta}_{gQ}$, $J^{a\,+}_{gQ}$ and $J^{a\,\mathrm{R}}_{gQ}$ are given by

$$\begin{aligned} J^{a\,\delta}_{gQ}(\mu, \epsilon, \alpha) &= \frac{1}{\epsilon} - \frac{1}{\epsilon} \ln\left(\frac{1 + \left(\frac{\mu}{x}\right)^2}{\left(\frac{\mu}{x}\right)^2} \right) - 2\mathrm{Li}_2(-\left(\frac{\mu}{x}\right)^2) - \frac{\pi^2}{3} \\ &\quad + 2 + 2\ln(\alpha) \Big[\ln\left(\frac{1 + \left(\frac{\mu}{x}\right)^2}{\left(\frac{\mu}{x}\right)^2} \right) - 1 \Big] \\ &\quad + \frac{1}{2} \ln^2\left(\frac{\mu}{x}\right)^2 + \frac{1}{2} \ln^2\left(1 + \left(\frac{\mu}{x}\right)^2\right) \\ &\quad - 2\ln\left(\frac{\mu}{x}\right)^2 \ln\left(1 + \left(\frac{\mu}{x}\right)^2\right) + \ln\left(\left(\frac{\mu}{x}\right)^2\right) \end{aligned} \tag{3.160}$$

$$J^{a\,+}_{gQ}(x, \mu, \alpha) = \Big[\ln\left(\frac{1 + \left(\frac{\mu}{x}\right)^2}{\left(\frac{\mu}{x}\right)^2} \right) - 1 \Big] \left(\frac{2}{1 - x} \right)_{1-\alpha}$$

$$[J^{a\,R}_{gQ}(x, \mu, \alpha)] = \left\{ \frac{1 - x}{2(1 - x + \mu^2)^2} + \frac{2}{(1 - x)} \ln\left(\frac{(2 - x + \mu^2)\left(\frac{\mu}{x}\right)^2}{(1 + \left(\frac{\mu}{x}\right)^2)(1 - x + \mu^2)} \right) \right\}$$

$$\cdot\Theta(x-1+\alpha), \tag{3.161}$$

where the $(1-\alpha)$ distribution is defined as

$$\int_0^1 dx\ f(x)\left(\frac{1}{1-x}\right)_{1-\alpha} = \int_{1-\alpha}^1 dx\ \frac{(f(x)-f(1))}{1-x}. \tag{3.162}$$

3.4.2.3 Spectator: final-state - Emitter: initial-state

Nr.	Case	DipoleTerm	Type	α IntDipole
121	$\bar{q} \to \bar{q}_a + g_i$	D_k^{gq}	$M_{sp} \neq 0$	I_{qq}^{Q}
121	$q \to q_a + g_i$	D_k^{gq}	$M_{sp} \neq 0$	I_{qq}^{Q}
122	$\bar{q} \to g_a + \bar{q}_i$	D_k^{gq}	$M_{sp} \neq 0$	$I_{qg}^{\mathbf{k}}$
122	$q \to g_a + q_i$	D_k^{gq}	$M_{sp} \neq 0$	$I_{qg}^{\mathbf{k}}$
124	$g \to q_a + \bar{q}_i$	D_k^{qq}	$M_{sp} \neq 0$	$I_{qq}^{\mathbf{k}}$
124	$g \to \bar{q}_a + q_i$	D_k^{qq}	$M_{sp} \neq 0$	$I_{qq}^{\mathbf{k}}$
125	$g \to g_a + g_i$	D_k^{gg}	$M_{sp} \neq 0$	$I_{gg}^{\mathbf{k}}$

Table 3.8: IS Emitter - FS Spectator
Index a labels a parton going into the hard process and Index i labels a final-state parton.

When an initial-state emitter and a final-state spectator are present, the phase-space factorization acquires an additional convolution due to the rescaling of the incoming momenta. The factorization is therefore similar to the case of a final-state emitter and an initial-state spectator, namely

$$\mathrm{d}\phi(p_i,p_j;Q+p_a) = \int_0^1 \mathrm{d}x\,\mathrm{d}\phi\Big(\widetilde{p}_j;Q+xp_a\Big)\int[\mathrm{d}p_i(\widetilde{p}_j;p_a,x)]. \tag{3.163}$$

The integration over the one parton subspace is given by

$$\begin{aligned}\int[\mathrm{d}p_i(\widetilde{p}_j;p_a,x)] \ &= \frac{1}{4}(2\pi)^{-3+2\varepsilon}(2\widetilde{p}_j p_a)^{1-\varepsilon}\int_0^1 \mathrm{d}x_{ij,a}\,\delta(x-x_{ij,a})\,(1-x+\mu_j^2)^{-\varepsilon} \\ &\times\int \mathrm{d}^{d-3}\Omega\int_0^{z_+(x)}\mathrm{d}\tilde{z}_i\ [z_+(x)-\tilde{z}_i]^{-\varepsilon}\,\tilde{z}_i^{-\varepsilon}\,,\end{aligned} \tag{3.164}$$

with the upper limit of the z-integration being

$$z_+(x) = \frac{1-x}{1-x+\mu_j^2}. \tag{3.165}$$

The integrated subtraction terms gain the α-dependency by multiplying Eq. (3.164) with $\Theta(\alpha - z_i)$, i.e.

$$\int[\mathrm{d}p_i(\widetilde{p}_j;p_a,x)] \to \int[\mathrm{d}p_i(\widetilde{p}_j;p_a,x)]\Theta(\alpha-z_i). \tag{3.166}$$

The possible splittings that can occur in this case are listed in the following. The index a labels the parton going into the hard process whereas i labels the parton contributing to the final-state.

1. $q(\overline{q}) \to q_a(\overline{q}_a) + g_i$ with massive spectator
2. $q(\overline{q}) \to g_a + q_i(\overline{q}_i)$ with massive spectator
3. $g \to q_a(\overline{q}_a) + \overline{q}_i(q_i)$ with massive spectator
4. $g \to g_a + g_i$ with massive spectator.

Initial-state massive partons are again not possible.

Case 1: $q(\overline{q}) \to q_a(\overline{q}_a) + g_i$

The integration of the corresponding splitting function is worked out in [24] and yields

$$
\begin{aligned}
I_Q^{qq}(x;\epsilon,\alpha) = C_F \Bigg\{ & -\frac{1}{\epsilon}\Big[\frac{2}{[1-x]_+} - 1 - x\Big] + \delta(1-x)\Bigg[\frac{1}{\epsilon^2} + \frac{\pi^2}{6} + \frac{1}{\epsilon}\ln(1+\Big(\frac{\mu}{x}\Big)^2) \\
+ \quad & 2\mathrm{Li}_2(-\Big(\frac{\mu}{x}\Big)^2) + 2\ln(\Big(\frac{\mu}{x}\Big)^2)\ln(1+\Big(\frac{\mu}{x}\Big)^2) - \frac{1}{2}\ln^2(1+\Big(\frac{\mu}{x}\Big)^2)\Bigg] \\
+ \quad & 4\left[\frac{\ln(1-x)}{(1-x)}\right]_+ - 2\,\frac{\ln(1+\tilde{\mu}^2)}{[1-x]_+} - \frac{2}{(1-x)}\ln\Big(\frac{2-x+x\left(\frac{\mu}{x}\right)^2}{1+\left(\frac{\mu}{x}\right)^2}\Big) \\
- \quad & \Theta(z_+-\alpha)\left[\left(\frac{2}{1-x}\right)\ln\left(\frac{z_+(1-x+\alpha)}{\alpha(1-x+z_+)}\right) - (1+x)\ln\left(\frac{z_+}{\alpha}\right)\right] \\
- \quad & (1+x)\ln\Big(\frac{(1-x)^2}{(1-x+x\left(\frac{\mu}{x}\right)^2)}\Big) + (1-x)\Bigg\} + \mathrm{O}(\epsilon)\,.
\end{aligned}
\tag{3.167}
$$

Case 2: $q(\overline{q}) \to g_a + q_i(\overline{q}_i)$

The case of a gluon initiating the hard process after being split from an initial-state quark is considered in [26] and yields the α-dependent result

$$
\begin{aligned}
I_Q^{qg}(x;\epsilon,\alpha) = C_F \Bigg\{ & \frac{\left(1+(1-x)^2\right)}{x} \\
\times \quad & \left[\ln\Big(\frac{(1-x)^2}{1-x+x\left(\frac{\mu}{x}\right)^2}\Big) - \frac{1}{\epsilon} - \Theta(z_+-\alpha)\ln\left(\frac{z_+}{\alpha}\right)\right] + \underline{2\left(\frac{\mu}{x}\right)^2} \\
\cdot \quad & \underline{\ln\left(\frac{x\left(\frac{\mu}{x}\right)^2}{1-x+x\left(\frac{\mu}{x}\right)^2}\right)} - \Theta(z_+-\alpha)2\left(\frac{\mu}{x}\right)^2\ln\left(\frac{1-z_+}{1-\alpha}\right) + x\Bigg\}
\end{aligned}
$$

$$+ \quad \mathrm{O}(\epsilon)\,. \tag{3.168}$$

Case 3: $g \to q_a(\overline{q}_a) + \overline{q}_i(q_i)$

The result for this case was also obtained in [26] and reads

$$\begin{aligned} I^{gq}(x;\epsilon,\alpha) &= T_R\Bigg\{\Big(x^2+(1-x)^2\Big)\times\Bigg[\ln\Big(\frac{(1-x)^2}{1-x+x\left(\frac{\mu}{x}\right)^2}\Big)-\frac{1}{\epsilon} \\ &\quad -\Theta(z_+-\alpha)\ln\left(\frac{z_+}{\alpha}\right)\Bigg]+2\;x(1-x)\Bigg\}+\mathrm{O}(\epsilon)\,. \end{aligned} \tag{3.169}$$

Case 4: $g \to g_a + g_i$

The result for the last case is according to [26]

$$\begin{aligned} I_Q^{gg}(x;\epsilon,\alpha) = {} & C_A\Bigg\{\delta(1-x)\Bigg[\frac{1}{\epsilon^2}+\frac{1}{\epsilon}\ln\left(1+\left(\frac{\mu}{x}\right)^2\right)+\frac{\pi^2}{6} \\ & +2\mathrm{Li}_2\left(-\left(\frac{\mu}{x}\right)^2\right)+2\ln\left(\left(\frac{\mu}{x}\right)^2\right)\ln\left(1+\left(\frac{\mu}{x}\right)^2\right)-\frac{1}{2}\ln^2\left(1+\left(\frac{\mu}{x}\right)^2\right)\Bigg] \\ & -\frac{1}{\epsilon}\,\frac{2}{[1-x]_+}-2\,\frac{\ln\left(1+\tilde{\mu}^2\right)}{[1-x]_+}+4\left[\frac{\ln(1-x)}{(1-x)}\right]_+ \\ & +2\left(x(1-x)+\frac{1-x}{x}-1\right)\Bigg[-\frac{1}{\epsilon}+\ln\left(\frac{(1-x)^2}{1-x+x\left(\frac{\mu}{x}\right)^2}\right)-\Theta(z_+-\alpha)\,\ln\left(\frac{z_+}{\alpha}\right)\Bigg] \\ & -\Theta(z_+-\alpha)\Bigg[2\left(\frac{\mu}{x}\right)^2\ln\left(\frac{1-z_+}{1-\alpha}\right)-\frac{2}{(1-x)}\ln\left(\frac{\alpha(1-x+z_+)}{z_+(1-x+\alpha)}\right)\Bigg] \\ & +2\left(\frac{\mu}{x}\right)^2\ln\left(\frac{x\left(\frac{\mu}{x}\right)^2}{1-x+x\left(\frac{\mu}{x}\right)^2}\right)-\frac{2}{(1-x)}\ln\left(\frac{2-x+x\left(\frac{\mu}{x}\right)^2}{1+\left(\frac{\mu}{x}\right)^2}\right)\Bigg\}. \end{aligned} \tag{3.170}$$

3.4.3 Collinear Subtraction Counterterm

We still have to account for the dependence on the factorization scale and on the factorization scheme. Reference [6] introduces a collinear-subtraction counterterm, which depends on both the factorization scheme and factorization scale. For a partonic process with the initial-state emitter a, the collinear-subtraction counterterm is given by

$$\mathrm{d}\sigma_a^{\mathrm{C}}(p;\mu_F^2) = -\frac{\alpha_s}{2\pi}\,\frac{1}{\Gamma(1-\epsilon)}\sum_b\int_0^1 dx\,\left[-\frac{1}{\epsilon}\left(\frac{4\pi\mu^2}{\mu_F^2}\right)^{\epsilon}P^{ab}(x)+K^{ab}_{\mathrm{F.S}}(x)\right]\mathrm{d}\sigma_b^{\mathrm{B}}(xp)\,. \tag{3.171}$$

Here $K^{ab}_{\mathrm{F.S}}(x)$ denotes the factorization scheme and $\sum_b$ the sum over all partons b that a can split into. $K^{ab}_{\mathrm{F.S}}(x) = 0$ indicates the $\overline{\mathrm{MS}}$ subtraction scheme. In order to

implement this term using the one-to-one correspondence of a dipole subtraction term and an integrated subtraction term, we rewrite it as follows

$$I_C^{ab}(x;\mu_F^2,\mu^2) = -\frac{\alpha_s}{2\pi}\,\frac{1}{\Gamma(1-\epsilon)}\left[-\frac{1}{\epsilon}\left(\frac{4\pi\mu^2}{\mu_F^2}\right)^{\epsilon} P^{ab}(x) + K_{\text{F.S.}}^{ab}(x)\right] . \tag{3.172}$$

By specifying the $\overline{\text{MS}}$ subtraction scheme, this yields

$$I_C^{ab}(x;\mu_F^2,\mu^2) = -\frac{\alpha_s}{2\pi}\,\frac{1}{\Gamma(1-\epsilon)}\left[-\frac{1}{\epsilon}\left(\frac{4\pi\mu^2}{\mu_F^2}\right)^{\epsilon} P^{ab}(x)\right] , \tag{3.173}$$

where $P^{ab}(x)$ are the usual four-dimensional Altarelli-Parisi splitting functions given in Eq. (3.186) - Eq. (3.189). For the sake of completeness, we point out two possible but equivalent representations and therefore implementations of +-distributions. This can lead to different results in a comparison at a given phase space point, but still yields the same result after phase space integration. The first term in Eq. (3.167) proportional to $\frac{1}{\varepsilon}$ should be cancelled by the corresponding collinear subtraction counterterm. If we only consider the coefficient of $\frac{1}{\varepsilon}$ and set $\mu = \mu_F$, we get

$$\begin{aligned} I_C^{qq}(x) + I_Q^{qq}(x) &= \frac{\alpha_s}{2\pi}\,\frac{(4\pi)^{\epsilon}}{\Gamma(1-\epsilon)}\left[\frac{1}{\epsilon}P^{qq}(x) - C_F\frac{1}{\epsilon}\Big[\frac{2}{[1-x]_+} - 1 - x\Big]\right] \\ &= \frac{\alpha_s}{2\pi}\,\frac{(4\pi)^{\epsilon}}{\Gamma(1-\epsilon)}\frac{1}{\epsilon}C_F\left[\left(\frac{1+x^2}{1-x}\right)_+\right. \\ &- \left.\Big[\frac{2}{[1-x]_+} - 1 - x\Big]\right] . \end{aligned} \tag{3.174}$$

Integrating this expression with a given test function $f(x)$, we find

$$\begin{aligned} &\int_0^1 \mathrm{d}x\mathrm{d}\Phi(x)\left(I_C^{qq}(x) + I_Q^{qq}(x)\right) f(\Phi(x)) \\ = \;& \frac{\alpha_s}{2\pi}\,\frac{C_F(4\pi)^{\epsilon}}{\Gamma(1-\epsilon)}\frac{1}{\epsilon}\left[\int_0^1 \mathrm{d}x\Phi(x)\,\left(\frac{1+x^2}{1-x}\right) - \Big[\frac{2}{[1-x]} - 1 - x\Big] f(\Phi(x))\right. \\ - \;& \left.\int_0^1 \mathrm{d}x\Phi(1)\,\left(\frac{1+x^2}{1-x}\right) - \Big[\frac{2}{[1-x]}\Big] f(\Phi(1))\right] \\ \overset{(1)}{=} \;& \frac{\alpha_s}{2\pi}\,\frac{C_F(4\pi)^{\epsilon}}{\Gamma(1-\epsilon)}\frac{1}{\epsilon}\left[-\int_0^1 \mathrm{d}x\Phi(1)\,(1+x)\,f(\Phi(1))\right] \\ \overset{(2)}{=} \;& \frac{\alpha_s}{2\pi}\,\frac{C_F(4\pi)^{\epsilon}}{\Gamma(1-\epsilon)}\frac{1}{\epsilon}\left[-\int_0^1 \mathrm{d}x\Phi(1)\,\frac{3}{2}\delta(1-x)\,f(\Phi(1))\right] . \end{aligned} \tag{3.175}$$

Both implementations (1) and (2) are possible and equivalent as shown.

3.4.4 Massless Integrated Subtraction Terms

In this Section, we focus on the massless subtractions terms that do not depend on the phase space restriction parameter α. They can be derived from the α-dependent integrated subtraction terms by setting $\alpha = 1$. This does not cause analytical or numerical issues in any of the cases above, since the phase-space restriction parameter α just shrinks the integration limits and therefore induces no singularities. The explicit expressions for the integrated subtraction terms in each of the cases above can be found in [6]. The integrated subtraction terms can be combined to a complete sum-formula. For the sake of completeness, we present the combined sum-formulas in each case.

3.4.4.1 No initial-state Hadron

If no initial-state hadron is involved, it is sufficient to combine the formulas in Section 3.4.1.1 to derive an expression for the **I**-Operator in Eq. (3.9). The **I**-Operator has generally the same structure as the one in Eq. (3.87) and is given by

$$\boldsymbol{I}(p_1,...,p_m;\epsilon) = -\frac{\alpha_s}{2\pi}\frac{1}{\Gamma(1-\epsilon)}\sum_i \frac{1}{\boldsymbol{T}_i^2}\,\mathcal{V}_i(\epsilon)\,\sum_{k\neq i}\boldsymbol{T}_i\cdot\boldsymbol{T}_k\,\left(\frac{4\pi\mu^2}{2p_i\cdot p_k}\right)^{\epsilon}\quad, \tag{3.176}$$

where

$$\mathcal{V}_i(\epsilon) = \boldsymbol{T}_i^2\left(\frac{1}{\epsilon^2}-\frac{\pi^2}{3}\right)+\gamma_i\,\frac{1}{\epsilon}+\gamma_i+K_i+\mathcal{O}(\epsilon)\ , \tag{3.177}$$

and K_i and γ_i are defined in Eq. (3.89). Following Eq. (3.9), the **I**-Operator has to be inserted in

$$\int_{m+1}\mathrm{d}\sigma^{\mathrm{A}} = \int_m\left[\mathrm{d}\sigma^{\mathrm{B}}\cdot\boldsymbol{I}(\epsilon)\right] \tag{3.178}$$

and can be added to the virtual correction of the full NLO-calculation.

3.4.4.2 One initial-state Hadron

This case involves not only subtraction terms due to singularities in the final-state, but also ones that account for initial-state singularities such as $\mathcal{D}_k^{ai}$. As explained in Section 3, this leads to **K**- and **P**- Operators that depend on the momentum fraction x carried by the colliding parton

$$\int_0^1 dx\int_m \mathrm{d}\sigma_a^{\mathrm{B}}\otimes(\boldsymbol{K}+\boldsymbol{P})\,, \tag{3.179}$$

where the index $_a$ in $\mathrm{d}\sigma_a^{\mathrm{B}}$ label the colliding parton from the initial-state hadron. The complete expression is summed up in [6]

$$\int_{m+1}\mathrm{d}\sigma^{\mathrm{A}}+\sum_{dipoles}\left[\int_m\mathrm{d}\sigma_a^{\mathrm{B}}\otimes\int_1\mathrm{d}V'_{\mathrm{dipole}}\right]$$

$$
\begin{aligned}
&= \int_m \mathrm{d}\sigma_a^{\mathrm{B}}(p) \otimes \boldsymbol{I}(\epsilon) + \int_0^1 dx \int_m \mathrm{d}\sigma_a^{\mathrm{B}}(xp) \otimes (\boldsymbol{K}+\boldsymbol{P}) \\
&= \int_m \left[\mathrm{d}\sigma_a^{\mathrm{B}}(p) \otimes \boldsymbol{I}(\epsilon)\right] \\
&\quad + \sum_b \int_0^1 dx \int_m \left[\left(\boldsymbol{K}^{a,b}(x) + \boldsymbol{P}^{a,b}(xp,x;\mu_F^2)\right) \otimes \mathrm{d}\sigma_b^{\mathrm{B}}(xp)\right] . \qquad (3.180)
\end{aligned}
$$

The Operators $\boldsymbol{I}$, $\boldsymbol{K}$ and $\boldsymbol{P}$ are disclosed in [6] and given by

$$
\begin{aligned}
\boldsymbol{I}(\{p\},p_a;\epsilon) = &- \frac{\alpha_s}{2\pi}\frac{1}{\Gamma(1-\epsilon)} \left\{ \sum_i \frac{1}{\boldsymbol{T}_i^2}\, \mathcal{V}_i(\epsilon) \left[\sum_{k\neq i} \boldsymbol{T}_i\cdot\boldsymbol{T}_k \left(\frac{4\pi\mu^2}{2p_i\cdot p_k}\right)^{\epsilon} \right.\right. \\
&\left.\left. + \boldsymbol{T}_i\cdot\boldsymbol{T}_a \left(\frac{4\pi\mu^2}{2p_i\cdot p_a}\right)^{\epsilon}\right] + \frac{1}{\boldsymbol{T}_a^2}\,\mathcal{V}_a(\epsilon) \sum_i \boldsymbol{T}_i\cdot\boldsymbol{T}_a \left(\frac{4\pi\mu^2}{2p_i\cdot p_a}\right)^{\epsilon} \right\} , \qquad (3.181)
\end{aligned}
$$

$$
\begin{aligned}
\boldsymbol{K}^{a,b}(x) &= \frac{\alpha_s}{2\pi}\left\{ \overline{K}^{ab}(x) - K^{ab}_{\mathrm{F.S}}(x). \right. \\
&+ \left. \delta^{ab} \sum_i \boldsymbol{T}_i\cdot\boldsymbol{T}_b \frac{\gamma_i}{\boldsymbol{T}_i^2}\left[\left(\frac{1}{1-x}\right)_+ + \delta(1-x)\right]\right\} \qquad (3.182)
\end{aligned}
$$

and

$$
\boldsymbol{P}^{a,b}(\{p\};xp_a,x;\mu_F^2) = \frac{\alpha_s}{2\pi}\, P^{ab}(x)\, \frac{1}{\boldsymbol{T}_b^2} \sum_i \boldsymbol{T}_i\cdot\boldsymbol{T}_b\, \ln\frac{\mu_F^2}{2xp_a\cdot p_i} \ . \qquad (3.183)
$$

The functions used to calculate the operators are defined as

$$
\begin{aligned}
&\overline{K}^{ab}(x) = \hat{P}'_{ab}(x) + P^{ab}_{\mathrm{reg}}(x)\, \ln\frac{1-x}{x} \\
&+ \delta^{ab}\left[\boldsymbol{T}_a^2\left(\frac{2}{1-x}\ln\frac{1-x}{x}\right)_+ - \delta(1-x)\left(\gamma_a + K_a - \frac{5}{6}\pi^2\,\boldsymbol{T}_a^2\right)\right] \qquad (3.184)
\end{aligned}
$$

and $\mathcal{V}_i(\epsilon)$ can be found in Eq. (3.177). The regular parts

$$
\begin{aligned}
&P^{ab}_{\mathrm{reg}}(x) = P^{ab}(x) \qquad \text{if } \ a\neq b \ , \\
&P^{qq}_{\mathrm{reg}}(x) = -C_F\,(1+x) \ , \quad P^{gg}_{\mathrm{reg}}(x) = 2\,C_A\left[\frac{1-x}{x} - 1 + x(1-x)\right] \qquad (3.185)
\end{aligned}
$$

of the Altarelli-Parisi splitting functions can be read of from

$$
P^{qg}(x) = P^{\bar{q}g}(x) = C_F\,\frac{1+(1-x)^2}{x} \ , \qquad (3.186)
$$

$$
P^{gq}(x) = P^{g\bar{q}}(x) = T_R\left[x^2+(1-x)^2\right] \ , \qquad (3.187)
$$

$$P^{qq}(x) = P^{\bar{q}\bar{q}}(x) = C_F \left(\frac{1+x^2}{1-x}\right)_+ , \tag{3.188}$$

$$P^{gg}(x) = 2C_A \left[\left(\frac{1}{1-x}\right)_+ + \frac{1-x}{x} - 1 + x(1-x)\right] + \delta(1-x)\left(\frac{11}{6}C_A - \frac{2}{3}N_f T_R\right) . \tag{3.189}$$

3.4.4.3 Two initial-state Hadrons

The case of two initial-state hadrons is closely related to the one with one hadron in the initial-state. One has to additionally correct for the correlation between the initial-state particles. The $\boldsymbol{I}$-operator is the same as in Eq. (3.181) except for the new (underlined) terms

$$\begin{aligned}
\boldsymbol{I}(\{p\}, p_a, p_b; \epsilon) = &- \frac{\alpha_s}{2\pi}\frac{1}{\Gamma(1-\epsilon)} \Bigg\{ \sum_i \frac{1}{\boldsymbol{T}_i^2}\, \mathcal{V}_i(\epsilon) \Bigg[\sum_{k\neq i} \boldsymbol{T}_i \cdot \boldsymbol{T}_k \left(\frac{4\pi\mu^2}{2p_i\cdot p_k}\right)^{\epsilon} \\
&+ \boldsymbol{T}_i \cdot \boldsymbol{T}_a \left(\frac{4\pi\mu^2}{2p_i\cdot p_a}\right)^{\epsilon} + \underline{\boldsymbol{T}_i \cdot \boldsymbol{T}_b \left(\frac{4\pi\mu^2}{2p_i\cdot p_b}\right)^{\epsilon}} \Bigg] \\
&+ \frac{1}{\boldsymbol{T}_a^2}\, \mathcal{V}_a(\epsilon) \left[\sum_i \boldsymbol{T}_i \cdot \boldsymbol{T}_a \left(\frac{4\pi\mu^2}{2p_i\cdot p_a}\right)^{\epsilon} + \underline{\boldsymbol{T}_b \cdot \boldsymbol{T}_a \left(\frac{4\pi\mu^2}{2p_b\cdot p_a}\right)^{\epsilon}} \right] \\
&+ \underline{\frac{1}{\boldsymbol{T}_b^2}\, \mathcal{V}_b(\epsilon) \left[\sum_i \boldsymbol{T}_i \cdot \boldsymbol{T}_b \left(\frac{4\pi\mu^2}{2p_i\cdot p_b}\right)^{\epsilon} + \boldsymbol{T}_b \cdot \boldsymbol{T}_a \left(\frac{4\pi\mu^2}{2p_b\cdot p_a}\right)^{\epsilon} \right]} \Bigg\} .
\end{aligned} \tag{3.190}$$

The insertion operators for $\boldsymbol{K}$ and $\boldsymbol{P}$ are also the same as in the one hadron initial-state case, apart from the red terms that are due to initial-state parton correlations

$$\begin{aligned}
\boldsymbol{K}^{a,a'}(x) = \frac{\alpha_s}{2\pi} \Bigg\{ &\overline{K}^{aa'}(x) - K_{\text{F.S}}^{aa'}(x) \\
&+ \delta^{aa'} \sum_i \boldsymbol{T}_i \cdot \boldsymbol{T}_a \frac{\gamma_i}{\boldsymbol{T}_i^2} \left[\left(\frac{1}{1-x}\right)_+ + \delta(1-x)\right] \Bigg\} - \underline{\frac{\alpha_s}{2\pi} \boldsymbol{T}_b \cdot \boldsymbol{T}_{a'} \frac{1}{\boldsymbol{T}_{a'}^2} \widetilde{K}^{aa'}(x)} ,
\end{aligned} \tag{3.191}$$

$$\begin{aligned}
&\boldsymbol{P}^{a,a'}(p_1, ..., p_m, p_b; x p_a, x; \mu_F^2) \\
&\quad = \frac{\alpha_s}{2\pi}\, P^{aa'}(x)\, \frac{1}{\boldsymbol{T}_{a'}^2} \Bigg[\sum_i \boldsymbol{T}_i \cdot \boldsymbol{T}_{a'}\, \ln\frac{\mu_F^2}{2x p_a \cdot p_i} \\
&\quad + \underline{\boldsymbol{T}_b \cdot \boldsymbol{T}_{a'}\, \ln\frac{\mu_F^2}{2x p_a \cdot p_b}} \Bigg] .
\end{aligned} \tag{3.192}$$

The final expression is given by

$$\int_{m+1} \mathrm{d}\sigma_{ab}^{\mathrm{A}} + \sum_{dipoles} \left[\int_m \mathrm{d}\sigma_{ab}^{\mathrm{B}} \otimes \int_1 \mathrm{d}V'_{\mathrm{dipole}} \right] = \int_m \left[\mathrm{d}\sigma_{ab}^{\mathrm{B}}(p, \bar{p}) \cdot \boldsymbol{I}(\epsilon) \right] \tag{3.193}$$

$$+\sum_{a'}\int_0^1 dx\ \int_m \Big[\Big(\boldsymbol{K}^{a,a'}(x)+\boldsymbol{P}^{a,a'}(xp,x;\mu_F^2)\Big)\otimes \mathrm{d}\sigma^{\mathrm{B}}_{a'b}(xp,\bar{p})\Big]$$
$$+\sum_{b'}\int_0^1 dx\ \int_m \Big[\Big(\boldsymbol{K}^{b,b'}(x)+\boldsymbol{P}^{b,b'}(x\bar{p},x;\mu_F^2)\Big)\otimes \mathrm{d}\sigma^{\mathrm{B}}_{ab'}(p,x\bar{p})\Big]\quad .$$

3.4.5 Massive Integrated Subtraction Terms

The massive integrated subtraction terms that do not depend on the phase-space restriction parameter can also be derived from the formulas in Section 3.4.2 by setting $\alpha = 1$. As stated above, the limit $\alpha \to 1$ causes no analytical or numerical issues. The α-independent integrated subtraction terms displayed in the following were calculated by [22].

3.4.5.1 No initial-state Hadrons

In order to simplify the equations, we introduce in the following Chapters some abbreviations. Some functions will depend on the masses of the emitter m_j and the spectator m_k, which we both denote with $\{m\}$. In the case of a splitting into a massive quark-antiquark pair, the masses of all possible massive quark flavours a gluon can split into will be in accordance to [22] denoted as $\{m_F\}$. Two kinematical variables ρ_1 and ρ_2 are also needed in the following formulas

$$\rho_1 = \sqrt{1-\frac{4m_F^2}{(Q_{jk}-m_k)^2}}\,, \qquad \rho_2 = \sqrt{1-\frac{4m_F^2}{Q_{jk}^2-m_k^2}} \tag{3.194}$$

which depend on $Q_{jk}^2 = 2p_jp_k + m_j^2 + m_k^2$. Since we do not consider initial-state hadrons in this case, we focus on Eq. (3.10). The $\boldsymbol{I}_m$-operator has a similar structure as Eq. (3.176) and is given by

$$\begin{aligned}\boldsymbol{I}_m(\epsilon,\mu^2;\{p\}) = &-\frac{\alpha_s}{2\pi}\frac{(4\pi)^\epsilon}{\Gamma(1-\epsilon)}\sum_j \frac{1}{\boldsymbol{T}_j^2}\sum_{k\neq j}\boldsymbol{T}_j\cdot\boldsymbol{T}_k\\ &\times\Bigg[\boldsymbol{T}_j^2\left(\frac{\mu^2}{s_{jk}}\right)^\epsilon\left(\mathcal{V}_j(s_{jk},\{m\},\{m_F\};\epsilon,\kappa)-\frac{\pi^2}{3}\right)+\Gamma_j(\mu,m_j,\{m_F\};\epsilon)\\ &+\gamma_j\ln\frac{\mu^2}{s_{jk}}+\gamma_j+K_j+\mathrm{O}(\varepsilon)\Bigg]\end{aligned} \tag{3.195}$$

The constants K_i and γ_i are defined in Eq. (3.89), $s_{jk} = 2p_jp_k$ and the function $\mathcal{V}_j$ are decomposed into a singular ($\mathcal{V}_j^{(S)}$) and a non-singular ($\mathcal{V}_j^{(NS)}$) part

$$\mathcal{V}_j(s_{jk},\{m\},\{m_F\};\epsilon,\kappa) = \mathcal{V}^{(\mathrm{S})}(s_{jk},\{m\};\epsilon) + \mathcal{V}_j^{(\mathrm{NS})}(s_{jk},\{m\},\{m_F\};\kappa)\,. \tag{3.196}$$

The first part cancels the singularities in ϵ arising from $\mathrm{d}\sigma^{\mathrm{V}}$, but also leads to finite contributions as the following expressions show

$$\begin{aligned}
\mathcal{V}^{(\mathrm{S})}(s_{jk}, m_j > 0, m_k > 0; \epsilon) &= \frac{1}{v_{jk}} \left[\frac{1}{\epsilon} \ln \rho - \frac{1}{4} \ln^2 \rho_j^2 - \frac{1}{4} \ln^2 \rho_k^2 - \frac{\pi^2}{6} \right] \\
&\quad + \frac{1}{v_{jk}} \ln \rho \ln \left(\frac{Q_{jk}^2}{s_{jk}} \right) , \\
\mathcal{V}^{(\mathrm{S})}(s_{jk}, m_j > 0, 0; \epsilon) &= \frac{1}{2\epsilon^2} + \frac{1}{2\epsilon} \ln \frac{m_j^2}{s_{jk}} - \frac{1}{4} \ln^2 \frac{m_j^2}{s_{jk}} - \frac{\pi^2}{12} \\
&\quad - \frac{1}{2} \ln \frac{m_j^2}{s_{jk}} \ln \frac{s_{jk}}{Q_{jk}^2} - \frac{1}{2} \ln \frac{m_j^2}{Q_{jk}^2} \ln \frac{s_{jk}}{Q_{jk}^2} , \\
\mathcal{V}^{(\mathrm{S})}(s_{jk}, 0, 0; \epsilon) &= \frac{1}{\epsilon^2} ,
\end{aligned} \tag{3.197}$$

where $\mu_n^2 \to m_n^2/Q_{jk}^2$ and $\tilde{v}_{ij,k} \to v_{jk}$. The non-singular functions $\mathcal{V}_j^{(NS)}$ are given in all three possible mass configurations

- $m_j > 0, m_k > 0$
- $m_j > 0, m_k = 0$
- $m_j = 0, m_k > 0$

and evaluated for both cases $j =$ quark or $j =$ gluon:

$$\begin{aligned}
\mathcal{V}_q^{(\mathrm{NS})}(s_{jk}, m_j, m_k) &= \frac{\gamma_q}{\boldsymbol{T}_q^2} \ln \frac{s_{jk}}{Q_{jk}^2} \\
&\quad + \frac{1}{v_{jk}} \left[\ln \rho^2 \ln(1+\rho^2) + 2\mathrm{Li}_2(\rho^2) - \mathrm{Li}_2(1-\rho_j^2) - \mathrm{Li}_2(1-\rho_k^2) - \frac{\pi^2}{6} \right] \\
&\quad + \ln \frac{Q_{jk} - m_k}{Q_{jk}} - 2 \ln \frac{(Q_{jk} - m_k)^2 - m_j^2}{Q_{jk}^2} - \frac{2m_j^2}{s_{jk}} \ln \frac{m_j}{Q_{jk} - m_k} \\
&\quad - \frac{m_k}{Q_{jk} - m_k} + \frac{2m_k(2m_k - Q_{jk})}{s_{jk}} + \frac{\pi^2}{2} ,
\end{aligned} \tag{3.198}$$

$$\mathcal{V}_q^{(\mathrm{NS})}(s_{jk}, m_j, 0) = \frac{\gamma_q}{\boldsymbol{T}_q^2} \ln \frac{s_{jk}}{Q_{jk}^2} + \frac{\pi^2}{6} - \mathrm{Li}_2 \left(\frac{s_{jk}}{Q_{jk}^2} \right) - 2 \ln \frac{s_{jk}}{Q_{jk}^2} - \frac{m_j^2}{s_{jk}} \ln \frac{m_j^2}{Q_{jk}^2} , \tag{3.199}$$

$$\mathcal{V}_q^{(\mathrm{NS})}(s_{jk}, 0, m_k) = \frac{\gamma_q}{\boldsymbol{T}_q^2} \left[\ln \frac{s_{jk}}{Q_{jk}^2} - 2 \ln \frac{Q_{jk} - m_k}{Q_{jk}} - \frac{2m_k}{Q_{jk} + m_k} \right] + \frac{\pi^2}{6} - \mathrm{Li}_2 \left(\frac{s_{jk}}{Q_{jk}^2} \right) , \tag{3.200}$$

$$\mathcal{V}_j^{(\mathrm{NS})}(s_{jk}, 0, m_k, \{m_F\}; \kappa) =$$

$$
\begin{aligned}
&\frac{\gamma_g}{\boldsymbol{T}_g^2}\left[\ln\frac{s_{jk}}{Q_{jk}^2}-2\ln\frac{Q_{jk}-m_k}{Q_{jk}}-\frac{2m_k}{Q_{jk}+m_k}\right]+\frac{\pi^2}{6}-\mathrm{Li}_2\left(\frac{s_{jk}}{Q_{jk}^2}\right)\\
&+\frac{4}{3}\frac{T_\mathrm{R}}{C_\mathrm{A}}\sum_{F=1}^{N_F^{jk}}\left[\ln\frac{Q_{jk}-m_k}{Q_{jk}}+\frac{m_k\,\rho_1^3}{Q_{jk}+m_k}+\ln\frac{1+\rho_1}{2}-\frac{\rho_1}{3}(3+\rho_1^2)-\frac{1}{2}\ln\frac{m_F^2}{Q_{jk}^2}\right]\\
&+\frac{2}{3}\frac{T_\mathrm{R}}{C_\mathrm{A}}\sum_{F=1}^{N_F}\ln\frac{m_F^2}{Q_{\mathrm{aux}}^2}+\left(\kappa-\frac{2}{3}\right)\frac{m_k^2}{s_{jk}}\left[\left(2\frac{T_\mathrm{R}}{C_\mathrm{A}}N_f-1\right)\ln\frac{2m_k}{Q_{jk}+m_k}\right.\\
&\qquad+2\frac{T_\mathrm{R}}{C_\mathrm{A}}\sum_{F=1}^{N_F^{jk}}\left(\rho_2^3\ln\left(\frac{\rho_2-\rho_1}{\rho_2+\rho_1}\right)\right.\\
&\qquad\left.\left.-\ln\left(\frac{1-\rho_1}{1+\rho_1}\right)-\frac{8\rho_1 m_F^2}{s_{jk}}\right)\right],
\end{aligned}
\tag{3.201}
$$

$$
\begin{aligned}
&\mathcal{V}_g^{(\mathrm{NS})}(s_{jk},0,0,\{m_F\})=\\
&\qquad\frac{4}{3}\frac{T_\mathrm{R}}{C_\mathrm{A}}\sum_{F=1}^{N_F^{jk}}\left[\ln\frac{1+\rho_1}{2}-\frac{\rho_1}{3}(3+\rho_1^2)-\frac{1}{2}\ln\frac{m_F^2}{s_{jk}}\right]\\
&\qquad+\frac{2}{3}\frac{T_\mathrm{R}}{C_\mathrm{A}}\sum_{F=1}^{N_F}\ln\frac{m_F^2}{Q_{\mathrm{aux}}^2}\,,
\end{aligned}
\tag{3.202}
$$

$$
\mathcal{V}_g^{(\mathrm{NS})}(s_{jk},0,0,\{\})=0. \tag{3.203}
$$

The index variable N_F occurring as upper limit for a sum in the last two equations denotes the number of heavy quark flavours a gluon can split into. N_{ij}^F is the number of heavy quark flavours for which $s_{jk} > 4m_F(m_F+m_k)$ and thus depends additionally on the phase space point. The arbitrary auxiliary mass scale Q_{aux} ensures finiteness in the massless limit and cancels against a contribution in $\Gamma_g(\{m_F\};\epsilon)$. The Γ_j functions read

$$
\Gamma_g(\{m_F\};\epsilon) = \frac{1}{\epsilon}\,\gamma_g-\frac{2}{3}\,T_\mathrm{R}\sum_{F=1}^{N_F}\ln\frac{m_F^2}{Q_{\mathrm{aux}}^2}\,, \tag{3.204}
$$

$$
\Gamma_q(\epsilon) = \frac{1}{\epsilon}\,\gamma_q\,, \tag{3.205}
$$

$$
\Gamma_q(\mu,m_q;\epsilon)=C_\mathrm{F}\left[\frac{1}{\epsilon}+\frac{1}{2}\ln\frac{m_q^2}{\mu^2}-2\right]. \tag{3.206}
$$

3.4.5.2 One initial-state Hadron

In the presence of one hadron in the initial-state the structure of the integrated subtraction terms is similar to the massless case. Due to collinear initial-state singularities the $\boldsymbol{K}$- and $\boldsymbol{P}$-operators arise, as was the case in the massive version of Eq. (3.180). The $\boldsymbol{I}$-operator decomposes

$$\boldsymbol{I}_{m+a}(\epsilon,\mu^2;\{p\},p_a) = \boldsymbol{I}_m(\epsilon,\mu^2;\{p\}) + \boldsymbol{I}_a(\epsilon,\mu^2;\{p\},p_a)\,, \tag{3.207}$$

into the $\boldsymbol{I}_m$ - operator of Eq. (3.195) and the $\boldsymbol{I}_a$ - operator that accounts for correlation between the initial and final-state

$$\begin{aligned}
\boldsymbol{I}_a(\epsilon,\mu^2;\{p_i,m_i\},p_a) = -\frac{\alpha_s}{2\pi}\,\frac{(4\pi)^\epsilon}{\Gamma(1-\epsilon)}\,\sum_j \Bigg\{ \\
\frac{1}{\boldsymbol{T}_j^2}\,\boldsymbol{T}_j\cdot\boldsymbol{T}_a \Bigg[\boldsymbol{T}_j^2 \left(\frac{\mu^2}{s_{ja}}\right)^\epsilon \left(\mathcal{V}_j(s_{ja},m_j,0,\{m_F\};\epsilon,\kappa) - \frac{\pi^2}{3}\right) + \Gamma_j(\mu,m_j,\{m_F\};\epsilon) \\
+\gamma_j \ln\frac{\mu^2}{s_{ja}} + \gamma_j + K_j \Bigg] \\
+\frac{1}{\boldsymbol{T}_a^2}\,\boldsymbol{T}_a\cdot\boldsymbol{T}_j \Bigg[\boldsymbol{T}_a^2 \left(\frac{\mu^2}{s_{aj}}\right)^\epsilon \left(\mathcal{V}_a(s_{aj},0,m_j,\{\};\epsilon,2/3) - \frac{\pi^2}{3}\right) + \frac{\gamma_a}{\varepsilon} \\
+\gamma_a \ln\frac{\mu^2}{s_{aj}} + \gamma_a + K_a \Bigg] \Bigg\}\,,
\end{aligned} \tag{3.208}$$

where $\mathcal{V}_j$ are given in Eq. (3.196). The $\boldsymbol{P}_m^{a,a'}$ and $\boldsymbol{K}_m^{a,a'}$ operators are calculated in [22] and read

$$\boldsymbol{P}_m^{a,a'}(x;\mu_F^2;\{p_i\},xp_a) = \frac{\alpha_s}{2\pi}\,P^{aa'}(x)\,\frac{1}{\boldsymbol{T}_{a'}^2}\sum_j \boldsymbol{T}_j\cdot\boldsymbol{T}_{a'}\,\ln\frac{\mu_F^2}{xs_{ja}}\,, \tag{3.209}$$

$$\begin{aligned}
\boldsymbol{K}_m^{a,a'}(x;\{p_i,m_i\},p_a) = \frac{\alpha_s}{2\pi}\Bigg\{ \overline{K}^{aa'}(x) - K^{ab}_{\text{F.S}}(x) - \sum_j \boldsymbol{T}_j\cdot\boldsymbol{T}_{a'}\,\mathcal{K}_j^{a,a'}(x;s_{ja},m_j,\{m_F\}) \\
-\frac{1}{\boldsymbol{T}_{a'}^2}\sum_j \boldsymbol{T}_j\cdot\boldsymbol{T}_{a'} \Bigg[P^{aa'}_{\text{reg}}(x)\,\ln\frac{(1-x)s_{ja}}{(1-x)s_{ja}+m_j^2} + \gamma_a\,\delta^{aa'}\,\delta(1-x) \\
\times\left(\ln\frac{s_{ja}-2m_j\sqrt{s_{ja}+m_j^2}+2m_j^2}{s_{ja}} + \frac{2m_j}{\sqrt{s_{ja}+m_j^2}+m_j}\right)\Bigg]\Bigg\}\,,
\end{aligned} \tag{3.210}$$

with

$$\mathcal{K}_q^{g,q}(x;s_{ja},m_j) \;= 0\,, \tag{3.211}$$

$$\begin{aligned}\mathcal{K}_q^{q,q}(x;s_{ja},m_j) &= 2\left[\left(\frac{\ln(1-x)}{1-x}\right)_+ - \frac{\ln(2-x)}{1-x}\right] + \left[J^a_{gQ}\left(x,\frac{m_j}{\sqrt{s_{ja}}}\right)\right]_+ \\ &\quad +2\left(\frac{1}{1-x}\right)_+ \ln\frac{(2-x)s_{ja}}{(2-x)s_{ja}+m_j^2} - \frac{\gamma_q}{C_\mathrm{F}}\delta(1-x) \\ &\quad +\delta(1-x)\left(\frac{m_j^2}{s_{ja}}\ln\frac{m_j^2}{s_{ja}+m_j^2} + \frac{1}{2}\frac{m_j^2}{s_{ja}+m_j^2}\right), \end{aligned} \tag{3.212}$$

$$\mathcal{K}_q^{q,g}(x;s_{ja},m_j) = 2\frac{C_\mathrm{F}}{C_\mathrm{A}}\frac{m_j^2}{xs_{ja}}\ln\frac{m_j^2}{(1-x)s_{ja}+m_j^2}, \tag{3.213}$$

$$\mathcal{K}_q^{g,g}(x;s_{ja},m_j) = \mathcal{K}_q^{q,q}(x;s_{ja},m_j) + \frac{C_\mathrm{A}}{C_\mathrm{F}}\mathcal{K}_q^{q,g}(x;s_{ja},m_j), \tag{3.214}$$

$$\begin{aligned}\mathcal{K}_g^{a,a'}(x;s_{ja},0,\{m_F\}) &= -\delta^{aa'}\frac{\gamma_g}{C_\mathrm{A}}\left[\left(\frac{1}{1-x}\right)_+ + \delta(1-x)\right] \\ &\quad +\delta^{aa'}\frac{T_\mathrm{R}}{C_\mathrm{A}}\sum_{F=1}^{N_F^{ja}}\Bigg\{\Big(\delta(1-x)-\delta(x_+-x)\Big) \\ &\quad\quad \cdot\left[\frac{2}{3}\left(\ln\frac{m_F^2}{s_{ja}}+\frac{5}{3}\right) - J^{a;\mathrm{NS}}_{Q\bar{Q}}\left(\frac{m_F}{\sqrt{s_{ja}}}\right)\right] \\ &\quad + \left[J^a_{Q\bar{Q}}\left(x,\frac{m_F}{\sqrt{s_{ja}}}\right)\right]_{x_+} + \delta(1-x)\,\frac{2}{3}\left(1-\frac{4m_F^2}{s_{ja}}\right)^{3/2}\Bigg\} \end{aligned} \tag{3.215}$$

and $\overline{K}^{aa'}(x)$ of Eq. (3.184). The upper limit N_F^{ij} of the last sum is the number of flavours with $s_{ja} > 4m_F^2$ and $x_+ = 1 - 4\frac{m_F^2}{s_{ja}}$. The x_+-distribution is defined as

$$\int_0^1 \mathrm{d}x \left(f(x)\right)_{x_+} g(x) \equiv \int_0^1 \mathrm{d}x\, f(x)\Theta(x_+-x)\left[g(x)-g(x_+)\right], \tag{3.216}$$

and its evaluation will be explained in more detail in Section 3.4.6. The complete sum formula for the case with one initial-state hadron is given in Eq. (3.180) with the operators displayed in this Section.

3.4.5.3 Two initial-state Hadrons

In this case, correlations between the initial-state partons come into play. The operators $\boldsymbol{I}_{m+a+b}$, $\boldsymbol{P}^{a,a'}_{m+b}$ and $\boldsymbol{K}^{a,a'}_{m+b}$ additionally depend on the incoming partons a and b and acquires an interference contribution proportional to $\boldsymbol{T}_a\boldsymbol{T}_b$

$$\begin{aligned}&\boldsymbol{I}_{m+a+b}(\epsilon,\mu^2;\{p\},p_a,p_b) = \\ &\quad \boldsymbol{I}_m(\epsilon,\mu^2;\{p\}) + \boldsymbol{I}_a(\epsilon,\mu^2;\{p\},p_a) + \boldsymbol{I}_b(\epsilon,\mu^2;\{p\},p_b)\end{aligned}$$

$$-\frac{\alpha_s}{2\pi}\frac{(4\pi)^\epsilon}{\Gamma(1-\epsilon)}\left(\frac{1}{\boldsymbol{T}_a^2}\boldsymbol{T}_a\cdot\boldsymbol{T}_b\left[\left(\frac{\mu^2}{s_{ab}}\right)^\epsilon\left(\frac{\boldsymbol{T}_a^2}{\epsilon^2}+\frac{\gamma_a}{\varepsilon}\right)-\boldsymbol{T}_a^2\frac{\pi^2}{3}+\gamma_a+K_a\right]\right.$$
$$\left.+(a\leftrightarrow b)\right), \tag{3.217}$$

$$\boldsymbol{P}_{m+b}^{a,a'}(x;\mu_F^2;\{p_i\},xp_a,p_b) = \boldsymbol{P}_m^{a,a'}(x;\mu_F^2;\{p_i\},xp_a)$$
$$+\frac{\alpha_s}{2\pi}P^{aa'}(x)\frac{1}{\boldsymbol{T}_{a'}^2}\boldsymbol{T}_b\cdot\boldsymbol{T}_{a'}\ln\frac{\mu_F^2}{xs_{ab}}, \tag{3.218}$$

and

$$\boldsymbol{K}_{m+b}^{a,a'}(x;\{p\},p_a,p_b) = \boldsymbol{K}_m^{a,a'}(x;\{p\},p_a)$$
$$-\frac{\alpha_s}{2\pi}\boldsymbol{T}_b\cdot\boldsymbol{T}_{a'}\left\{\frac{1}{\boldsymbol{T}_{a'}^2}P_{\rm reg}^{aa'}(x)\ln(1-x)\right.$$
$$\left.+\delta^{aa'}\left[2\left(\frac{\ln(1-x)}{1-x}\right)_+-\frac{\pi^2}{3}\delta(1-x)\right]\right\}. \tag{3.219}$$

These operators plugged into the formula of Eq. (3.193) also account for the two hadron initial-state case.

3.4.6 Evaluation of x_+ and + distributions

In this Section we explain the evaluation of the x_+- and +-distributions in more detail. First we restrict to +-distributions only, which are defined as

$$\int_0^1 \mathrm{d}x\left(f(x)\right)_+ g(x) \equiv \int_0^1 \mathrm{d}x\, f(x)\left[g(x)-g(1)\right]. \tag{3.220}$$

The calculation of the **K**-Operator includes the evaluation of the symbolic +-distribution $[J_{gQ}^a(x,\mu_Q)]_+$ where μ_Q is itself a function of the mass m_Q and $s_{ja}=2\tilde{p_{ij}}p_a$. Since the +-prescription acts on both variables x and $\tilde{p_{ij}}$, it is according to [6] important to notice that $\tilde{p_{ij}}$ has to be kept fixed during the subtraction prescription in Eq. (3.220). Schematically, with $[J(x,s_{ja}^{(x)})]_+$ acting on a testfunction $g(x)$, the following integral has to be calculated:

$$\int_0^1 \mathrm{d}x\int \mathrm{d}\Phi(x)\left[J\left(x,s_{ja}^{(x)}\right)\right]_+ g(x). \tag{3.221}$$

Hence, the (x) in $s_{ja}^{(x)}$ indicates that $s_{ja}^{(x)}$ is calculated out of the final-state momentum p_j in the x- dependent phase space $\Phi(x)$ and of the initial-state momentum p_a in the

phase space $\Phi(1)$. As this seems inconvenient, [6] describes a simplification by inserting unity $\int_{-\infty}^{+\infty} \mathrm{d}\bar{s}_{ja}\, \delta\left(\bar{s}_{ja} - s_{ja}^{(x)}\right)$ in the above equation, yielding

$$\begin{aligned}
&\int_0^1 \mathrm{d}x \int \mathrm{d}\Phi(x) \int_{-\infty}^{+\infty} \mathrm{d}\bar{s}_{ja}\, \delta\left(\bar{s}_{ja} - s_{ja}^{(x)}\right) \left[J\left(x, \bar{s}_{ja}\right)\right]_+ g(x) \\
&\quad = \int_0^1 \mathrm{d}x \int_{-\infty}^{+\infty} \mathrm{d}\bar{s}_{ja}\, J\left(x, \bar{s}_{ja}\right) \left\{ \int \mathrm{d}\Phi(x) \delta\left(\bar{s}_{ja} - s_{ja}^{(x)}\right) g(x) \right. \\
&\qquad\qquad \left. - \int \mathrm{d}\Phi(1) \delta\left(\bar{s}_{ja} - s_{ja}^{(1)}\right) g(1) \right\}. \qquad (3.222)
\end{aligned}$$

Integrating over $\mathrm{d}\bar{s}_{ja}$ eliminates the δ-function $\delta\left(\bar{s}_{ja} - s_{ja}^{(x)}\right)$ and gives

$$\begin{aligned}
&\int_0^1 \mathrm{d}x \int \mathrm{d}\Phi(x) \left[J\left(x, s_{ja}^{(x)}\right)\right]_+ g(x) \\
&\quad = \int_0^1 \mathrm{d}x \left\{ \int \mathrm{d}\Phi(x)\, J\left(x, s_{ja}^{(x)}\right) g(x) - \int \mathrm{d}\Phi(1)\, J\left(x, s_{ja}^{(1)}\right) g(1) \right\}. \qquad (3.223)
\end{aligned}$$

The last equation shows that s_{ja} is now always evaluated in the corresponding phase space. If the second argument of $[J\left(x, \mu(s_{ja})\right)]_+$ is a function of s_{ja}, one can see in which phase space s_{ja} has to be evaluated when plugging the following schematic form

$$\left[J\left(x, \mu(s_{ja})\right)\right]_+ = \left(f_1\left(x, \mu(s_{ja})\right)_+ + \left(f_2\left(x, \mu(s_{ja})\right)_+ f\left(x, \mu(s_{ja})\right), \qquad (3.224)$$

into Eq. (3.223):

$$\begin{aligned}
&\int_0^1 \mathrm{d}x \int \mathrm{d}\Phi(x) \left[J\left(x, \mu(s_{ja}^{(x)})\right)\right]_+ g(x) \\
&\quad = \int_0^1 \mathrm{d}x \left\{ \int \mathrm{d}\Phi(x)\, g(x) \left(f_1\left(x, \mu(s_{ja}^{(x)})\right) + f_2\left(x, \mu(s_{ja}^{(x)})\right) f\left(x, \mu(s_{ja}^{(x)})\right)\right) \right. \\
&\qquad\qquad - \int \mathrm{d}\Phi(1)\, g(1) \left(f_1\left(x, \mu(s_{ja}^{(1)})\right)\right. \\
&\qquad\qquad \left. \left. + f_2\left(x, \mu(s_{ja}^{(1)})\right) f\left(x, \mu(s_{ja}^{(1)})\right)\right)\right\}. \qquad (3.225)
\end{aligned}$$

It is important to notice that $\mu(s_{ja})$ is evaluated even inside the +-prescription in the corresponding phase spaces. The x_+-distribution, which occurs only if $g \to Q\bar{Q}$ splitting with massive quarks Q is included and is defined through

$$\int_0^1 \mathrm{d}x \left(f(x)\right)_{x_+} g(x) \equiv \int_0^1 \mathrm{d}x\, f(x) \Theta(x_+ - x) \left[g(x) - g(x_+)\right], \qquad (3.226)$$

is evaluated analogously. The x_+ itself is calculated using $s_{ja}^{(x)}$ from the x-dependent phase space $\Phi(x)$ via

$$x_+ = 1 - \frac{4m_F}{s_{ja}^{(x)}}. \qquad (3.227)$$

The corresponding evaluation of the integral is given by

$$\begin{aligned}
&\int_0^1 \mathrm{d}x \int \mathrm{d}\Phi(x) \left[J\left(x, \mu(s_{ja}^{(x)})\right)\right]_{x_+} g(x) \\
&= \int_0^{x_+} \mathrm{d}x \left\{ \int \mathrm{d}\Phi(x_+)\, g(x_+) \left(f_1\left(x, \mu(s_{ja}^{(x_+)})\right) + f_2\left(x, \mu(s_{ja}^{(x_+)})\right) f\left(x, \mu(s_{ja}^{(x_+)})\right)\right)\right. \\
&\qquad - \int \mathrm{d}\Phi(1)\, g(1) \left(f_1\left(x, \mu(s_{ja}^{(1)})\right)\right. \\
&\qquad \left.\left. + f_2\left(x, \mu(s_{ja}^{(1)})\right) f\left(x, \mu(s_{ja}^{(1)})\right)\right)\right\}, \qquad (3.228)
\end{aligned}$$

implicitly assuming that in the last line it has already be taken care of $\Theta(x_+ - x)$ from the definition of the x_+-distribution.

4

Implementation

In this Chapter, we focus on the implementation of the different parts of the program. First, we review the recursion relation for building up the phase space in both LO and NLO and present the mappings used in the code. A set of basic tests for the main parts of the Monte Carlo Event generator follows the details of the implementation of the dipole subtraction terms and the corresponding integrated subtraction terms.

4.1 Phase Space

In this Section we focus on the details of the implementation of the different parts of the Monte Carlo Event generator. Parts of the implementation are closely related to [28]. Cross Sections in particle physics involve integrations over the phase space and, in the case of hadron colliders, over the momentum fractions x_1 and x_2 of the incoming partons. The total cross section at LO can be factorized into a partonic part $\hat{\sigma}_{ab}$ and parton distribution functions

$$\sigma = \int \mathrm{d}r_1 \mathrm{d}r_2 \int \mathrm{d}\Phi_m \frac{f_a(x_1(r_1),\mu^2) f_b(x_2(r_2),\mu^2)}{g_{f_a}(x_1(r_1)) g_{f_b}(x_2(r_2))}\, \hat{\sigma}_{ab}(x_1 p_a, x_2 p_2, \mu^2), \tag{4.1}$$

where

$$\mathrm{d}\Phi_m(p_a,p_b,\{p_i\}) = (2\pi)^{(4-3m)} \delta^4 \left(p_a + p_b - \sum_{i=1}^{m} p_i \right) \prod_{i=1}^{m} \mathrm{d}^4 p_i \delta(p_i^2 - m_i^2) \Theta(p_i^0), \tag{4.2}$$

f_a is the parton distribution function of parton a in the considered initial-state hadron and $g_{f_a}(x)$ is the density of the mapping of the momentum fraction x, which is introduced in Section 4.4. The total cross Section at NLO including both the virtual and the subtracted real part can be written as

$$\delta\sigma^{\mathrm{NLO}} = \int \underline{\mathrm{d}r_1 \mathrm{d}r_2} \int_{m+1} \underline{\mathrm{d}\Phi_{m+1}} \frac{f_a(x_1(r_1),\mu^2) f_b(x_2(r_2),\mu^2)}{g_{f_a}(x_1(r_1)) g_{f_b}(x_2(r_2))} \left[\underline{\underline{d\sigma^{\mathrm{R}}_{ab}}} - \underline{d\sigma^{\mathrm{A}}_{ab}} \right]$$

$$+ \int \underline{\mathrm{d}r_1 \mathrm{d}r_2} \int_m \underline{\mathrm{d}\Phi_m} \frac{f_a(x_1(r_1),\mu^2) f_b(x_2(r_2),\mu^2)}{g_{f_a}(x_1(r_1)) g_{f_b}(x_2(r_2))} \left\{ \left[\underline{\underline{d\sigma^{\mathrm{V}}_{ab}}} + \underline{\underline{d\sigma^{\mathrm{B}}_{ab}}} \otimes \underline{\mathbf{I}_{ab}} \right] \right.$$
$$\left. + \int \underline{\mathrm{d}x} \left[\underline{\underline{d\sigma^{\mathrm{B}}_{ab}}} \otimes \underline{(\mathbf{K}_{ab}(x) + \mathbf{P}_{ab}(x))} \right] \right\}. \tag{4.3}$$

The underlined parts in the equation above are tasks of the Monte Carlo Event generator and the double underlined parts are user inputs. The next Sections explain in detail how each of the steps is evaluated and implemented in the program.

4.2 LO Phase Space Generator

The main goal of a phase-space generator is to optimize the $\mathrm{d}\Phi_m$ part of the integration. Large variations of the integrand come from the peaking structure of the squared matrix element [29]. They decrease the efficiency of the phase-space integration. One way out is a Multi-Channel Monte Carlo with appropriately constructed mappings as described in Chapter 2. The squared matrix element exhibits its peaking structure through the propagators occurring in the corresponding Feynman diagrams. The propagators have a well-defined representation in the topologies of the underlying Feynman diagrams. Thus, the goal is to combine the mapping in such a way that they smoothen the peaking behaviour of the integrand. We call the set of mappings according to the propagator structure of one Feynman diagram a *channel*. Usually, many Feynman diagrams contribute to a complete process. We refer to the combination of all channels (i.e. diagrams) contributing to a given process as a *generator*. The phase-space mappings that map random numbers into variables out of which four momenta can be built have to be continuously differentiable so that integration by substitution can be applied. The aim of the algorithm is to build up the phase-space mappings recursively. Fixing a channel (i.e. a Feynman diagram), the recursion is based on the decomposition of the phase space. In order to cover all possible peaking structures of a given process, it is necessary to decompose the phase space in all possible ways. This means, one has to find all tree-level topologies contributing as Feynman diagrams to the process under consideration. A Feynman diagram is identified by a sequence of vertices $\{V_1, \ldots, V_n\}$ and propagating particles $\{P_{1_{1,\ldots,3}}, \ldots, P_{n_{1,\ldots,3}}\}$. Hence, we can represent one decomposition of the phase space by a Feynman diagram.

We denote $\mathrm{d}\Phi_m(Q; p_1, \ldots, p_n)$ with the phase space, where Q corresponds to the incoming momenta and $\{p_1, \ldots, p_n\}$ are the outgoing momenta. Thus, Q^2 is the invariant mass of the system that is formed by $\{p_1, \ldots, p_n\}$. An important property of the phase space in Eq. (4.2) is the decomposition

$$\mathrm{d}\Phi_n(p_a, p_b; p_1, \ldots, p_n) = \left(\prod_{i=1}^{m} \frac{\mathrm{d}Q_i^2}{2\pi} \right) \mathrm{d}\Phi_m(p_a + p_b; Q_1, \ldots, Q_m)$$

$$\times \, \mathrm{d}\Phi_{n_1}(Q_1; r_1^{Q_1}, \ldots, r_{n_1}^{Q_1}) \\ \times \, \ldots \, \times \, \mathrm{d}\Phi_{n_m}(Q_m; r_1^{Q_m}, \ldots, r_{n_m}^{Q_m}), \tag{4.4}$$

where the subsets $\{r_1^{Q_i}, \ldots, r_{n_i}^{Q_i}\}$ are arbitrary covering partitions of $\{p_1, \ldots, p_n\}$. Feynman diagrams are a realization of such a decomposition which allows an algorithm to recursively build up the phase space. As an example one possibility of the decomposition of the six particle phase space out of decays is given by

$$\begin{aligned} \mathrm{d}\Phi_n(p_a, p_b; p_1, \ldots, p_6) &= \left(\prod_{i=1}^{2} \frac{\mathrm{d}Q_i^2}{2\pi} \right) \mathrm{d}\Phi_2(p_a + p_b; Q_1, Q_2) \\ &\quad \times \mathrm{d}\Phi_3(Q_1; p_1, \ldots, p_3) \mathrm{d}\Phi_3(Q_2; p_4, \ldots, p_6) \\ &= \left(\prod_{i=1}^{2} \frac{\mathrm{d}Q_i^2}{2\pi} \right) \mathrm{d}\Phi_2(p_a + p_b; Q_1, Q_2) \\ &\quad \times \left[\frac{\mathrm{d}K_2^2}{2\pi} \mathrm{d}\Phi_2(Q_1; p_1, K_2) \mathrm{d}\Phi_2(K_2; p_2, p_3) \right] \\ &\quad \times \left[\frac{\mathrm{d}L_2^2}{2\pi} \mathrm{d}\Phi_2(Q_2; p_4, L_2) \mathrm{d}\Phi_2(L_2; p_5, p_6) \right] \end{aligned} \tag{4.5}$$

with its corresponding Feynman topology shown in Figure 4.1. The following recursion

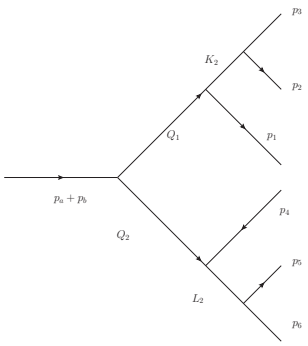

Figure 4.1: Topology to Eq. 4.5

leads for example to a sequence of decays, where each decay produces one final-state parton and another decaying parton. This phase-space decomposition reads

$$\begin{aligned} \mathrm{d}\Phi_n(p_a, p_b; p_1, \ldots, p_6) &= \left(\prod_{i=1}^{2} \frac{\mathrm{d}Q_i^2}{2\pi} \right) \mathrm{d}\Phi_2(p_a + p_b; Q_1, Q_2) \\ &\quad \times \mathrm{d}\Phi_1(Q_1; p_1) \mathrm{d}\Phi_3(Q_2; p_2, \ldots, p_6) \\ &= \mathrm{d}\Phi_2(p_a + p_b; p_1, K_1) \frac{\mathrm{d}K_1^2}{2\pi} \mathrm{d}\Phi_2(K_1; p_2, K_2) \\ &\quad \times \frac{\mathrm{d}K_2^2}{2\pi} \mathrm{d}\Phi_2(K_2; p_3, K_3) \frac{\mathrm{d}K_3^2}{2\pi} \mathrm{d}\Phi_2(K_3; p_4, K_4) \end{aligned}$$

$$\times \frac{\mathrm{d}K_4^2}{2\pi}\mathrm{d}\Phi_2(K_4; p_5, p_6) \tag{4.6}$$

with its corresponding Feynman topology (figure 4.2). In this recursive way all existing

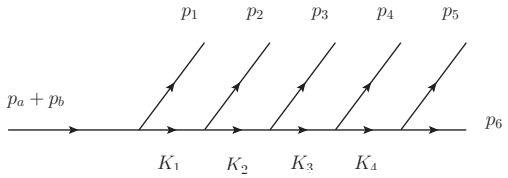

Figure 4.2: Topology to Eq. 4.5

Feynman topologies can be built up. In order to recursively construct the phase space, it need to be defined, which types of $\mathrm{d}\Phi_{n_m}(Q_m; r_1^{Q_m}, \ldots, r_{n_m}^{Q_m})$ are used. We will refer to these as the so-called building blocks. The main building blocks of the phase space of our code are the decay $\mathrm{d}\Phi_d$ and the $2 \to 2$-process phase spaces $\mathrm{d}\Phi_p$. The main task of the algorithm that provides the channels (topologies) to a given process, is to output a sequence of vertices and propagators according to which the phase-space building blocks are chosen.

A vertex V_i can be characterized by one incoming timelike momentum Q ($Q^2 > 0$) and two outgoing momenta P_1 and P_2 via $V_i : Q \to P_1 + P_2$. (A more complicated case with two incoming momenta (t-channel) will be explained later on.) The case described refers to a decay

$$\begin{aligned}
\int \mathrm{d}\Phi_d(Q; P_1, P_2) &= \int \mathrm{d}^4P_1\mathrm{d}^4P_2\delta(P_1^2 - m_1^2)\theta(P_1^0)\delta(P_2^2 - m_2^2)\theta(P_2^0)\delta^{(4)}(Q - P_1 - P_2) \\
&= \int \mathrm{d}^4P_1\delta(P_1^2 - m_1^2)\Theta(P_1^0)\delta((Q - P_1)^2 - m_2^2) \\
&= \frac{\lambda^{\frac{1}{2}}(Q^2, P_1^2, P_2^2)}{8Q^2}\int_0^{2\pi}\mathrm{d}\phi^*\int_{-1}^{1}\mathrm{d}\cos\theta^*
\end{aligned} \tag{4.7}$$

of Q into of P_1 and P_2. In the following we will denote $\mathrm{d}P_1^2/2\pi$ with $\mathrm{d}\Phi_s(P_1)$. One can rewrite the part of the phase-space decomposition, where a parton with momentum Q decays into two partons with momenta P_1 and P_2 with the building block $\mathrm{d}\Phi_d$ as follows

$$\begin{aligned}
\mathrm{d}\Phi_m &= \ldots\frac{\mathrm{d}P_1^2}{2\pi}\frac{\mathrm{d}P_2^2}{2\pi}\mathrm{d}\Phi_d(Q; P_1, P_2)\ldots \\
&= \ldots\mathrm{d}\Phi_s(P_1)\mathrm{d}\Phi_s(P_2)\frac{\lambda^{\frac{1}{2}}(Q^2, P_1^2, P_2^2)}{8Q^2}\mathrm{d}\phi^*\mathrm{d}\cos\theta^*\ldots \qquad .
\end{aligned} \tag{4.8}$$

In Eq (4.8) we assume that P_1 and P_2 belong to internal lines. If the momenta P_1 and P_2 belong to outgoing particles, there is no integration to perform over $\mathrm{d}P_1^2/2\pi$ or

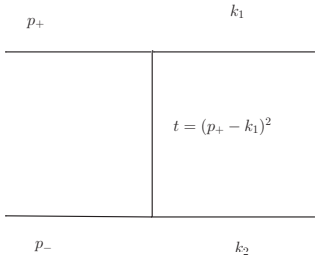

Figure 4.3: Topology of t-channel process

$\mathrm{d}P_2^2/2\pi$. The angular variables have to be built in their integration boundaries out of random numbers by the mappings

$$\phi = 2\pi r_\phi \ , \qquad \cos\theta^* = 2r_{\theta^*} - 1 \tag{4.9}$$

introducing new Jacobians which lead to a modified decomposition

$$\begin{aligned} \mathrm{d}\Phi_m &= \dots \mathrm{d}\Phi_s(P_1)\mathrm{d}\Phi_s(P_2)\mathrm{d}\Phi_d(Q;P_1,P_2)\dots \\ &= \dots \frac{\mathrm{d}P_1^2}{2\pi}\frac{\mathrm{d}P_2^2}{2\pi}\frac{\pi\lambda^{\frac{1}{2}}(Q^2,P_1^2,P_2^2)}{2Q^2}\mathrm{d}r_\phi \mathrm{d}r_{\theta^*}\dots \qquad , \end{aligned} \tag{4.10}$$

where we denote the density g_d as follows:

$$g_d(Q,P_1^2,P_2^2) = \frac{\pi\lambda^{\frac{1}{2}}(Q^2,P_1^2,P_2^2)}{2Q^2}. \tag{4.11}$$

The phase-space building block $\mathrm{d}\Phi_p(p_+,p_-,k_1,k_2)$ corresponds to a t-channel-process with the two incoming partons p_+ and p_- and the two outgoing partons k_1 and k_2. Given the masses of the outgoing partons and fixed initial-state momenta, the Feynman topology (figure 4.3) to this process includes a propagator transferring a space-like momentum $t = (p_+ - k_1)^2 < 0$. With a mapping $\phi^* = 2\pi r_{\phi^*}$ for the polar angle ϕ^* and $p = p_+ + p_-$, the phase space $\mathrm{d}\Phi_d$ reads

$$\begin{aligned} &\int \mathrm{d}\Phi_p(p_+,p_-,k_1,k_2) \\ &= \int \mathrm{d}^4k_1\mathrm{d}^4k_2\delta\left(k_1^2-m_1^2\right)\theta(k_1^0)\delta\left(k_2^2-m_2^2\right)\theta(k_2^0)\delta^{(4)}(p-p_1-p_2) \\ &= \frac{\pi}{2\lambda^{\frac{1}{2}}(p^2,p_+^2,p_-^2)}\int_0^1 \mathrm{d}r_1 \int_{-t_{\max}}^{-t_{\min}} \mathrm{d}|t|. \end{aligned} \tag{4.12}$$

For the integration limits, one has to calculate the azimuthal-angle dependence θ^* of t

$$t = k_1^2 + p_+^2$$

$$- \quad \frac{(p^2+k_1^2-k_2^2)(p^2+p_+^2-p_-^2)-\lambda^{\frac{1}{2}}(p^2,k_1^2,k_2^2)\lambda^{\frac{1}{2}}(p^2,p_+^2,p_-^2)\cos\theta^*}{2p^2} \tag{4.13}$$

and find the extrema of t in $\cos\theta^*$. If no cut on θ^* is imposed, the maximum of t is reached at $\cos\theta^* = 1$ and the minimum at $\cos\theta^* = -1$. This leads to the phase-space decomposition

$$\begin{aligned} \mathrm{d}\Phi_m &= \ldots \frac{\mathrm{d}P_1^2}{2\pi}\frac{\mathrm{d}P_2^2}{2\pi}\mathrm{d}\Phi_p(p_+,p_-;P_1,P_2)\ldots \\ &= \ldots \mathrm{d}\Phi_s(P_1)\mathrm{d}\Phi_s(P_2)\frac{\pi}{2\lambda^{\frac{1}{2}}\left((p_++p_-)^2,p_+^2,p_-^2\right)}\mathrm{d}r_{\phi^*}\mathrm{d}|t|\ldots \quad . \end{aligned} \tag{4.14}$$

The phase space can now be built recursively according to the decomposition formula Eq. (4.4), using the building blocks

$$\mathrm{d}\Phi_m = \prod_{i=1}^{n_s}\mathrm{d}\Phi_s^{(i)} \quad \prod_{j=1}^{n_d}\mathrm{d}\Phi_d^{(j)} \quad \prod_{l=1}^{n_p}\mathrm{d}\Phi_p^{(l)} \quad , \tag{4.15}$$

which leads to the product of phase-space variables

$$\mathrm{d}\Phi_m \to \prod_{i=1}^{n_s}\mathrm{d}s^{(i)} \quad \prod_{j=1}^{n_d}\mathrm{d}r_{\theta^*}^{(j)}\mathrm{d}r_{\phi}^{(j)} \quad \prod_{l=1}^{n_p}\mathrm{d}r_{\phi^*}^{(l)}\mathrm{d}|t|^{(l)} \quad . \tag{4.16}$$

The variables r_{θ^*},r_ϕ and r_{ϕ^*} are random numbers in the interval $[0,1]$. The number of phase-space variables $3n-4$ is composed of in total

- $n-2$ invariants such as $s^{(i)}$ and $|t|^{(l)}$ and
- $2(n-1)$ angles such as θ^*, ϕ and ϕ^*.

The variables $s^{(i)}$ and $|t|^{(l)}$ are invariants of propagators and have to be mapped via h out of random numbers r

$$s(r) = h(r, m^2, \nu, s_{\min}, s_{\max}) \tag{4.17}$$

and, accordingly,

$$|t(r)| = h(r, m^2, \nu, -t_{\max}, -t_{\min}), \tag{4.18}$$

such that the Jacobian g_s of h with respect to r smoothens the corresponding propagator

$$\begin{aligned} \int_{s_{\min}}^{s_{\max}}\mathrm{d}s &= \int_{s_{\min}}^{s_{\max}}\frac{\mathrm{d}h(r,m^2,\nu,s_{\min},s_{\max})}{\mathrm{d}r}\mathrm{d}r \\ &= \int_0^1 \frac{\mathrm{d}r}{g_s(s(r),m^2,\nu,s_{\min},s_{\max})}. \end{aligned} \tag{4.19}$$

The typical propagators in amplitudes are either of Breit–Wigner type

$$\frac{1}{(k^2-m^2)^2+m^2\Gamma^2}, \tag{4.20}$$

or, in case of a propagator with vanishing width, of the form

$$\frac{1}{(k^2-m^2)^\nu}. \tag{4.21}$$

The mappings and densities belonging to Eq. (4.21) are in the case of $\nu \neq 1$

$$\begin{aligned} h(r,m^2,\nu,s_{\min},s_{\max}) &= \Big[r(s_{\max}-m^2)^{1-\nu}+(1-r)(s_{\min}-m^2)^{1-\nu}\Big]^{\frac{1}{1-\nu}}+m^2, \\ g_s(s,m^2,\nu,s_{\min},s_{\max}) &= \frac{1-\nu}{\Big[(s_{\max}-m^2)^{1-\nu}-(s_{\min}-m^2)^{1-\nu}\Big](s-m^2)^\nu} \end{aligned} \tag{4.22}$$

and in the case of $\nu = 1$

$$\begin{aligned} h(r,m^2,1,s_{\min},s_{\max}) &= \exp\Big[r\ln(s_{\max}-m^2)-(1-r)\ln(s_{\min}-m^2)\Big]+m^2, \\ g_s(s,m^2,1,s_{\min},s_{\max}) &= \frac{1}{\Big[\ln(s_{\max}-m^2)-\ln(s_{\min}-m^2)\Big](s-m^2)}. \end{aligned} \tag{4.23}$$

Calculating $1/g(k^2) = |\partial h(r)/\partial r|$ shows the desired property

$$\begin{aligned} \frac{1}{g(k^2)} &= \left|\frac{\partial h(r)}{\partial r}\right| = \frac{1}{1-\nu}\Big[r(k_{\max}^2-m^2)^{(1-\nu)}+(1-r)(k_{\min}^2-m^2)^{(1-\nu)}\Big]^{\frac{\nu}{1-\nu}} \\ &\quad\times\ \Big((k_{\max}^2-m^2)^{(1-\nu)}+(k_{\min}^2-m^2)^{(1-\nu)}\Big) \\ &= \frac{1}{1-\nu}\Big((k_{\max}^2-m^2)^{(1-\nu)}+(k_{\min}^2-m^2)^{(1-\nu)}\Big)\left(k^2-m^2\right), \end{aligned} \tag{4.24}$$

with $\nu \neq 1$ and correspondingly if $\nu = 1$

$$\begin{aligned} \frac{1}{g(k^2)} &= \left(\exp\left(r\ln\left(k_{\max}^2-m^2\right)+(1-r)\ln\left(k_{\min}^2-m^2\right)\right)\right) \\ &\quad\times\ \left(\ln\left(k_{\max}^2-m^2\right)-\ln\left(k_{\min}^2-m^2\right)\right) \\ &= \left(k^2-m^2\right)\left(\ln\left(k_{\max}^2-m^2\right)-\ln\left(k_{\min}^2-m^2\right)\right). \end{aligned} \tag{4.25}$$

In the Breit–Wigner case Eq. (4.20), the mapping and density is given by

$$\begin{aligned} h(r,m^2-\mathrm{i}m\Gamma,2,s_{\min},s_{\max}) &= m\Gamma\tan\Big[y_1+(y_2-y_1)r\Big]+m^2, \\ g_s(s,m^2-\mathrm{i}m\Gamma,2,s_{\min},s_{\max}) &= \frac{m\Gamma}{(y_2-y_1)[(s-m^2)^2+m^2\Gamma^2]} \end{aligned} \tag{4.26}$$

where

$$y_{1/2} \quad = \quad \arctan\left(\frac{s_{\min/\max} - m^2}{m\Gamma}\right). \tag{4.27}$$

The free parameter ν can be used to tune the Monte Carlo Event generator. It should be chosen close to 1. Setting the parameter $\nu = 0$ (flat mappings), allows the calculation of the phase space volume (e.g. including cuts) which is often needed for checks. With the definition of the mappings the density of the t-channel can be written as

$$g_p(p^2, p_+^2, p_-^2, t, m^2, \nu, t_{\min}, t_{\max}) = \frac{2\lambda^{\frac{1}{2}}\left((p_+ + p_-)^2, p_+^2, p_-^2\right)}{\pi} g_s(-t, m^2, \nu, -t_{\max}, -t_{\min}). \tag{4.28}$$

Combining all the densities derived above the phase space is finally decomposed in terms of random-number variables r_i and the corresponding Jacobians as follows

$$\mathrm{d}\Phi_m = \prod_{i=1}^{n_s} \frac{1}{g_{s^{(i)}}} \mathrm{d}r_{s^{(i)}} \quad \prod_{j=1}^{n_d} \frac{1}{g_{d^{(j)}}} \mathrm{d}r_{\theta^*}^{(j)} \mathrm{d}r_{\phi}^{(j)} \quad \prod_{l=1}^{n_p} \frac{1}{g_{p^{(l)}}} \mathrm{d}r_{\phi^*}^{(l)} \mathrm{d}r_{|t|^{(l)}} \quad . \tag{4.29}$$

Construction of Final-State Momenta

Once the phase space is decomposed into all possible channels according to the scheme above, the final-state momenta can be constructed for a chosen channel. Since we have two basic building blocks for the phase-space decomposition we need recipes for the momentum construction. At first the proper Lorentz transformations are introduced. In order to transform momentum P into the rest frame of a particle with momentum Q, the Lorentz transformation reads [18], [19]

$$P' \quad = \quad \mathcal{B}(Q_0, \mathbf{Q})P \tag{4.30}$$

with the boost $\mathcal{B}(Q_0, \mathbf{Q})$ explicitly acting on P as follows

$$P_0' \quad = \quad \gamma P_0 + \mathbf{bP}, \qquad \mathbf{P}' = \mathbf{P} + \mathbf{b}\frac{\mathbf{bP}}{1-\gamma} + \mathbf{b}P_0, \tag{4.31}$$

where $\mathbf{b} = -\mathbf{Q}/m$, $\gamma = Q_0/m$ and $m = \sqrt{Q^2}$. In addition we need rotations that leave the 0 component of a four vector invariant. The rotation that turns a four vector about the z axis through the angle ϕ is e.g. given by

$$\mathcal{R}_z(\phi) = \begin{pmatrix} 1 & 0 & 0 & 0 \\ 0 & \cos\phi & \sin\phi & 0 \\ 0 & -\sin\phi & \cos\phi & 0 \\ 0 & 0 & 0 & 1 \end{pmatrix}. \tag{4.32}$$

In the following we construct the momenta according to the two phase-space building blocks $\mathrm{d}\Phi_d$ and $\mathrm{d}\Phi_p$. The idea is to find a reference frame to a given phase-space building block, where the momenta can be fixed, and then transform the momenta into the laboratory frame. First we consider the isotropic decay into two particles. Let Q be the momentum of the particle that decays into two particles with momenta P_1 and P_2 and ϕ and θ be the polar and azimuthal angle respectively in the rest frame of the decaying particle. In the rest frame of the decaying particle we can write the outgoing momenta P_1^* and P_2^* due to the isotropy of the decay as follows

$$P_1^* = \begin{pmatrix} \frac{Q^2+P_1^2-P_2^2}{2\sqrt{Q^2}} \\ 0 \\ 0 \\ \frac{\lambda^{\frac{1}{2}}(Q^2,P_1^2,P_2^2)}{2\sqrt{Q^2}} \end{pmatrix}, \quad \text{and } P_2^* = Q - P_1^*. \tag{4.33}$$

With the rotation given by

$$\begin{aligned} \mathcal{R}(\phi,\cos\theta) &= \begin{pmatrix} 1 & 0 & 0 & 0 \\ 0 & \cos\phi & \sin\phi & 0 \\ 0 & -\sin\phi & \cos\phi & 0 \\ 0 & 0 & 0 & 1 \end{pmatrix} \begin{pmatrix} 1 & 0 & 0 & 0 \\ 0 & \cos\theta & 0 & \sin\theta \\ 0 & 0 & 1 & 0 \\ 0 & -\sin\theta & 0 & \cos\theta \end{pmatrix} \\ &= \begin{pmatrix} 1 & 0 & 0 & 0 \\ 0 & \cos\theta\cos\phi & \sin\phi & \sin\theta\cos\phi \\ 0 & -\cos\theta\sin\phi & \cos\phi & -\sin\theta\sin\phi \\ 0 & -\sin\theta & 0 & \cos\theta \end{pmatrix} \end{aligned} \tag{4.34}$$

the momenta of the outgoing particles read

$$P_1 = \mathcal{B}(Q_0,-\mathbf{Q})\mathcal{R}(\phi^*,\cos\theta^*) \begin{pmatrix} \frac{Q^2+P_1^2-P_2^2}{2\sqrt{Q^2}} \\ 0 \\ 0 \\ \frac{\lambda^{\frac{1}{2}}(Q^2,P_1^2,P_2^2)}{2\sqrt{Q^2}} \end{pmatrix}, \quad \text{and } P_2 = Q - P_1. \tag{4.35}$$

This allows to construct two outgoing momenta P_1 and P_2 out of an incoming momentum Q in an isotropic decay by generating the polar and azimuthal angle according to Eq. (4.9).

The second basic building blocks of the phase space are $2 \to 2$ processes with incoming momenta p_+ and p_- and two outgoing momenta k_1 and k_2. The propagator of the underlying Feynman diagram depends on the Mandelstam variable $t = (p_+ - k_1)^2$.

In the rest frame of $Q = p_+ + p_-$ the external particles can be written as [19]

$$p_\pm^* = \begin{pmatrix} \frac{Q^2+p_\pm^2-p_\mp^2}{2\sqrt{Q^2}} \\ 0 \\ 0 \\ \pm\frac{\lambda^{\frac{1}{2}}(Q^2,p_+^2,p_-^2)}{2\sqrt{Q^2}} \end{pmatrix}, \qquad k_1^* = \mathcal{R}(\phi,\cos\theta) \begin{pmatrix} \frac{Q^2+k_1^2-k_2^2}{2\sqrt{Q^2}} \\ 0 \\ 0 \\ \frac{\lambda^{\frac{1}{2}}(Q^2,k_1^2,k_2^2)}{2\sqrt{Q^2}} \end{pmatrix}, \quad (4.36)$$

and k_2^* is due to momentum conservation given by $k_2^* = p_+^* + p_-^* - k_1^*$. The angle $\cos\theta$ can be calculated from (4.13) and ϕ is randomly chosen via $\phi = 2\pi r_\phi$. The following Lorentz transformations transform the final-state momenta into the laboratory frame

$$k_1 = \mathcal{B}(Q_0,-\mathbf{Q})\mathcal{R}(-\hat{\phi},\cos\hat{\theta})k_1^*, \;\; k_2 = \mathcal{B}(p_0,-\mathbf{p})\mathcal{R}(-\hat{\phi},\cos\hat{\theta})k_2^*, \quad (4.37)$$

where the angles are given by

$$\hat{\phi} = \begin{cases} \arctan\left(\frac{\hat{p}_{+2}}{\hat{p}_{+1}}\right) & , \quad \hat{p}_{+1} > 0 \\ \arctan\left(\frac{\hat{p}_{+2}}{\hat{p}_{+1}}\right) + \pi & , \quad \hat{p}_{+1} < 0 \end{cases}, \qquad \cos\hat{\theta} = \frac{\hat{p}_{+3}}{|\hat{\mathbf{p}}_+|} \quad (4.38)$$

with $\hat{p}_+ = \mathcal{B}(Q_0,\mathbf{Q})p_+$.

Generic Cuts

Already during the generation of the momenta, we take generic physical cuts such as invariant-mass cuts into account. For a given channel, we calculate for each internal particle l the minimal invariant out of the masses of the external particles and given cuts on the angles between pairs of outgoing particles. For a given internal particle l the masses of all external particles m_i that are included in particle l, are summed up

$$s_{l,\text{invm}} = \left(\sum_{i\in\{N_l^{\text{incl}}\}} m_i\right)^2, \quad (4.39)$$

where $\{N_l^{\text{incl}}\}$ stands for the set of particles included in l. Consecutively for all pairs i and j of included particles the new invariant mass is calculated according to

$$\begin{aligned} s_{l,\text{invm}}^{\text{cut}} &= s_{l,\text{invm}} + \sum_{i,j\in\{N_l^{\text{incl}}\}} \Big(-(m_i+m_j)^2 \\ &+ \max\left[s_{i,j}^{\text{cut}}, m_i^2+m_j^2+2\sqrt{(E_i^2-m_i^2)(E_j^2-m_j^2)}\cos\theta_{i,j}^{\text{cut}}\right]\Big) . \end{aligned} \quad (4.40)$$

Here $s_{i,j}^{\text{cut}}$ accounts for an invariant mass cut on particles i and j and $\theta_{i,j}^{cut}$ for cuts on the angles between the corresponding pair particles.

4.3 NLO Phase-Space Generator

The NLO phase space $\mathrm{d}\Phi_{m+1}$ can be generated in two different ways. One can use the algorithm of Section 4.2 for $m+1$ final-state partons. Since $\mathrm{d}\sigma^{\mathrm{A}}$ is evaluated on the $\mathrm{d}\Phi_{m+1}$ phase space, it might be of advantage to decompose the phase space via the mappings according to $\mathrm{d}\Phi_m$ (from above) and additional mappings that account for the soft and collinear regions. As seen in Section 3.2, the behaviour to be mapped is proportional to $1/s_{ij}$. The term $\mathrm{d}\sigma^{\mathrm{A}}$ is a sum of dipole subtraction terms and thus accounts for many different $1/s_{ij}$ behaviours. The strategy of this approach for a NLO phase-space decomposition is to take a hard m-parton phase space channel out of $\mathrm{d}\Phi_m$ and add a momentum p_j that is mapped according to the occurring singularity. Let p_i and p_k be two momenta from the hard phase space $\mathrm{d}\Phi_m$ and $s_{ij} = (p_i' + p_j)^2$, $s_{jk} = (p_j + p_k')^2$ and $s_{ik} = (p_i' + p_j + p_k')^2$ such that momentum conservation is ensured $(p_i + p_k)^2 = (p_i' + p_j + p_k')^2$. The basis for this algorithm is the decomposition of the $m+1$-parton phase space into the m-parton phase space and the product of a propagator and the three-parton phase space

$$\mathrm{d}\Phi_{m+1} = \mathrm{d}\Phi_{m-1}\frac{\mathrm{d}K^2}{2\pi}\mathrm{d}\Phi_3(K; p_i', p_j, p_k'). \tag{4.41}$$

Applying the phase-space decomposition of Eq. (4.4) to $\mathrm{d}\Phi_3$,

$$\mathrm{d}\Phi_3(K; p_i', p_j, p_k') = \mathrm{d}\Phi_2(K; p_i', Q)\frac{\mathrm{d}Q^2}{2\pi}\mathrm{d}\Phi_2(Q; p_j, p_k'), \tag{4.42}$$

and using the parametrization for the two-body phase space, we get for Eq. (4.41)

$$\begin{aligned}
\mathrm{d}\Phi_{m+1} &= \mathrm{d}\Phi_{m-1}\frac{\mathrm{d}K^2}{2\pi}\mathrm{d}\Phi_2(K; p_i', Q)\frac{\mathrm{d}Q^2}{2\pi}\mathrm{d}\Phi_2(Q; p_j, p_k') \\
&= \mathrm{d}\Phi_m\frac{\mathrm{d}Q^2}{2\pi}\mathrm{d}\Phi_2(Q; p_j, p_k') \\
&= \mathrm{d}\Phi_m\,\frac{1}{4(2\pi)^3 s_{ik}}\mathrm{d}s_{ij}\mathrm{d}s_{jk}\mathrm{d}\phi_j.
\end{aligned} \tag{4.43}$$

The idea of Eq. (4.41) is pictorially shown in Figure 4.4. Reference [30] assumes a minimal value $s_{\min}$ for s_{ij} and s_{jk} and restricts $s_{ij} + s_{jk} < s_{ik}$. In order to absorb the poles in s_{ij} and s_{jk} into the measure, [30] suggests the mappings

$$s_{ij} = s_{ik}\left(\frac{s_{\min}}{s_{ik}}\right)^{r_1}, \qquad s_{jk} = s_{ik}\left(\frac{s_{\min}}{s_{ik}}\right)^{r_2} \tag{4.44}$$

where r_1 and r_2 are random numbers in the interval $[0,1]$. With $\mathrm{d}s_{ij} = s_{ij}\ln(\frac{s_{\min}}{s_{ik}})\mathrm{d}r_1$ the phase space decomposition reads

$$\mathrm{d}\Phi_{m+1} = \mathrm{d}\Phi_m\frac{1}{4(2\pi)^3}\frac{s_{ij}s_{jk}}{s_{ik}}\ln^2\left(\frac{s_{\min}}{s_{ik}}\right)\Theta(s_{ij}+s_{jk}<s_{ik})\mathrm{d}r_1\mathrm{d}r_2\mathrm{d}\phi_s. \tag{4.45}$$

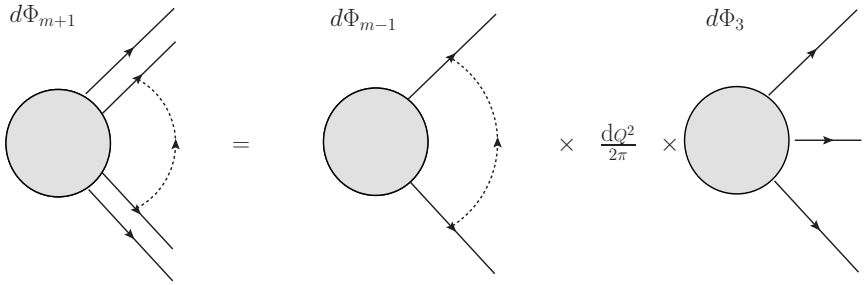

Figure 4.4: Factorization of $\mathrm{d}\Phi_{m+1}$

The angle ϕ_s is chosen according to the mapping $\phi_s = 2\pi r_3$. The final weight for the $m+1$-parton phase space w_{m+1} in terms of the weight w_m of the hard phase space is given by

$$w_{m+1} \quad = \quad w_m \quad \frac{\pi}{2(2\pi)^3} \frac{s_{ij}s_{jk}}{s_{ik}} \ln^2\left(\frac{s_{\min}}{s_{ik}}\right). \tag{4.46}$$

Construction of Final-State Momenta

Using this decomposition of the real radiation (NLO) phase space the $m+1$ final-state momenta are created out of a given m-parton (hard) phase space and three additional random variables r_1, r_2 and r_3. We pick, according to [30], two momenta k_1 and k_2 out of the hard m-parton phase space and create k_1', k_2' and k_r'. After calculating

$$s_{12} = (k_1 + k_2)^2 \ , \tag{4.47}$$

we use Eq. (4.44) in order to generate the invariants s_{1r} and s_{r2}, i.e.

$$s_{1r} = s_{12}\left(\frac{s_{\min}}{s_{12}}\right)^{r_1}, \qquad s_{r2} = s_{12}\left(\frac{s_{\min}}{s_{12}}\right)^{r_2}. \tag{4.48}$$

The azimuthal angle of the additional NLO-phase-space momentum k_r is calculated out of the random variable r_3 acording to

$$\phi_r = 2\pi r_3. \tag{4.49}$$

As required above, the event is rejected if $(s_{1r} + s_{r2}) < s_{12}$ is not fulfilled. Since we consider the case $s_{1r} \to 0$, we check if $s_{1r} < s_{r2}$, otherwise we exchange 1 and 2. In order to fix the final-state momentum k_r' we transform k_1 and k_2 into the centre-of-mass system of $k_1 + k_2$ gaining p_1', p_2' and p_r and perform a rotation such that p_r is parallel to the $z$axis. With

$$\cos\theta_{12} \quad = \quad 1 - \frac{s_{12} - s_{1r} - s_{r2}}{2E_1E_2},$$

$$\cos\theta_{r2} = 1 - \frac{s_{r2}}{2E_sE_2} \tag{4.50}$$

we have

$$p_1' = \begin{pmatrix} \frac{s_{12}-s_{r2}}{2\sqrt{s_{12}}} \\ \frac{s_{12}-s_{r2}}{2\sqrt{s_{12}}}\ \sin\theta_{12}\cos(\phi_r+\pi) \\ \frac{s_{12}-s_{r2}}{2\sqrt{s_{12}}}\ \sin\theta_{12}\sin(\phi_r+\pi) \\ \frac{s_{12}-s_{r2}}{2\sqrt{s_{12}}}\cos\theta_{12} \end{pmatrix}, \quad p_r = \begin{pmatrix} \frac{s_{1r}+s_{r2}}{2\sqrt{s_{12}}} \\ \frac{s_{1r}+s_{r2}}{2\sqrt{s_{12}}}\sin\theta_{r2}\cos\phi_r \\ \frac{s_{1r}+s_{r2}}{2\sqrt{s_{12}}}\sin\theta_{r2}\sin\phi_r \\ \frac{s_{1r}+s_{r2}}{2\sqrt{s_{12}}}\sin\theta_{r2} \end{pmatrix}, \tag{4.51}$$

and

$$p_2' = \begin{pmatrix} \frac{s_{12}-s_{1r}}{2\sqrt{s_{12}}} \\ 0 \\ 0 \\ \frac{s_{12}-s_{1r}}{2\sqrt{s_{12}}} \end{pmatrix}. \tag{4.52}$$

In order to transform the momenta p_1', p_r and p_2' into the NLO final-state momenta k_1', k_2' and k_r' the following Lorentz transformations have to be performed

$$\begin{aligned} k_1' &= \mathcal{B}(Q_0,\mathbf{Q})\mathcal{R}(\phi,\cos\theta)p_1' \\ k_r &= \mathcal{B}(Q_0,\mathbf{Q})\mathcal{R}(\phi,\cos\theta)p_r \\ k_2' &= \mathcal{B}(Q_0,\mathbf{Q})\mathcal{R}(\phi,\cos\theta)p_2' \,, \end{aligned} \tag{4.53}$$

where $Q = k_1 + k_2$ and

$$\theta = \arcsin\left(\frac{\mathbf{p}_2^t}{\mathbf{p_2}}\right), \quad \phi = \arctan\left(\frac{p_2^y}{p_2^x}\right). \tag{4.54}$$

With the above prescription a $m+1$-parton NLO final state is created out of a given hard m-parton phase space in order to account for the soft and collinear regions in the phase space.

4.4 Additional Mappings

In the previous Sections, we focussed on smoothing the peaking structure which belongs to the squared matrix element in both LO and NLO phase space. Peaks of the integrand are also due to factors like the parton distributions functions and the flux factor with at least one initial-state hadron. Especially in the low-energy limit $x_1, x_2 \to 0$ both the flux factor $1/2x_1x_2s$ and the parton distribution functions diverge. As already indicated in Eqs. (4.1) and (4.3) we introduced additional mappings g_{f_a} and g_{f_b} in order to improve the integration of these parts. The basis for the following optimization procedure is the

technique of importance sampling (see Section 2.3.2) and a cut on the minimal partonic centre-of-mass energy $s_{\min}$ in order to avoid the divergence at $x_1, x_2 \to 0$. In

$$\sigma = \int_0^1 \mathrm{d}x_1 \int_0^1 \mathrm{d}x_2 \int \mathrm{d}\Phi_m \frac{f_a(x_1,\mu^2) f_b(x_2,\mu^2)}{2x_1 x_2 s}\, \hat{\sigma}_{ab}(x_1 p_a, x_2 p_2, \mu^2) \tag{4.55}$$

we perform the variable transformation

$$\tau \to x_1 x_2, \quad x \to x_2 \tag{4.56}$$

with the corresponding Jacobian

$$J = \left| \frac{\partial(\tau, x)}{\partial(x_1, x_2)} \right| = x_2 \tag{4.57}$$

and find

$$\sigma = \int_{\tau_{min}}^1 \mathrm{d}\tau_1 \int_\tau^1 \mathrm{d}x \int \mathrm{d}\Phi_m \frac{f_a(\frac{\tau}{x},\mu^2) f_b(x,\mu^2)}{2\tau x s}\, \hat{\sigma}_{ab}(x_1 p_a, x_2 p_2, \mu^2), \tag{4.58}$$

where $\tau_{\min} = s_{\min}/s$. As pointed out in Reference [31] this variable transformation without any mapping already smoothens the contribution from the pdfs to some extent. Now the factor $1/(\tau x)$ from the flux factor still has to be flattened. This is done by the following mappings

$$\tau(r_1) = \tau_{\min}^{\sqrt{1-r_1}}, \quad x(r_2) = \tau^{1-r_2} \tag{4.59}$$

with their corresponding Jacobians

$$g_\tau(\tau)^{-1} = \frac{\ln^2(\tau_{\min})\tau}{-2\ln(\tau)}, \quad g_x(x)^{-1} = -x\ln(\tau). \tag{4.60}$$

Also other singular terms occur during the calculation of the integrated subtraction terms, namely +-prescriptions such as $1/[z(1-z)]_+$ and $1/[(1-z)]_+$, which are divergent, if $z \to 1$ and/or $z \to 0$. In both cases we proceed as above with the importance sampling technique by finding appropriate mappings and cuts and, following [31]. The factor $1/(1-z)$ diverges, if $z \to 1$. With an upper integration limit of $z_{\max}$, the mapping reads

$$z_1(r) = 1 - \mathrm{e}^{\mathrm{r}\ln(1-\mathrm{z_{max}})} \tag{4.61}$$

with its corresponding density

$$g_{z_1}(z_1)^{-1} = -\ln(1-z_{\max})(1-z_1). \tag{4.62}$$

For the factor $1/z(1-z)$, we additionally find a divergence in $z \to 0$. Hence, we impose a cut on the lower integration boundary $z_{\min}$. The specific mapping is given by

$$z(r) = \frac{\mathrm{e}^{\frac{\mathrm{r-b}}{\mathrm{a}}}}{1 - \mathrm{e}^{\frac{\mathrm{r-b}}{\mathrm{a}}}} \tag{4.63}$$

and its Jacobian reads

$$g_z(z)^{-1} = \frac{z(1-z)}{a}, \tag{4.64}$$

where

$$a = \ln\left(\frac{z_{\max}(1-z_{\min})}{(1-z_{\max})z_{\min}}\right)^{-1}, \quad b = -a\ln\left(\frac{z_{\min}}{1-z_{\min}}\right). \tag{4.65}$$

The mappings discussed in this Section are implemented separately, as Table 4.1 shows.

Peak	Subroutine
$\frac{f_a(x_1,\mu^2)f_b(x_2,\mu^2)}{2x_1x_2s}$	`mapxpdf`
$\frac{1}{(1-z)}$	`map_omz`
$\frac{1}{z(1-z)}$	`map_zomz`

Table 4.1: Additional mappings and subroutines

4.5 Structure of the Program

In the following, we describe the basic structure of the program and its usage. As a Monte Carlo integrator including an implementation of the dipole subtraction formalism, the program consists of two main parts. On the one hand side, it creates all the information needed to integrate the complete NLO process out of the input of the Born process and the corresponding NLO process. This means, it first creates a list of all possible LO and NLO generators and checks if they exist. In a next step, the program identifies all the colour-correlated Born matrix elements needed in the dipole subtraction formalism and creates the following files:

- `list.gen`: List of all existing LO/NLO generators with their corresponding processes.
- `list.dsf`: List of all dipole subtraction terms for all real-radiation generators (including the number of the dipole subtraction term and the explicit splitting).
- `RequiredSubroutines`: List of the subroutines the user has to provide.
- `user_subroutines.f90`: Input scheme for the required subroutines.

The subroutines listed in `RequiredSubroutines` have to be implemented in the file `me_calls.f90`.
The process-dependent files are written into a subdirectory `mcrun/`. After providing the required subroutines the program can be compiled in `mcrun/`.
For the integration itself we provide four different integration routines listed in Table

Subroutine	Role
`integrationBorn`	Integration Routine for Φ_m according to 4.2
`integrationreal`	Integration Routine for Φ_{m+1} according to 4.2
`integrationrealps`	Integration Routine for Φ_{m+1} according to 4.3
`integrationvirtual`	Integration Routine for Φ_m according to 4.2

Table 4.2: Integration Subroutines

4.2 and explained in Section 4.5.2 In the following we explain in detail the structure and usage of the program.

4.5.1 Initialization

The initialization phase of the main program contains multiple steps. At first, the process with its parameters is set up, and the parameters for the Monte Carlo run are initialized, e.g. number of events and technical cuts. Next, all possible LO (Born) generators are generated out of the input. In case of a composite particle such as a proton, all possible combinations of initial states are built and it is checked if the underlying process exists. Only the processes that exist in the Standard Model are considered as a Born generator. As a next step, all NLO generators are created and checked for their existence. The subroutines `create_nlo_generators` and `check_gen` create the generators for the real radiation process by adding the additionally radiated particle to all given LO generators and check if the process exists. The Born generators also form the basis for the generators of the virtual corrections, since they obey the same phase space. Therefore, we use the same generators for the Born process and the virtual corrections. For the integration of the real and virtual corrections, the information for the dipole subtraction formalism has to be set up next. The subroutine `subtractiontermtable` checks for all possible dipole subtraction terms of the real radiation generators and stores the corresponding numbers (see Tables in Chapter 3) in variables like `D_AS_BS`, where `AS` and `BS` can denote `F`inal and/or `I`nitial `S`tate. This finalizes the initialization.

4.5.2 Structure of Integration

The main program loops over the number of generators for each phase space (Born, real, virtual) and calls — depending on what flags are set — the following subroutines in each step of the loop:

- `subroutine integrationBorn`
- `subroutine integrationreal`

- `subroutine integrationrealps`
- `subroutine integrationvirtual`

Born Phase Space

The Born-integration routine loops over the number of events N_{events}. The first step in each loop is the generation of random numbers by calling `subroutine RANLUX`, which is declared in the file `mod_ranlux.f`. The amount n_{rn} of random numbers needed depends on phase space, number of incoming hadrons and chosen mappings

$$n_{\text{rn}} = 3n_{\text{out}} - 4 + n_{\text{mpdf}} + n_{\text{momz}}, \tag{4.66}$$

where n_{out} is the number of outgoing particles, n_{mpdf} the number of incoming hadrons increased by one (one chooses the order x_1 and x_2 distributed over pdf_1 and pdf_2) and n_{momz} denotes the number of random variables needed for the mappings of the poles in $1/1-z$ as seen in Chapter 4.4. In case of initial-state hadrons, `mapxpdf` is called in order to smoothen the behaviour of the parton distribution functions according to the chosen mappings (`flpdfmap` – see Section 4.6). As a next step, the momenta for the LO phase space are generated by calling `generate_momenta`. This subroutine is provided by the module `density` and generates the final-state momenta out of a given set of random numbers according to a randomly chosen channel of the considered generator. With the final-state momenta at hand, cuts can now be applied via the subroutine `recombination`. If the set of final states passes the cuts, the squared Born matrix element is evaluated in the subroutine `integrandBorn`, which has to be provided by the user. As a next step, the program calculates according to the multi-channel approach the sum of all single-channel densities and combines all calculated densities to $g_{\text{tot}}^{\text{LO}}$. One loop iteration finishes with the calculation of the weight according to Eq. (4.78) and summing the weight and the square of the weight in order to compute the standard deviation of calculation as shown in Chapter 2 . If N_{events} are accepted, the result will be written into the file `result.dat`.

Real Corrections

For the integration of Bremsstrahlung processes, we implemented two different routines that differ in the way the NLO phase space is built. The subroutine `integrationreal` acts according to the method described in Chapter 4.2, whereas `integrationrealps` creates the final-state momenta and the corresponding densities according to Chapter 4.3. The basic structure of both subroutines is closely related to the Born integration routine, only three steps are different. After the evaluation of the squared real radiation matrix element via `integrandreal` the sum of all contributing dipole subtraction terms $\mathrm{d}\sigma^{\text{A}}$ is calculated in the subroutine `dipole_all_real_subterms`, which is declared in

the module `subtractionmodule`. The weight here is consequently calculated according to Eq. (4.80) and summed up as shown above.

Virtual Corrections

The structure of the integration of the virtual contribution is similar to the real radiation integration. The momenta and densities are created according to the underlying Born phase space. The virtual matrix element is evaluated in the subroutine `integrationvirtual`. All contributing integrated subtraction terms are calculated in `dipole_al_int_terms` and `mass_dipole_all_int_terms` and contribute to the weight as shown in Eq. (4.81).

Module `density` contains all necessary functions and subroutines to generate the momenta and compute the corresponding densities. In order to generate the momenta according to Chapters 4.2 and 4.3, we implemented the subroutine `generate_momenta`. The densities of Eq. (4.29) are computed in `generate_densities`.

4.5.3 Clustering and Recombination algorithm

In order to compute multijet cross Sections we implemented a recombination and clustering algorithm (se e.g. References [32], [33]). In the algorithm the final-state particles are — under certain conditions — recursively recombined into clusters, until no further recombination is possible. In our code we implemented three different clustering algorithms (anti-k_T, Cambrigde/Aachen and k_T-algorithm) and the E-scheme (four-vector addition) for recombination. For the clustering algorithm it is essential to know, which particles of the given process contribute in the clustering and recombination procedure. We encode this with a flag `typepart(i)` in `setup.f90` that can have the following values:

- `typepart(i) = 1`: Particle i is a jet and can merge to jets (e.g. quarks, gluons)
- `typepart(i) = -1`: Particle i is not a jet, but can merge to jets (e.g. photons)
- `typepart(i) = 0`: Particle i is not a jet and does not merge to jets.

The procedure of the algorithm is as follows:

1. For every pair of final-state objects k and l, which cluster according to `typepart(k)` and `typepart(l)`, the values $d_k = k^p_{\mathrm{T},k}$, $d_l = k^p_{\mathrm{T},l}$ and the parameter

$$d_{kl} = \min(k^p_{\mathrm{T},k}, k^p_{\mathrm{T},l}) \frac{\Delta R_{kl}}{D^2} \tag{4.67}$$

are calculated. Therein $\Delta R_{kl} = (y_k - y_l)^2 + (\Phi_k - \Phi_l)^2$ and y_l and Φ_l are respectively the rapidity and azimuthal angle of objects l and D is an additional parameter. The exponent p can be chosen to be

- $p = -1$ corresponding to the anti-k_T-algorithm,
- $p = 0$ corresponding to the Cambrigde/Aachen-algorithm,
- $p = 1$ corresponding to the k_T-algorithm.

2. Find the smallest value among the d_k and d_{kl}.

3. If d_{kl} is the smallest value, then recombine the objects k and l to a new object (kl) by adding their four-momenta $p_{(kl)} = p_k + p_l$. If d_k is the smallest value, the object k is not mergable and is defined as jet. Thus, the variable `typejet(k)` is set to `1`.

4. Repeat until all mergable objects have been included into jets.

The momenta of all objects and jets are stored in `kjet` and their corresponding types in `typejet`. Both are return values of our clustering subroutine `ktcluster` and are passed on to the cut algorithm, which is explained in the following Section.

4.5.4 Cuts

We also implemented a basic, generic cut scheme that allows to impose cuts on the final-state momenta. The cut function is a logical function `passcut` that returns `true` or `false`, if the final-state momenta pass the cuts or not. We structured and arranged the type of cuts that can be imposed in the following way:

1. We apply cuts to jets, if `jetcut` in `setup.f90` is set to `true`, by calling the subroutine `cut_jets`. Cuts on jets are only applied to the momenta i with `typejet(i)=1`. This subroutine ensures that at least `numjet` jets with a minimum transverse momentum of `ptjetcut` and a maximum pseudorapidity of `etajetcut` are present in the final state. Furthermore a list of jets ordered by decreasing p_T is produced, which will be needed in step 3. The first `numjet` jets in this list are called *tagging jets*. If `numjet` is set to 0, the cuts of step 3 are applied to all jets passing the minimum transverse momentum and the maximum pseudorapidity cut. The default value for `numjet` is 0.

2. As a next step cuts to leptons are applied, if `lepcut` in `setup.f90` is set to `true`. This subroutine `lep_cuts` cuts only on momenta i with `chargedlep(i)=1` and ensures that `numlep` leptons with a minimum transverse momentum of `ptlepcut` and a maximum rapidity of `etalepcut` are present in the final state. Also here a list of leptons ordered by decreasing p_T is produced, which will be needed in step 4. If `numlep` is set to 0, the cuts of step 4 are applied to all leptons passing the minimum transverse momentum and the maximum rapidity cut. The default value for `numlep` is 0.

3. Now cuts to pairs of jets are applied, if `jjcut` in `setup.f90` is set to `true`. The subroutine `jet_jet_cuts` is applied to all pairs of tagging jets and checks for a minimal separation angle between two jets in the rapidity-azimuthal angle plane and for minimal invariant mass of the two jets.

4. If `llcut` is set to `true`, we apply cuts to lepton pairs, which can be built out of the list of leptons produced in step 2. This is done in the subroutine `lep_lep_cuts` that can apply the same cuts as to pairs of jets.

5. If `ljcut` is set to `true`, we apply cuts to all pairs of jets and leptons. If `numjet` and/or `numlep` are set to a non-zero value, we take only the first `numjet` jets and/or `numlep` leptons into account. The subroutine `lep_jet_cuts` applies rapidity-azimuthal angle cuts and minimal invariant mass cuts.

We point out that this is only the basic setup of generic cuts, which can easily be supplemented with cuts from user. Table 4.3 shows the basic set of cuts that we already have implemented. Each of the functions listed in the Table above returns `.true.` or

Logical Function	Role
`minenergycut`	Minimum Energy of outgoing particle
`minptcut`	Minimum p_t of outgoing particle
`mininvmcut`	Minimum invariant mass
`maxrapiditycut`	Maximum rapidity
`pseudorapiditycut`	Maximum pseudorapidity
`minrapsepcut`	Minimum Rapidity Separation
`deltarsepcut`	Minimum Delta Separation
`opphemiscut`	Require two partons to be in opposite detector hemispheres

Table 4.3: Function: Cuts

`.false.` whether the cut is passed (`.true.`) or is not passed (`.false.`). In the arguments of following subroutines we denote the momenta of the actual phase-space point with `kin` and `i` stands for the parton number the cut is applied to. In order to consider events that have large enough energy we have implemented the logical function

```
logical function minenergycut(i,kin,minecut,gen,errorflag)
```

and for ensuring a large enough transverse momentum

```
logical function minptcut(i,kin,ptcut,gen,errorflag),
```

which requires

$$k_{\mathrm{T}} = \sqrt{k_x^2 + k_y^2} > k_{\mathrm{T,cut}}. \tag{4.68}$$

Another kinematic, dimensionless variable is the reference-frame-dependent rapidity defined as

$$y_i = \frac{1}{2} \ln \frac{k_i^0 + k_i^3}{k_i^0 - k_i^3}. \tag{4.69}$$

The logical function

`maxrapiditycut(i,kin,maxrapcut,gen,errorflag)`

cuts on the maximum rapidity of parton `i` and analogously the function

`pseudorapiditycut(i,kin,maxrapcut,gen,errorflag)`

cuts on the maximum pseudorapidity. A cut on the rapidity separation and thus accounts for the spatial separation of two partons, i.e.

$$|y_i - y_j| = \left| \frac{1}{2} \ln \frac{k_i^0 + k_i^3}{k_i^0 - k_i^3} - \frac{1}{2} \ln \frac{k_j^0 + k_j^3}{k_j^0 - k_j^3} \right|. \tag{4.70}$$

is performed by the logical function

`minrapsepcut(pind1,pind2,kjet,minrapcut,gen,errorflag)`

We impose a lower $y_{\min}$ cut on the absolute value of the difference of rapidites $|y_i - y_j| > y_{\min}$. The rapidity allows to check if two particles are in opposite detector hemispheres. This is accounted for in the logical function `opphemiscut(i,j,kin,gen,errorflag)`, which checks

$$y_i \times y_j < 0. \tag{4.71}$$

We can also impose cuts on pseudo rapidity via the logical function , which is defined as

$$\eta = -\ln \tan \frac{\theta}{2}, \tag{4.72}$$

where θ is the angle between the considered parton and the beam axis. It can also happen that the detector cannot resolve two particles which hit the detector too close to each other. To impose a minimal separation angle between two partons we implement a rapidity-azimuthal angle separation cut. In

`logical function deltarsepcut(i,j,kin,deltarcut,gen,errorflag)`

we calculate

$$\Delta R_{i,j} = \sqrt{(\eta_i - \eta_j)^2 - (\phi_i - \phi_j)^2} \tag{4.73}$$

where ϕ_i denotes the azimuthal angle of parton i and we impose a lower cut `deltarcut` on $\Delta R_{i,j}$. We also implemented a cut on the minimal invariant mass of two partons i and j via the

`logical function mininvmcut(i,j,kin,invmcut,gen,errorflag),`

where the invariant mass of the partons i and j is calculated and a lower cut `invmass` is demanded.

4.5.5 Implementation of Dipole Subtraction Terms

The dipole subtraction terms are implemented in the file `subtractionmodule.f95` that produces a module named `subtractionmodule`. It fulfills two main tasks, creating a Table of all possible subtraction terms to a given generator and calculating the corresponding subtraction terms. The subroutine `subtractiontermtable` calls

- `call table_D_FS_FS`
- `call table_D_IS_FS`
- `call table_D_FS_IS`
- `call table_D_IS_IS`.

These subroutines check if a dipole subtraction term for the corresponding spectator emitter pair is needed and store an according value to the global variables `D_AS_BS` — where $A, B \in \{F, I\}$. All of the four subroutines listed above call `check_subtraction` which goes through all possible emitter–spectator pairs and returns an integer value if a subtraction term exists. The subroutine `dipole_all_real_subterms` calculates the sum of all dipole subtraction terms by calling five subroutines

1. `call dipole_real_FSem_FSsp`
2. `call dipole_real_FSem_ISsp`
3. `call dipole_real_ISem_FSsp`
4. `call dipole_real_ISem_ISsp`
5. `call dipole_sum`.

The first four subroutines calculate the appearing subtraction terms and store their results in the `real` variables

1. `Dsub_FS_FS`
2. `Dsub_FS_IS`
3. `Dsub_IS_FS`
4. `Dsub_IS_IS`,

where the first part of the variable name (FS, IS) labels the emitter and the second part the spectator. These variables are declared as

```
double precision, dimension(n_part,n_part,n_part,maxg) :: Dsub_AS_BS.
```

Nr.	Case	Subroutine
1	$q \to g + q$	`dipole_FSem_FSsp_gl_q`
2	$g \to g + g$	`dipole_FSem_FSsp_gl_gl`
3	$g \to q + \bar{q}$	`dipole_FSem_FSsp_q_q`
101	$Q \to g + Q$	`dipole_mass_FSem_FSsp_gl_q`
102	$g \to g + g$	`dipole_mass_FSem_FSsp_gl_gl`
103	$g \to Q + \bar{Q}$	`dipole_mass_FSem_FSsp_q_q`

Table 4.4: Subroutines: FS emitter - FS spectator

Nr.	Case	Subroutine
21	$q \to q_a + g_i$	`dipole_ISem_FSsp_gl_q`
22	$q \to g_a + q_i$	`dipole_ISem_FSsp_gl_qbar`
24	$g \to q_a + \bar{q}_i$	`dipole_ISem_FSsp_q_q`
25	$g \to g_a + g_i$	`dipole_ISem_FSsp_gl_gl`
121	$q \to q_a + g_i$	`dipole_mass_ISem_FSsp_gl_q`
122	$q \to g_a + q_i$	`dipole_mass_ISem_FSsp_gl_qbar`
124	$g \to q_a + \bar{q}_i$	`dipole_mass_ISem_FSsp_q_q`
125	$g \to g_a + g_i$	`dipole_mass_ISem_FSsp_gl_gl`

Table 4.5: Subroutines: IS emitter - FS spectator

The first index stands for the spectator, the second for the emitter which emits the parton that is labelled by index three. The fourth and last index is the generator in which the subtraction term occurs. Hence `Dsub_FS_IS(1,5,6,4)` stands for the subtraction term $\mathcal{D}^1_{56}$ of generator 4. The subroutine `call dipole_sum` sums all the non-zero subtraction terms and returns the value `dipolesum` that is equal to $\mathrm{d}\sigma^{\mathrm{A}}$ at the given phase-space point. The subroutines `dipole_real_ASem_BSsp` calculate all possible dipole subtraction terms in the given emitter–spectator case ($A, B \in \{F, I\}$). The integer variable `D_AS_BS` contains a coded number that refers to one specific dipole subtraction term according to the Tables in Chapter 3. This numbering is unique for the subtraction terms, but not for the integrated subtraction terms. The reason for this is that, in the presence of massive particles, the structure of the integrated subtraction terms depends on which of the particles (emitter and/or spectator) is massive. The structure of the subtraction terms for the real correction does instead not depend on that. If one of the `D_AS_BS` values is non-zero the corresponding subroutine calculating the subtraction term is called. The result of the term is stored in `Dsub_AS_BS`. The subroutines that can be called from `dipole_real_ASem_BSsp` are listed in the following Tables and are either of the form `dipole_ASem_BSsp_C_D` or of the form `dipole_mass_ASem_BSsp_C_D`, where $A, B \in \{F, I\}$ and $C, D \in \{q, \bar{q}, gl\}$.

The basic structure of the subroutines

Nr.	Case	Subroutines
11	$q \to g + q$	`dipole_FSem_ISsp_gl_q`
12	$g \to g + g$	`dipole_FSem_ISsp_gl_gl`
13	$g \to q + \bar{q}$	`dipole_FSem_ISsp_q_q`
111	$q \to g + q$	`dipole_mass_FSem_ISsp_gl_q`
112	$g \to g + g$	`dipole_mass_FSem_ISsp_gl_gl`
113	$g \to q + \bar{q}$	`dipole_mass_FSem_ISsp_q_q`

Table 4.6: Subroutine: FS emitter - IS spectator

Nr.	Case	Subroutines
31	$q \to q_a + g_i$	`dipole_ISem_ISsp_gl_q`
32	$q \to g_a + q_i$	`dipole_ISem_ISsp_gl_qbar`
33	$g \to q_a + \bar{q}_i$	`dipole_ISem_ISsp_q_q`
34	$g \to g_a + g_i$	`dipole_ISem_ISsp_gl_gl`

Table 4.7: Subroutines: IS emitter - IS spectator

`dipole_ASem_BSsp_C_D`

or

`dipole_mass_ASem_BSsp_C_D`

is as follows:

```
subroutine dipole_(mass_)ASem_BSsp_C_D

! declarations
 call  map_(mass_)ASem_BSsp
!  calculate variables needed for the subtraction term
call reducedMEsquared
! calculate the final result and store it in the global variable
Dsub_AS_BS

end subroutine dipole_mass_ASem_BSsp_C_D
```

The names of the subroutines and the splittings they correspond to can be found in Tables 4.4 – 4.11. The functions `map_(mass_)ASem_BSsp` return the momenta and other kinematical variables needed according to the mappings defined in Chapter 3. The correlated colour-projected reduced matrix element is the return value of the subroutine `reducedMEsquared` and the final result of the subtraction term is stored in `Dsub_AS_BS`. The α dependence, i.e. if a subtraction term is evaluated at the given phase space point, is realized with an `if` statement after the corresponding kinematical

variable is calculated. There are four different cases to which the phase-space restriction parameter α can be applied to. The variables in the code are intuitively named as `alpha_ASem_BSsp`.

In the cases of a gluon splitting either into a gluon–gluon pair or a quark–anti-quark pair the splitting functions obey a Lorentz structure like [34]

$$\boldsymbol{V}^{\mu\nu} \propto \left(-g^{\mu\nu} + C_1 u^\mu u^\nu\right). \tag{4.74}$$

In order to calculate the corresponding dipole subtraction term in a generic way, one uses the spin sum

$$\sum_{\lambda=+,-} \epsilon^\mu(k,\lambda)\epsilon^{*\nu}(k,\lambda) = -g_{\mu\nu} - \frac{k^\mu k^\nu}{(k\cdot n)^2} n^2 + \frac{n^\nu k^\mu + n^\mu k^\nu}{k\cdot n}. \tag{4.75}$$

The first term of relation (4.74) results in

$$\begin{aligned}
\mathcal{M}^*_\mu(-g_{\mu\nu})\mathcal{M}_\nu &= \mathcal{M}^*_\mu \left(\sum_{\lambda=+,-} \epsilon^\mu(k,\lambda)\epsilon^{*\nu}(k,\lambda) + \frac{k^\mu k^\nu}{(k\cdot n)^2} n^2 - \frac{n^\nu k^\mu + n^\mu k^\nu}{k\cdot n} \right) \mathcal{M}_\nu \\
&= \sum_{\lambda=+,-} \mathcal{M}^*_\mu \epsilon^\mu(k,\lambda) \mathcal{M}_\nu \epsilon^{*\nu}(k,\lambda) \\
&= \sum_{\lambda=+,-} \left|\mathcal{M}_\lambda\right|^2,
\end{aligned} \tag{4.76}$$

where we used $\mathcal{M}_\nu k^\nu = 0$, $u\cdot k = 0$ and denoted $\mathcal{M}_\lambda = \mathcal{M}_\mu \epsilon^{*\mu}(k,\lambda)$. The second part of relation (4.74) $u^\mu u^\nu \mathcal{M}^*_\mu \mathcal{M}_\nu$ using Eq. (4.75) can be rewritten as [34]

$$\begin{aligned}
u^\mu u^\nu \mathcal{M}^*_\mu \mathcal{M}_\nu &= u_\rho u_\sigma \mathcal{M}^*_\mu \mathcal{M}_\nu \left(\sum_{\lambda=+,-} \epsilon^\mu(k,\lambda)\epsilon^{*\rho}(k,\lambda) + \frac{k^\mu k^\rho}{(k\cdot n)^2} n^2 - \frac{n^\rho k^\mu + n^\mu k^\rho}{k\cdot n} \right) \\
&\cdot \left(\sum_{\lambda=+,-} \epsilon^\nu(k,\lambda)\epsilon^{*\sigma}(k,\lambda) + \frac{k^\nu k^\sigma}{(k\cdot n)^2} n^2 - \frac{n^\sigma k^\nu + n^\nu k^\sigma}{k\cdot n} \right) \\
&= \sum_{\lambda=+,-} \left(\left|\mathcal{M}_\lambda\right|^2 \left|u\cdot\epsilon(k,\lambda)\right|^2 \right) \\
&+ 2\mathcal{R}\left(\mathcal{M}^*_+ \mathcal{M}_- \left(u\cdot\epsilon^*(k,+)\right)\left(u\cdot\epsilon(k,-)\right) \right).
\end{aligned} \tag{4.77}$$

In the case of a gluon splitting into two partons, four values are needed as an input for a generic implementation of the dipole subtraction formalism namely $|\mathcal{M}_-|^2$, $|\mathcal{M}_+|^2$, $\mathcal{M}^*_+\mathcal{M}_-$ and $\mathbf{T}_i\mathbf{T}_k \left|\mathcal{M}^{i,k}\right|^2$. In our implementation, the `subroutine reducedMEsquared` is called with arguments i and k labeling the wanted colour projection. In the case of a gluon splitting into a gluon pair or a quark–anti-quark pair, the subroutine has the following three return values:

- `rescmplx` corresponds to $\mathbf{T}_i\mathbf{T}_k\mathcal{M}_+^{i,k^*}\mathcal{M}_-^{i,k}$,
- `resp` corresponds to $\mathbf{T}_i\mathbf{T}_k\left|\mathcal{M}_+^{i,k}\right|^2$,
- `resm` corresponds to $\mathbf{T}_i\mathbf{T}_k\left|\mathcal{M}_-^{i,k}\right|^2$,
- `respm` corresponds to $\mathbf{T}_i\mathbf{T}_k\left|\mathcal{M}^{i,k}\right|^2$.

4.5.6 Implementation of Integrated Subtraction Terms

There are four categories of integrated subtraction terms, two of which are implemented. In general the implementation structure of the α-dependent differs from α-independent integrated subtraction terms. In the α-independent case we have two different but equivalent implementations. We can use the integrated subtraction terms that are combined to a sum of contributions presented in Chapters 3.4.4 and 3.4.5. The second possibility is to use the separately integrated dipole subtraction terms. This means that for every dipole subtraction term for the real radiation matrix element the corresponding integrated subtraction term is evaluated. The latter is completely flexible, i.e. it is possible to use different values for α for different initial-state final-state combinations and all different combinations of massless and massive particles can be accounted for. The formulas of Chapters 3.4.4 and 3.4.5 can only be used in the α-independent case. Thus, it is recommended to use the implementation of the separately integrated dipole subtraction terms.

4.5.6.1 Implementation of α-dependent Integrated Subtraction Terms

The α-dependent integrated subtraction terms are implemented using the one to one correlation of subtraction term to integrated subtraction term. Therefore, the structure of this implementation is closely related to the one of Chapter 4.5.5. The output of the subroutine `subtractiontermtable`, which was already run during initialization, is used to calculate the integrated subtraction terms. The sum over all these terms is calculated in the routine `dipole_al_int_terms`, calling the following five functions

1. `alint_dipole_real_FSem_FSsp`
2. `alint_dipole_real_ISem_FSsp`
3. `alint_dipole_real_FSem_ISsp`
4. `alint_dipole_real_ISem_ISsp`
5. `int_dipole_sum`.

The first four subroutines calculate the integrated subtraction terms for one particular emitter–spectator pair. Each of them checks the values stored in `D_AS_BS` with $A, B \in \{F, I\}$ and calls the correlated subroutine, calculating the specific integrated subtraction term. All the occurring cases are listed in the following Tables 4.8 – 4.9.

Nr.	Case	Subroutine
1	$q \to g + q$	`al_dipole_FSem_FSsp_I_gl_q`
2	$g \to g + g$	`al_dipole_FSem_FSsp_I_gl_gl`
3	$g \to q + \bar{q}$	`al_dipole_FSem_FSsp_I_q_q`
101	$Q \to g + Q$	`al_dipole_mass_FSem_FSsp_I_gl_q`
102	$g \to g + g$	`al_dipole_mass_FSem_FSsp_I_gl_gl`
103	$g \to Q + \bar{Q}$	`al_dipole_mass_FSem_FSsp_I_qm_qm`

Table 4.8: Subroutines integrated subtraction terms: FS emitter - FS spectator

The results are stored into global variables such as

```
real(kind=dp), dimension(n_part,n_part,n_part,0:4,0:3,maxg) :: al_Int_AS_BS.
```

The fourth index going from 0 to 4 accounts for the different phase spaces the integrated subtraction term have to be evaluated in, such that

- index 0 stands for the x-dependent phase space and
- index 1 stands for the phase space with $x = 1$.

Details on the calculation of the distributions in the different cases are explained in Chapter 3.4.6. The fifth index going from 0 to 3 returns the coefficients from the ϵ-poles in the **I**-operator, where index i correspond to ϵ^{-i}, i.e.

- index $0 \leftrightarrow \epsilon^0$
- index $1 \leftrightarrow \epsilon^{-1}$

Nr.	Case	Subroutine
21	$q \to q_a + g_i$	`al_dipole_ISem_FSsp_I_q_q`
22	$q \to g_a + q_i$	`al_dipole_ISem_FSsp_I_q_gl`
24	$g \to q_a + \bar{q}_i$	`al_dipole_ISem_FSsp_I_gl_q`
25	$g \to g_a + g_i$	`al_dipole_ISem_FSsp_I_gl_gl`
121	$q \to q_a + g_i$	`al_dipole_mass_ISem_FSsp_I_q_q`
122	$q \to g_a + q_i$	`al_dipole_mass_ISem_FSsp_I_q_gl`
124	$g \to \bar{q}_a + q_i$	`al_dipole_mass_ISem_FSsp_I_gl_q`
125	$g \to g_a + g_i$	`al_dipole_mass_ISem_FSsp_I_gl_gl`

Table 4.9: Subroutines integrated subtraction terms: IS emitter - FS spectator

Nr.	Case	Subroutines
11	$q \to g + q$	`al_dipole_FSem_ISsp_I_gl_q`
12	$g \to g + g$	`al_dipole_FSem_ISsp_I_gl_gl`
13	$g \to q + \bar{q}$	`al_dipole_FSem_ISsp_I_q_q`
111	$q \to g + q$	`al_dipole_mass_FSem_ISsp_I_q_ql`
112	$g \to g + g$	-
113	$g \to q + \bar{q}$	`dipole_mass_FSem_ISsp_I_q_q`

Table 4.10: Subroutine integrated subtraction terms: FS emitter - IS spectator

Nr.	Case	Subroutines
31	$q \to q_a + g_i$	`al_dipole_ISem_ISsp_I_q_q`
32	$q \to g_a + q_i$	`al_dipole_ISem_ISsp_I_q_gl`
33	$g \to q_a + \bar{q}_i$	`al_dipole_ISem_ISsp_I_gl_q`
34	$g \to g_a + g_i$	`al_dipole_ISem_ISsp_I_gl_gl`

Table 4.11: Subroutines integrated subtraction terms: IS emitter - IS spectator

- index $2 \leftrightarrow \epsilon^{-2}$.

Subroutine `int_dipole_sum` sums up all the integrated subtraction terms returning the array

```
double precision,dimension(0:4,0:3) :: intdipolesum,
```

where the two indices are the same as the ones explained above. The coefficients of the ϵ-poles can be used to check the **I**-operator with the virtual corrections. The ϵ-poles of the **I**-operator and the virtual corrections should cancel at any arbitrary phase-space point. The implementation of the massive α-dependent subtraction terms is straightforward and the corresponding subroutines and functions are already listed in the Tables above. The α-independent subtraction terms can of course also be calculated in this module by setting $\alpha = 1$. Nevertheless, we have a second implementation according to the sum formulas. The two implementations allow for consistency checks of the code, due to their thoroughly different design.

4.5.6.2 Implementation of sum formula of integrated subtraction terms

This type of implementation is based on the sum formulas given in the Chapters 3.4.4 and 3.4.5. The three different cases depending on the number of initial-state partons present are in the massless case represented by the subroutines

- `Iop_no_ishadrons`
- `Iop_one_ishadrons`

- `Iop_two_ishadrons`

and in the massive case given by

- `massIop_no_ishadron`
- `massIop_one_ishadrons`
- `massIop_two_ishadrons` .

In the massless case of no initial state hadron, `Iop_no_ishadrons` mainly contains two loops according to the sums in Eq. (3.176), where the subroutines `intcalvi` and `virtualBorn` are called. Subroutine `intcalvi` calculates the result of Eq. (3.177) and returns a array, whose index represents the coefficient in front of the ϵ-poles, and `virtualBorn` returns the colour-projected Born matrix element. The result of `Iop_no_ishadrons` is a three-dimensional array accounting for the poles in ϵ. In the presence of one initial state hadron, the subroutine `Iop_one_ishadrons` is called, which calculates the result of Eq. (3.180) taking Eq. (3.181) – Eq. (3.183) into account. The **I**-operator of Eq. (3.181) is calculated in subroutine `Iop_a` and the **K** and **P** operators in the corresponding subroutines `intpabvec` and `intkabvec`. The result of subroutine `Iop_one_ishadrons` is stored in the variable

```
real(kind=dp),dimension(0:4,0:3) :: ioponeres,
```

where the indices again account for phase spaces and coefficients of ϵ-poles. The subroutine `Iop_two_ishadrons` calculates the case of two initial-state hadrons according to Eq. (3.190) - Eq. (3.192). The straightforward named subroutines calculating each one of the equations are `iop_ab`, `intpabvectwo` and `intkabvectwo`. The result is given in an array that has the same array dimensions as `ioponeres`. In the case of massive partons the Eq. (3.195), Eq. (3.207) – Eq. (3.210) and Eq. (3.217) – Eq. (3.219) are implemented in a straightforward way, as their sum formulas suggest.

4.5.7 Calculation of Weights

Now we have all values at hand and can combine them to the final weight, out of which the integration result can be calculated. This is done in the main integration routine in `integration.f90`. For the Born result, we only have to take LO phase space into account, which leads to the density $g_{\text{tot}}^{\text{LO}}$ calculated according to Eq. (2.83). In case of one initial-state hadron we need a mapping for one parton distribution function. In order to smoothen the pdf behaviour we have the mapping $z_{\text{1ish}}(r) = (1/x_0 - 1)/r$ and x_0 is the lower integration bound. The default value for x_0 is 10^{-6}. The corresponding density is given by $g_{\text{1ish}}^{-1} = -(1/x_0 - 1)/r^2$ and we replace in Eqs. (4.78),(4.80) and (4.81) $1/(g_\tau g_x)$ with g_{1ish}^{-1}. In case of two initial-state hadrons we acquire the additional

weights $g_\tau(\tau)$ and $g_x(x)$ as defined in Eq. (4.60). With the value for the Born matrix element squared $\mathcal{M}^2_{\text{Born}}$, we have

$$w_{\text{LO}} = \frac{1}{g_\tau g_x} \frac{\mathcal{M}^2_{\text{Born}}}{g^{\text{LO}}_{\text{tot}}} \tag{4.78}$$

for the weight, which is summed up as follows

$$res = res + w_{\text{LO}}, \quad ressq = ressq + w^2_{\text{LO}}. \tag{4.79}$$

In NLO real-radiation phase space we additionally have the value for the sum of the subtraction terms $\mathrm{d}\sigma^{\text{A}}$ that is subtracted from the squared real radiation matrix element $\mathcal{M}^2_{\text{real}}$. The final weight is calculated to

$$w_{\text{real}} = \frac{1}{g_\tau g_x} \frac{\mathcal{M}^2_{\text{Born}} - \sum D_{ij} \otimes \mathcal{M}^{2\,\text{CP}}_{\text{Born}}}{g^{\text{real}}_{\text{tot}}}, \tag{4.80}$$

where $g^{\text{real}}_{\text{tot}}$ can be calculated either according to Chapter 4.2 or Chapter 4.3, the sum in $\sum D_{ij} \otimes \mathcal{M}^{2\,\text{CP}}_{\text{Born}}$ denotes a sum over all possible emitter-spectator pairs and $\mathcal{M}^{2\,\text{CP}}_{\text{Born}}$ stands for the corresponding colour-projected Born matrix element.The virtual corrections have the same underlying phase space as the Born process. But since we want to compute the integrated subtraction terms as well, we also have to evaluate +-distributions in case of initial-state hadrons as explained in Chapter 3.4.6. This means, we have to take two phase spaces $\mathrm{d}\Phi(x)$ and $\mathrm{d}\Phi(1)$ into account, the x-independent ($x = 1$) and the x-dependent. For that reason, the colour-projected Born matrix elements required for the computation of the integrated subtraction terms have to be evaluated in both phase spaces. This also leads to two different weights $g^{x,\text{virt}}_{\text{tot}}$ and $g^{1,\text{virt}}_{\text{tot}}$ for each of them. As outlined in Chapter 4.4 we can smoothen the singularities arising from $1/(1-z)$ or $1/(z(1-z))$ with the densities g_{z_1} and g_z of Eq. (4.62) and Eq. (4.64) respectively. Combining all this leads to

$$\begin{aligned} w_{\text{virt}} &= \frac{1}{g_x g_\tau} \frac{\mathcal{M}^2_{\text{virt}}(\Phi(1)) + \sum \left(\int D_{ij}\right) \otimes \mathcal{M}^{2\,\text{CP}}_{\text{Born}}(\Phi(1))}{g_z g^{1,\text{virt}}_{\text{tot}}} \\ &- \frac{1}{g_x g_\tau} \frac{\sum \left(\int D_{ij}\right) \otimes \mathcal{M}^{2\,\text{CP}}_{\text{Born}}(\Phi(x))}{g_z g^{\text{x,virt}}_{\text{tot}}}, \end{aligned} \tag{4.81}$$

where $\int D_{ij}$ stands for the integrated subtraction term corresponding to the emitter–spectator pair ij. The final result for each of the three cases (Born, real and virtual corrections) is calculated as shown in Chapter 2 and printed into the file `result.dat`.

4.6 HowTo Run the Program

In this Section we outline the installation and running of the program. After downloading and unpacking the program via `tar -xzvf mcint.tar.gz` one can start to set up a process. Each step is explained in detail in the following.

4.6.1 Input of Process

The initialization of a full NLO process contains two main steps. In a first step all the information for the generators and a scheme for the subtraction has to be created. For this one has to modify the file `setup.f90` correctly. We show the setup of the file for the LO process $\mathrm{pr} + \mathrm{pr} \to \mathrm{d} + \bar{\mathrm{d}}$:

```
!#########################
!LO PROCESS
!#########################

!number of external particles in lo-process
nextloproc(1)=4
!number of particles in the proton defined
npartpr(1)=3
 pr(1:3)=  (/'gl ','u  ','u~ '/)
 loproc(1) = 'pr '
 loproc(2) = 'pr '
 loproc(3) = 'd  '
 loproc(4) = 'd~ '
```

Since we want to produce all corresponding NLO processes we further set:

```
!#########################
!NLO PROCESS
!#########################

!number of particles in the jet defined
npartjet(1)=1
jet(1:1)=  (/'gl  '/)
nloproc(1) = 'pr '
nloproc(2) = 'pr '
nloproc(3) = 'd  '
nloproc(4) = 'd~ '
nloproc(5) = 'jet'
```

The subroutine that initializes all subtraction terms first checks for the parton by which the initialization of the NLO process `nloproc` differs from the LO process `loproc` — in the above example this is `nloproc(5)`. As a next step the initilization subroutine build all subtraction terms, where `nloproc(5)` is the emitted parton. For considering more possible singularities we included the variable `proc_lo(i)`. If one sets `proc_lo(i)=.true.`, particle `i` is also included as an emitted parton and all corresponding subtraction terms are set up. As default only for the parton by which the NLO process differs from the LO process `proc_lo` is set to `.true.`. As a next step we

have to specify, which part of the process we want to integrate. We implemented three flags for this – each of them is a logical variable:

- `flborn`: If `flborn` is set to `.true.` the leading-order process is integrated, otherwise not.
- `flreal`: If `flreal` is set to `.true.` the real radiation corrections are integrated, otherwise not.
- `flvirt`: If `flvirt` is set to `.true.` the virtual corrections are integrated, otherwise not.

Since we implemented two different methods for the phase-space integration of the real radiation matrix elements, we implemented an additional flag `flrealLO`. If this flag is set to `.true.` the real radiation matrix element is integrated according to Chapter 4.3, otherwise Chapter 4.2 is used for the phase-space integration. In the first case only the mappings according to Chapter 4.3 are used, i.e. we do not additionally include the mappings from Chapter 4.2 here.

```
!########################################################################
!########################################################################
!What to integrate?
flborn=.false.
flreal=.true.
flvirt=.false.

!If flreal == TRUE, choose according to which scheme the PS is built up
!if flrealLO == true, then the phase space is built as the LO
!                     phase space
!if flrealLO == false, then the phase space is built with
!                     additional mappings
!for coll/soft singularities
flrealLO=.false.
```

Once all this is set up one can type `./initscript.sh`. This script compiles all the needed files according to the setup, creates a new folder `mcrun/` and produces some new output files, such as `list.gen` and `list.dsf`. The file `list.gen` provides a list of all possible generators at LO and NLO. It is structured into three parts – the LO, the real radiation and the virtual generators – and reads as follows:

```
 ------------------------------------------------
             List of LO GENERATORS
 ------------------------------------------------
 LO Process:
```

```
pr +pr  ->             d   + d~
Nr of LO gens:            3
-------------------------------------------------
 GEN            1 :
     gl +gl  ->             d   + d~

 GEN            2 :
     u  +u~  ->             d   + d~

 GEN             3 :
     u~ +u   ->             d   + d~

-------------------------------------------------
            List of NLO GENERATORS
              REAL CORRECTIONS
-------------------------------------------------
NLO Process:
pr +pr  ->             d   + d~  + jet
  Nr of REAL NLO gens:           3
-------------------------------------------------
GEN            4 :
gl +gl  ->             d   + d~  + gl

GEN            5 :
u  +u~  ->             d   + d~  + gl

GEN            6 :
u~ +u   ->             d   + d~  + gl
  -------------------------------------------------

-------------------------------------------------
            List of NLO GENERATORS
              VIRTUAL CORRECTIONS
-------------------------------------------------
NLO Process:
pr +pr  ->             d   + d~
 Nr of VIRTUAL NLO gens:           3
-------------------------------------------------

GEN            7 :
gl +gl  ->             d   + d~

GEN            8 :
```

```
 u  +u~  ->             d   + d~

 GEN            9 :
 u~ +u   ->             d   + d~

-------------------------------------------------
```

The file `list.dsf` contains all the information about the dipole subtraction terms. It has the following form:

```
 -------------------------------------------------
             List of DSF TERMS
             GENERATOR           4
 -------------------------------------------------
 Process
 gl +gl  ->             d   + d~  + gl
 Number
  1 + 2  ->             3  +  4  +  5

IS Spectator - IS Emitter
 -------------------------------------------------
     D^{25}^{1}  : gl  -> gl +gl     D:  34   LOREF  1
     D^{15}^{2}  : gl  -> gl +gl     D:  34   LOREF  1
 -------------------------------------------------
 IS Spectator - FS Emitter
 -------------------------------------------------
     D_{35}^{1}  : d   -> d  +gl       D:  11   LOREF  1
     D_{45}^{1}  : d~  -> d~ +gl       D:  11   LOREF  1
     D_{35}^{2}  : d   -> d  +gl       D:  11   LOREF  1
     D_{45}^{2}  : d~  -> d~ +gl       D:  11   LOREF  1
 -------------------------------------------------
 FS Spectator - IS Emitter
 -------------------------------------------------
     D^{15}_{3}  : gl  -> gl +gl     D:  25   LOREF  1
     D^{25}_{3}  : gl  -> gl +gl     D:  25   LOREF  1
     D^{15}_{4}  : gl  -> gl +gl     D:  25   LOREF  1
     D^{25}_{4}  : gl  -> gl +gl     D:  25   LOREF  1
 -------------------------------------------------
 FS Spectator - FS Emitter
 -------------------------------------------------
     D_{45}_{3}  : d~  -> d~ +gl       D:   1   LOREF  1
     D_{35}_{4}  : d   -> d  +gl       D:   1   LOREF  1
```

For example the line

```
D^{25}^{1}  : gl  -> gl +gl     D:  34   LOREF  1
```

means, that the subtraction term, where the initial-state parton 2 emits the final-state parton 5 and spectator is initial-state parton 1, is internally numbered by `D_IS_IS=34` and corresponds to the dipole subtraction term of Table 3.5. All other corresponding dipole terms are listed in Tables 3.2 – 3.4. The parameter `LOREF` references the generator of the born process, which is to evaluate in order to compute the dipole subtraction term. A detailed explanation on this notation can be found in Chapter 4.5.5. For the dipole subtraction the program needs the colour-projected Born matrix elements as an input. The file `RequiredSubroutines` provides a list of all colour-projected matrix elements that are needed for the process. The corresponding template subroutines are written into the file `user_subroutines.f90` and have to be provided by the user. This finalizes the first step of the setup.

4.6.2 Input of Parameters

After all the required matrix elements have been provided the physical parameters such as masses and couplings have to be set. This is also done in the file `setup.f90` and must be done either before running the `initscript.sh` or in the the path `mcrun/setup.f90` as the following excerpt shows:

```
!################################################
!################################################
!# PHYSICAL PARAMETERS
!################################################
!################################################
!Parameters PDG 2010
mcalpha  = 1d0/132.3489045d0
mcalphas = 1.18d-01
mcGfermi = 1.16637d-005
mcwmass  = 8.03990000D+01
mcwwidth = 2.085D+00
mczmass  = 9.11876000D+01
mczwidth = 2.4952D00
mchmass  = 120.0d0
mchwidth = 3.48D-03

!additional masses
mcdmass=0.0d0
mcumass=0.0d0
mcsmass=0.0d0
mccmass=0.0d0
mctmass=174.3d0
```

```
mcbmass=0.0d0
mcelmass=0.0d0
mcmumass=0.0d0
mctaumass=0.0d0

!Energy
energy = 1000d0
```

4.6.3 Input of Cuts

As pointed out in 4.5.4 we implemented a generic cut scheme. The type and kind of cuts applied can also be regulated in the file `setup.f90`. We show the corresponding excerpt of `setup.f90` and refer to Chapter 4.5.4 for details:

```
!#################################################
!# Recombination
!#################################################
!Which clustering algorithm?
p=1
! p =-1: anti-kT Algorithm
! p = 0: Cambridge Algorithm
! p = 1: kT Algorithm

ktd = 0.8
!D - parameter in clustering Algorithm


!#################################################
!# CUTS
!#################################################
!What kind of particles are required?

!-----------------------------------------
!SECTION: Cuts on Jets
!-----------------------------------------
jetcut=.true.

!number of required jets
numjet=2
!transverse momentum of jets
ptjetcut =20d0
!pseudorapidity of jets
etajetcut =4.5d0
```

```
!-------------------------------------------
!END SECTION: Cuts on Jets
!-------------------------------------------

!-------------------------------------------
!SECTION: Cuts on (charged) leptons
!-------------------------------------------
lepcut=.true.

!number of required leptons
numlep=2
!transverse momentum of leptons
ptlepcut = 20d0
!pseudorapidity of leptons
etalepcut = 2.5d0


!-------------------------------------------
!END SECTION: Cuts on (charged) leptons
!-------------------------------------------
!###########################################
!###########################################
!###########################################

!-------------------------------------------
!SECTION: Cuts on pairs of jets
!-------------------------------------------
jjcut=.true.

!deltaRcut between two jets
deltaRjjcut = 0.4d0
!invariant mass cut between two jets
invmassjetcut=600d0
!require two jets to be in opposite detector hemisphere
opphemjet=.true.

!-------------------------------------------
!END SECTION: Cuts on pairs of jets
!-------------------------------------------

!-------------------------------------------
!SECTION: Cuts on pairs of (charged) leptons
!-------------------------------------------
```

```
llcut=.true.

!number of leptons
numlep=2
!deltaRcut between two leptons
deltaRllcut = 0.4d0
!invariant mass cut between two leptons
invmassllcut=600d0
!require two lep to be in opposite detector hemisphere
opphemlep=.true.

!-------------------------------------------
!END SECTION: Cuts on pairs of (charged) leptons
!-------------------------------------------

!-------------------------------------------
!SECTION: Cuts on a jet - lepton pair
!-------------------------------------------
ljcut=.true.

!deltaRcut between jet - lepton
deltaRljcut = 0.4d0
!invariant mass cut between jet - lepton
invmassljcut=600d0

!-------------------------------------------
!END SECTION: Cuts on jet - lepton pair
!-------------------------------------------

!################################################
!# CUTS
!################################################
```

The user can easily complement the given set of cuts, by implementing them and calling them in the corresponding functions:

- `jetcut`
- `lepcut`
- `jet_jet_cuts`
- `lep_lep_cuts`
- `lep_jet_cuts`.

The technical parameters explained in Chapter 4.7 are also set in `setup.f90` and reads:

```
!################################
!# TECHPARAM
!################################
!technical cuts
!real(kind=dp),dimension(3) ::techparam

!dimension 1: technical cut : 1-cost.gt.-1*techparam(1)
!dimension 2: technical cut : cut on tmax: tmax.lt.techparam(2) -> tmax=0d0
!dimension 3: technical cut : small mass parameter for mapping function h

!Technical Parameters for the MonteCarlo

 techparam(1)=1d-10  ! allowed uncertainty on 1-cost
 techparam(2)=1d-10*energy**2    ! allowed uncertainty tmax in process
 techparam(3)=1d-4               ! small negative mass in h-function

!################################
!# Input for Generator
!################################

powermap=0.8d0
```

Finally, the technical parameters for the subtraction can be set as follows:

```
!################################
!# Input for Subtraction
!################################

!Factorization Scale
scalemuf=91.188d00
!Renormalisation Scale
scalemur=91.188d0

epsilon=0d0
kappa=2d0/3d0

!alpha-parameter
alpha_FSem_FSsp = 1.0d0
alpha_ISem_FSsp = 1.0d0
alpha_FSem_ISsp = 1.0d0
alpha_ISem_ISsp = 1.0d0
```

In case `epsilon != 0` the dipole subtraction terms and the corresponding integrated subtraction terms are evaluated including the ϵ-dependent parts. The parame-

ter κ can be chosen to simplify the evaluation of either the subtraction terms or of the integrated subtraction terms. For more details to the choice of κ we refer to paragraph 3.3.3.2.

4.6.4 Input of Parton Distribution Function

For the parton distribution functions we provide a generic setup for MRST [35] and CTEQ6 [36]. We also provide the Les Houches Accord PDF interface [37]. We implemented some flags and variables in order to control which kind of parton distribution functions are chosen and what specific settings are used in the file `setup.f90`:

```
!################################
!#PDF Settings
!################################
flpdf = 1
             !flpdf = 1 : MRST
             !flpdf = 2 : CTEQ
             !flpdf = 5 : LHApdf

!MRST settings
isetMRST  = 0  ! which MRST set to load
prefix = "Grids/"

!CTEQ settings
isetCTEQ = 1   ! which CTEQ set to load

!LHApdf settings
lhapath=''
```

The parameters `isetMRST` and `isetCTEQ` are used to initialize a specific set of parton distribution functions as explained in References [35] and [36] respectively. The variable `prefix` chooses the path where to find the corresponding set. The user can of course use different parton distribution functions. The corresponding changes have to be done in the subroutine `pdfconv` in the file `integration.f90`. Whenever the value of a parton distribution function is needed, the subroutine `pdfconv` is called.

4.6.5 Run the program

After setting up the process with all the parameters and cuts and providing the subroutines for the (colour-projected) matrix elements the user still has to adapt the makefile in the folder `mcrun/`. In `makefile` we provide the template variables `MGMATSRC`, `MGMATOBJ` and `ADDOBJ`. If the user provides subroutines that still have to be compiled,

the source files should be listed in `MGMATSRC` and the corresponding object files in `MGMATOBJ`. If the user already provides compiled object files, they should be listed in `ADDOBJ`. Te user has to take care that the same compiler for both his files and the files of the Monte Carlo is used. The program can be run with `./multich` after compiling with `make` in the folder `mcrun/`.

4.7 Technical Parameters

In this Section we review implemented technical parameters. Some of the technical cuts presented are mandatory (e.g. to ensure $|\cos\theta| \leq 1$) and some can help to increase the stability of the integration. Numerical instabilities can arise due to issues explained in appendix A. We implemented the following technical parameters:

1. accuracy for momentum conservation: `acc`
2. exponent of mappings ν: `powermap`
3. technical cuts on $\cos\theta$, $t_{\max}$ and masses m_i: `techparam`
4. technical cut on invariant s_{ij}: `tcsij`

The details of each of the parameters are explained in the following:

1. The parameter `acc` is used in the subroutine `checkmom` to check for energy-momentum conservation and on-shellness up to the given accuracy `acc`, i.e. with n outgoing particles

$$k_1^i + k_2^i - \sum_{j=3}^{n+2} k_j^i < \text{acc} \times \left|k_1^0 + k_2^0\right| \ , \ \forall i \in \{0, \ldots, 3\} \tag{4.82}$$

   and

$$\left(k_i^0\right)^2 - \sum_{j=1}^{3} \left(k_i^j\right)^2 < \text{acc} \times \left|k_1^0 + k_2^0\right|^2 \ , \ \forall i \in \{1, \ldots, n\}. \tag{4.83}$$

   Typical values for the accuracy `acc` are 10^{-12} and smaller.

2. The parameter ν was introduced in Section 4.2. It accounts for the power of the denominator of the propagator. Due to cancellations of the poles in the propagator with the nominator, the parameter should be chosen around $0.8 - 0.9$.

3. The array `techparam` accounts for different technical cuts. With the first entry of the array `techparam` we check for deviations of $\cos\theta$ from 1 during the generation of the momenta. If $1 < \cos\theta < 1 +$ `techparam(1)`, we set $\cos\theta = 1$. Thus, typical values for `techparam(1)` are 10^{-10} and smaller. The calculation

of the integration boundary $t_{\max}$ in the density of a $2 \to 2$ process according to Eq. (4.13) can become larger than one. In the case of $t_{\max} > 0$ we set $t_{\max} = 0$, if `techparam(2)` $> t_{\max}/E^2_{\mathrm{CMS}}$, otherwise we reject the event. Typical values for `techparam(2)` are 10^{-10} and smaller. The third entry of the array `techparam` increases the stability of the integration, when masses are neglected. In order to avoid instabilities occurring in the case of $s_{\min} = 0$ e.g. in Eq. (4.23), `techparam(3)` allows for a small technical mass $m^2 = -$`techparam(3)` with values of 10^{-4} and smaller.

4. In the case of soft and/or collinear limit at NLO, both the squared real radiation matrix element and the dipole subtraction terms behave as $1/s_{ij}$. This can lead to numerical instabilities if s_{ij} is very small. Therefore we implemented an additional cut related to the parameter `tcsijparam`. We reject such an event, if $s_{ij} <$ `tcsijparam` $\cdot E^2_{\mathrm{CMS}}$, where typical values for `tcsijparam` are 10^{-9} and smaller depending on E^2_{CMS}.

We also provide a basic error handling concept, which is explained in Appendix B.

4.8 Parallelization

The Monte Carlo integration is inherently parallelizable in a very efficient way. By distributing the evaluation of the squared matrix element onto np processors, one can reach a significant speedup in overall computing time. We also provide a parallel code for the integration algorithm, where we use OpenMPI as basis for the parallel code. In our parallelization the complete procedure of generating phase space points and evaluating the squared matrix element is not only done on one processor, but on np processors (see Figure 4.5). If one wants to generate 10^6 phase space points on 256 processors, one processor has to evaluate only 3907 events. Since most of the computing time goes into the evaluation of the squared matrix element, this leads to a significant improvement and speedup.

The setup of the parallel code is the same as explained in Section 4.6 with two exceptions. The specification of the process, which is to be integrated, is different. We additionally included three logical flags:

- `flbornparallel`: If `flbornparallel` is set to `.true.` the leading-order process is integrated with the parallel code, otherwise not.
- `flrealparallel`: If `flrealparallel` is set to `.true.` the real radiation process is integrated with the parallel code, otherwise not.
- `flvirtparallel`: If `flvirtparallel` is set to `.true.` the virtual process is integrated with the parallel code, otherwise not.

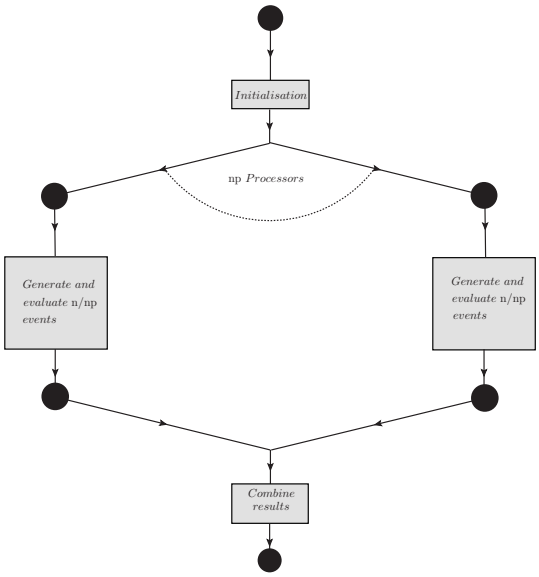

Figure 4.5: Parallel evaluation of events

These flags can be set in the file `setup.f90` as follows:

```
!####################################################################################
!####################################################################################
!What to integrate?
flbornparallel=.false.
flrealparallel=.true.
flvirtparallel=.false.
```

After these flags are set one has to type `./initscriptparallel.sh` in order to create the folder `mcrunparallel/`. Everything else is set as explained in Section 4.6.

4.9 Checks

Testing the program is a critical element in developing software. It has two main purposes — verification and bug finding. Verification confirms that the program meets the functional specifications which define the output, given specific input conditions. A bug is a disagreement between actual and expected output of the program, which has to be tracked back to specific faults in the code. Once modifications based on found errors have been made, regression tests are necessary which in principal ensure a consistent validation after each change to an application. For each check, particular test cases have to be created. Some of the most important test cases that each check a specific part of the program are described in the following subsections. In order to

illustrate the importance of the test, we consider the representation of Eq. (4.3) in our code

$$\begin{aligned}\sigma^{\mathrm{NLO}} &= \sum_{i=1}^{N_{\Phi_{m+1}}} \int \mathrm{d}r_1 \mathrm{d}r_2 \mathrm{d}\mathbf{r}_{\Phi_{m+1}} \; \frac{f_a(x_1(r_1),\mu^2) f_b(x_2(r_2),\mu^2)}{g_{f_a}(x_1(r_1)) g_{f_b}(x_2(r_2))} \frac{\left[d\sigma^{\mathrm{R}}_{ab} - d\sigma^{\mathrm{A}}_{ab}\right]}{g_{\mathrm{tot}}\left(\Phi_i(\mathbf{r})\right)} \\ &+ \sum_{i=1}^{N_{\Phi_m}} \int \mathrm{d}r_1 \mathrm{d}r_2 \mathrm{d}\mathbf{r}_{\Phi_m} \; \frac{f_a(x_1(r_1),\mu^2) f_b(x_2(r_2),\mu^2)}{g_{f_a}(x_1(r_1)) g_{f_b}(x_2(r_2))} \frac{\left[d\sigma^{\mathrm{V}}_{ab} + d\sigma^{\mathrm{B}}_{ab} \otimes \mathbf{I_{ab}}\right]}{g_{\mathrm{tot}}\left(\Phi_i(\mathbf{r})\right)} \\ &+ \sum_{i=1}^{N_{\Phi_m}} \int \mathrm{d}r_1 \mathrm{d}r_2 \mathrm{d}\mathbf{r}_{\Phi_m} \; \frac{f_a(x_1(r_1),\mu^2) f_b(x_2(r_2),\mu^2)}{g_{f_a}(x_1(r_1)) g_{f_b}(x_2(r_2))} \frac{\left[d\sigma^{\mathrm{B}}_{ab} \otimes \left(\mathbf{K}_{ab}(x) + \mathbf{P}_{ab}(x)\right)\right]}{g_{\mathrm{tot}}\left(\Phi_i(\mathbf{r})\right)},\end{aligned} \tag{4.84}$$

where N_{Φ_m} is the number of channels in the phase space Φ_m, and explain the checks in the following subsections.

4.9.1 Phase Space Volume

One main part of the program to check is the correct implementation of the phase-space generator. A generated event has to fulfill momentum conservation. This is checked up to a given accuracy (see Chapter 4.7) at each phase-space point after the generation of the event during runtime with the subroutine `checkmom`. In order to check the consistent implementation of the mappings $\Phi_i(\mathbf{r})$ and their corresponding Jacobians, we can integrate the phase space over the function $f(\Phi) = 1$. The result of this integral is the phase-space volume, which we can compare to the analytical formula in the case of massless final-state particles

$$\int \prod_{i=1}^{m} \mathrm{d}^4 p_i \delta(p_i^2 - m_i^2) \Theta(p_i^0) (2\pi)^{(4-3m)} \delta^4 \left(p - \sum_{i=1}^{m} p_i \right) = \left(\frac{\pi}{2}\right)^{n-1} \frac{p^{2m-4}}{\Gamma(m)\Gamma(m-1)}. \tag{4.85}$$

In order to check the implementation of the densities g_i that are included in g_{tot}, we focus on the first line of Eq. (4.84). Setting

$$f_a(x_1) = 1,\; f_b(x_2) = 1,\; g_{f_a}(\mathbf{r}) = 1,\; g_{f_a}(\mathbf{r}) = 1,\; \left(\mathrm{d}\sigma^{\mathrm{R}}_{ab} - \mathrm{d}\sigma^{\mathrm{A}}_{ab}\right) = 1, \tag{4.86}$$

this yields

$$vol_{\mathrm{PS}} = \sum_{i=1}^{N_{\Phi_{m+1}}} \int \mathrm{d}\mathbf{r}_{\Phi_m} \frac{1}{g_{\mathrm{tot}}\left(\Phi_i(\mathbf{r})\right)}. \tag{4.87}$$

Since the integrand $1/g_{\mathrm{tot}}\left(\Phi_i(\mathbf{r})\right)$ clearly exhibits a peaking structure according to the process — and therefore mappings — chosen, we recommend a strategy to improve the convergence. We implemented a flag `smap` that allows for flat mappings, i.e. setting the masses in the mappings and densities of the propagating particles (see Chapter 4.2) to

a small positive value $m \propto 10^{-5}$ and the widths to zero. Thus we avoid an extensive peaking structure in the integrand $1/g_{\text{tot}}\left(\Phi_i(\mathbf{r})\right)$ and get way better convergence, if compared to the case where we keep the original masses. In fact, if the flag `smap` is set to 0, the masses of the particles are set to small but different values each. It is necessary to set the masses to different values to ensure that all channels of the original case — where we kept the masses — are also present in the test case, because during initialization of the channels the algorithm checks if the channel already exists for the given generator. In the case that a channel already exists, it is not taken into account, since it does not optimize the integration. But for test purposes we of course want to check all possible channels, which is the reason for setting the masses to different values.

4.9.2 Dipole Subtraction Terms

The implementation of the dipole subtraction terms has been checked in various ways. We performed extensive checks with MadGraph and MadDipole[38], [39], [40] and performed additional consistency checks. We checked the mappings from the $\mathrm{d}\Phi_{m+1}$ to the $\mathrm{d}\Phi_m$ phase space for all different emitter–spectator cases with both massive and massless particles — in total 7 different mappings — against the corresponding mappings in Madgraph and found full agreement. Furthermore we checked all 28 dipole subtraction terms for all emitter-spectator cases with both massive and massless particles against the corresponding terms in Madgraph and found full agreement for all dipole subtraction terms. Another check we performed is the subtraction itself, i.e. in a given collinear and/or soft limit the ratio of the sum of the dipole subtraction terms $D_{\text{sum}} = \sum D_{ij} \otimes \mathcal{M}^{2\,\text{CP}}_{\text{Born}}$ and the real radiation matrix element $\mathcal{M}_{\text{R}}$ yield due to Eq. (3.24)

$$\frac{|\mathcal{M}_{\text{R}}|^2}{\sum D_{ij} \otimes \mathcal{M}^{2\,\text{CP}}_{\text{Born}}} \to 1. \tag{4.88}$$

The program therefore provides a subroutine producing a trajectory of continually more singular phase-space points. The subroutine inverses for each of the four cases (final–final, final–initial, initial–final, initial–initial) the mappings from the $m+1$ parton to the m parton phase space given in Chapter 3. In the following we show some plots as examples for the subtraction behaviour.

In Figure 4.6 we plot the dependency of $D_{\text{sum}}/\left|\mathcal{M}_{\text{R}}\right|^2$ with respect to the ratio s_{25}/s_{12} for the process $\mathrm{e}^-(1) + \mathrm{u}(2) \to \mathrm{e}^-(3) + \mathrm{u}(4) + \mathrm{g}(5)$ at 1 TeV centre-of-mass energy, where we took 100 phase-space points with continually decreasing invariant s_{25}. As seen in Chapter 3 both the real radiation matrix element $\left|\mathcal{M}_{\text{R}}\right|^2$ and the subtraction term diverge like $1/s_{25}$, if the corresponding invariant mass s_{25} goes to zero, and thus their ratio goes to one as Eq. (4.88) shows.

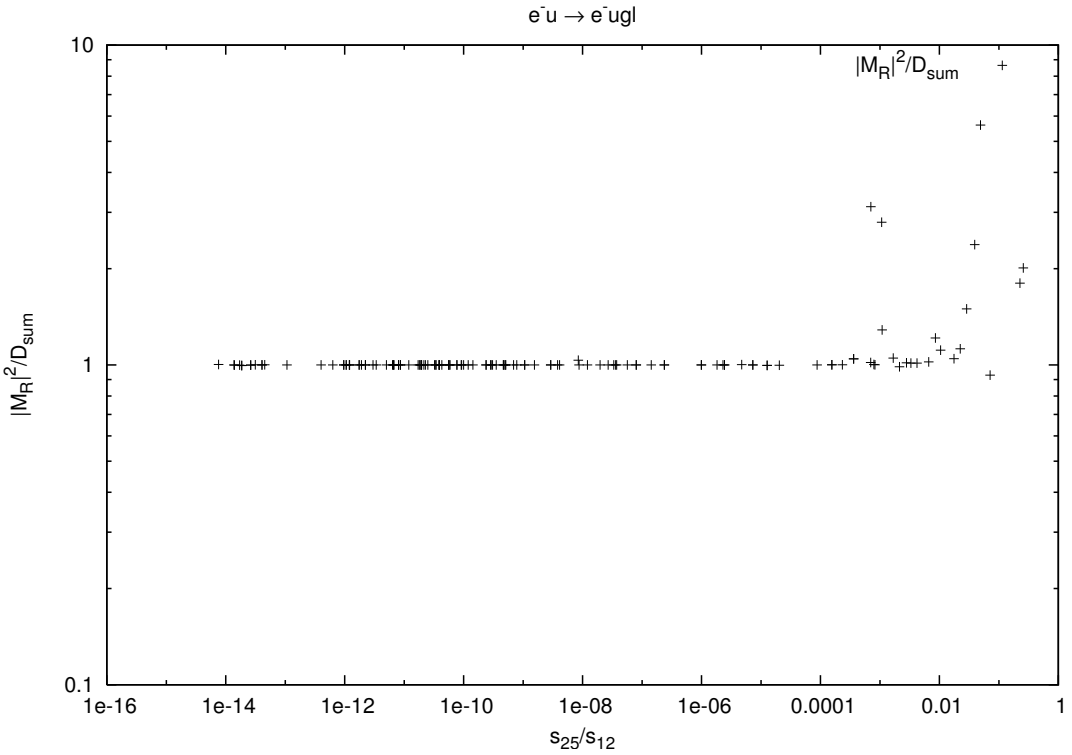

Figure 4.6: $|M_R|^2/D_{\text{sum}}$ for the process $\text{e}^-\text{u} \to \text{e}^-\text{ug}$

As another example for the subtraction we present a histogram in Figure 4.7 , which is created with 10^8 events for the same process. We divided the x-axis into 100 bins and plotted the real radiation matrix element $|\mathcal{M}_{\text{R}}|^2$, the dipole sum D_{sum} and the difference $|\mathcal{M}_{\text{R}}|^2 - D_{\text{sum}}$ for the technical cut $tcsij = 10^{-12}$ on the invariants. The Figure shows that for this process up to a value for s_{45}/s_{12} of around 10^{-4} the sum of all dipole subtraction terms is subtracts the squared matrix element very well. The smaller the ratio of invariants s_{45}/s_{12} the bigger the error and thus the worse the subtraction gets.

4.9.3 Integrated subtraction terms

We checked the implementation of the integrated dipole subtraction terms in two different ways. We checked every single integrated subtraction term against the corresponding term in MadDipole and performed consistency checks in terms of independence of the phase-space restriction parameter α. As pointed out in Chapter 3 the dipole subtraction terms and the integrated subtraction terms depend on the phase-space-restriction parameter α — but the sum of both contributions must be independent of

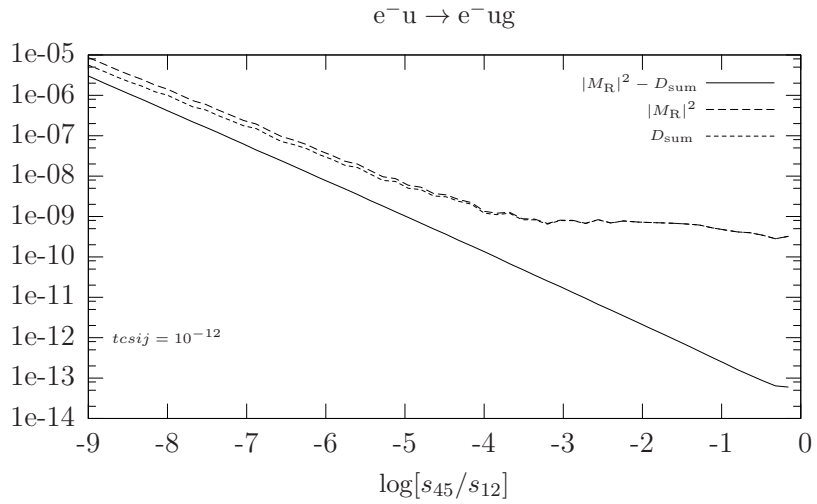

Figure 4.7: Histograms: $e^- u \to e^- ug$ (s_{45}-dependence) with 10^8 events

α. Thus it is a good check to numerically validate

$$\int_{m+1} \left(\mathrm{d}\sigma^{\mathrm{R}} - \mathrm{d}\sigma^{\mathrm{A}}\right) + \int_m \left(\int_1 \mathrm{d}\sigma^{\mathrm{A}}_{\mathrm{fin}}\right) = \text{const.} \tag{4.89}$$

We exemplarily show this in Figure 4.8 for the process $e^+e^- \to u\bar{u}g$, where we denote $\int_{m+1} \left(\mathrm{d}\sigma^{\mathrm{R}} - \mathrm{d}\sigma^{\mathrm{A}}\right)$ with $\sigma^{\mathrm{Real}}_{\mathrm{sub}}$ and $\int_m \left(\int_1 \mathrm{d}\sigma^{\mathrm{A}}_{\mathrm{fin}}\right)$ with $\sigma^{\mathrm{Virt}}_{\mathrm{sub}}$ and only consider the finite (i.e. ϵ-independent) terms of $\sigma^{\mathrm{Virt}}_{\mathrm{sub}}$. Since we mainly want to illustrate the α independence in Figure 4.8, we use an arbitrary normalization and add also the result of the Born process for comparison. For the check with MadDipole we checked the finite terms, the $1/\epsilon$ and the $1/\epsilon^2$ poles for different values of the phase-space restriction parameter α at different phase-space points. We first point out some differences between the MadDipole implementation and our implementation. In the final-state emitter and final-state spectator splittings $Q \to Q + g$ with massive and massless spectator, $q \to q+g$ with massive spectator and $g \to q+\bar{q}$ with massive spectator we implemented the symmetric part of the eikonal integral (see explanation after Eq. (3.126)), which is completely sufficient for the calculation of physical cross Sections. MadDipole implemented the complete eikonal integral, i.e. both the symmetric and the antisymmetric part. In the case of an initial-state emitter and a final-state spectator we implemented Eq. (3.168) including the underlined term, whereas MadDipole left out this term. In all other massless and massive cases we find full agreement with MadDipole.

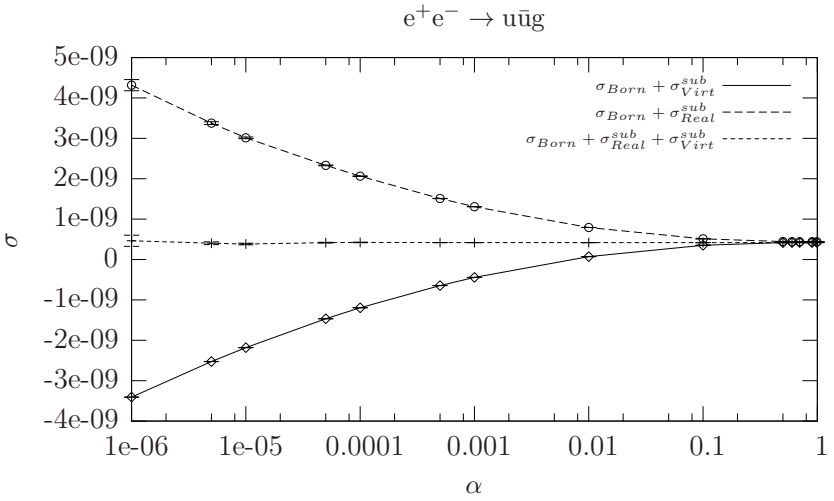

Figure 4.8: α-dependence in $e^+e^- \to u\bar{u}g$

5

Application to weak boson fusion

The search for the Higgs boson and thus the understanding of electroweak symmetry breaking and fermion-mass generation is one of the goals of the CERN Large Hadron Collider (LHC). In Figure 5.1 Standard Model cross sections are shown for various mechanisms of Higgs production. The largest cross section for the Higgs production at LHC is expected in the gluon-fusion channel ($gg \to h$), where the Higgs boson is produced via a heavy-quark loop (see Figure 5.2). In combination with subsequent Higgs decay channels such as $h \to \gamma\gamma$, $h \to WW$ and $h \to ZZ$ this is the most important production mechanism for the Higgs-mass range $100\text{GeV} \lesssim m_h \lesssim 1\text{TeV}$ [41]. The LO cross section of this process is increased by the QCD radiative corrections at NLO by about $80 - 100\%$ at the LHC. The second largest Higgs-production cross section is predicted for Weak Boson Fusion (WBF) ($qq \to qqVV \to qq$) Figure (5.3). In contrast to gluon fusion, the QCD NLO corrections in WBF are relatively small, typically of order $\mathcal{O}(5\%)$ [42].

The W and Z production in combination with 2 jets is an important background for Higgs-boson searches. This makes it necessary to extract the corresponding signals. In order to distinguish the Higgs-boson signal, where the Higgs boson is produced via WBF, from background channels restrictive cuts are required [43–52]. The main advantage of the WBF signal is the presence of the two energetic forward jets, which are at LO formed by the two scattered quarks. Next to the detection of the two tagging jets cuts on the decay products of the Higgs boson have to be applied to suppress background processes. As another important feature of the WBF channel there is no colour-exchange between the initial-state quarks, which leads to low hadronic activity between the two tagging jets. Hence, there is in comparison to the gluon-fusion channel a significantly decreased amount of gluon radiation in the central region. One can exploit this fact in order to distinguish between the two channels by imposing a veto on soft jets in the central region between the two tagging jets. The tagging jets however are produced mainly with large rapidity, i.e. at small angles, since the momentum

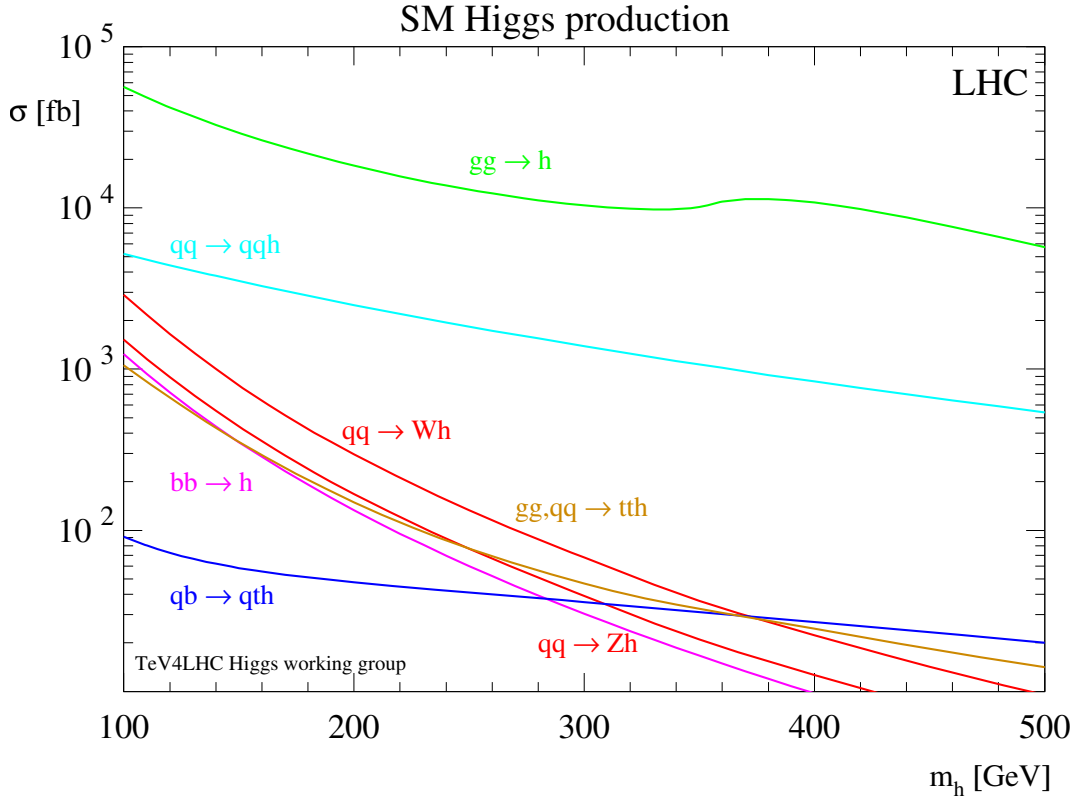

Figure 5.1: Higgs-boson production cross sections (fb) at the LHC, taken from Reference [1]

transfer is small compared to the quark-jet energy. Another important process with a Higgs plus two jets signal is Higgsstrahlung ($qq \to Wh$ and $qq \to Zh$), where a Higgs boson is radiated from a W or Z gauge boson in an s-channel process Figure 5.4.

For the extraction of the WBF signal various cuts on experimentally measurable quantities have to be applied based on the kinematics of the process. First of all we require at least two hard jets with

$$\begin{aligned} p_{\mathrm{Tj}} &> 20 \text{ GeV}, \\ |\eta_{\mathrm{j}}| &\leq 4.5. \end{aligned} \tag{5.1}$$

Since WBF has two energetic forward jets one requires a large rapidity gap between the two jets. A high cut on the dijet mass eliminates much of the QCD background and the gluon fusion channel. Additionally it ensures avoiding the threshold of the W/Z boson mass in the s-channel Higgsstrahlungs process. The cut $\eta_{\mathrm{j1}} \times \eta_{\mathrm{j2}} < 0$ ensures that we only consider events where the jets are in opposite detector hemispheres. This results in the following basic set of WBF cuts:

$$\Delta\eta_{\mathrm{j_1 j_2}} = |\eta_{\mathrm{j_1}} - \eta_{\mathrm{j_2}}| > 4,$$

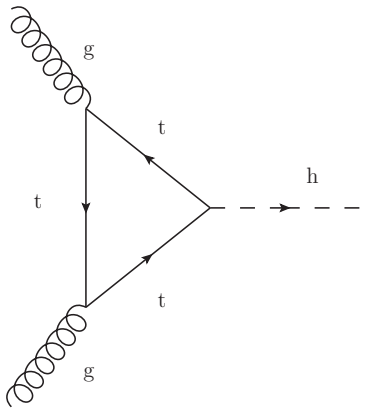

Figure 5.2: Leading-order diagram for gluon fusion

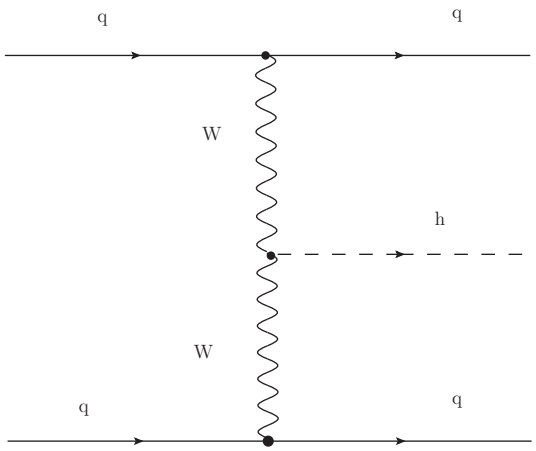

Figure 5.3: Leading-order diagram for weak boson fusion

$$\begin{aligned} \eta_{j1} \times \eta_{j2} &< 0, \\ M_{jj} &> 600 \text{ GeV}. \end{aligned} \tag{5.2}$$

5.1 W^+jj

5.1.1 Setup

One important WBF process is the electroweak production of a W^+ plus two jets W^+jj. The consecutive leptonical decay of the W boson $W^+ \to e^+\nu_e$ leads to the final state $e^+\nu_e jj$. As stated above these type of processes are an important background to Higgs boson searches in WBF. At LO we have 10 Feynman diagrams contributing to W^+jj. Two scattered quarks exchanging a colourless gauge boson, where additionally one of the quark lines emits a W^+ boson decaying into $l^+\nu_l$ lead to 5 Feynman diagrams. 5

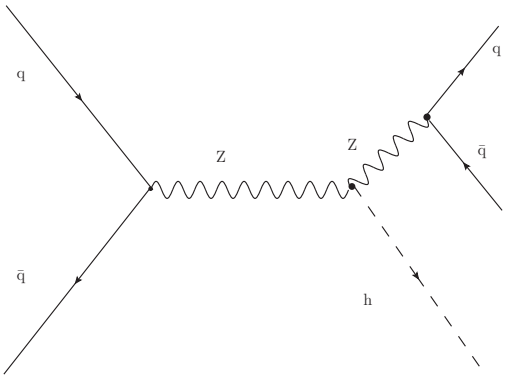

Figure 5.4: Leading-order diagram for Higgsstrahlung

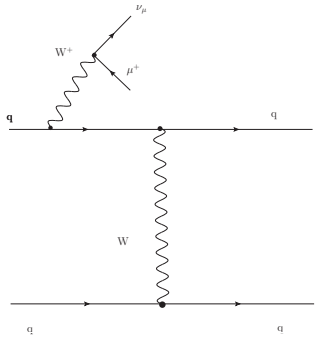

Figure 5.5: Leading-order topology for process $qq \to qq\mu^+\bar{\nu}_\mu$

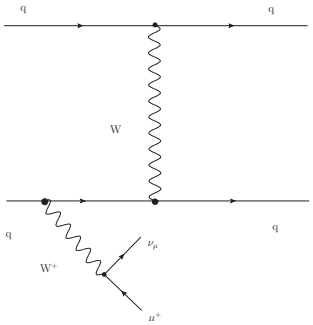

Figure 5.6: Leading-order topology for process $qq \to qq\mu^+\bar{\nu}_\mu$

more diagrams are produced via a t-channel exchange of two weak bosons fusing into the leptonic part $l^+\nu_l$ of the final state $l^+\nu_l jj$. In case of identical quark flavours on the two quark lines additional subprocesses occur, which we do not consider. We neglect contributions from s-channel diagrams and any interferences. The LO topologies of the Feynman diagrams are shown in Figures (5.5),(5.6),(5.7) and (5.8). The LO results of a similar process (W^+W^+jj) show that these diagrams lead to a negligible contribution to the total cross section (see LO results in Section 5.2.2). In order to obtain the real radiation matrix element for the QCD corrections we need to attach the gluon to the quark lines in all possible ways, which gives rise to 45 Feynman diagrams. The initial-state gluon contributions are obtained by crossing these diagrams, i.e. the final-state gluon becomes an initial-state particle and an initial-state (anti)quark becomes a final-state parton. Since we neglected s-channel and any interference contributions at LO, we have to remove these contributions also at NLO for consistency reasons. Thus, we do not consider diagrams, where two time-like vector bosons are produced, as well as diagrams, where the initial-state gluon couples to initial-state fermion line. The details

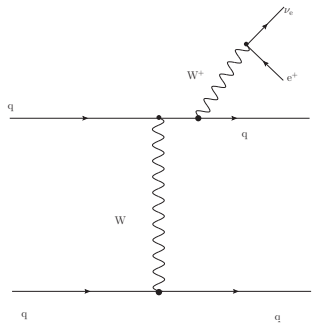

Figure 5.7: Leading-order topology for process $qq \to qq\mu^+\bar{\nu}_\mu$

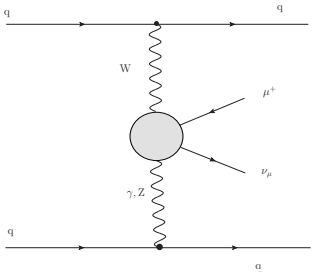

Figure 5.8: Leading-order topology for process $qq \to qq\mu^+\bar{\nu}_\mu$

of the calculation of the all contributing tree-level and virtual amplitudes are worked out in Reference [53].

5.1.2 Results

The amplitudes (see Reference [53]) that contribute to $pp \to e^+\nu_e jj$ have been implemented in the Monte Carlo code presented in Chapter 4. All quark masses are neglected throughout the calculation. At LO we use the CTEQ6L1 parton distribution functions and at NLO the CTEQ6M parton distributions with $\alpha_S(m_Z) = 0.118$. We take the same input parameters as in Reference [54], i.e. as electroweak input parameters we use

$$\begin{aligned} m_W &= 80.419 \text{ GeV}, \\ m_Z &= 91.188 \text{ GeV}, \\ \Gamma_W &= 2.099 \text{ GeV}, \\ \Gamma_Z &= 2.510 \text{ GeV}, \\ G_F &= 1.66 \times 10^{-5} \text{ GeV}^{-2}. \end{aligned} \tag{5.3}$$

With the following electroweak tree-level relations

$$\begin{aligned} \sin^2\theta_W &= 1 - \frac{m_W^2}{m_Z^2}, \\ \alpha_{QED} &= \frac{1}{\pi} G_F \sqrt{2} m_W^2 \sin^2\theta_W. \end{aligned} \tag{5.4}$$

we calculate the other parameters such as $\alpha_{QED} = 1/132.51$ and $\sin^2\theta_W = 0.2223$. For the reconstruction of final-state jets we only take massless partons with pseudorapidity $|\eta| < 5$ into account and use the k_T algorithm with resolution parameter $D = 0.8$. We require at least two hard jets with

$$p_{Tj} > 20 \text{ GeV},$$

$$|\eta_{\mathrm{j}}| \leq 4.5, \tag{5.5}$$

where the two jets with highest transverse momentum are called „tagging jets“. In order to suppress backgrounds to WBF we require a large rapidity gap between the two tagging jets

$$\Delta\eta_{\mathrm{j_1 j_2}} = |\eta_{\mathrm{j_1}} - \eta_{\mathrm{j_2}}| > 4. \tag{5.6}$$

Since we want to ensure a well observed lepton, we impose the following cuts

$$\begin{aligned} p_{\mathrm{Tl}} &> 20 \text{ GeV}, \\ |\eta_{\mathrm{l}}| &\leq 2.5, \\ \Delta R_{\mathrm{jl}} &\geq 0.4, \end{aligned} \tag{5.7}$$

where ΔR_{jl} denotes the jet-lepton separation in the rapidity–azimuthal angle plane (4.5.4). Additionally we require that the charged leptons fall in between the rapidity of the two tagging jets, i.e.

$$\eta_{\mathrm{j,min}} < \eta_{\mathrm{l}} < \eta_{\mathrm{j,max}}. \tag{5.8}$$

By imposing the above cuts, we render the LO finite. At NLO the initial-state singularities for the splittings $\mathrm{q} \to \mathrm{qg}$ and $\mathrm{g} \to \mathrm{q\bar{q}}$ are properly taken into account. But in the case of t-channel photons an additional collinear singularity due to the $\mathrm{q} \to \mathrm{q}\gamma$ occurs in phase-space regions with vanishing momentum transfer of the virtual photon. In order to avoid this singularity we impose an additional cut on quark lines only. In the case of a qq, $\bar{\mathrm{q}}\mathrm{q}$ and $\mathrm{q\bar{q}}$ initial-state we require

$$|k_1 - k_3|^2 > 4 \text{ GeV}^2, \tag{5.9}$$

$$|k_1 - k_4|^2 > 4 \text{ GeV}^2, \tag{5.10}$$

$$|k_2 - k_3|^2 > 4 \text{ GeV}^2, \tag{5.11}$$

$$|k_2 - k_4|^2 > 4 \text{ GeV}^2. \tag{5.12}$$

In the gluon-initiated processes we only impose the cuts on the quark lines, i.e. in the processes gq and $\mathrm{g\bar{q}}$ we require the cuts (5.11) and (5.12) and in the processes qg and $\bar{\mathrm{q}}\mathrm{g}$ we appply the cuts (5.9) and (5.10). For the numerical integration of the process we used the code presented in Chapter 4. At LO the phase-space generator uses 10 channels and at NLO 45 channels for the integration, which in both cases agrees with the number of tree-level diagrams present in the process. For the LO result without the cuts of Eqs. (5.9) – (5.12) we find $\sigma^{\mathrm{LO}}_{\mathrm{wocuts}} = (1052.37 \pm 4.1)$ fb. The results for the LO and NLO cross sections with the cuts of Eqs. (5.9) – (5.12) are shown in table 5.1, where we chose for the factorization scale $\mu_{\mathrm{F}} = m_{\mathrm{W}}$ and for the renormalization scale $\mu_{\mathrm{R}} = m_{\mathrm{W}}$, and found agreement with Reference [54]. As kinematical distributions we present the transverse momentum distributions of the tagging jet with highest p_{T} (see Figure 5.9) and of the lepton (see Figure 5.10)

σ^{LO}	σ^{NLO}
1042.16 ± 2.0 (fb)	1107.4 ± 9.7 (fb)

Table 5.1: Results

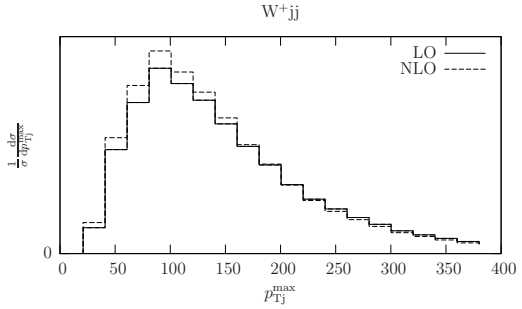

Figure 5.9: Transverse momentum distribution of the tagging jet with highest p_T.

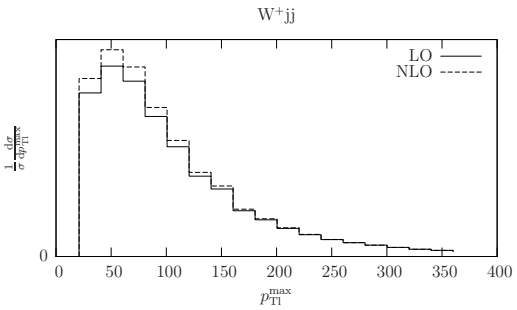

Figure 5.10: Transverse momentum distribution of the charged lepton.

5.2 W^+W^+jj

5.2.1 Setup

In the following we present the application of the programme — presented in Chapter 4 — to the process $jje^+\bar{\nu}_e\mu^+\bar{\nu}_\mu$ via WBF [53]. At LO, i.e. α^6, the two scattered quarks exchange a weak gauge boson via a t-channel process with a subsequent emission of W^+ boson, which decay leptonically afterwards. There are four main t-channel topologies, which result in the final state $jje^+\bar{\nu}_e\mu^+\bar{\nu}_\mu$. In two of them a W^+, subsequently decaying into $l\nu$, is emitted either from only one quark line or from different quark lines as shown in Figures (5.11) and (5.12). In a third topology the two inital-state quarks each emit a W^+ with successive leptonical decay $W^+W^+ \to e^+\bar{\nu}_e\mu^+\bar{\nu}_\mu$ (see Figure 5.14). In the fourth topology a W or Z boson and a W^+ boson is emitted from each of the quark lines resulting in $e^+\bar{\nu}_e$. The other $l\nu$-pair is produced via the W^+ emission from one of the quark lines 5.13. Next to t-channel processes also u-channel processes and their interferences with t-channel processes contribute to processes with identical flavours in the final state. The s-channel contribution will be suppressed by the chosen set of cuts, but they are included in the calculation of [53].

5.2.2 Results

The amplitudes [53] contributing to $pp \to jje^+\bar{\nu}_e\mu^+\bar{\nu}_\mu$ discussed above have been implemented in the Monte Carlo code presented in Chapter 4. We use the CTEQ6L1 parton distributions at LO. Throughout the calculation quark masses are neglected.

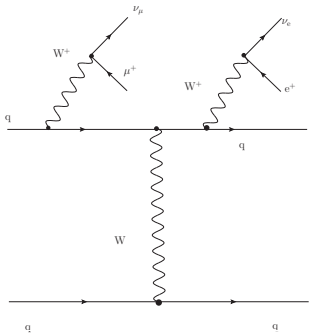

Figure 5.11: Leading-order topology for process $qq \to qqe^+\bar{\nu}_e\mu^+\bar{\nu}_\mu$

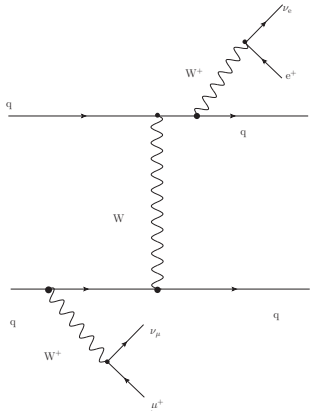

Figure 5.12: Leading-order topology for process $qq \to qqe^+\bar{\nu}_e\mu^+\bar{\nu}_\mu$

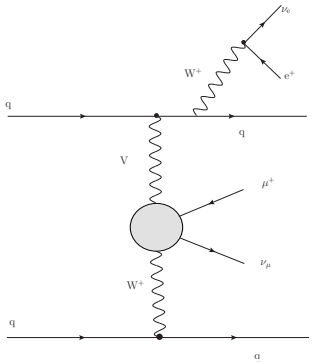

Figure 5.13: Leading-order topology for process $qq \to qqe^+\bar{\nu}_e\mu^+\bar{\nu}_\mu$

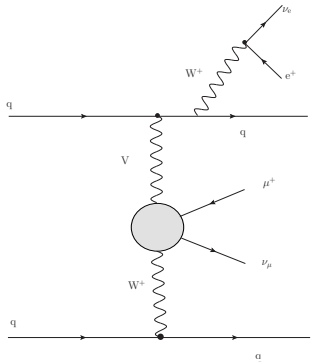

Figure 5.14: Leading-order topology for process $qq \to qqe^+\bar{\nu}_e\mu^+\bar{\nu}_\mu$

As input parameters we chose

$$\begin{aligned} m_{\mathrm{W}} &= 80.423\ \mathrm{GeV}, \\ m_{\mathrm{Z}} &= 91.188\ \mathrm{GeV}, \\ m_{\mathrm{H}} &= 120.0\ \mathrm{GeV}, \\ \Gamma_{\mathrm{W}} &= 2.04759951\ \mathrm{GeV}, \\ \Gamma_{\mathrm{Z}} &= 2.44140351\ \mathrm{GeV}, \\ \Gamma_{\mathrm{H}} &= 3.48 \times 10^{-3}\ \mathrm{GeV}, \\ G_{\mathrm{F}} &= 1.66 \times 10^{-5}\ \mathrm{GeV}^{-2}. \end{aligned} \tag{5.13}$$

The other parameters such as α_{QED} and $\sin^2\theta_{\mathrm{W}}$ are calculated with the following electroweak tree-level relations

$$\begin{aligned} \sin^2\theta_{\mathrm{W}} &= 1 - \frac{m_{\mathrm{W}}^2}{m_{\mathrm{Z}}^2}, \\ \alpha_{\mathrm{QED}} &= \frac{1}{\pi} G_{\mathrm{F}} \sqrt{2} m_{\mathrm{W}}^2 \sin^2\theta_{\mathrm{W}}. \end{aligned} \tag{5.14}$$

For the reconstruction of the jets the k_{T} algorithm is used according to Section 4.5.3 with the resolution parameter $D = 0.7$. The integration is performed for LHC with center-of-mass energy of $\sqrt{s} = 14$ TeV. We employ the WBF cuts from Eq. (5.2). Additionally we impose the following cuts on leptons

$$\begin{aligned} p_{\mathrm{Tl}} &> 20 \text{ GeV}, \\ |\eta_{\mathrm{l}}| &\leq 2.5, \\ \Delta R_{\mathrm{ll}} &\geq 0.1, \\ \Delta R_{\mathrm{jl}} &\geq 0.4, \end{aligned} \tag{5.15}$$

where ΔR_{ll} and ΔR_{jl} stand for the lepton–lepton and the jet-lepton separation in the rapidity–azimuthal angle plane (4.5.4). As explained in Section 5 all the leptonic activity in the WBF $jje^+\bar{\nu}_e\mu^+\bar{\nu}_\mu$ production falls in between the two hard tagging jets we also require that the rapidity of the charged leptons is in between the rapidity of the two tagging jets, i.e.

$$\eta_{\mathrm{j,min}} < \eta_{\mathrm{l}} < \eta_{\mathrm{j,max}}. \tag{5.16}$$

First of all we performed technical checks to ensure that the subtraction terms and the integrated subtraction terms are correct. For the check of the dipole subtraction terms we exemplarily present in Figure 5.15 the ratio $|M_{\mathrm{R}}|^2/D_{\mathrm{sum}}$ for the gluon-initiated process $dg \to use^+\bar{\nu}_e\mu^+\bar{\nu}_\mu\bar{c}$. In contrast to Figure 4.6 — where we randomly generated phase-space points and picked the more singular ones — we created the more singular phase-space points with the subroutine mentioned in Section 4.9.2. The deviation from 1 between 10^{-2} and 10^{-3} is due to the fact that the other ratios of invariants s_{39}/s_{12} and s_{49}/s_{12} have the order of magnitude 10^{-4} and thus the subtraction of the singularity in s_{29} does not have to work in that region. A table of all contributing dipole subtraction terms to each of the three channels qq, qg and gq can be found in Table 5.2.

For the virtual matrix element we checked the ϵ-dependence of the integrand in the sum

$$\int_m \left[\mathrm{d}\sigma^V + \int_1 \mathrm{d}\sigma^{\mathrm{A}} \right] = \text{const}, \tag{5.17}$$

when varying ϵ. In Figure 5.16 we denoted the sum of the integrated dipole terms $\int_1 \mathrm{d}\sigma^{\mathrm{A}}$ with $\mathrm{IntD}_{\mathrm{sum}}$ and clearly verify that the sum in Eq. (5.17) is independent on ϵ.

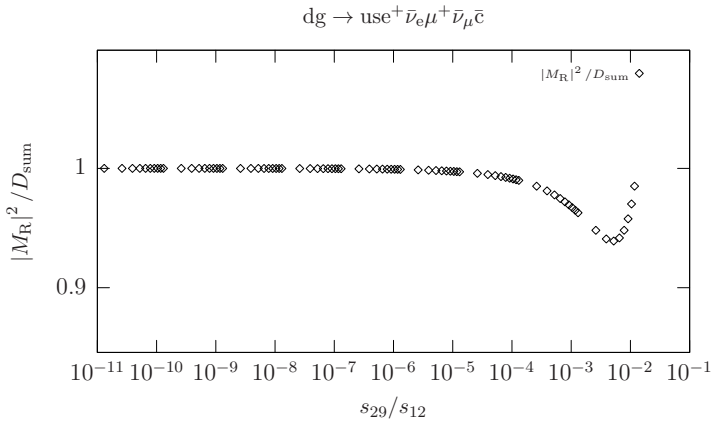

Figure 5.15: $|M_{\mathrm{R}}|^2/D_{\mathrm{sum}}$ for the process $\mathrm{dg} \to \mathrm{use}^+\bar{\nu}_{\mathrm{e}}\mu^+\bar{\nu}_\mu\bar{\mathrm{c}}$

Initial-state partons	Dipole subtraction terms
qq	$\mathcal{D}^{29,1}$, $\mathcal{D}^{19,2}$, $\mathcal{D}^{1}_{39}$, $\mathcal{D}^{1}_{49}$, $\mathcal{D}^{2}_{39}$, $\mathcal{D}^{2}_{49}$, $\mathcal{D}^{19}_{3}$, $\mathcal{D}^{29}_{3}$, $\mathcal{D}^{19}_{4}$, $\mathcal{D}^{29}_{4}$, $\mathcal{D}_{49,3}$, $\mathcal{D}_{39,4}$
qg	$\mathcal{D}^{24,1}$, $\mathcal{D}^{29,1}$,$\mathcal{D}^{24}_{3}$,$\mathcal{D}^{29}_{3}$, $\mathcal{D}^{29}_{4}$, $\mathcal{D}^{24}_{9}$
gq	$\mathcal{D}^{13,2}$, $\mathcal{D}^{19,2}$, $\mathcal{D}^{19}_{3}$, $\mathcal{D}^{13}_{4}$, $\mathcal{D}^{19}_{4}$, $\mathcal{D}^{13}_{9}$

Table 5.2: Dipole subtraction terms

For the numerical integration we used the parallel version of the code presented in Chapter 4. The phase-space generator therein is initialized by identifying all channels that are needed to account for the peaking structures that occur in the squared matrix elements. For the process $\mathrm{jje}^+\bar{\nu}_{\mathrm{e}}\mu^+\bar{\nu}_\mu$ 92 channels at LO are used to integrate the process. A further reduction of the integration error is achieved by using the adaptive optimization scheme (see 2.5), where we take 10% of the total number of events to perform 10 optimization steps. At LO we investigated three cross sections:

1. The full process (σ^{full}) includes weak-boson exchange in the s-channel, all t and u-channel contributions as well as — in the case of subprocesses with identical flavour in the final state (such as $\mathrm{uu} \to \mathrm{dde}^+\bar{\nu}_{\mathrm{e}}\mu^+\bar{\nu}_\mu$)— the interferences of t and u-channel contributions.

2. The process ($\sigma^{\mathrm{s,t,u}}$) includes s, t and u-channel contributions, but not the interferences of t and u-channel as above.

3. The process ($\sigma^{\mathrm{t,u}}$) includes t and u-channel contributions.

The LO results for the factorization scale chosen to be $\mu_{\mathrm{F}} = m_{\mathrm{W}}$ with the cuts of (5.15), (5.16) and (5.6) are shown in Table 5.3. The result is in full agreement with the corresponding result $\sigma^{\mathrm{cuts}}_{\mathrm{LO}}(\mu_0 = m_W) = 1.478$ fb in [48]. Table 5.3 also shows that the

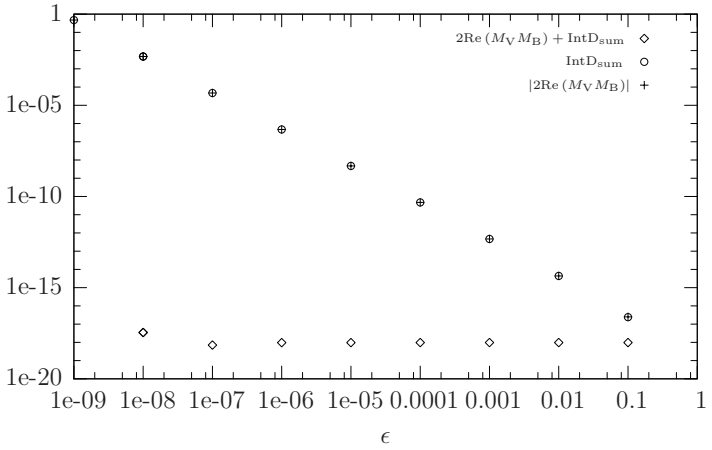

Figure 5.16: ϵ-dependence

σ^{full}	$\sigma^{\mathrm{s,t,u}}$	$\sigma^{\mathrm{t,u}}$
1.474 ± 0.004 (fb)	1.484 ± 0.005 (fb)	1.475 ± 0.004 (fb)

Table 5.3: LO results

s-channel and interference contributions to the total cross section is less than 1%. The following kinematical distributions are produced according to the full process (σ^{full}). As pointed out in Section 5 the two tagging jets are located in the far-forward and far-backward regions of the detector, which can be seen in the rapidity distributions in Figures 5.20 and 5.21. Since there is no colour exchange between the initial-state quarks in the WBF channel the central-rapidity range of the detector encounters little jet activity. In Figures 5.18 and 5.19 we present the transverse momentum distribution of the tagging jets with lowest and highest p_{T}, respectively.

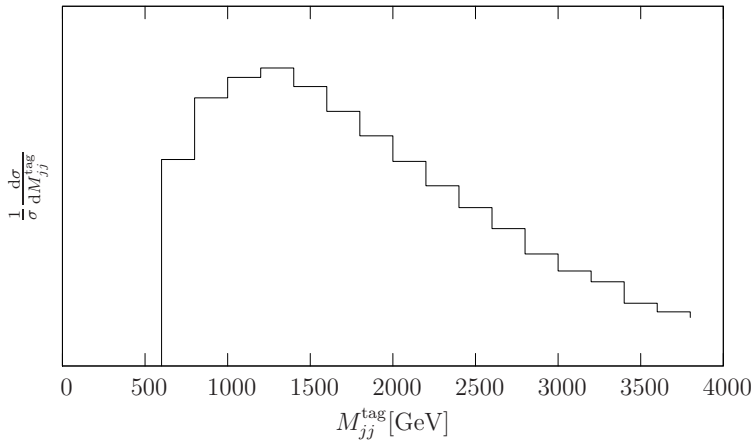

Figure 5.17: Invariant mass distribution of the two tagging jets.

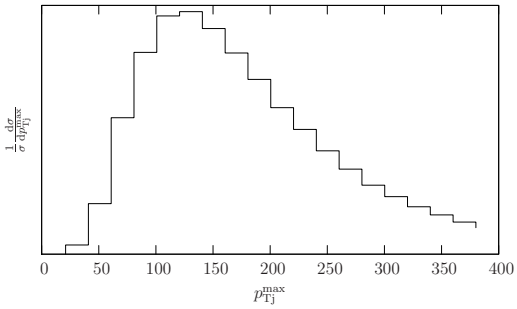

Figure 5.18: Transverse momentum distribution of the tagging jet with highest p_{T}.

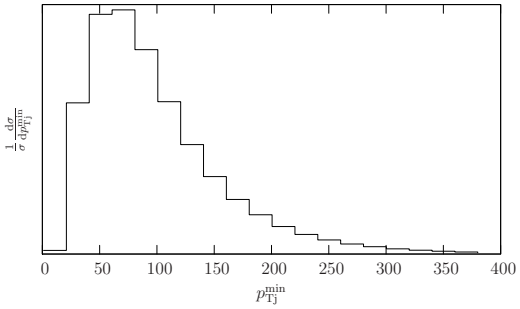

Figure 5.19: Transverse momentum distribution of the tagging jet with lowest p_{T}.

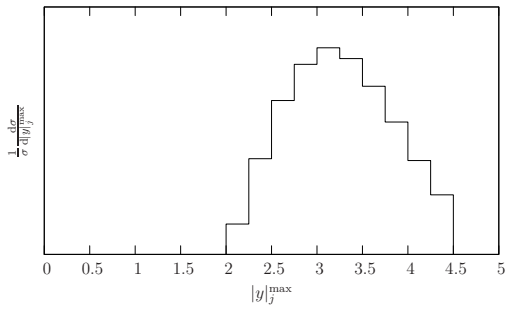

Figure 5.20: Rapidity distribution of the tagging jet with highest absolute value of the rapidity $|y_j|$.

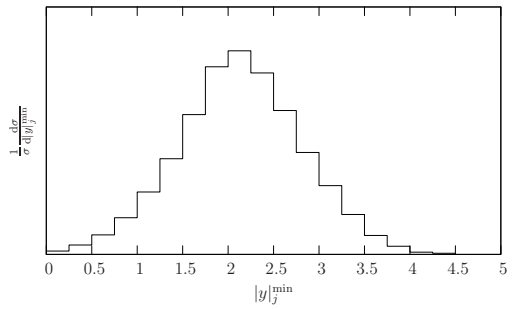

Figure 5.21: Rapidity distribution of the tagging jet with lowest absolute value of the rapidity $|y_j|$.

Acknowledgements

First of all I wish to thank my supervisor Prof. Dr. Ansgar Denner for assigning the topic of the thesis. His continuous support, his patience and criticism were invaluable. He always found time to answer all my questions.
I would also like to thank Prof. Dr. Thomas Gehrmann and Prof. Dr. Daniel Wyler, who gave me the great opportunity to work at the Institute and provided the support at the University of Zürich.
Special thanks go to Prof. Dr. Ben Moore for providing fooseball, billiard, ping-pong and most-importantly the annual „Christmas Dinner“.
I would also like to express my gratitude to Doug Potter and Roland Bernet for providing excellent computing infrastructure.
My special thanks also go to Rikkert Frederix and Nicolas Greiner for their great help concerning all questions and comparisons with MadGraph and MadDipole.
I am also very grateful to Prof. Dr. Ansgar Denner and Oriana Schällibaum for carefully reading through the manuscript. Their hints and comments led to significant improvements in both its substance and organization. I also would like to thank Andrea Ferroglia and Cedric Studerus for many comments on the manuscript.
Furthermore I am very grateful to all my colleagues at the Institute for Theoretical Physics of the University of Zürich and at the Paul Scherrer Institute in Villigen for creating a pleasant working environment and the numerous fruitful discussions and conversations. I very much enjoyed their company and the time we spent together. In particular I would like to emphasize Andreas Bleuler, Sebastian Elser, Marc Guillioz, Nico Hamaus, Antoine Klein, Lucas Lombriser, Thomas Lübbert, Aurel Schneider, Erich Weihs as well as Stefano Actis, Grigorios Chachamis, Stefan Kallweit, Timo Schmidt, Michael Spira and Qiang Li for enduring joyful entertainment at lunch and coffee breaks. I would also like to thank my office mates Christian Kurz, Lucia Hošeková, Pier Francesco Monni, Jaiyul Yoo and Thomas Lübbert (in order of appearance) for many discussions and for providing much appreciated distraction.
Outside the world of physics I had a bunch of friends with whom life in Zürich was a lot of fun. I would like to set apart Zoé Kilchenmann, Dominik Leuenberger, Doug Potter, Oriana Schällibaum and Cedric Studerus for long conversations about anything

but physics — and physics.
I am indebted to my parents Carmen and Martin Motz for their continuous and indefatigable support throughout all the years. Last but not least I thank my brother Michael Motz for sharing his enthusiastic optimism, encouraging me and for the refreshing conversations we had.

You all shaped the scenes that were my last four years in Zurich.
Thank you!

Appendix A

Numerics

In this section we review the origin of instabilities in floating-point operations and follow [55]. Since the set A of numbers representable in a computer machine is finite, the question arises how to approximate a number $x \notin A$ with a machine number $g \in A$. Given the machine precision eps, a rounding mapping is defined as follows

$$\begin{aligned} rd &: \mathcal{R} \mapsto A, \\ rd(x) &= x(1+\epsilon) \quad \text{with} \quad |\epsilon| \leq eps \; \forall x \in \mathcal{R}. \end{aligned} \tag{A.1}$$

For a good approximation of an element $x \notin A$ in terms of a machine number g one requires

$$|x - rd(x)| \leq |x - g|, \quad \forall g \in A. \tag{A.2}$$

The result of the arithmetic operations $x \pm y$, $x \cdot y$, x/y of elements $x, y \in A$ need not necessarily be an element of A. Therefore floating-point operations are usually defined as follows

$$\begin{aligned} x +^* y &:= rd(x+y) \\ x -^* y &:= rd(x-y) \\ x \times^* y &:= rd(x \times y) \\ x/^* y &:= rd(x/y) \end{aligned} \tag{A.3}$$

for $x, y \in A$. Because of (A.1), it holds

$$\begin{aligned} x +^* y &:= (x+y)(1+\epsilon_1) \\ x -^* y &:= (x-y)(1+\epsilon_2) \\ x \times^* y &:= (x \times y)(1+\epsilon_3) \\ x/^* y &:= (x/y)(1+\epsilon_4) \end{aligned} \tag{A.4}$$

with $\|\epsilon_i\| \leq eps$. As an example, we consider the sums $y = (a+b)+c$ and $z = a+(b+c)$. With respect to floating-point operations the results are the approximations $\tilde{y}$ and $\tilde{z}$ instead of y and z, for which the following holds

$$\begin{aligned} \alpha &= rd(a+b) = (a+b)(1+\epsilon_1) \\ \tilde{y} &= rd(\alpha+c) = (\alpha+c))(1+\epsilon_2) \\ &= [(a+b)(1+\epsilon_1)+c](1+\epsilon_2) \\ &= (a+b+c)\left[1+\frac{a+b}{a+b+c}\epsilon_1(1+\epsilon_2)+\epsilon_2\right]. \end{aligned} \tag{A.5}$$

Neglecting higher-order terms, the relative error $\epsilon_y = (\tilde{y}-y)/y$ of $\tilde{y}$ is given by

$$\epsilon_y \approx \frac{a+b}{a+b+c}\epsilon_1 + 1\cdot\epsilon_2. \tag{A.6}$$

The amplification factors $(a+b)/(a+b+c)$ and 1 show, how the rounding errors ϵ_1, ϵ_2 affect ϵ_y. The factor $(a+b)/(a+b+c)$ shows, that - depending on whether $\|a+b\|$ or $\|b+c\|$ is smaller - it is numerically more stable to build the sum $a+b+c$ according to $(a+b)+c$ or $a+(b+c)$. The formula of error propagation in an operation ϕ

$$\epsilon_{y_i} = \sum_{j=1}^{n} \frac{x_j}{\phi_i}\cdot\frac{\partial\phi_i(x)}{\partial x_j}\cdot\epsilon_{x_j} \tag{A.7}$$

shows how a relative error in x_j affects the relative error in y_i. For arithmetic operations $x \pm y$, $x\cdot y$, x/y, we get

$$\begin{aligned} \phi(x,y) := x\cdot y: &\quad \epsilon_{xy} = \epsilon_x + \epsilon_y \\ \phi(x,y) := x/y: &\quad \epsilon_{x/y} = \epsilon_x - \epsilon_y \\ \phi(x,y) := x\pm y: &\quad \epsilon_{x\pm y} = \tfrac{x}{x\pm y}\epsilon_x \pm \tfrac{y}{x\pm y}\epsilon_y. \end{aligned} \tag{A.8}$$

In the summation the critical amplification factors arise if x and y have opposite signs and are of comparable magnitude, i.e. $y \approx -x$. This amplifies the factors $\frac{x}{x+y}$, $\frac{y}{x+y}$ and also the resulting relative error.

Appendix B

Error Handling

During runtime of the program some issues can occur that may lead to the abortion of the program. Some of these issues can be due to numerical issues as explained in Appendix A, where e.g. huge cancellations appear. In order to absorb those issues during runtime we implemented a basic error handling concept, which takes care for such errors. The file `error.dat` contains the information, how often an error appeared. The index of the array `error` denotes a specific error:

```
Index 09: function jacobian: xmin>xmax (case nu = 0)
Index 10: function jacobian: xmax=mass2 (case nu > 1)
Index 11: function jacobian: xmin=mass2  (case nu > 1)
Index 15: function jacobian: x-mass2<0 (case nu = 1)
Index 16: function jacobian: xmin>xmax (case nu != 0)
Index 17: function jacobian: x-mass2<0 (case nu=1)
Index 18: function jacobian: xmax < mass2
Index 19: function jacobian: xmin < mass2

Index 12: function h: xmax=mass2 (case nu > 1)
Index 13: function h: xmin=mass2 (case nu > 1)

Index 20: subroutine rotation: cost > 1
Index 21: subroutine boost: m2<0

Index 22: subroutine density_inv: denum=0 (case width=0)
Index 29: subroutine density_inv: denum<0 (case width=0)
Index 23: subroutine density_inv: denum<=0 (case width>0)

Index 24: subroutine generate_decay: lambda<=0
Index 25: subroutine generate_decay: s<=0
Index 26: subroutine generate_decay: cost > 1
```

```
Index 27: subroutine density_decay: lambda <=0
Index 28: subroutine density_decay: denum <=0

Index 30: subroutine generate_process: lambdas<=0
Index 31: subroutine generate_process: lambdat<=0
Index 32: subroutine generate_process: cost > 1
Index 33: subroutine generate_process: costhat > 1

Index 35: subroutine density_process: lambdas<=0
Index 36: subroutine density_process: lambdat<=0
Index 37: subroutine density_process: denum<=0 (case width>0)
Index 38: subroutine density_process: denum=0 (case width=0)
Index 40: subroutine density_process: denum<0 (case width=0)

Index 39: subroutine generate_process: s<0
Index 42: subroutine generate_process: tmax <= tmin

Index 50: subroutine generate_density: error in calling density_inv
Index 51: subroutine generate_density: error in calling density_process
Index 52: subroutine generate_density: error in calling density_decay

Index 55: subroutine generate_momentum: error in calling generate_inv
Index 56: subroutine generate_momentum: error in calling generate_process
Index 57: subroutine generate_momentum: error in calling generate_decay

Index 60: subroutine generate_density called with errorcode.ne.0
Index 62: subroutine generate_inv called with errorcode.ne.0
Index 63: subroutine density_inv called with errorcode.ne.0
Index 64: subroutine generate_decay called with errorcode.ne.0
Index 65: subroutine density_decay called with errorcode.ne.0
Index 66: subroutine generate_process called with errorcode.ne.0
Index 67: subroutine generate_process tmax gt 0

Index 70: subroutine generate_inv: Errorcode from function h
Index 71: subroutine density_inv: Errorcode from function jacobian

Index 80: subroutine density_inv: smin > smax
Index 81: subroutine generate_momenta: error from checkmom


!RECOMBINATION ALGORITHM
Index 101: subroutine ktcluster: |cos(deltaphi)| > 1
Index 110: subroutine applyjetcut: lt 2 hard jets
```

```
Index 111: subroutine applyjetcut: tagging jet rapidity separation cut not fullfille
Index 112: subroutine applyjetcut:  opposite detector hemisphere cut not fullfilled
Index 113: subroutine applyjetcut: invariant mass jet cut not fullfilled

Index 120: subroutine applylepcut:deltaRll cut not fullfilled
Index 121: subroutine applylepcut:deltaRlj cut not fullfilled
Index 122: subroutine applylepcut: ptlep cut not fullfilled
Index 123: subroutine applylepcut: etalep cut not fullfilled
Index 124: subroutine applylepcut: invmassll cut not fullfilled
Index 125: subroutine applylepcut: charged lep rapidity not between tagging jet ones

!VEGAS
Index 45: subroutine density_process: problem in recovering random number
```

Bibliography

[1] T. Hahn, S. Heinemeyer, F. Maltoni, G. Weiglein, and S. Willenbrock, "SM and MSSM Higgs boson production cross-sections at the Tevatron and the LHC," `hep-ph/0607308`. Published in 'Tevatron for LHC report: Higgs'(hep-ph/0612172).

[2] R. Eckhard, "Stan Ulam, John Von Neumann and the Monte Carlo method," *Los Alamos Science,* **15,** (1987) 131–136.

[3] N. Metropolis, "The beginning of the Monte Carlo method," *Los Alamos Science,* **15,** (1987) 125–130.

[4] I. Morgenstern, "Physikalische Optimierungsmethoden." Lecture, 2005.

[5] N. Metropolis, A. Rosenbluth, M. Rosenbluth, A. Teller, and E. Teller, "Equation of state calculations by fast computing machines," *J.Chem.Phys.* **21** (1953) 1087–1092.

[6] S. Catani and M. H. Seymour, "A general algorithm for calculating jet cross sections in NLO QCD," *Nucl. Phys.* **B485** (1997) 291–419, `hep-ph/9605323`.

[7] U. Krengel, *Einführung in die Wahrscheinlichkeitstheorie und Statisik.* Friedr. Vieweg & Sohn Verlagsgesellschaft mbH, Braunschweig/Wiesbaden 2002.

[8] W. Hackenbroch, "Einführung in die Wahrscheinlichkeitstheorie und Statistik." Lecture, 2004.

[9] G. Lepage, "A New Algorithm for Adaptive Multidimensional Integration," *J.Comput.Phys.* **27** (1978) 192. Revised version.

[10] G. Lepage, "VEGAS: AN ADAPTIVE MULTIDIMENSIONAL INTEGRATION PROGRAM,".

[11] T. Ohl, "Vegas revisited: Adaptive Monte Carlo integration beyond factorization," *Comput.Phys.Commun.* **120** (1999) 13–19, `hep-ph/9806432`.

[12] R. P. R. Kleiss, "Weight optimization in multichannel Monte Carlo," `hep-ph/9405257v2`.

[13] C. Dutang and P. Savicky, *randtoolbox: Generating and Testing Random Numbers*, 2010. R package version 1.10.

[14] K. M. S.K. Park, "Random Number Generators: Good Ones Are Hard To Find," *Communications of the ACM* **31** (1988) 1192–1201.

[15] T. N. M. Matsumoto, "Mersenne twister: a 623-dimensionally equidistributed uniform pseudo-random number generator," *Communications of the ACM* **8** (1998) 3–30.

[16] P. L'Ecuyer, "Random numbers for simulation," *Communications of the ACM* **33** (1990) 85–97.

[17] F. James, "RANLUX: A Fortran implementation of the high-quality pseudorandom number generator of Lüscher," *Comp. Phys. Comm.* **79** (1994) 11–114.

[18] E. Byckling and K. Kajantie, *Particle Kinematics*. John Wiley and Sons, 1973.

[19] M. Roth, *Precise Predictions for Four-Fermion Production in Electron-Positron Annihilation*. PhD thesis, ETH Zurich, 2000. `hep-ph/0008033v1`.

[20] J. Hilgart, R. Kleiss, and F. Le Diberder, "An Electroweak Monte Carlo for four fermion production," *Comput.Phys.Commun.* **75** (1993) 191–218.

[21] F. A. Berends, P. Daverveldt, and R. Kleiss, "Monte Carlo Simulation of Two Photon Processes. 1. Radiative Corrections to Multiperipheral e+ e- mu+ mu- Production," *Comput.Phys.Commun.* **40** (1986) 271–284.

[22] S. Catani, S. Dittmaier, M. H. Seymour, and Z. Trocsanyi, "The Dipole formalism for next-to-leading order QCD calculations with massive partons," *Nucl.Phys.* **B627** (2002) 189–265, `hep-ph/0201036`.

[23] Z. Nagy and Z. Trocsanyi, "Next-to-leading order calculation of four jet observables in electron positron annihilation," *Phys.Rev.* **D59** (1999) 014020, `hep-ph/9806317`.

[24] J. M. Campbell, R. Ellis, and F. Tramontano, "Single top production and decay at next-to-leading order," *Phys.Rev.* **D70** (2004) 094012, `hep-ph/0408158`.

[25] R. Frederix, T. Gehrmann, and N. Greiner, "Integrated dipoles with MadDipole in the MadGraph framework," *JHEP* **1006** (2010) 086, `1004.2905`.

[26] J. M. Campbell and F. Tramontano, "Next-to-leading order corrections to Wt production and decay," *Nucl.Phys.* **B726** (2005) 109–130, hep-ph/0506289.

[27] G. Bevilacqua, M. Czakon, C. Papadopoulos, R. Pittau, and M. Worek, "Assault on the NLO Wishlist: pp $\to$ t anti-t b anti-b," *JHEP* **0909** (2009) 109, 0907.4723.

[28] A. Denner, S. Dittmaier, M. Roth, and D. Wackeroth, "RACOONWW1.3: A Monte Carlo program for four fermion production at e+ e- colliders," *Comput.Phys.Commun.* **153** (2003) 462–507, hep-ph/0209330.

[29] C. G. Papadopoulos, "PHEGAS: A Phase space generator for automatic cross-section computation," *Comput.Phys.Commun.* **137** (2001) 247–254, hep-ph/0007335.

[30] S. Weinzierl, "Introduction to monte carlo methods." Research School Subatomic Physics, Amsterdam, 2000.

[31] C. Meier, *Electroweak Corrections to Dilepton-plus-Photon Production at the LHC*. PhD thesis, University of Zürich, 2005.

[32] S. Catani, Y. L. Dokshitzer, M. H. Seymour, and B. R. Webber, "Longitudinally invariant K(t) clustering algorithms for hadron hadron collisions," *Nucl. Phys.* **B406** (1993) 187–224.

[33] S. D. Ellis and D. E. Soper, "Successive combination jet algorithm for hadron collisions," *Phys. Rev.* **D48** (1993) 3160–3166, hep-ph/9305266.

[34] S. Kallweit, *Precision Calculations for Gauge-Boson Pair Production with a Hadronic Jet at Hadron Colliders*. PhD thesis, LMU München, 2008.

[35] A. Martin, W. Stirling, R. Thorne, and G. Watt, "Update of parton distributions at NNLO," *Phys.Lett.* **B652** (2007) 292–299, 0706.0459.

[36] J. Pumplin, D. Stump, J. Huston, H. Lai, P. M. Nadolsky, *et al.*, "New generation of parton distributions with uncertainties from global QCD analysis," *JHEP* **0207** (2002) 012, hep-ph/0201195.

[37] M. R. Whalley, D. Bourilkov, and R. C. Group, "The Les Houches Accord PDFs (LHAPDF) and Lhaglue," hep-ph/0508110.

[38] T. Stelzer and W. Long, "Automatic generation of tree level helicity amplitudes," *Comput.Phys.Commun.* **81** (1994) 357–371, hep-ph/9401258.

[39] F. Maltoni and T. Stelzer, "MadEvent: Automatic event generation with MadGraph," *JHEP* **0302** (2003) 027, hep-ph/0208156.

[40] J. Alwall, P. Demin, S. de Visscher, R. Frederix, M. Herquet, *et al.*, "MadGraph/MadEvent v4: The New Web Generation," *JHEP* **0709** (2007) 028, 0706.2334.

[41] **LHC Higgs Cross Section Working Group** Collaboration, S. Dittmaier *et al.*, "Handbook of LHC Higgs Cross Sections: 1. Inclusive Observables," 1101.0593.

[42] T. Figy, C. Oleari, and D. Zeppenfeld, "Next-to-leading order jet distributions for Higgs boson production via weak boson fusion," *Phys.Rev.* **D68** (2003) 073005, hep-ph/0306109.

[43] T. Plehn and D. L. Rainwater, "Higgs decays to muons in weak boson fusion," *Phys.Lett.* **B520** (2001) 108–114, hep-ph/0107180.

[44] T. Figy, S. Palmer, and G. Weiglein, "Higgs Production via Weak Boson Fusion in the Standard Model and the MSSM," 1012.4789. * Temporary entry *.

[45] D. Green, "Kinematics in vector boson fusion," hep-ph/0603022.

[46] D. L. Rainwater and D. Zeppenfeld, "Searching for H $\rightarrow$ gamma gamma in weak boson fusion at the LHC," *JHEP* **9712** (1997) 005, hep-ph/9712271.

[47] N. Kauer, T. Plehn, D. L. Rainwater, and D. Zeppenfeld, "H $\rightarrow$W W as the discovery mode for a light Higgs boson," *Phys.Lett.* **B503** (2001) 113–120, hep-ph/0012351.

[48] B. Jäger, C. Oleari, and D. Zeppenfeld, "Next-to-leading order QCD corrections to W+ W+ jj and W- W- jj production via weak-boson fusion," *Phys.Rev.* **D80** (2009) 034022, 0907.0580.

[49] B. Jäger, C. Oleari, and D. Zeppenfeld, "Next-to-leading order QCD corrections to Z boson pair production via vector-boson fusion," *Phys.Rev.* **D73** (2006) 113006, hep-ph/0604200.

[50] M. Ciccolini, A. Denner, and S. Dittmaier, "Electroweak and QCD corrections to Higgs production via vector-boson fusion at the LHC," *Phys.Rev.* **D77** (2008) 013002, 0710.4749.

[51] M. Ciccolini, A. Denner, and S. Dittmaier, "Strong and electroweak corrections to the production of Higgs + 2jets via weak interactions at the LHC," *Phys.Rev.Lett.* **99** (2007) 161803, 0707.0381.

[52] A. Denner, S. Dittmaier, T. Kasprzik, and A. Muck, "Electroweak precision for W+jet production," *PoS* **RADCOR2009** (2010) 058, 1001.2468. * Temporary entry *.

[53] L. Hošeková *to be published.* PhD thesis, University of Zürich.

[54] C. Oleari and D. Zeppenfeld, "Next-to-leading order QCD corrections to W and Z production via vector-boson fusion," *Phys. Rev.* **D69** (2004) 093004, hep-ph/0310156.

[55] J. Stoer, *Numerische Mathematik 1.* Springer Verlag Berlin, 8th ed., 2002.

[56] A. Denner, S. Dittmaier, M. Roth, and L. Wieders, "Electroweak corrections to four-fermion production in e+ e- annihilation," hep-ph/0505253.

[57] A. Denner, S. Dittmaier, M. Roth, and L. Wieders, "Electroweak corrections to e+ e- $\to$ 4 fermions," *Nucl.Phys.Proc.Suppl.* **157** (2006) 68–72, hep-ph/0601122.

[58] M. E. Peskin and D. V. Schroeder, *An Introduction to quantum field theory.* Reading, USA: Addison-Wesley (1995) 842 p.

[59] F. Halzen and A. D. Martin, *Quarks and leptons: an introductory course in modern particle physics.* New York, Usa: Wiley (1984) 396 p.

[60] M. Böhm, A. Denner, and H. Joos, *Gauge theories of the strong and electroweak interaction.* Stuttgart, Germany: Teubner (2001) 784 p.

[61] R. K. Ellis, W. J. Stirling, and B. R. Webber, *QCD and collider physics*, vol. 8. 1996.

[62] Z. Nagy, "Next-to-leading order calculation of three jet observables in hadron hadron collision," *Phys.Rev.* **D68** (2003) 094002, hep-ph/0307268.

[63] T. Gleisberg and F. Krauss, "Automating dipole subtraction for QCD NLO calculations," *Eur.Phys.J.* **C53** (2008) 501–523, 0709.2881.

[64] S. Catani, Y. L. Dokshitzer, M. Olsson, G. Turnock, and B. R. Webber, "New clustering algorithm for multi - jet cross-sections in e+ e- annihilation," *Phys. Lett.* **B269** (1991) 432–438.

[65] D. L. Rainwater and D. Zeppenfeld, "Observing H $\to$ W(*) W(*)$\to$ e+- muon-+ missing-p(T) in weak boson fusion with dual forward jet tagging at the CERN LHC," *Phys.Rev.* **D60** (1999) 113004, hep-ph/9906218.

[66] C. Anastasiou and K. Melnikov, "Higgs boson production at hadron colliders in NNLO QCD," *Nucl.Phys.* **B646** (2002) 220–256, hep-ph/0207004.

[67] T. Plehn, D. Rainwater, and D. Zeppenfeld, "Determining the structure of higgs couplings at the cern large hadron collider," *Phys. Rev. Lett.* **88** (Jan, 2002) 051801.

[68] S. Palmer, *Higgs production via weak boson fusion in the Standard Model and the MSSM*. PhD thesis, Institute for Particle Physics Phenomenology, Durham University, 2009.

[69] G. Bozzi, B. Jäger, C. Oleari, and D. Zeppenfeld, "Next-to-leading order QCD corrections to W+ Z and W- Z production via vector-boson fusion," *Phys.Rev.* **D75** (2007) 073004, `hep-ph/0701105`.

[70] B. Jäger, C. Oleari, and D. Zeppenfeld, "Next-to-leading order QCD corrections to W+W- production via vector-boson fusion," *JHEP* **0607** (2006) 015, `hep-ph/0603177`.